Thermo-economic assessment of small-scale organic Rankine cycle for low-grade industrial waste heat recovery based on an experimental application

DOCTORAL THESIS

presented by
BERNARDO PERIS PÉREZ

supervised by
DR. JOAQUÍN NAVARRO ESBRÍ

Castellón de la Plana (Spain), July 2017

Thermo-economic assessment of small-scale organic Rankine cycle for low-grade industrial waste heat recovery based on an experimental application

A dissertation submitted to

Universitat Jaume I, Castelló de la Plana, Espanya
Escola Superior de Tecnologia i Ciències Experimentals
Departament d'Enginyeria Mecànica i Construcció
Programa de doctorat en Tecnologies Industrials, Materials i Edificació

for the mention of

International Doctorate

presented by

Bernardo Peris Pérez

supervised by

Dr. Joaquín Navarro Esbrí

reviewed by

Dr. Juan Manuel Belman Flores
Universidad Guanajuato. Salamanca, Mexico

Dr. Luis Carlos Mendoza Toledo
Ecole Polytechnique Fédérale de Lausanne. Neuchâtel, Switzerland

Thesis committee

Dr. Alberto Coronas Salcedo
Universitat Rovira i Virgili. Tarragona, Spain

Dr. Francisco Molés Ribera
Universitat Jaume I. Castelló de la Plana, Spain

Dr. Luis Carlos Mendoza Toledo
Ecole Polytechnique Fédérale de Lausanne. Neuchâtel, Switzerland

Dr. Gumersindo Jesús Verdú Martín
Universitat Politècnica de València, Spain

Dr. Rafael Miró Herrero
Universitat Politècnica de València, Spain

Castellón de la Plana (Spain), July 2017

ACKNOWLEDGMENTS

AGRADECIMIENTOS

Quisiera agradecer al director de la tesis, el Dr. Joaquín Navarro Esbrí, la oportunidad brindada y la confianza depositada en mí durante estos años. Gracias por esos consejos que me han permitido llegar hasta aquí.

A mis amigos y compañeros del grupo de investigación ISTENER, Fran, Adrián, y Ángel habéis sido un apoyo fundamental para la consecución de este trabajo. A Fran especialmente quiero reconocerle la ayuda que me ha prestado para que este proyecto salga adelante.

Hay buenos amigos que estoy seguro han marcado el carácter de esta tesis. Ivan Calvet, quiero agradecerte la fuerza que me has transmitido en cada uno de esos cafés. Sergio Balderrama, gracias por ese punto de vista siempre tan acertado. Y Miguel Manuel de Villena, no olvidaré la experiencia vivida a tu lado.

Por supuesto, no hay paciencia más grande que la de aquél que te quiere. Así que gracias a mi familia, Peris – Pérez – Górriz – Pellicer – Llobregat, Baena – Urueña.

Para mis padres, un ejemplo a seguir,
y para Mar, con quien seguir el ejemplo.

ABSTRACT

Nowadays, the environmental concern is leading researchers to focus on more sustainable energy systems. In this way, small-scale Organic Rankine Cycles (ORC) are receiving an increasing attention to produce electricity from low-grade heat sources.

Among the different applications for the ORC adoption, this study focuses on industrial processes. This application raises a great interest due to its high amount of waste heat recoverable, but lacks of in-depth experimental investigations on the topic.

Being aware of the economic feasibility relevance for the ORC adoption in practical applications, more cost-effective solutions are being explored in the literature through thermo-economic optimizations. However, the results achieved cannot be discussed with respect to actual projects implemented in industry, due to its absence.

In light of this, this thesis proposes as novelty to conduct the thermo-economic optimization from an experimental application in industry. In this manner, a comprehensive model of the system can be developed and validated from actual data. Accordingly, more realistic results can be reached to assess the economic feasibility of the optimized proposal under the different economic scenarios.

The main results obtained in this study show that, by means of a multivariable optimization using cost-effective indicators as objective function, a net electricity increase of 6.2% and specific investment cost reduction of the project of 19.1% with respect to the reference case are achieved. In other words, the optimization allows a mean discounted payback period reduction about 2 years under the best economic regime currently available in the industry addressed. The results extrapolation to other economic scenarios shows that the less advantageous is the scenario, the more significant is the improvement in the discounted payback period due to the optimization. In the most favorable scenario, discounted payback periods below 5 years could be achieved. In addition, the wealth and reliability of the project using the optimized system result more advantageous, being the optimization a guarantee to reach the best cost-effective solution for a new project.

RESUMEN

Actualmente, la preocupación por el medioambiente está guiando a los investigadores hacia el estudio de sistemas energéticos más sostenibles. En este sentido, los ciclos Rankine orgánicos (ORC por las siglas en inglés) de pequeña escala están recibiendo cada vez más atención para la producción de electricidad a partir de fuentes térmicas de baja temperatura.

De entre las diferentes aplicaciones para el uso del ORC, este trabajo se centra en los procesos industriales. Se trata de una aplicación que suscita un gran interés debido a su elevado potencial de calor residual recuperable, pero con escasa investigación experimental detallada sobre el tema.

Siendo conscientes de la relevancia de la viabilidad económica para la aplicación práctica de los sistemas ORC, en la literatura se está explorando soluciones más rentables a través de optimizaciones termo-económicas. Sin embargo, la discusión de los resultados alcanzados no puede hacerse con respecto a proyectos reales implementados en industria, dada su ausencia.

A la luz de esto, esta tesis propone como novedad llevar a cabo la optimización termo-económica a partir de una aplicación experimental en industria. De esta forma, un modelo íntegro del sistema puede desarrollarse y validarse a partir de datos reales. En consecuencia, pueden alcanzarse resultados más realistas con los que evaluar la viabilidad económica de la propuesta bajo los diferentes escenarios económicos.

Los principales resultados que se han obtenido en este trabajo muestran que por medio de una optimización multivariable, que utilice los indicadores oportunos como función objetivo, se consigue aumentar la producción de electricidad neta en un 6.2% y reducir el coste específico de la inversión del proyecto en un 19.1% con respecto al caso de referencia. O dicho de otro modo, la optimización permite reducir en 2 años el periodo descontado de retorno medio en el mejor régimen económico actualmente disponible en la industria analizada. La extensión de los resultados a otros escenarios económicos muestra que cuanto menos ventajoso sea el escenario, más importante es la mejora sobre el periodo descontado de retorno debida a la optimización. En el caso más favorable, se podrían conseguir periodos descontados de retorno por debajo de 5 años. Además, la riqueza y viabilidad del proyecto salen beneficiadas de la optimización, siento ésta una garantía para alcanzar la mejor solución en un proyecto nuevo.

CONTENTS

LIST OF FIGURES

LIST OF TABLES

NOMENCLATURE

Acronyms

ALT	Atmospheric Lifetime (yr)
BPHE	Brazed Plate Heat Exchanger
DPP	Discounted Payback Period (yr)
GWP	Global Warming Potential
HCFO	Hydrochlorofluoroolefin
HFC	Hydrofluorocarbon
HFO	Hydrofluoroolefins
HRVG	Heat recovery vapor generator (Eco + Eva)
IRR	Internal Rate of Return (%)
LCOE	Levelized Cost of Electricity (€/MWh)
LMTD	Logarithmic mean temperature difference (K)
NPV	Net present value (€)
NTU	Number of Transfer Units
ODP	Ozone Depletion Potential
ORC	Organic Rankine cycle
PI	Profitability Index
PID	Proportional-Integral-Derivative
SIC	Specific Investment Cost (€/kW)
SP	Single Phase
TP	Two Phase
USD	United States Dollar
WHR	Waste Heat Recovery

Nomenclature

A	Area (m^2)
A_c	Cross sectional area (m^2)
b	Pressing depth (m)
Bo	Boiling number (-)
C	Thermal capacitance (kW$\cdot$K^{-1})
	Constant coefficient (-)
	Cost (€)
c_p	Specific heat at constant pressure (kJ$\cdot$kg$^{-1}\cdot$K^{-1})
D	Diameter (m)
D_h	Hydraulic diameter (m)
E	Electrical energy (kWh)
Eco	Economizer
Eva	Evaporator
f	Friction factor (-)
F	LMTD correction factor (-)
Fc	Correction factor (-)
FpM	Fins per meter (-)
g	Gravitational acceleration (m$\cdot$s^{-2})
G	Mass flux (kg$\cdot$s$^{-1}\cdot$m^{-2})
Gr	Grashof
h	Enthalpy (kJ$\cdot$kg^{-1})
	Convection coefficient (kW$\cdot$m$^{-2}\cdot$K^{-1})

hr	Hour
k	Thermal conductivity (kW·m^{-1}·K^{-1})
K	Exponent coefficient (-)
L	Length (m)
L_M	Air inlet height (m)
$\dot{m}$	Mass flow rate (kg·s^{-1})
m	Fins efficiency coefficient
M	Number of a parameters (-)
	Mass (kg)
N	Number of a parameters (-)
Nu	Nusselt numbre (-)
P	Pressure (bar)
P_{un}	Unmixed ratio
Pr	Prandtl number (-)
Q	Thermal power (kW)
r	Radius (m)
	Ratio (-)
	Discount ratio
R	Thermal resistance (K·kW^{-1})
	Ratio (-)
R^2	Coefficient of determination (%)
Re	Reynolds number (-)
s	Entropy (kJ·Kg^{-1}·K^{-1})
S_D	Diagonal pitch (m)
S_L	Longitudinal pitch (m)
S_T	Transverse pitch (m)
t	Thickness (m)
	Number of time periods
	Tons unit
T	Temperature (ºC)
U	Uncertainty (%)
	Overall heat transfer coefficient (kW·m^{-2}·K^{-1})
v	Velocity (m·s^{-1})
$\dot{V}$	Volumetric flow rate (m^3·s^{-1})
V_r	Built-in volume ratio (-)
w	Width (m)
W	Electrical power (kW)
x	Independent variable
y	Prandtl exponent
	Dependent variable
yr	Year

Greek symbols

β	Chevron angle (º)
	Volumetric coefficient of thermal expansion (K^{-1})
Δ	Differential
ε	Effectiveness (-)
η	Efficiency (-)
μ	Dynamic viscosity (Pa·s)
ρ	Density (kg·m^{-3})
σ	Standard deviation
χ	Vapor dryness (-)
	Capacity ratio (-)
	Error
ψ	Fins efficiency coefficient(-)

Subscrits

c	Cold fluid
conv	Convection
cond	Conduction
	Condenser
e	Electrical
em	Electro-mechanical
eq	Equivalent
f	Friction
fl	Full load
g	Gross
h	Hot fluid
i	Input
	Individual variable
ise	Isentropic
l	Liquid saturated
lv	Between liquid and vapor
m	Mechanical
mom	Momentum
mx	Mixed fluid
o	Output
oil	Thermal oil
p	Pump
pl	Partial load
r	Ratio (-)
reg	Regenerator
s	Surface conditions
sat	Saturated
tp	Two-phase
v	Vapor saturated
	Volumetric
w	Fouling factor
wf	Working fluid
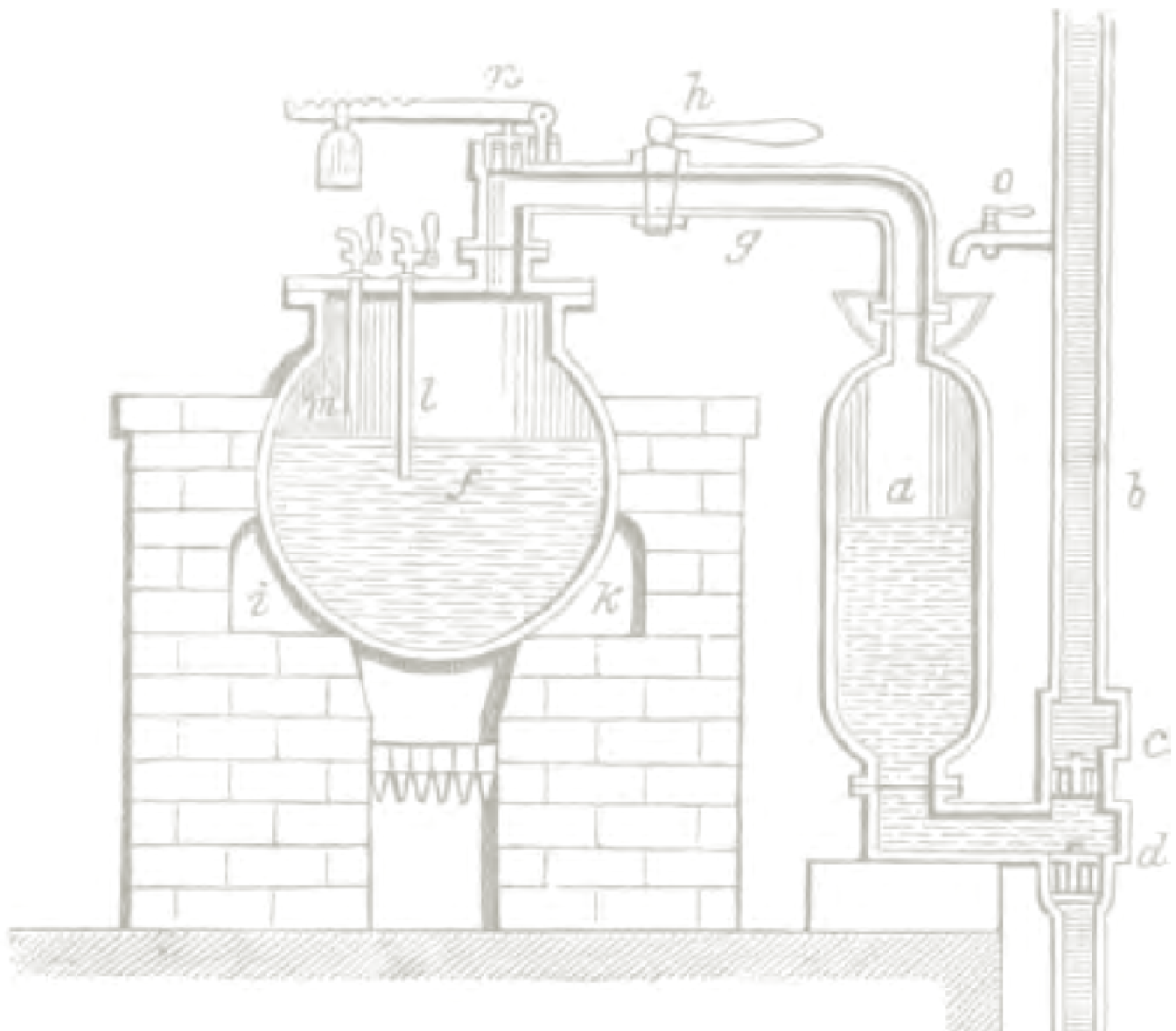
Introduction

Savery's Engine (1697).

1.   INTRODUCTION

W ORLDWIDE, the annual mean temperature is rising. To deal with this challenge, countries are committed to stabilizing atmospheric greenhouse gas concentrations. The proposed strategies are based on a sustainable growth by means of greener and more efficient energy systems.

This posture can also be seen in innovative investigations, with proposals such as the addressed in this doctoral thesis. In particular, this dissertation deals with the ORC (Organic Rankine Cycle), which is a system able to take advantage of low-grade waste heat to produce useful electricity.

To frame the investigation performed, this section goes from the historical context to the current status of the topic.

1.1.   Environmental issue

The ecological awareness emerged in the mid-twentieth century. First consequences of industrialization were revealed in the form of pollution, deforestation, resources depletion, and effects on humans [1].

To address this ecological concern, worldwide leaders were invited to the United Nations Conference on the Human Environment, held in Stockholm (Sweden) in 1972 [2]. For the first time, the environmental issue was considered as a global problem that required urgent actions [3].

Measures began with the adoption of the Geneva Convention on Long-Range Transboundary Air Pollution, signed in 1979 [4], and the agreement of the Vienna Convention for the Protection of the Ozone Layer, adopted in 1985 [5]. Meanwhile, the acid rain manifested its effects in Europe and North America [6].

The magnitude that the environmental issue was acquiring demanded a deeper understanding. For this reason, the IPCC (Intergovernmental Panel on Climate Change) was consolidated in 1988 [7]. In their first report, that contained investigations of 400 scientists, they provided evidence about the global warming and demanded the international community cooperation [8].

One year later, measures for the ozone layer protection were undertaken, through the entry into force of the Montreal Protocol and the Helsinki Declaration [9]. Moreover, the global warming issue was addressed in the UNCED (United Nations Conference on Environment and Development), held in Rio de Janeiro (Brazil) in 1992 [10]. From there, a new framework of international environmental treaties emerged, such as the stabilization of atmospheric GHG (Greenhouse Gases) concentrations caused by humans

and its regular monitoring through the meetings of the COP (Conference of the Parties) [11].

The first COP was held in Berlin (Germany) in 1995, establishing commitments among member countries. The agreement was reached in 1997 at the COP 3 of Kyoto (Japan), through a protocol for the reduction of GHG emissions by 5% in 2012 compared to 1990 levels [11]. After its entry into force, in 2007, there was a great milestone for negotiations and long-term objectives, the fourth IPCC report [12]. In this report, it was warned about the catastrophic consequences that would be unleashed by an increase of over 2 ºC in the average annual global temperature. Thus, such thermal limit was recognized as a common goal in 2009 at the COP 15 of Copenhagen (Denmark) and established the negotiations at the COP 18 of Doha (Qatar) for the Kyoto Protocol extension [13]. In 2015, the negotiations reached a horizon beyond 2020 at the COP 21 of Paris (France), with a legally binding global climate agreement approved by 195 countries [14].
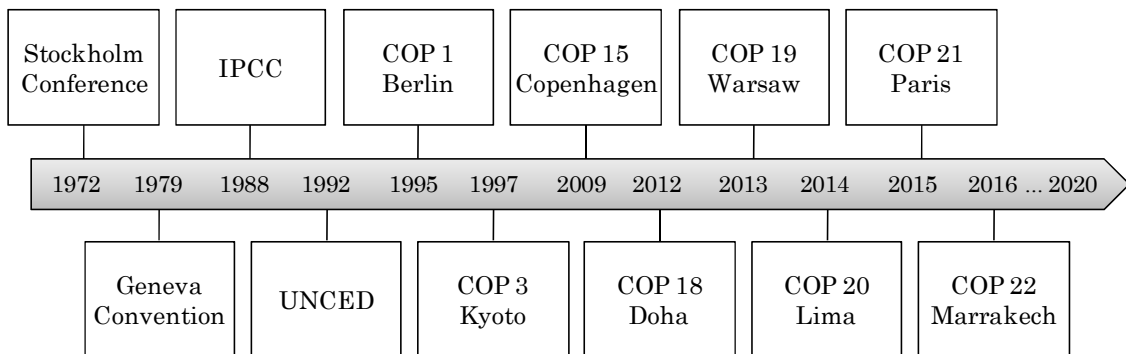
Fig. I.1. *United Nations Framework Conventions on Climate Change.*

As a result of these efforts, the European Union (EU-12) achieved the commitment established for the first period of the Kyoto Protocol. They accomplished a 12% reduction of emissions compared to pre-industrial levels. In recent years, the European Union (EU-28) is already close to the target of 20% reduction set for the second period of the Kyoto Protocol. Nevertheless, despite the progress achieved, it still remains far from the target of 40% established for 2030. According to forecasts, only a reduction of 22% can be reached in 2030 [15]. This means that the world is heading towards an increase in the annual mean temperature around 3.5 ºC [16], such as Fig. I.2 shows.

To prevent this rising trend, a sustainable growth is being promoted by institutions [17]. This fact, in turn, encourages researchers to focus on greener and more efficient energy systems [18].
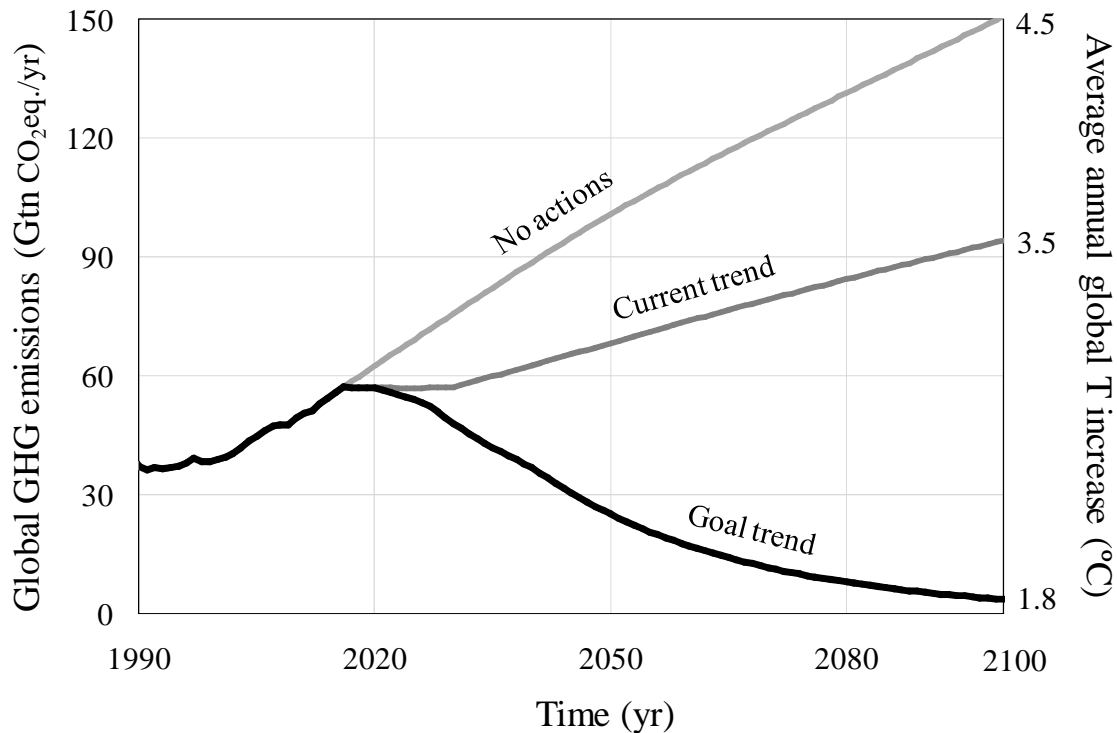
Fig. I.2. *Graphical summary of GHG emissions and annual temperature increase over time. (Source: Ref.* [19]*)*

1.2. From heat engines to the ORC development

In this section, the subject addressed in the investigation is presented. To do this, a brief historical overview is described, starting from the heat engines invention to the well-known steam Rankine cycle consolidation. The motivation that steered the ORC development and its evolution along the early years is described. Finally, the current status of the ORC is addressed.

1.2.1. Historical overview of heat engines

The earliest document mentioning a mechanism to produce work from heat dates from 130 BC and appeared reflected in the *Pneumatica* of the mathematician and engineer Hero of Alexandria. It was a primitive steam turbine known as *Aeolipile* [20].

A similar device was described in 1601 by Giovanni Battista della Porta. This scientific also included the possibility to take profit from the vacuum, which is caused by the steam condensation, to raise water and fill the vessel again. Shortly after, in 1615, the French engineer Solomon De Caus described an engine to propel a jet of water to a great height by using the steam pressure produced in the same vessel. A new innovation was proposed in 1663 by Edward Somerset, which consisted of the use of a separate boiler from the vessel that contained the water to propel.

The combination of these three innovations led to the first steam engine,

devised by Thomas Savery in 1697. It was a heat engine used to raise large quantities of water by means of the steam pressure produced in a separated boiler, but also that utilized the vacuum to elevate more water to the level of the engine. This heat engine was extensively used for draining mines and water distribution in small communities [21].

In 1705 Savery, Thomas Newcomen and John Cawley improved this engine by introducing a mechanism that consisted of a vertical cylinder and a piston, developed by Denis Papin in 1690. Thereby, the atmospheric engine for pumping mines was invented, which is shown in Fig. I.3.

After several adjustments in the atmospheric engine, John Smeaton started the series production. Though soon, he would be overcome by the innovations of James Watt. In 1763, this remarkable Scottish inventor realized about the enormous waste of energy that occurred in the cylinder during heating and cooling processes. Six years later, he patented an engine that surpassed their predecessors' ones.

The success was such that in 1802 William Symington used the steam engine to navigate the *Charlotte Dundas* tugboat. Subsequently, in 1807, Robert Fulton used it to sail a boat on the Hudson River. This heat engine reached such state of improvement that, in 1829, George Stephenson adapted it to a locomotive nicknamed *The Rocket* [20].

This evolution scenario did not develop driven by means of the theory, but rather by empiric advances. The first person who raised the key question was the engineer Nicolas Sadi Carnot in 1824. At a time when it was still accepted the theory that heat was a substance called caloric, Carnot argued that the ideal engine is the one that produces motive power without any "flow" of waste heat. Thus, he conceived a cyclic process in which only the thermal sources intervened, he demonstrated that it cannot be devised an engine more efficient than his and he consolidated the basis of modern thermodynamics [22].

During the decade between 1850 and 1860, and especially due to the endeavor of a group of scientists: William Thomson, Peter Guthrie Tait, Macquorn Rankine, James Clerk Maxwell, Rudolf Clausius and Fleeming Jenkin; it was formed the idea that heat, work, electricity, magnetism, and light became manifestations of the same concept, energy. Thereby, the statement of energy conservation played a unifying role of physical phenomena under concepts of transformation [23].

The unifying theories of energy were concentrated on the steam engine in 1859 by Rankine, in his famous piece *A Manual of the steam engine and*

other prime movers [21]. In this document, Rankine consolidated the word thermodynamics, established the terminology of first and second law, and suggested the possibility of a direct conversion between mechanical and electrical power with efficiencies close to the unit. For all these reasons, Rankine was recognized among the scientific community, who designated the thermodynamic cycle of steam engines as Rankine cycle.
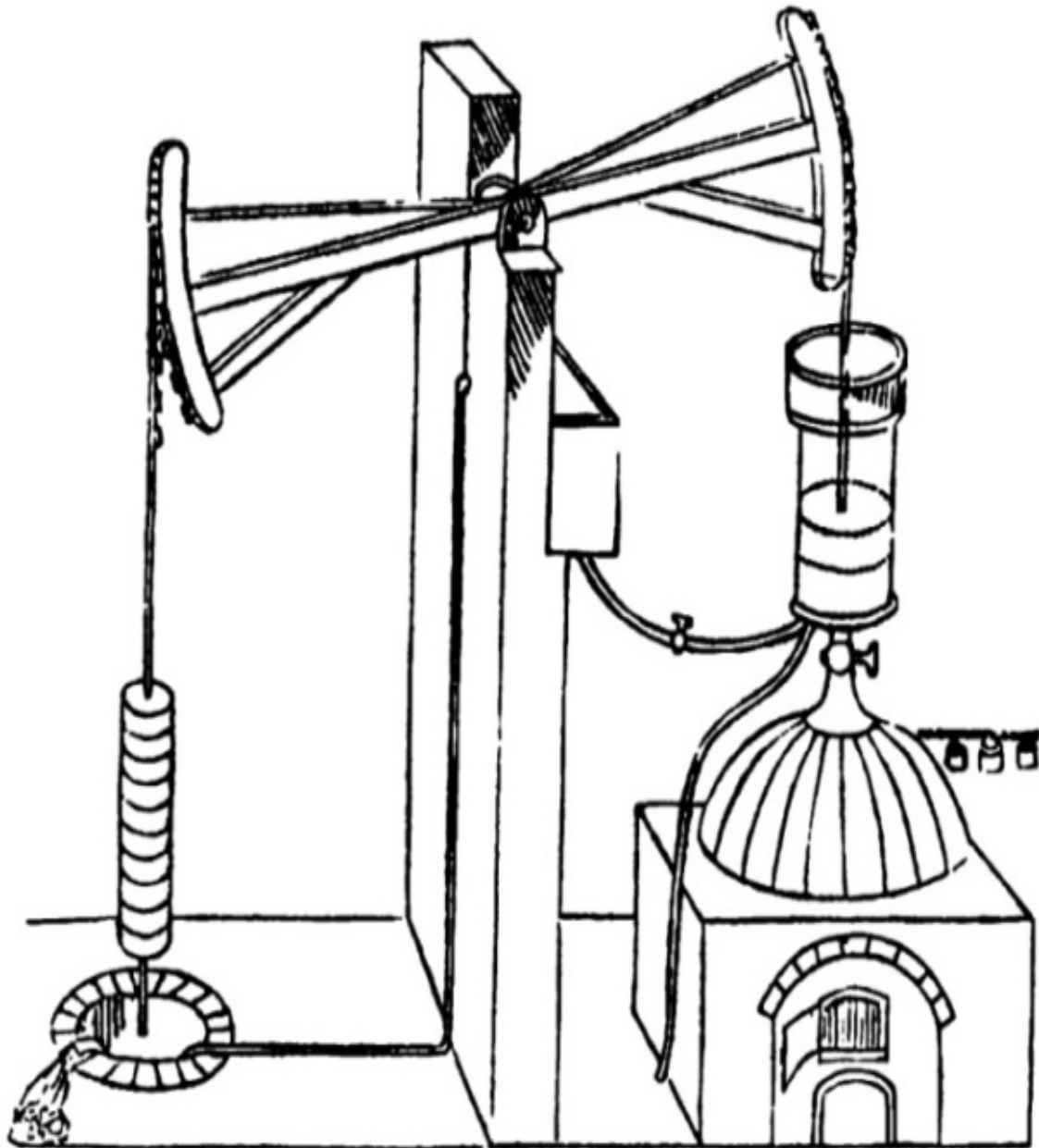
Fig. I.3. *Atmospheric Engine. (Source: Ref.* [21]*)*

1.2.2. ORC development

The idea of water replacement in steam engines was firstly implemented in 1826. Thomas Howard patented the concept of using alcohol or ether to improve the heat engines performance within similar operating conditions. Everything suggests that one of these systems, of 18 kW, was operating for a short period time in Rotherhithe (England) [24].

As soon as this improvement was known, its use was extended to naval applications. Around 1850, the French engineer Du Tremblay combined a steam engine with an ether engine in a binary system. The engine was installed in several ships, but its construction was interrupted in 1856 after an explosion in the harbor of Bahia (South America) [25]. In 1885, the US naval engineers commission published favorable results by using a mixture of water and methyl alcohol. However, they indicated that the high fluid cost and excessive leakages made the technology unfeasible.

At that time, several replacement options were considered to enhance the performance of the heat engines of the ships. The most popular were built by Frank W. Ofeldt from 1897, which used naphtha as working fluid [26].

As its own name suggests, the ORC refers to the use of organic working fluids. Nevertheless, inorganic fluids also received attention throughout history. Some examples are Campbell engines, which were patented in 1890 and that used a mixture ammonia-water as working fluid. Also Henry E. Willsie engines, which were built in 1904 to take advantage of solar thermal energy by using sulfur dioxide [24].

The pioneer who tested an ORC in a solar thermal source was Frank Shuman in 1907. This engineer used ether as working fluid, the source temperature was 120 ºC, and a mechanical power of 2.6 kW was produced. In the field of solar thermal energy conversion, the Italian Tito Romagnoli was able, in 1923, to produce a mechanical power of 1.5 kW using for that a heat source at only 55 ºC and methyl chloride as working fluid [27].

These continuous improvements led to new low-temperature applications and commercial developments. In 1952, the first commercial plant with an ORC in a geothermal source was installed. It was located in Kiabukwa (Republic of Congo) and produced 200 kW of electricity from hot water at 91 °C. The second oldest geothermal plant was installed on the Kamchatka Peninsula (Siberia) in 1967. The ORC was able to use water at 80 °C to produce an electrical power up to 670 kW and using Freon CFC-12 as working fluid [27]. The success achieved in the course of time would impulse commercial ORC systems to new low-temperature applications.

1.2.3. Current status of ORC systems

Nowadays, the ORC causes a great interest among the scientific community [28], being the main reason the possibilities that this system offers to contribute to a sustainable growth.

Before exploring these opportunities, a description of the ORC as it is currently known is necessary. To do this, their main components are illustrated in Fig. I.4, along with a generic thermodynamic cycle. Paying attention to the components, it can be seen that the ORC can be classified as an exothermic engine, since the heat is recovered from external sources through a HRVG (Heat Recovery Vapor Generator) [29]. In this HRVG, the pressurized organic working fluid is evaporated, feeding the expander with superheated vapor at high pressure. This vapor reduces its enthalpy during the expansion, causing the expander rotation and power production. Generally, the power output is turned into electricity through an electric generator, but it can also be directly used in a mechanical process [30]. Subsequently, the low-pressure vapor enters into the condenser. In this heat exchanger, the working fluid transfers the latent heat to a colder fluid, that can be later used for cogeneration applications or rejected to the ambient as a power only system [31]. Once the working fluid is in the liquid phase, it flows to the pump to be pressurized again and restart the thermodynamic cycle.
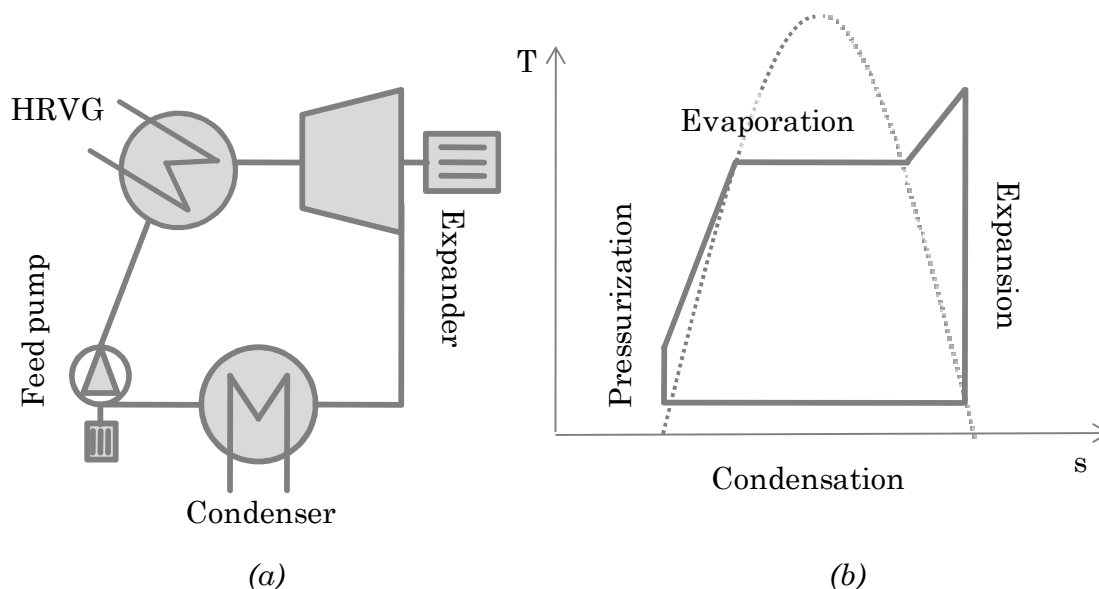
Fig. I.4. ORC generic scheme: (a) main components, (b) temperature-entropy diagram.

There are more types of heat engines capable of producing work from heat. Each one is indicated for specific operating conditions and, hence, suggested for certain applications.

In light of this, Fig. I.5 is presented to check the operating conditions in which the ORC is suggested. Different technologies of heat engines are shown, that are classified in function of their capacity and operating temperature range. Focusing on the ORC, the suitability for its application in low-temperature heat sources is confirmed. Such sources present a greater difficulty for the heat to work conversion than high-temperature heat sources [32]. Therefore, according to exergetic nomenclature, these sources are commonly known as low-grade or low-quality heat sources [33]. Despite this obstacle, in this type of heat sources is where the ORC has been proven as more adequate than other exothermic engines, like Stirling engine, closed Brayton cycle or externally fired gas turbine [27]. Among direct ORC competitors the Kalina cycle highlights, along with those emerged from modifications on them, like Goswami cycle, transcritical cycle or trilateral flash. Even though it was demonstrated that Kalina cycle reaches better efficiencies, the difference in performance shown experimentally with respect to the ORC was merely 3% [34]. In addition, the ORC is significantly less complex and needs a lower maintenance [35].
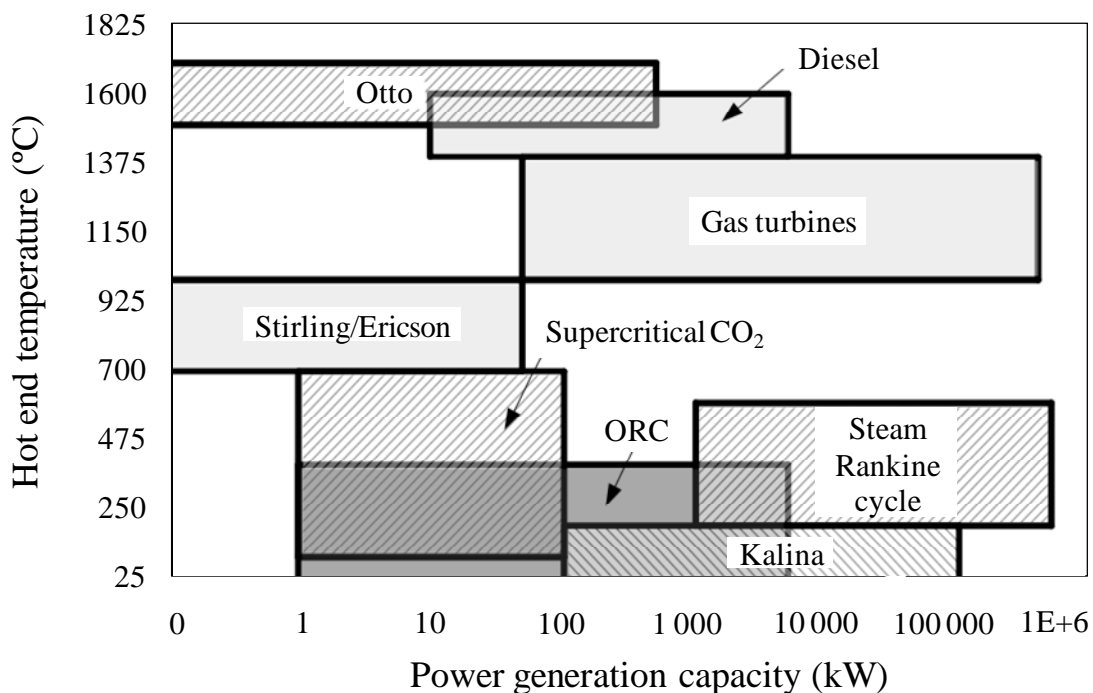
Fig. I.5. *Comparative chart of heat engines with applicable temperature range.*
(Source: Ref. [36]*)*

Besides heat engines, there are more systems that produce work from heat. Although they are still considered less mature technologies compared to ORC system [37].

Once presented the inherent condition of the ORC to recover low-grade heat from external sources, its scope can be focused. Nowadays, the ORC system is being widely studied to benefit from renewable and waste heat sources. For instance, geothermal [38], biomass [39], solar thermal [40], bottoming power cycles [41], industrial waste heat [42], oceanic [37] or other types of applications [43].

Some of the aforementioned heat sources raise a greater interest. The main reason is the available potential or development perspective that represent. In this topic focused Southon *et al.* [44], whose results are illustrated in Fig. I.6. As the researchers concluded, the geothermal application had the greatest growth over the years. On the other hand, the applications that have recently emerged and that represent an opportunity to take into consideration are WHR (Waste Heat Recovery), biomass and solar thermal.
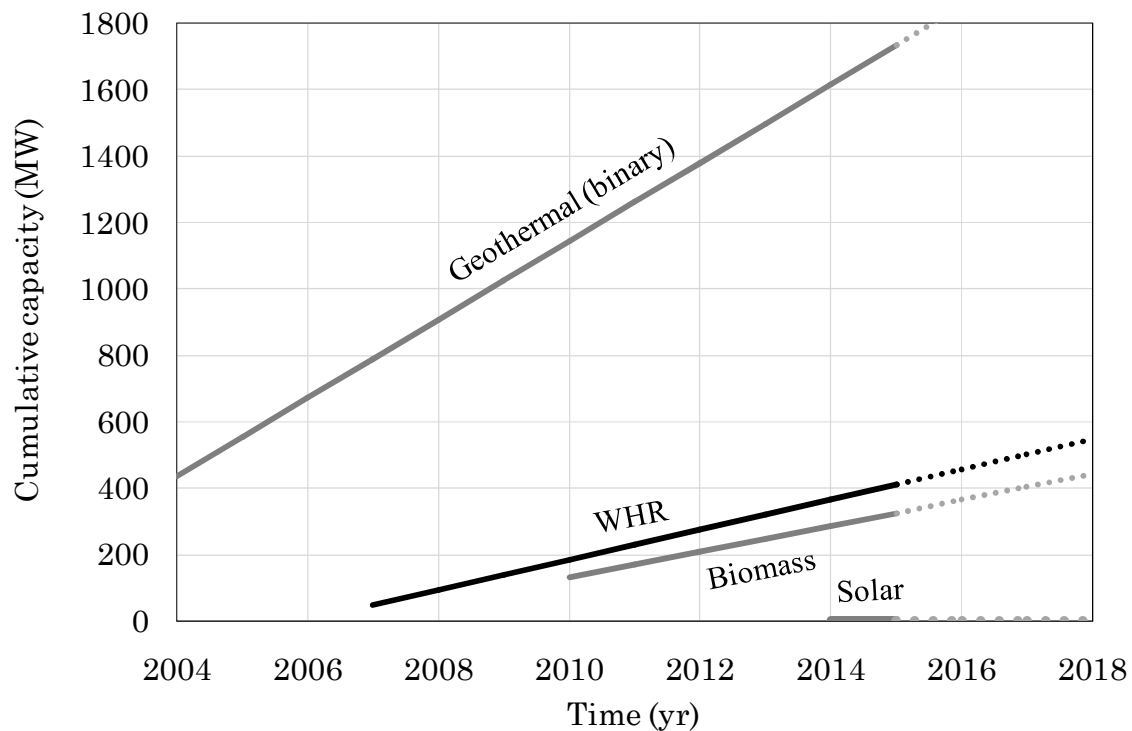
Fig. I.6. *Linear capacity growth trends for the ORC applications over time. (Source: Ref. [44])*

The ORC application for WHR and, in particular, for industrial processes has been proven as advantageous in literature. A study conducted in the European Union (EU-27) estimated that an electrical power of 2.7 GW could be produced annually, which would save 1,957 million euros and avoid 8.1 million tons emissions to the atmosphere [45]. It must also be noted that over 50% of industrial heat rejections are considered as low-grade waste heat, whose temperatures do not exceed 300-350 ºC [46]. A non-exhaustive

review of waste heat temperatures available in industrial processes is collected in Table I.1.

In most situations, the industries reject this low-grade heat due to its low thermal potential recoverable, which is insufficient to offset the transportation and reuse costs [47]. For this reason, the use of small-scale ORC systems, generally referred to systems that reach an electrical power up to 100 kW [48], is considered as an improvement that would contribute with significant energy, environmental and economic benefits.

Table I.1. *Temperatures of industrial gases.*

Industry	Process	Temperature (ºC)	Ref.
Cement	Kiln exhaust gases	200-350 / 300-450	[37]
	Kiln cooling gas	200-300	
Steel	Electric arc furnaces	250	[45]
	Rolling mills	300-450	
	Coke oven stack gas	190	[49]
	Blast furnace stoves	250-300	
	Finishing soaking pit	200-600 / 300-400	
Glass	Container glass melting	160-200 / 140-160	
	Flat glass	160-200 / 300-500	
	Fiberglass melting	140-160	
Chemical	Processing furnaces exhaust	340	
	Boiler exhaust	230	
	Refinery gases	150-300	[50]
	Gas turbines	370-540	[37]
Food	Fryers	120-212	[51]
	Exhaust gases	164	
Ceramic	Kiln exhaust gases	220	[52]
	Kiln cooling gas	200-300	[53]

The relevance of this application has not gone unnoticed. This fact can be seen in two clear upward trends. The first one is the exponential growth of investigations on the topic, which is depicted in Fig. I.7. The second one is appreciable in the commercial small-scale ORC systems increase in the market in recent years [54].
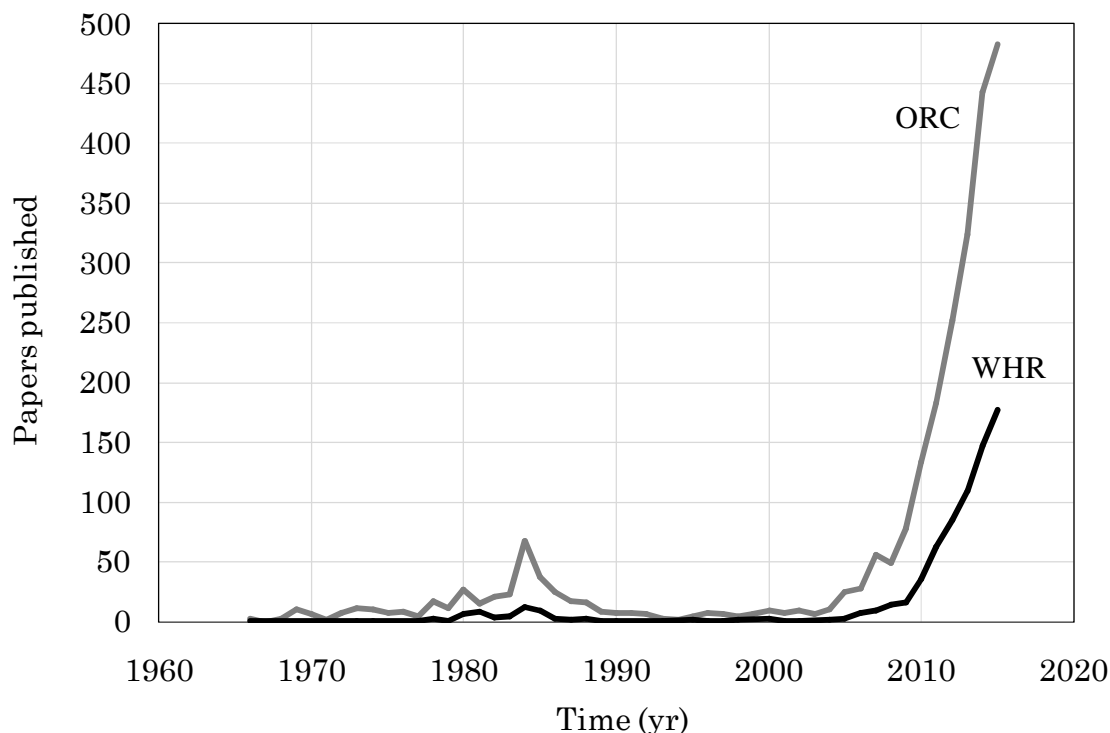
Fig. I.7. *Documents indexed in Scopus database. Screened from title, abstract and keywords. (Source: Ref.* [55]*)*

2. THEORETICAL GAP

From the introduction, it is noted the importance that acquires the investigation of small-scale ORC systems for low-grade waste heat recovery in industrial processes. Most of these investigations have a technical character, which is at the core of ORC development [56]. Nonetheless, the ORC adoption in practical applications does not merely depend on technical, but also the economic feasibility. For this reason, an increasing number of publications conduct thermo-economic (a combination of thermodynamic and economic) optimizations [57]. This method of analysis consists of the system optimization according to cost-effective indicators, instead of just using performance ratios as objective functions [58]. However, due to the lack of knowledge about experimental applications [59], the results achieved cannot be discussed with respect to actual projects installed in industries [60].

With this in mind, this dissertation proposes as a novelty to address the thermo-economic optimization from an experimental application in industry. In particular, it is used a project that was materialized in Spain thanks to a financial support program for business innovation [61]. The application consisted of the installation of a pre-competitive ORC prototype, of a rated electrical power of 20 kW, in a ceramic furnace to take advantage of the low-grade waste heat available in the exhaust air.

3.   OBJECTIVE

The objective of this thesis is to contribute to the adoption of small-scale ORC systems in industrial processes for low-grade WHR.

This general objective can be split into these particular ones:

- To address the experimental application, monitoring the facility and conducting tests to obtain actual data of operation.

- To develop a comprehensive model of the WHR system according to the requirements of a thermo-economic optimization.

- To calibrate and validate the model from actual data of operation.

- To use the model to conduct a thermo-economic optimization of the system.

- To assess the economic feasibility reachable with the optimized system under the different economic scenarios, and to compare it with respect to the reference case.

4.   METHODOLOGY

To accomplish these objectives, the investigation is conducted according to the following methodology.

Firstly, a review of state-of-the-art is conducted on the topic. The purpose is to refresh the technical characteristics of small-scale ORC systems, to identify the economic feasibility expected in industrial applications, and to establish the background of thermo-economic optimizations.

Secondly, the experimental tasks are carried out. The facility is monitored and a testing procedure is conducted to obtain actual data of operation.

Thirdly, a comprehensive model of the WHR system is developed according to the needs of the analysis. Specifically, the model should allow the performance simulation, cost correlations establishment and to address the thermo-economic optimization. For that, the equations that define the model are implemented in the software EES (Engineering Equation Solver) [62], along with its module to call properties from REFPROP [63].

Fourthly, the model is calibrated through performance ratios extracted from the analysis of operating data. Then, a simulation of these same data is used

to validate the results and to reveal the accuracy of the model.

Finally, a year of operation is simulated to establish the profitability of the reference case. Subsequently, the thermo-economic optimization is conducted, and the economic feasibility of the optimized proposal is assessed under the different economic scenarios.

5. SCOPE AND EXPECTED RESULTS

This study aims to contribute to the ORC adoption in practical applications. In this way, the investigation conducted is based on a specific experimental application. Thus, realistic results of the economic feasibility that could be reached through an optimized WHR system are expected. But also, it is expected to contribute with useful information extensible to other application cases, such as the extent of improvement that a thermo-economic optimization offers or which are the main topics to pay attention to achieve cost-effective solutions.

6. THESIS OUTLINE

The rest of the document is organized in accordance with the established methodology, as follows:

- Chapter II. A review of the state-of-the-art on the topic is conducted. In particular, the technology of small-scale systems, the economic feasibility reachable in industrial applications, and the background of thermo-economic optimizations are addressed.

- Chapter III. The experimental part of the thesis is conducted, which comprises the facility description, monitoring with metering devices, testing procedure carried out, and acquisition and treatment of the data.

- Chapter IV. The comprehensive model of the WHR system is developed from the geometric and thermodynamic description of the main components. Furthermore, cost correlations and profitability indicators are defined.

- Chapter V. The calibration and validation of the model is accomplished from actual data of operation. In this manner, the accuracy of the model is revealed.

- Chapter VI. The results of the thesis are discussed. For that, firstly, the economic feasibility of the reference case is analyzed. Secondly, a thermo-economic optimization is conducted to achieve the most cost-effective solution. And finally, the economic feasibility reachable through the optimized system is assessed under the different economic scenarios, as well as compared to the reference case.

- Chapter VII. The main conclusions that have been extracted throughout the chapters are summarized. Moreover, recommendations and future action lines are suggested.

The appendices collect relevant information to complement the document and allowing the reproducibility of results.
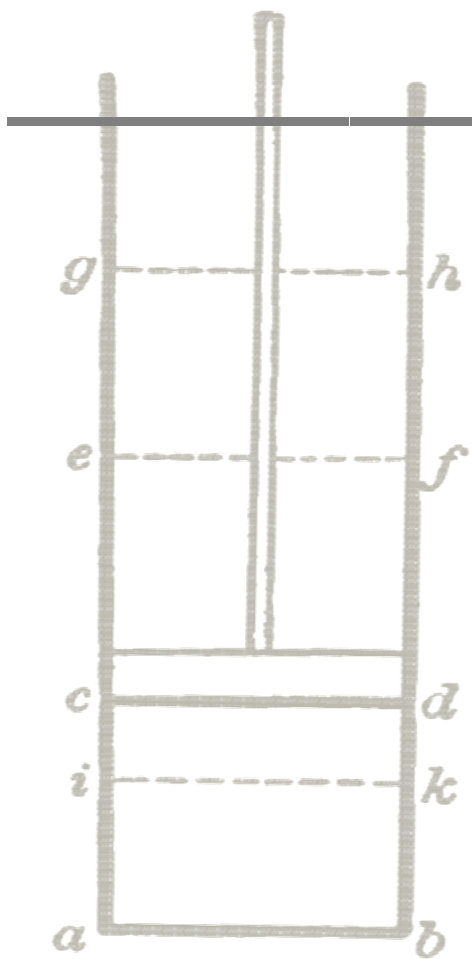
State of the Art

FIG. 1.

Cylindrical vessel and piston used by N.L.S. Carnot to reflect on the Motive Power of Heat (1824).

1. INTRODUCTION

This Chapter reviews the state of the art of ORC systems. In particular, the technology of small-scale systems, the economic feasibility reachable in industrial applications, and the background of thermo-economic optimizations are addressed below.

2. TECHNOLOGY

Technical studies are at the core of the ORC development. Numerous technological improvements are proposed in the literature to reach more efficient, reliable, and sustainable systems.

Taking this into account, a review of the current status of the technology used in small-scale ORC systems is presented.

2.1. Organic working fluid

The working fluid selection is one of the main topics that is continuously being investigated in the literature of small-scale ORC systems, since numerous possibilities are currently available in the market. For instance, Bao *et al.* [64] collected a list of almost 80 pure fluids that have been proposed for their use in ORC systems. In addition, it should be noted that numerous zeotropic mixtures are also recommended to improve the exergetic efficiency of ORC systems ([65], [66]), besides to achieve more cost-effective solutions [67].

Among the wide list of working fluids proposed, there is no a single best candidate. The main reason is due to the multiple requirements demanded, such as chemical stability, non-toxicity, non-flammability, good handling, compatibility with materials, low specific volume of vapor, moderate pressures, high latent heat, and low cost. In addition to several environmental features as a consequence of the growing ecological concern, such as a null ODP (Ozone Depletion Potential), low GWP (Global Warming Potential), and short ALT (Atmospheric Lifetime). Therefore, the investigations establish their own screening criteria in accordance with the characteristics of each application [68].

Focusing on pure fluids, Rahbar *et al.* [69] recently presented a summary of the most promising alternatives. This list is displayed in Fig. II.1 in function of operating temperatures, which are also related to the critical point of the fluids.

Fig. II.1. *List of the best fluids obtained from the literature survey and categorized based on heat source and critical temperatures. (Source: Ref.* [69]*)*

Nowadays, with the Kigali amendment approved, an effort to gradually phase down the usage of hydroflourocarbons (HFC) is being made [70]. With this in mind, different low GWP alternatives are currently being proposed to replace the hydrofluorocarbon HFC-245fa, which is the most popular working fluid among small-scale ORC manufacturers and that has a GWP of 858 [71].

In this way, Huck *et al.* [72] analyzed the fluids of Fig. II.2, and concluded that the hydrochlorofluoroolefins HCFO-1233zd(E) is a promising replacement alternative with a GWP of 1. Eyerer *et al.* [73] also proposed this fluid as drop-in replacement for HFC-245fa in existing ORC systems. The researchers pointed that, in addition to the advantage of the low GWP, a higher efficiency is reachable, but a slight reduction in electrical power occurs. Molés [74] also demonstrated experimentally that HCFO-1233zd(E) can be used as drop-in replacement for HFC-245fa, as well as the slight reduction in electrical power. Furthermore, the suitability of other low GWP candidates, such as the hydrofluoroolefins HFO-1234ze(Z) with a GWP of 1 and HFO-1336mzz(Z) with a GWP of 2, was theoretically assessed. Recently, Navarro-Esbrí *et al.* [75] experimentally confirmed the validity of the HFO-1336mzz(Z) as working fluid for ORC systems. Usman *et al.* [76] argued that also economically the HCFO-1233zd(E) has potential to replace the HFC-245fa if heat sources around 145 ºC are used. Petr *et al.* [77] underlined the suitability of the HFO-1234ze(Z) due to their similar thermophysical properties to the HFC-245fa. In the same way, Ziviani *et al.* [78] showed that HFO-1234ze(Z) achieves a slight increase in power output compared to HFC-245fa.
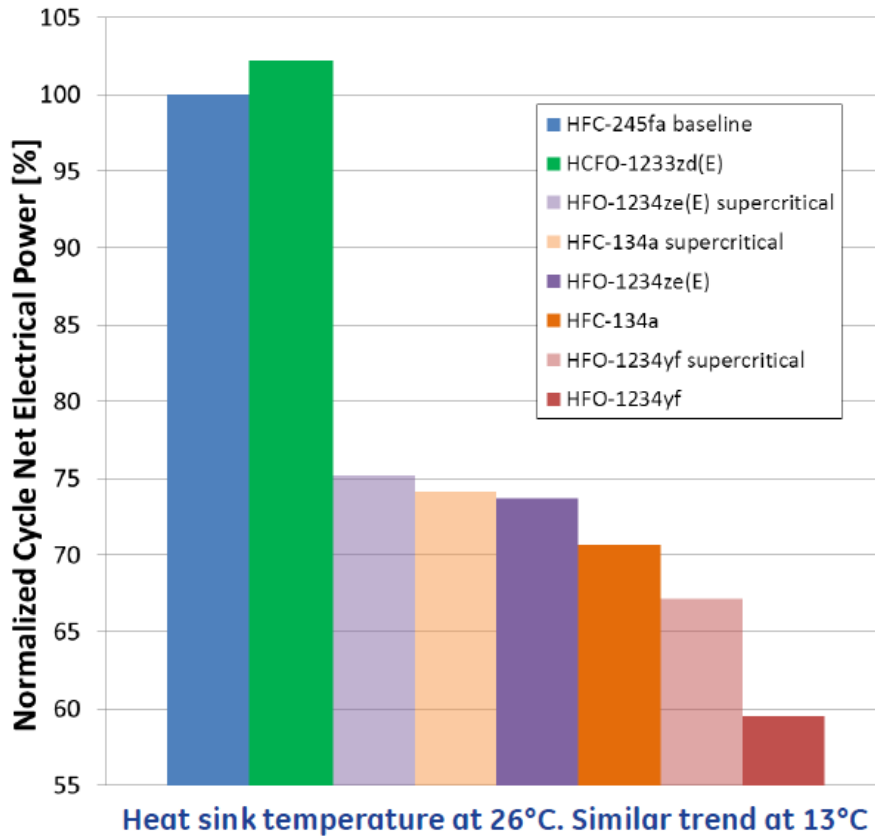
Fig. II.2. *Modeling results of ORC net power output in function of organic working fluid. (Source: Ref.* [72]*)*

2.2. Expander devices

The technology of expansion is one of the main topics experimentally investigated related to small-scale ORC systems, since it has been proven as a critical component to reach cost-effective solutions [64].
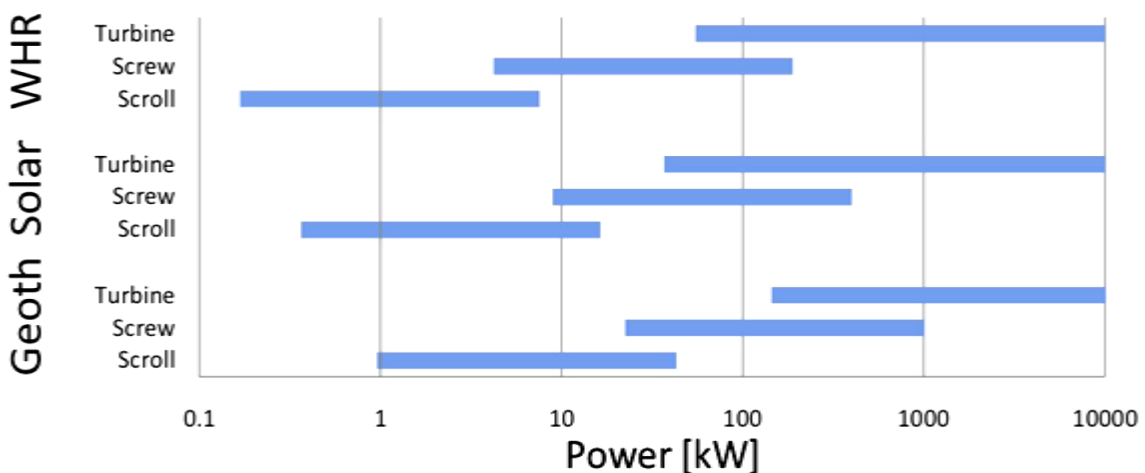
Fig. II.3. *Allowed power range for low-temperature applications and type of expansion machine. (Source: Ref.* [79]*)*

From a general point of view, volumetric (or positive displacement) machines are more appropriate than turbo-machines for micro and small-scale applications, such as Fig. II.3 shows. This is because volumetric machines are characterized by lower flow rates, higher pressure ratios, much lower rotational speed, besides to tolerate liquid phase during the process of expansion [80]. On the other hand, turbo-machines are a more compact alternative from electrical power outputs of 70 kW [81].

Focusing on the application range of volumetric machines, different technologies can be distinguished. In this way, Fig. II.4 establishes three categories according to the type of motion: orbital, rotary, and reciprocant [82]. Experimental investigations in each category can be found in the literature [69], which are addressed as follows.
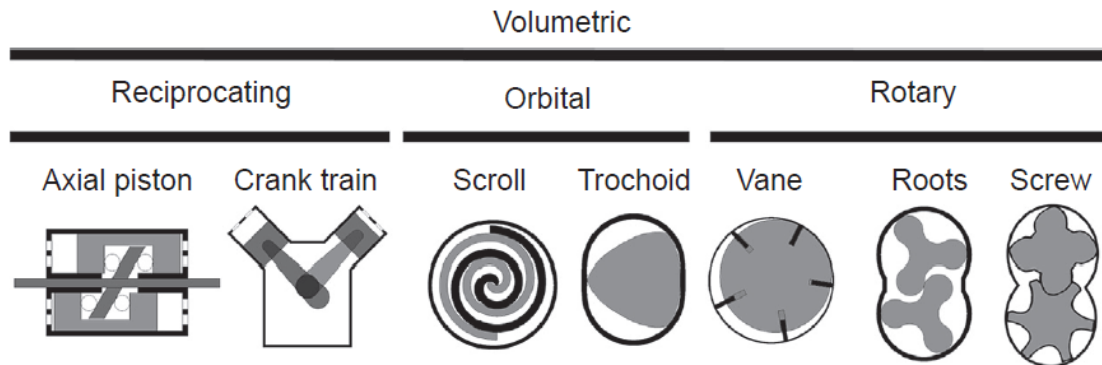
Fig. II.4. *Classification of positive displacement expanders according to the type of motion of the rotors. (Source: Ref.* [82]*)*

2.2.1. Orbital

Different types of orbital devices, *i.e.* scroll and trochoid, have been tested as expanders for micro-scale ORC systems (<10 kW) [32]. In particular, scroll devices have received a remarkable attention, since cost-effective solutions have been achieved through the reverse operation of commercial compressors [83]. In this way, three types of devices can be seen in Fig. II.5. Specifically, hermetic refrigeration compressors, automotive air conditioning compressors, and open drive air compressors can be distinguished. All of them operate as expander with the principle shown in Fig, II.6, which consists of the working fluid expansion by the volume increase between the two wraps.
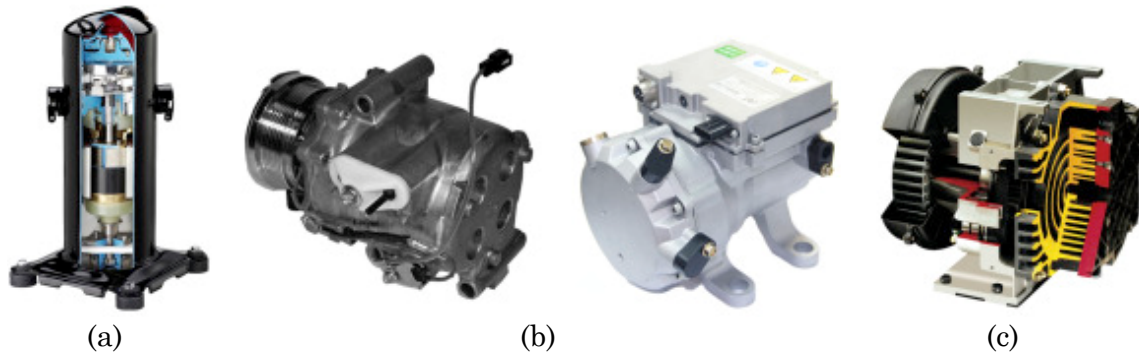
Fig. II.5. *Types of scroll compressors: (a) hermetic refrigeration, (b) automotive air-conditioning, (c) open drive air. (Source: Ref.* [83]*)*

First Vapour Pocket   Two intermediate Vapour Pockets   Final Vapour Pocket
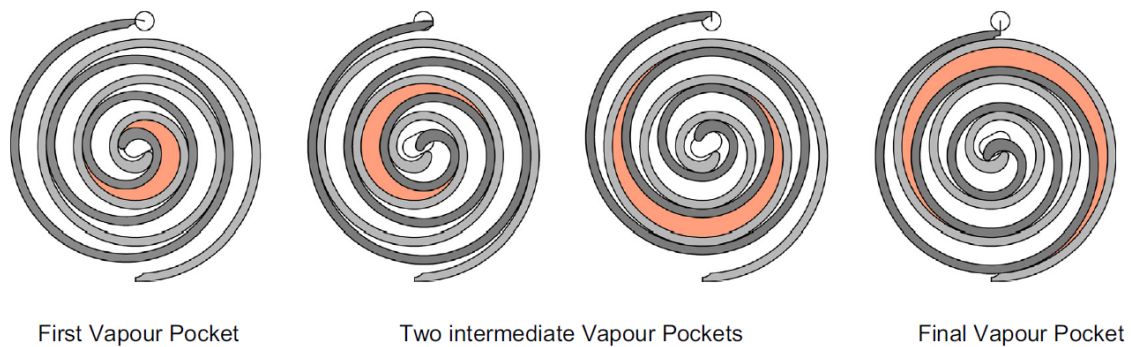
Fig. II.6. *Displacement process of the scroll expander. (Source: Ref.* [84]*)*

Different experimental investigations can be found in the literature for each type of scroll device. Thus, Kosmadakis *et al.* [85] tested a converted hermetic scroll expander in a 3 kW ORC prototype, which can be seen in Fig. II.7. The working fluid used was HFC-404A, and an electrical efficiency of almost 6% in subcritical conditions was reached. The researchers also pointed that supercritical conditions did not show a superior performance.

Miao *et al.* [86] tested the ORC of Fig. II.8, which used as expander the scroll compressor of a bus air conditioning system. The working fluid selected was HCFC-123, and a maximum shaft power of 2.63 kW was obtained. Moreover, a comprehensive model of the system was developed from sub-models of the components, demonstrating that a thermodynamic optimization could lead the system to double the electrical power output.

Similarly, Yang *et al.* [87] tested an ORC based on a scroll expander modified from a commercial air compressor, which can be seen in Fig. II.9. The organic working fluid used was HFC-245fa. Thereby, the prototype showed that a shaft power output of 2.64 kW and maximum net electrical efficiency of 3.93% can be reached with a constant heat source temperature of 100 ºC.

(a)   (b)
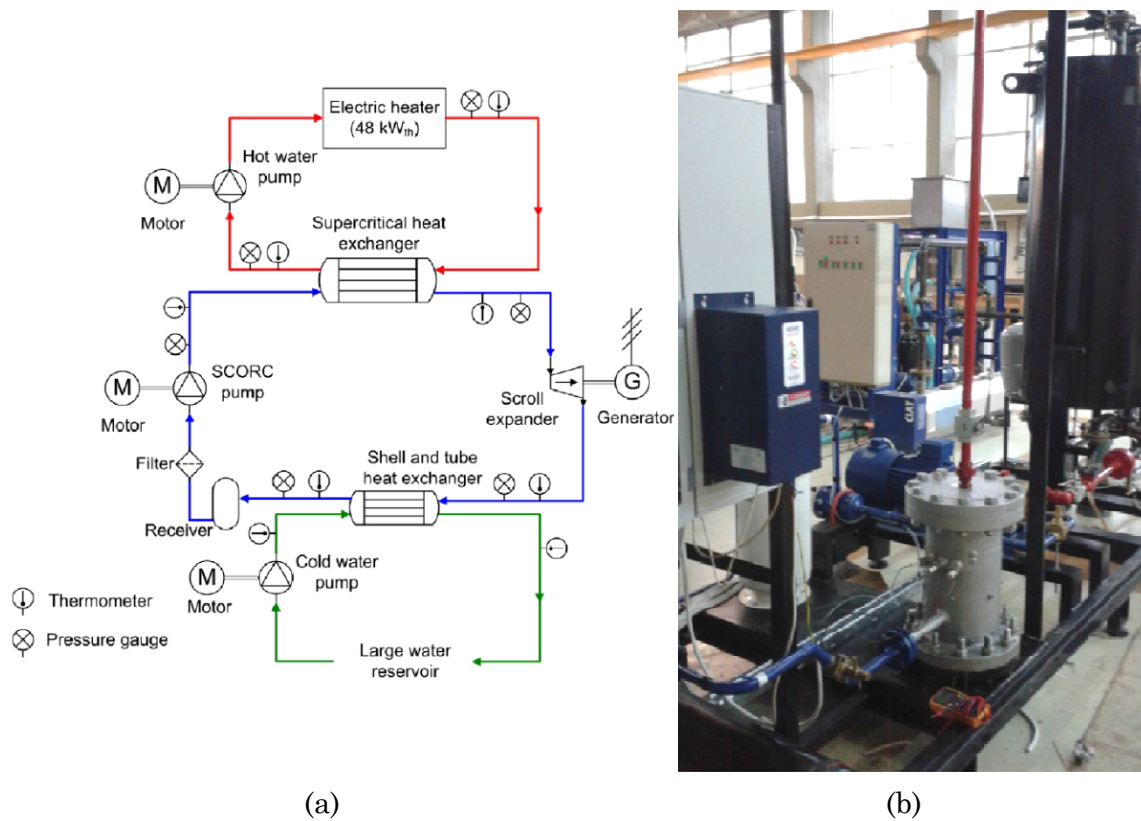
Fig. II.7. *ORC setup: (a) basic architecture, (b) view of the prototype in the test bench. (Source: Ref. [85])*
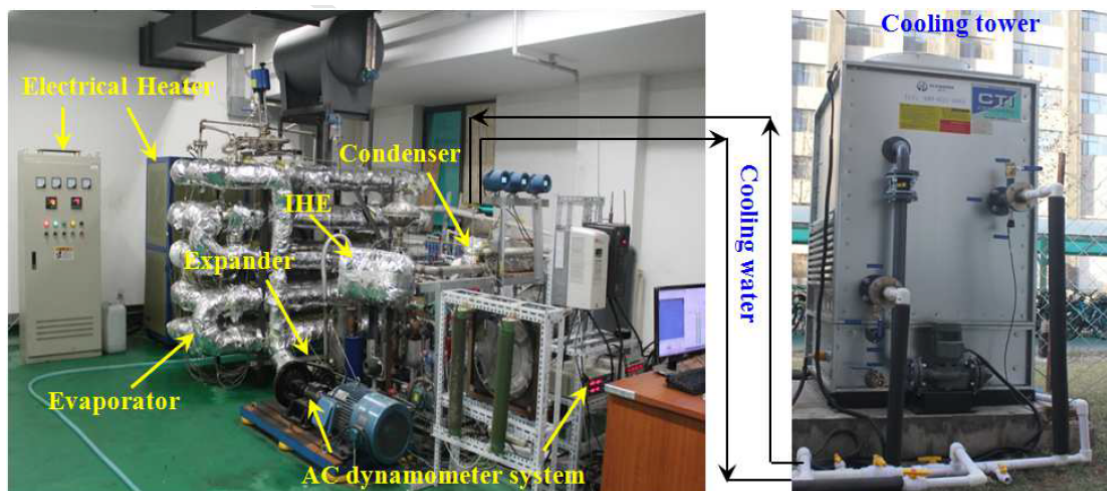
Fig. II.8. *Photos of the experimental setup. (Source: Ref. [86])*
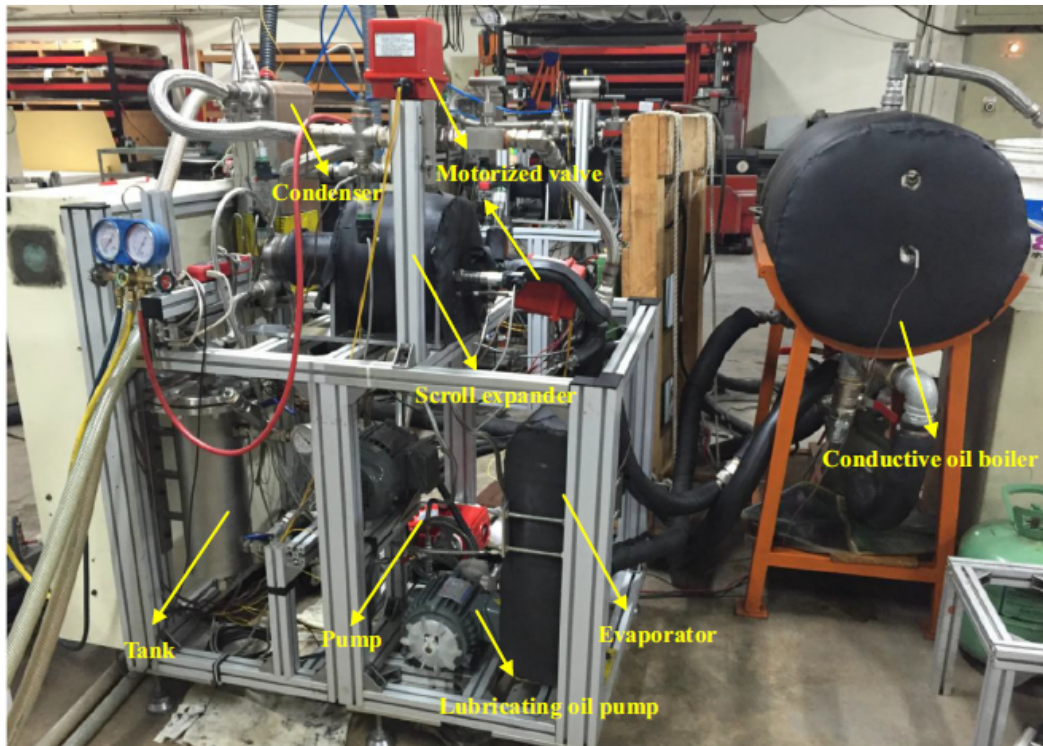
Fig. II.9. *Photos of experimental setup. (Source: Ref.* [87]*)*

2.2.2. Rotary

Rotary technology has also been extensively investigated to be used in micro and small-scale applications. For instance, Kolasiński *et al.* [88] proposed the use of vane and lobe expanders as suitable rotary alternatives to scroll machines in micro-scale applications. With regard to the range of small-scale systems, the twin-screw expander was pointed in the literature as the best candidate [89]. Its operating principle can be explained as follows. The fluid enters the casing through the inlet port at the top of the rotors, in flutes formed between the lobes, until the rotation cuts off their access (Fig. II.10.a). The expansion proceeds by a further rotation until the whole helical length is filled with the fluid (Fg. II.10.b). Finally, the rotation continues until the discharge process starts and the vapor leaves through the outlet port (Fig. II.10.c). An example of this process in function of volume and port area change is illustrated in Fig. II.11 [90]. The abscissa value set to zero corresponds to the cut-off of the expander. This position determines the machine built-in volume ratio (V_r), which is a determinant parameter of the expander performance.

In this way, Hsu *et al.* [91] experimentally investigated the performance of a 50 kW ORC using a twin-screw expander and HFC-245fa as working fluid, which can be seen in Fig. II.12. Their results showed a maximum expander isentropic efficiency of 72.4% and a cycle efficiency of 10.5%.

(a)   (b)   (c)
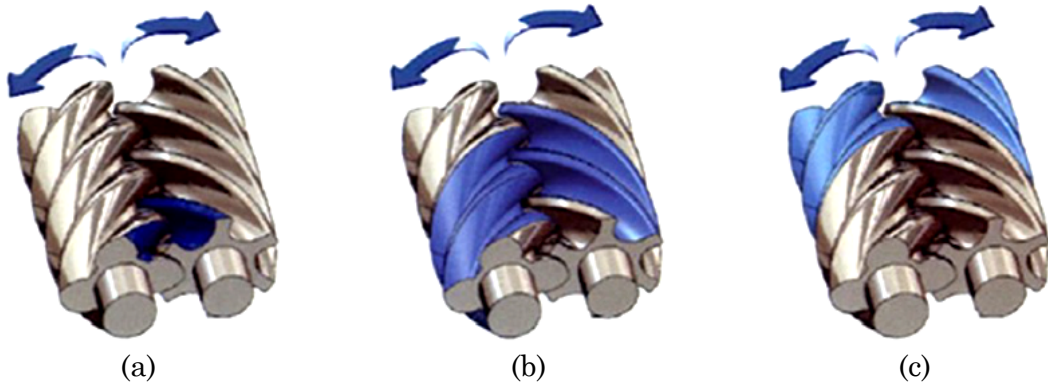
Fig. II.10. *Expansion process of twin-screw machine. (Source: Ref.* [92]*)*
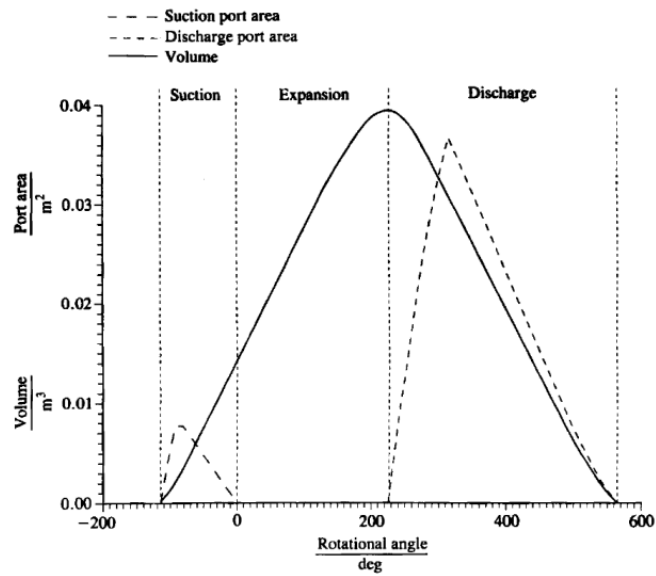
Fig. II.11. *Example of expansion sequence of a twin-screw expander. (Source: Ref.* [90]*)*

(a)   (b)
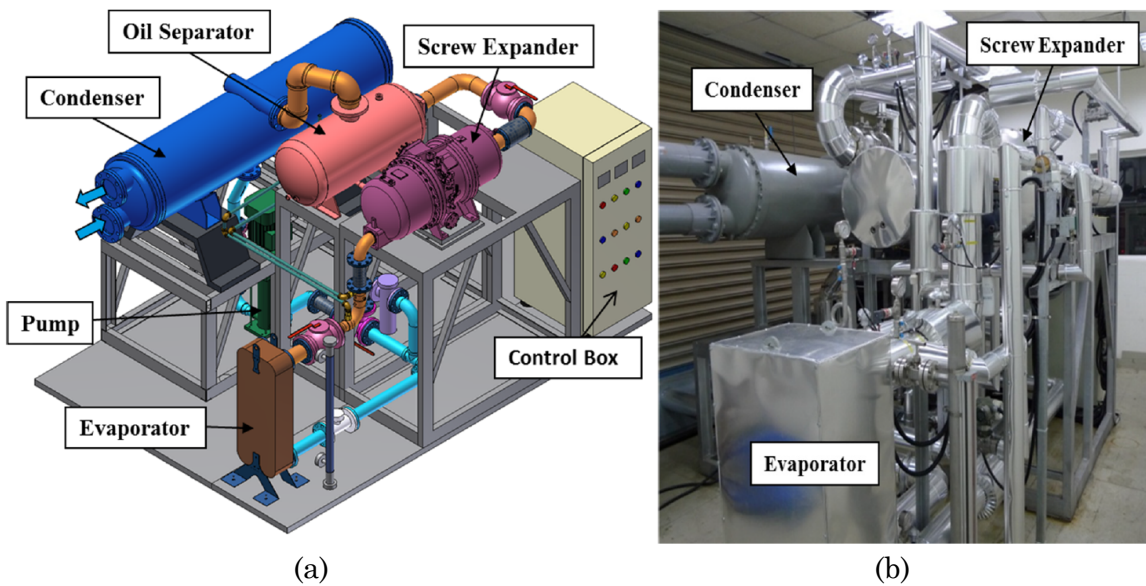
Fig. II.12. *50 kW ORC system with twin-screw expander: (a) three-dimensional layout, (b) photo of the unit. (Source: Ref.* [91]*)*

Besides twin-screw devices, single-screw machines have also been proposed as a suitable rotary technology for small-scale applications. In this way, Desideri *et al.* [93] tested an 11 kW ORC unit, shown in Fig. II.13, that used a single screw expander obtained by modifying a compressor. Two different organic working fluids were tested, SES36 and HFC-245fa. Thus, a maximum expander isentropic efficiency of 60% was reached using SES36, and a value of 52% using HFC-245fa.
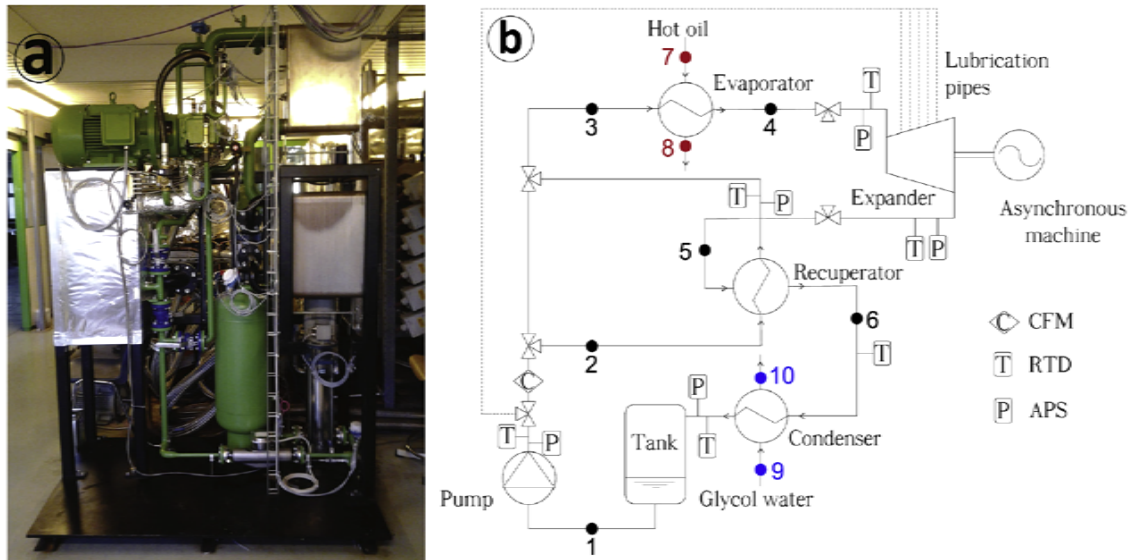
Fig. II.13. *11 kW ORC system with single screw expander: (a) front view of ORC test ring, (b) process flow diagram. (Source: Ref.* [93]*)*

2.2.3. Reciprocant

Piston devices have been proven as an efficient technology for micro-scale application in which the expansion process requires a high pressure ratio [94]. The main reason was underlined by Lemort *et al.* [95], which is due to the larger built-in volume ratios that can reach, typically between 6 and 14. For comparisons, scroll machines exhibit values from 1.5 to around 4, and screw machines typically reach maximum values about 5.

Taking this into account, Oudkerk *et al.* [96] conducted an experimental study of a piston expander in a small-scale ORC. The working fluid used was HFC-245fa. Thereby, the results showed a maximum expander isentropic efficiency of 53%. Moreover, a semi-empirical simulation model was proposed and calibrated to be used in the analysis of different heat sources.

2.3.   Cycle and architecture

Different typologies of ORC systems have been investigated to improve their performance. One of the most commonly used is the regenerative architecture, which can be performed in three ways: with an internal heat exchanger (IHE) [40], with open and closed feed fluid heaters using turbine bleeding [97], or using a vapor injector as a regenerator [98]. Among these, the architecture with IHE is widely recommended for small-scale ORC systems. This is due to the type of organic working fluid used, which typically have a dry or isentropic slope of the vapor saturated line, such as Fig. II.14 shows. This architecture allows the reuse of the heat that leaves from the expander to preheat the liquid that leaves from the pump. Nonetheless, despite this typology improves the cycle efficiency, it is not always recommended to enhance the power output [58].

| (a) | (b) | (c) |
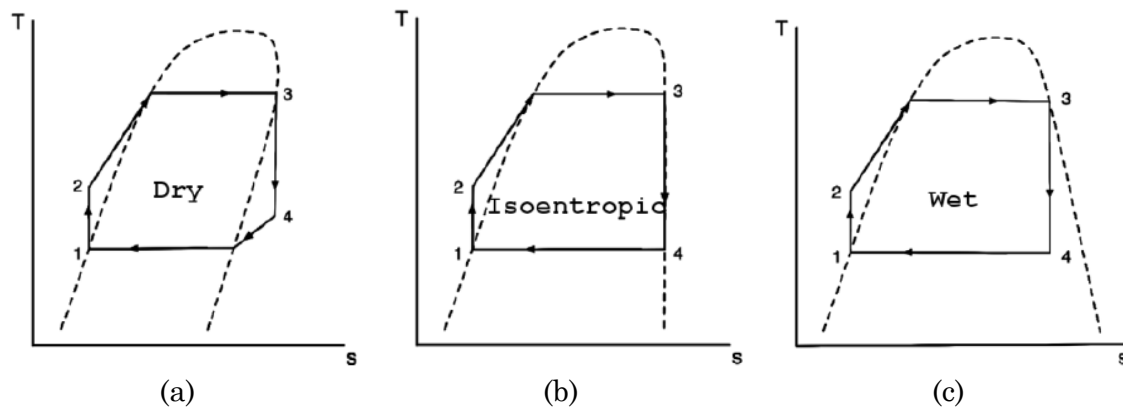
Fig. II.14. *Shape of saturated vapor line of dry, isentropic, and wet fluids. (Source: Ref. [99])*

Lecompte *et al.* [100] argued that despite the basic architecture is gradually being adopted, the need to achieve more cost-effective systems leads to the use of better architectures. Thus, a revision of different cycles was conducted. In particular, transcritical cycle, trilateral cycle, the usage of zeotropic mixtures, cycle with multiple evaporation pressures, flash cycle, regenerative with IHE, regenerative with turbine bleeding, with vapor injector, cascade cycles, and with reheaters. In conclusion, researchers pointed that in spite of the promising improvement reachable in performance, it is not clear that these typologies represent economically viable solutions. Additionally, Lecompte *et al.* [101] conducted a thermo-economic optimization of different ORC architecture applied to a case of study in industry. The researchers concluded that transcritical cycles are less cost-effective compared to subcritical systems.

Similarly, the analysis of the different architectures shown in Fig. II.15 was conducted by Peris *et al.* [56]. We concluded that all options increase the efficiency compared to the basic ORC. However, it was also observed that small improvements on the cycle allow similar gains compared to the most complex schemes proposed, being the regenerative (with IHE) the recommended typology.
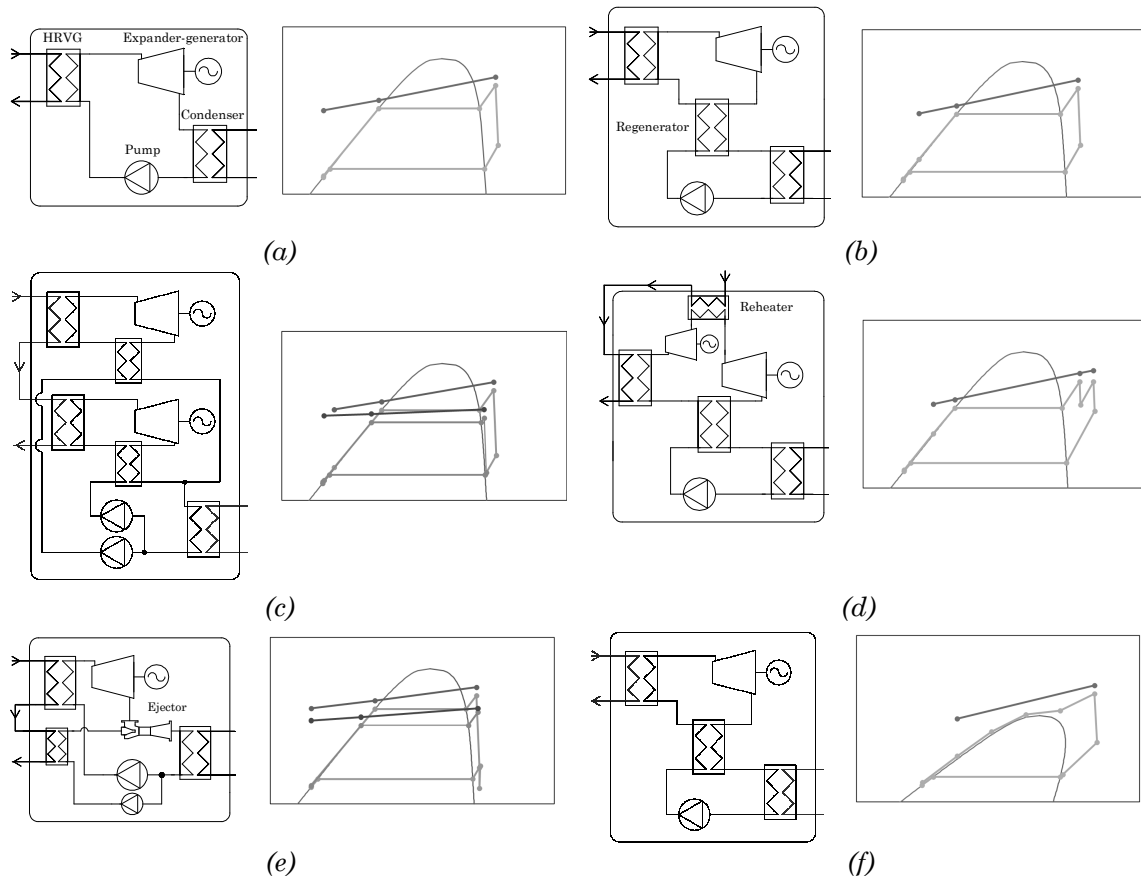
***Fig. II.15**. ORC architectures and thermodynamic cycles in temperature-entropy diagram: (a) basic, (b) regenerative with internal heat exchanger, (c) double regenerative, (d) reheat regenerative, (e) ejector, (f) transcritical regenerative. (Source: Ref. [56])*

For more information, an extensive review of different architectures in function of expansion technology, working fluid, and type of application can be seen in the study performed by B. Obi [102].

2.4.   Other relevant topics

In summary of the review previously conducted, the main topics addressed in the literature about the technology of small-scale ORC systems refer to working fluids, expansion technologies, and system architectures. However, there are other relevant topics addressed in a lesser extent.

For instance, the feed pump is a component that also plays a key role in the cycle. Thus, Bianchi *et al.* [103] tested an ORC prototype based on sliding vane rotary technology. The researchers focused the study on the feed pump, analyzing the energy losses occurred and pointing that electrical efficiencies obtained were below 50%, such as Fig. II.16 shows. Similarly, Landelle *et al.* [104] investigated a reciprocating pump driven by an induction motor with variable speed drive. The maximum pump efficiency achieved was 82%. However, a global efficiency (pump & drive) of 41% was observed. In the same magnitude order of efficiencies are the values reported by Quoilin [105], which are displayed in Fig. II.17 in function of pump technology: diaphragm, plunger, piston, and gear.

(a)   (b)
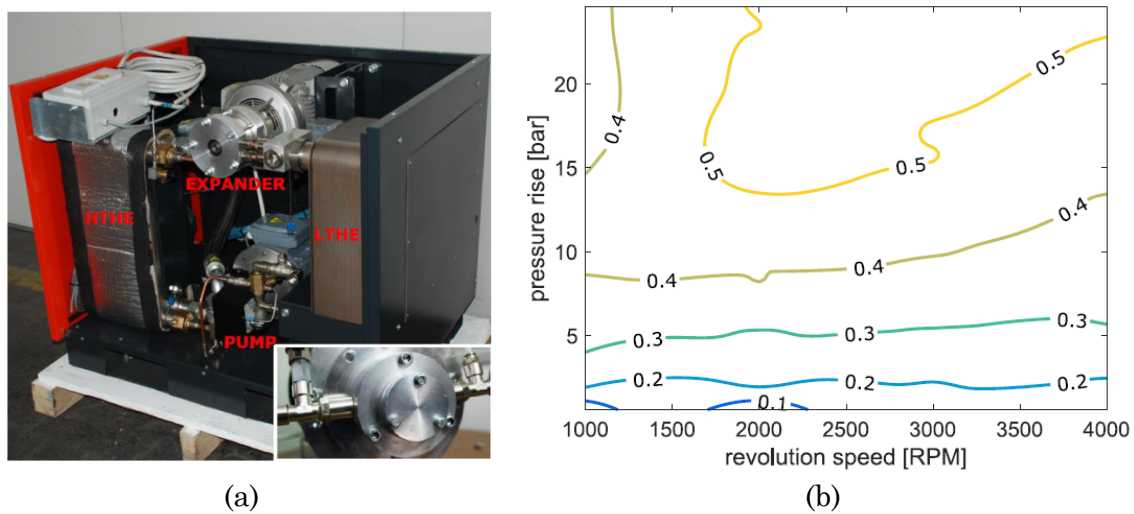
Fig. II.16. *Sliding vane rotary technology: (a) ORC prototype and pump view (bottom right), (b) total efficiency map of the pump. (Source: Ref. [103])*
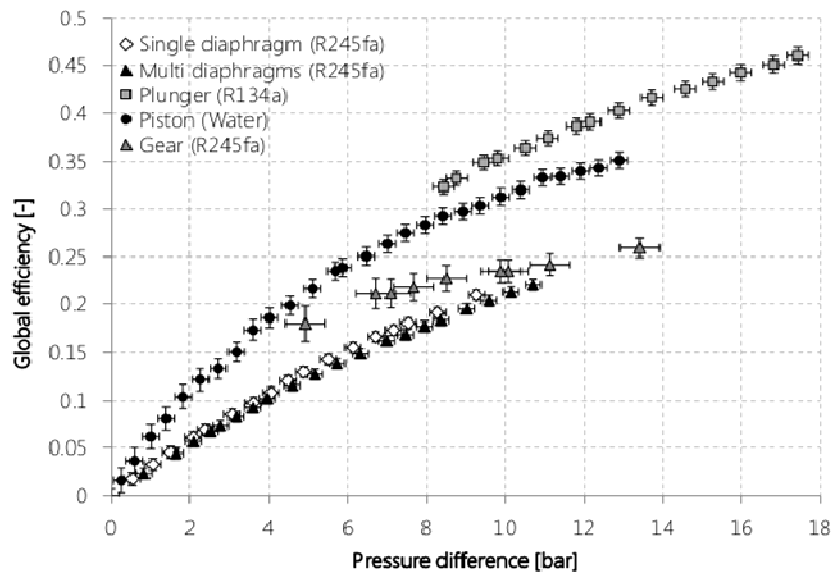
Fig. II.17. *Global efficiency of feed pumps in function of type of technology, working fluid and operating conditions. (Source: Ref. [105])*

Heat exchangers have also received attention to contribute to achieving more cost-effective solutions. In this way, Lazova *et al.* [106] proposed an innovative helical coil heat exchanger for supercritical ORC systems that improved the heat transfer coefficient and, hence, the cycle efficiency. Hossain and Bari [12] adapted a commercial shell-and-tube heat exchanger to recover waste heat from exhaust gases and they concluded about its suitability for the use in ORC systems. Hu *et al.* [107] argued that heat exchangers require not only being designed to improve thermal efficiency, but also to save charge of working fluid. Therefore, the researchers investigated heat transfers with the fluid HFC-245fa in a brazed plate heat exchanger as evaporator. A comparison of different ORC configurations using both plate and sell-and-tube heat exchangers was conducted by Walraven *et al.* [108]. As a main conclusion, it was observed that an ORC with all plate heat exchangers performs better than an ORC with all shell-and-tube heat exchangers. Zhang *et al.* [109] used a thermo-economic model to compare different heat exchanger configurations, and concluded that finned tube bundles with circular fins as evaporator and a shell-and-tube heat exchanger as condenser is the most cost-effective solution.

Control strategies are also investigated in the literature. Generally, the superheating is controlled to maximize efficiency, as well as to avoid the liquid droplet at the inlet of the expander [110]. In this topic focused Hernandez *et al.* [111], who proposed a multivariable predictive control strategy. This proposal demonstrated similar performance compared to conventional control strategies based on PID (Proportional, Integral, and Derivative) when stable heat sources are used, but a significant improvement of net power output in the case of unsteady thermal energy sources. Li *et al.* [112] not only conducted the control over the superheating of the expander, but also the fans of the cooling tower that allowed to regulate condensing conditions. The researchers concluded that to improve the efficiency and to maintain a safe operation, superheating degree and condensing conditions require being maintained as low as possible.

2.5. Commercial systems

A non-exhaustive review of small-scale ORC suppliers has been conducted. The results are listed in Table II.1, which includes the electrical power capacity of ORC units, organic working fluids used, and expansion technologies adopted. As can be seen, the working fluid HFC-245fa is the most popular among the reviewed ORC suppliers. It also highlights that some companies already include new generation working fluids with low GWP. Regarding expansion machines, different technologies can be appreciated, being radial turbines the most repeated.

Table II.1. Non-exhaustive list of ORC suppliers.

Manufacturer	Capacity (kW)	Organic fluid	Expander	Ref.
Clear Power (USA)	77	HFC-245fa	Scroll	[113]
ElectraTherm (USA)	35 – 110	HFC-245fa	Twin screw	[114]
Enertime (FR)	>100	HFC, Low-GWP	Axial turbine	[115]
Enogia (IT)	5 – 100	HFC-245fa, Low-GWP	Radial turbine	[116]
E-rational (BEL)	<500	HFC-245fa, SES36	Single screw	[117]
GE clean energy (USA)	125	HFC-245fa	Radial turbine	[118]
Icenova (IT)	10 – 30	HFC-245fa	Scroll	[81]
Infinity Turbine (USA)	5 –100	HFC-245fa, HFC-134a	Radial turbine	[119]
Rank (SP)	1 – 100	HFC-245fa, Low-GWP	Twin screw, other	[54]
Triogen (NLD)	100 – 170	Toluene	Radial turbine	[120]
Zuccato Energy (IT)	30 – 300	HFC	Radial turbine	[121]

3. ECONOMIC FEASIBILITY

Being aware of the economic feasibility relevance for the ORC adoption in practical applications, a review of the profitability of the projects is conducted.

For that, firstly, the different economic regimes that frame industrial projects are analyzed. Then, the profitability reported in the literature is reviewed.

3.1. Economic regime

The economic regime that involves a project depends on the price of the electricity generated and the specific regulation.

3.1.1. Electricity price

The price at which industries buy the electricity is directly related to the revenue of a project when the investment is paid back from the saving in the energy bill, which is known as self-consumption. From a general point of view, Fig. II.18 shows that this electricity price depends on the country where the project is implemented. In particular, this figure displays the electricity price variation in the European Union during 2016 for industrial consumers in the range of power between 500 MWh and 2,000 MWh. As can be deduced, within the same country, the electricity price also depends on the year assessed, as well as the type the industry. For instance and focusing on the specific case of Spain, Fig. II.19 depicts the electricity price evolution over recent years. The variable tendency of this price makes difficult to predict its evolution during the lifetime of a project. Moreover, Fig. II.20 shows that, within the same country and year, the electricity price also depends on the size of the industry. In this case, the clear tendency reveals that the higher the energy consumption of the factory, the lower the price paid. Consequently, countries with high electricity prices and small industries are preferable to reach the profitability of a project with ORC systems using the economic regime of self-consumption.
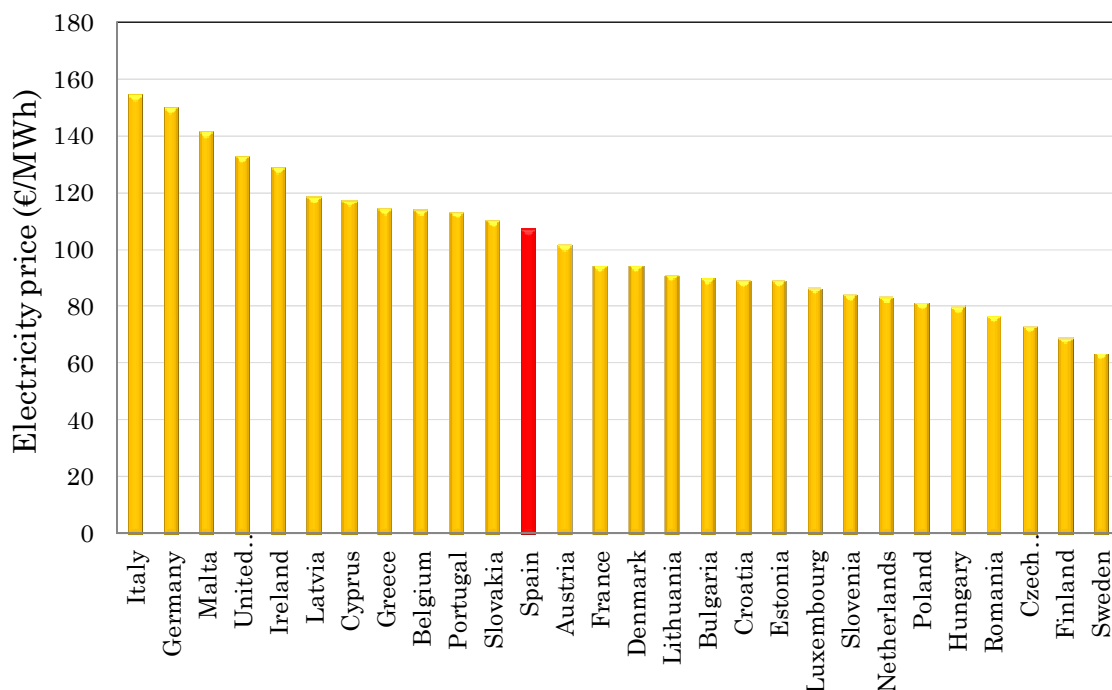
***Fig. II.18.** Electricity price for industrial consumers (500 MWh – 2,000 MWh) of EU-28 in 2016, excluding VAT and other recoverable taxes and levies. (Source: Ref. [122])*
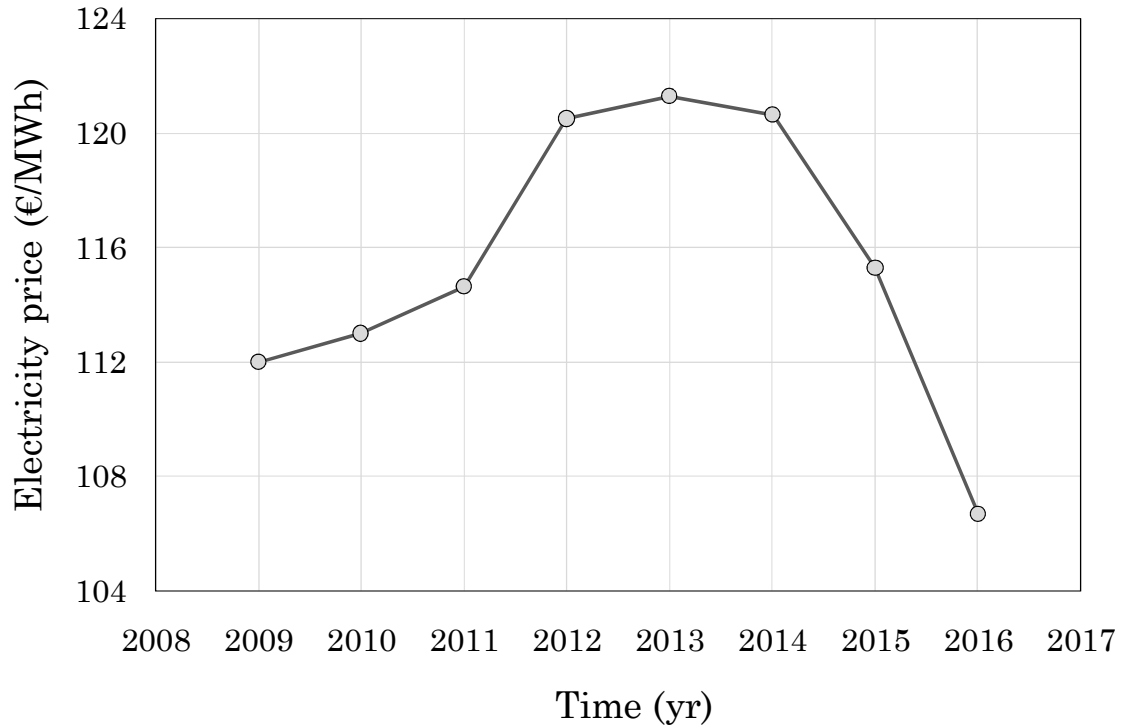
Fig. II.19. *Electricity price for industrial consumers (500 MWh – 2,000 MWh) of Spain in function of the year, excluding VAT and other recoverable taxes and levies. (Source: Ref.* [122]*)*
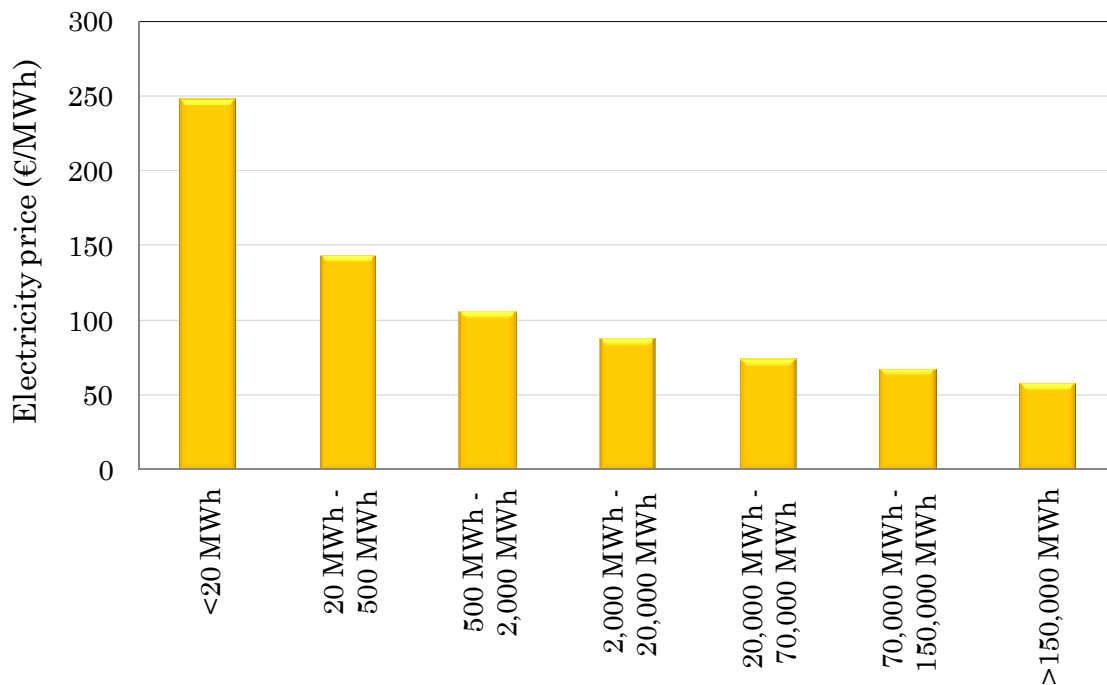
Fig. II.20. *Electricity prices in 2016 for industries of Spain in function of annual energy consumption, excluding VAT and other recoverable taxes and levies. (Source: Ref.* [122]*)*

On the other hand, there are different alternatives to the self-consumption. For instance, the energy generated by the power plant could be injected into the network of the energy supplier. In that case, the economic regime could consist of the continuous energy sale to the energy market (at the pool price [123]) or to take advantage of other regimes, if any, such as net-metering [81]. In this way, Fig. II.21 shows a comparison between purchase and sale prices in European countries in absence of incentives during the year 2016. As it highlights, the profitability of a project highly depends on the economic regime adopted.
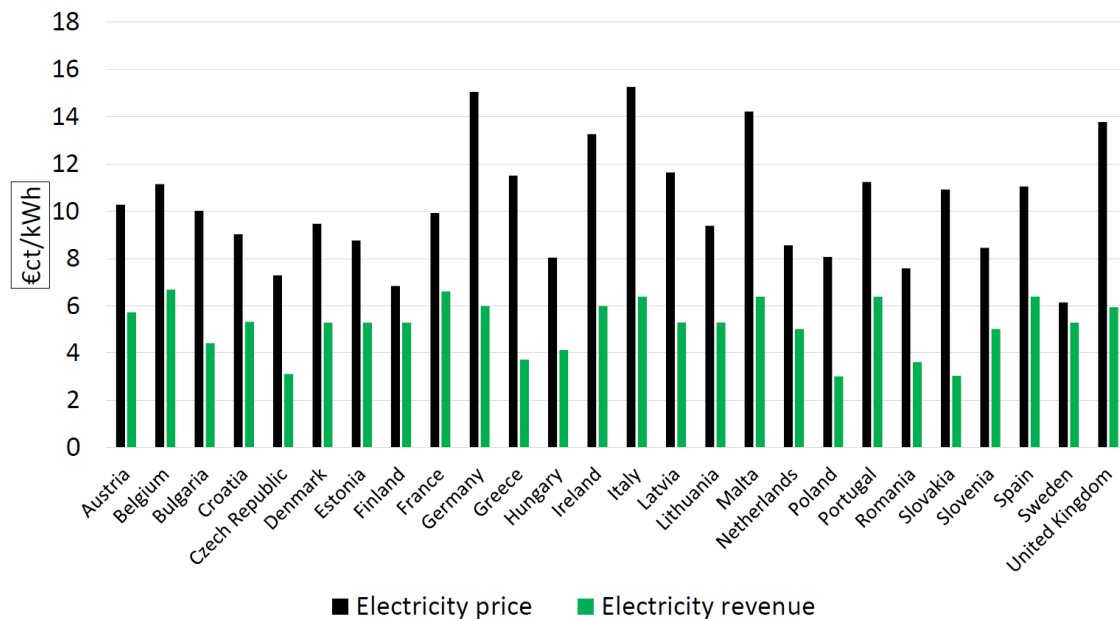
Fig. II.21. *Purchase and sale electricity prices of European countries in 2016. (Source: Ref.* [81]*)*

3.1.2. Incentives and economic charges

The previous electricity prices vary upwards or downwards depending on the specific regulation. For instance, a project integrated into an industry of Spain receives an economic retribution if the electricity is sold to the energy market [124], but it must assume an economic charge if the energy is self-consumed [125].

Regardless the economic regime, the use of ORC systems in industry is recognized by institutions as an energy efficiency measure that saves fossil fuel consumption and avoids CO_2 emissions in comparison to the electrical generation by means of conventional power systems. Therefore, aiming to promote this type of projects, an economic retribution is provided [126]. In this way, Forni *et al.* [127] valued this incentive in the form of white certificates as a saving around 15% of the total investment cost of the

project. For the specific case of Spain, this incentive would reach up to the 30% of the total investment cost [128].

3.2. Projects profitability

There are few studies that focus on the profitability of actual small-scale ORC systems in industrial processes. This fact was underlined by Cavazzini *et al.* [129], who also pointed the importance to develop models of commercial ORC systems, and to consider direct and indirect costs, in order to correctly evaluate the profitability of new projects in industry. Thus, the economic feasibility of a hypothetical scenario using a commercial ORC unit was analyzed. The results revealed the unprofitability of the project, even with the use of the energy efficiency incentive. Nonetheless, researchers highlighted that an improvement in performance and investment cost could lead to more reliable solutions. In contrast, a great profitability is expected in this type of applications. For instance, Casci *et al.* [52] tested a 40 kW ORC prototype and estimated that its application in a ceramic kiln could result in a payback period lower than 4 years. Similarly, Tocci *et al.* [81] analyzed generic small-scale ORC systems under different economic scenarios and assumed payback periods of 3 years.

As can be appreciated, there is a lack of knowledge about the actual profitability reachable in the range of small-scale applications. So to shed light on the magnitude order, a review of medium and large-scale applications in conducted. In these ranges of power, there are already projects implemented in industry. For instance, Fig. II.22 shows a medium-scale ORC of 500 kW used to recover waste heat from the hot gases of several ceramic kilns [130]. A list of large-scale ORC systems installed worldwide for waste heat recovery in industries is collected in Table. II.2.

With respect to the profitability obtained in the medium-scale range, Jung *et al.* [131] developed a financial model to examine a 250 kW ORC for low-grade waste heat recovery in a petroleum refinery. The researchers concluded that, in compliance with a target cost of $3000/kW for a feasible system, a reasonable internal rate of return of 21.8% and a payback period of 6.8 years could be achieved. David *et al.* [132] analyzed the use of exhaust gas from a coke plant to produce electricity with a 250 kW ORC unit. The scheme proposed is shown in Fig. II.23.a. An intermediate loop is used to recover the thermal energy and transport it to two commercial units of 125 kW (expected net power of 200 kW). The total investment cost was estimated about 1.1 million euros. Other assumptions were a system lifetime of 15 years, the absence of subsidies, and a discount rate of 2%. In this manner, the payback variation in function of electricity price was

analyzed, as it is shown in Fig. II.23.b. The study of the project profitability in France showed that due to electricity prices lower than 75 €/MWh, payback periods were around 9 years.

Fig. II.22. *ORC plant of 500 kW. Heat source of hot gases collected with pipes from several ceramic kilns, Sundstrand 1983. (Source: Ref.* [130]*)*

Table II.2. *ORC recovery plants in industries worldwide. (Source: Ref.* [133]*)*

Year	Plant	Group, Country	Supplier	Power (MW)
1999	Cement	Heidelberg Zement, Germany	Ormat	1.5
2010	Cement	Italcementi, Marocco	Turboden	1.8
2011	Glass	Vetrerie Sangalli Manfredonia, Italy	Ormat	2
2012	Glass	AGC Cuneo, Italy	Turboden	1.3
2012	Cement	Holcim, Romania	Turboden	4
2013	Cement	Jura Cement, Switzerland	ABB	2
2014	Cement	Holcim, Slovakia	Turboden	5

(a)   (b)
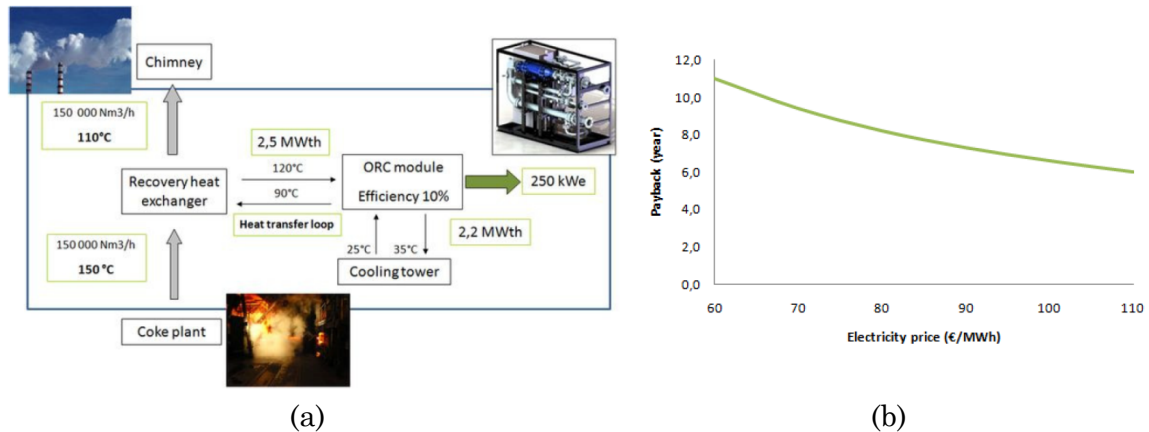
Fig. II.23. *Case study of waste heat recovery from coke plant: (a) schematic of the system, (b) simple payback period in function of electricity price. (Source: Ref.* [132])

Regarding the profitability of the large-scale range, Battisti *et al.* [134] compared various strategies to recover waste heat from a case of study in an iron foundry. For that, a large-scale ORC unit of 20 MW was considered. The investment cost of the plant was quantified as 1.43 million €, the lifetime assumed was 25 years, 2,300 hours of operation were considered, and a cost of electricity of 160 €/MWh. The results showed that the project was considered unfeasible. Nonetheless, the researchers concluded that applications with continuous periods of operation are preferable to reach the profitability of the projects. Taking that into account, Forni *et al.* [127] analyzed more favorable cases of study in cement, float glass, and steel industries. From the results, collected in Table II.3, various conclusions were extracted. In the first place, large operating periods around 8,000 hours per year can be seen, which were pointed as preferable in terms of profitability. A high difference between the cost of the ORC unit and the total investment cost of the project is appreciable, which changes radically the conclusions of an economic feasibility study. In particular, a simple payback period around 9 years was obtained in absence of incentives, which was pointed as a consequence of the low electricity price of 80 €/MWh. Nonetheless, considering white certificates and its multiplying factor for the promotion of energy efficiency measures, the simple payback period drops to about 4 years thanks to the incentives.

Table II.3. Economic feasibility analysis cases. (Source: Ref. [127]*)*

Industry	Cement	Float glass	Steel
Heat source	Kiln and clinker cooler gas	Oven exhaust gas	Preheating oven exhaust gas
Thermal power (MW)	25	5.6	5.5
Net electrical power (MW)	4.6	1.1	0.95
Electrical efficiency (%)	18.4	19.6	17.3
Time operation (hr/yr)	7,900	8,100	8,000
ORC unit (million €)	5	1.5	2
Total cost (million €)	17.6	3.8	3.1
SIC ORC (€/kW)	1087	1364	2105
SIC process (€/kW)	3826	3455	3263
Electricity price (€/MWh)	80	80	75
Net present value (million €)	1.05	0.5	0.28
Internal rate of return (%)	9	11	10
Simple payback period (yr)	9.2	8.4	8.8
Payback with incentives (yr)	4.2	3.8	3.8
Avoided CO_2 (t/yr)	22,894	5,613	4,788

4. THERMO-ECONOMIC ASSESSMENT

From the above information, it can be highlighted that there is a lack of knowledge about experimental small-scale ORC systems integrated into industrial processes. The main reason is that the profitability of the projects is not guaranteed, even for medium and large-scale systems. Therefore, thermo-economic optimizations emerge as a way to achieve more cost-effective solutions.

With this in mind, firstly, the objective functions used in thermo-economic optimizations are reviewed. Secondly, the magnitude order of the main cost-effective indicator is underlined. And finally, the background of thermo-economic optimizations is established.

4.1. Objective functions

Thermo-economic optimizations use cost-effective indicators, instead of just using performance ratios, as objective functions. A comparison between both modes of optimization was conducted by Quoilin *et al.* [58] applied to small-scale ORC systems in waste heat recovery applications. Thus, it was

demonstrated that different objective functions for the same working fluid lead to different operating conditions. In addition, thermodynamic and thermo-economic optimizations lead to the selection of different working fluids.

A review of different objective functions was reported by Lecompte *et al.* [101], which is listed in Table II.4. Among the different options proposed, the SIC (Specific Investment Cost) was highlighted as the most frequently used. Moreover, the reviewers proposed to use multi-objective functions when the parameters weighing are not fixed.

Table II.4. *List of objective functions used in thermo-economic optimizations. (Source: Ref.* [101]*)*

Objective function	Comments
Min. specific area (m²/kW)	Easy to calculate
	Not direct financial interpretation
Max. net present value, NPV (€)	The best to make financial appraisal
	Many assumptions needed
Min. specific investment cost, SIC (€/kW)	Easy to calculate
	Frequently used in literature
	It is not necessarily the highest NPV
Min. simple payback period (yr)	Identical to SIC if annual cash flow is
	dominated by the electricity sold
Min. Levelized cost of electricity, LCOE (€/kWh)	Useful to compare technologies
	Not convenient to assess a single project

4.2.   Specific Investment Cost (SIC)

The use of small-scale ORC systems in waste heat recovery applications better needs to be more cost-effective than efficient, as was reported by Tchanche *et al.* [135]. The reviewers demonstrated that results of optimizations focused on efficiency and cost-effective ratio do not match, as can be appreciated in Fig. II.24. The main reason was pointed due to the thermodynamic properties influence over the system performance and components sizing. Consequently, it was highlighted that SIC minimization is preferable than electrical power maximization for the ORC adoption.
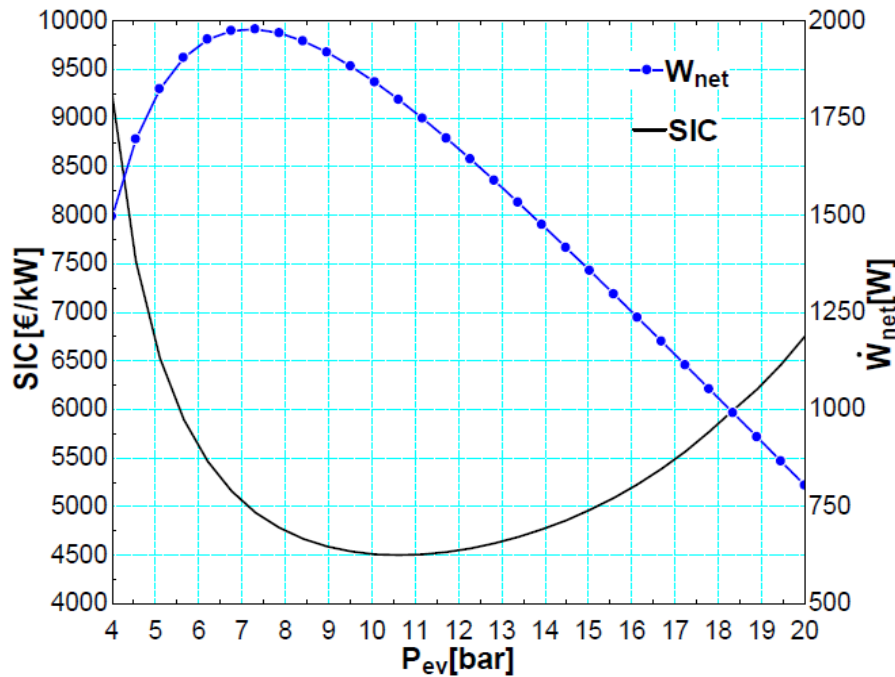
Fig. II.24. *Difference between using SIC or net power as objective function in a thermo-economic optimization (Source: Ref.* [135]*)*

Recently, Tocci *et al.* [81] pointed that the lack of experimental applications and the scarce number of commercial systems in the small-scale range are due to the high value of SIC. With this in mind, the researchers compared SIC values of ORC systems to other technologies currently available in the market to produce electricity. Thus, it was concluded that to achieve competitive systems, ORC units should not exceed a SIC value of 3,500 €/kW for micro-scale applications (<10 kW) and 2,500 €/kW for small-scale applications (10 − 100 kW). However, these values are far from actual costs. For instance, Cavazzini *et al.* [129] estimated that the SIC of a small-scale project using a commercial 30 kW ORC was about 5,000 €/kW. In the medium-scale range, Lemmens *et al.* [136] reported a SIC of 4,216 €/kW$_{gross}$ referred to a project using a 375 kW ORC to recover flue gas stream from an industrial plant. SIC values of large-scale plants can be extracted from the previous Table II.3, which range between 3,000 − 4,000 €/kW. As it highlights, the lower the scale of the application, the less cost-effective is the SIC of the project.

Other values reported in the literature for all scales in the different applications were displayed by Lemmens *et al.* [60] in Fig. II.25. This figure also distinguishes between SIC of ORC module (M) and SIC of the projects (P). The researchers also underlined that SIC values tend to decrease as the electrical power increases, which explains why small-scale projects are less profitable than large-scale applications.
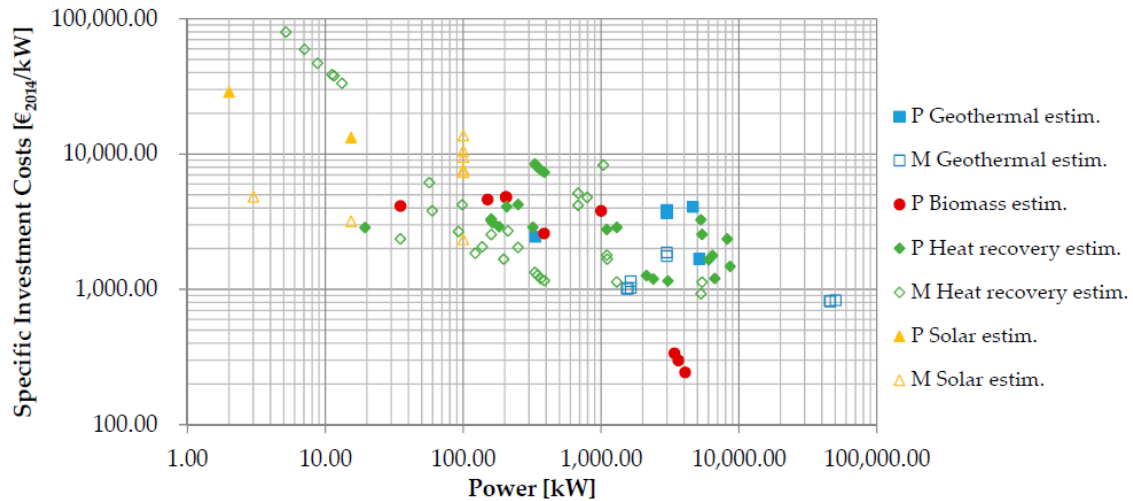
Fig. II.25. *Estimated costs of ORC Projects (P) and Modules (M) in literature, in 2014 Euros. (Source: Ref. [60])*

4.3.   Optimization

As it was mentioned, thermo-economic optimizations use cost-effective indicators as objective functions, being SIC the ratio most extensively used. In this way, Lecompte *et al.* [101] conducted the optimization of a generic medium-scale ORC applied to a case of study in an incinerator. Thus, the SIC evolution with respect to the net power output is depicted in Fig. II.26.a. As can be seen, there is an optimum of 4,114 €/kW referred to the subcritical ORC module, which is related with a simple payback period of 8.5 years. Moreover, the SIC variation with respect to pinch point values of evaporator and condenser can be seen in Fig.26.b and Fig.26.c, respectively.

The results of another investigation of Lecompte *et al.* [137] are illustrated in Fig. II.27. In this case, the thermo-economic optimization was conducted using data from a retail company. Thus, results showed that there is an optimum for each parameter assessed. Among these parameters, researchers focused on the built-in volume ratio of the expander, as well as heat exchange surfaces. Moreover, the importance of the part-load operation was highlighted. For that, a map of operation was developed to be used for the annual performance simulation of the case of study.
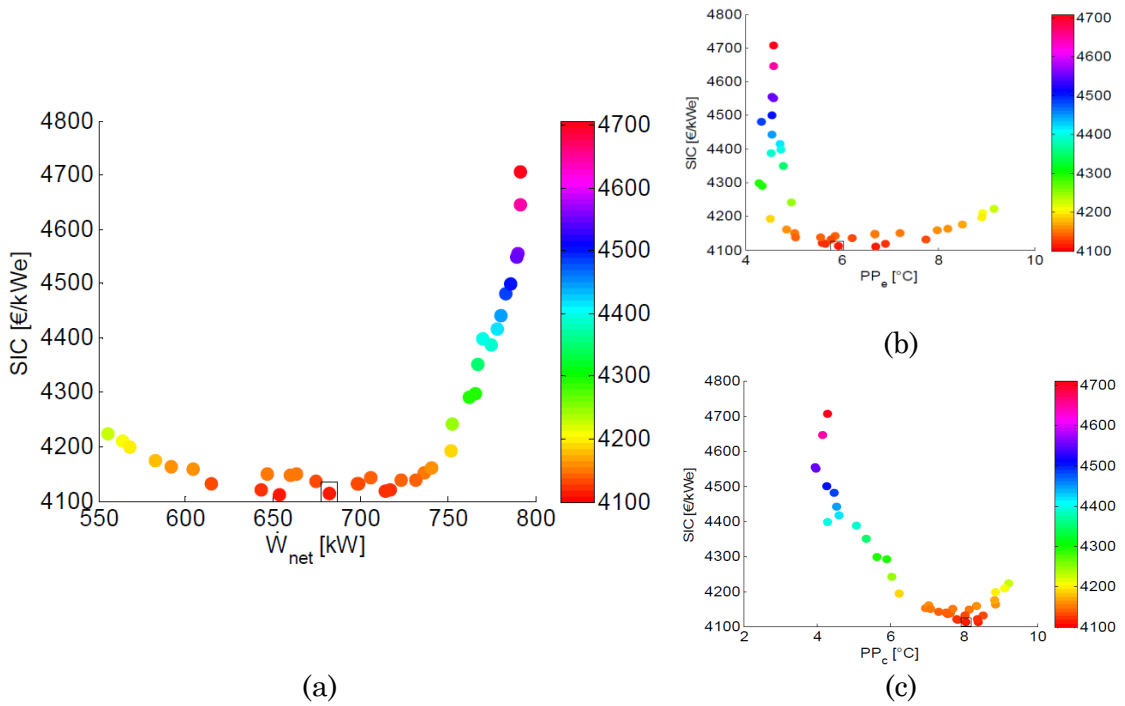
Fig. II.26. *SIC optimization in subcritical ORC in function of: (a) electrical power; (b) pinch-point evaporator; (c) pinch-point condenser. (Source: Ref.* [101]*)*
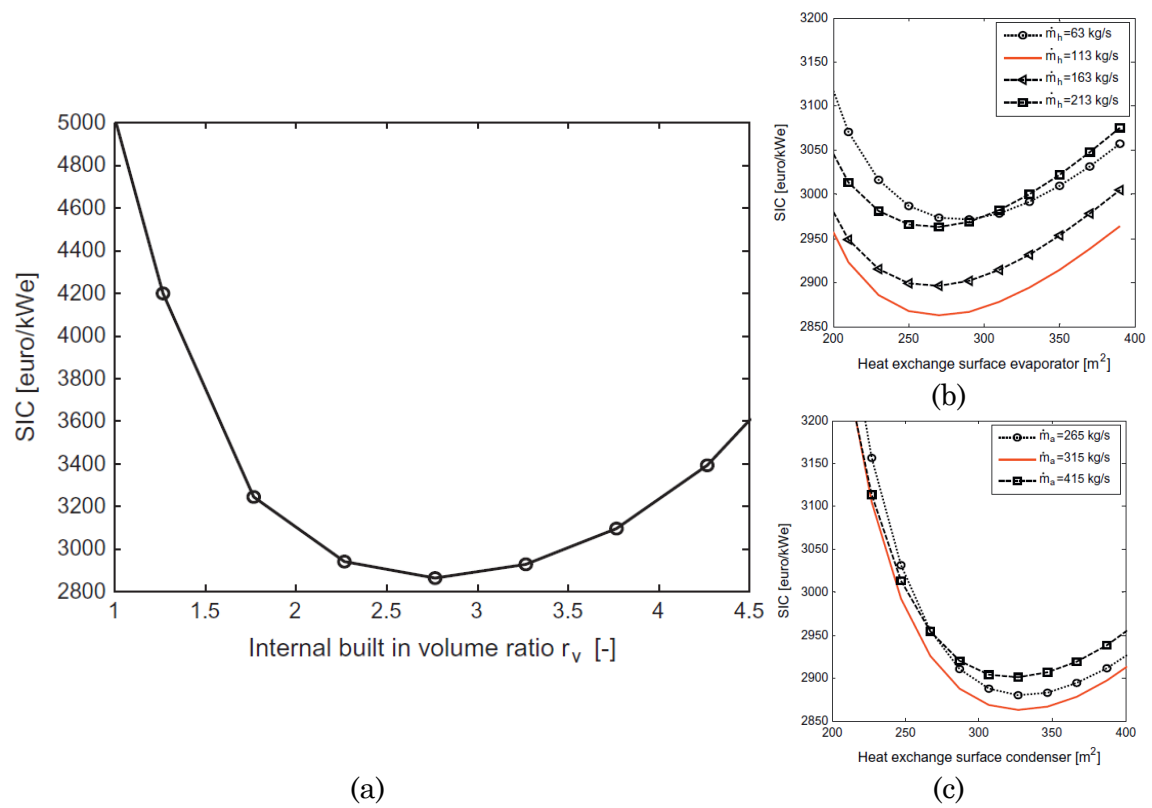
Fig. II.27. *Thermo-economic optimization of: (a) built-in volume ratio of expander, (b) heat exchange surface of evaporator, (c) heat exchange surface of condenser. (Source: Ref.* [137]*)*

Garg *et al.* [138] conducted the thermo-economic assessment of different applications. Regarding waste heat recovery applications, Fig. II.28 shows that the results of the optimization also depend on the scale of the unit. The parameters investigated were the working fluid (HFC-152a was the optimum in SIC), heat source temperature, pinch point in the condenser, HRVG and regenerator, expander inlet pressure, and air-cooled condenser surface.
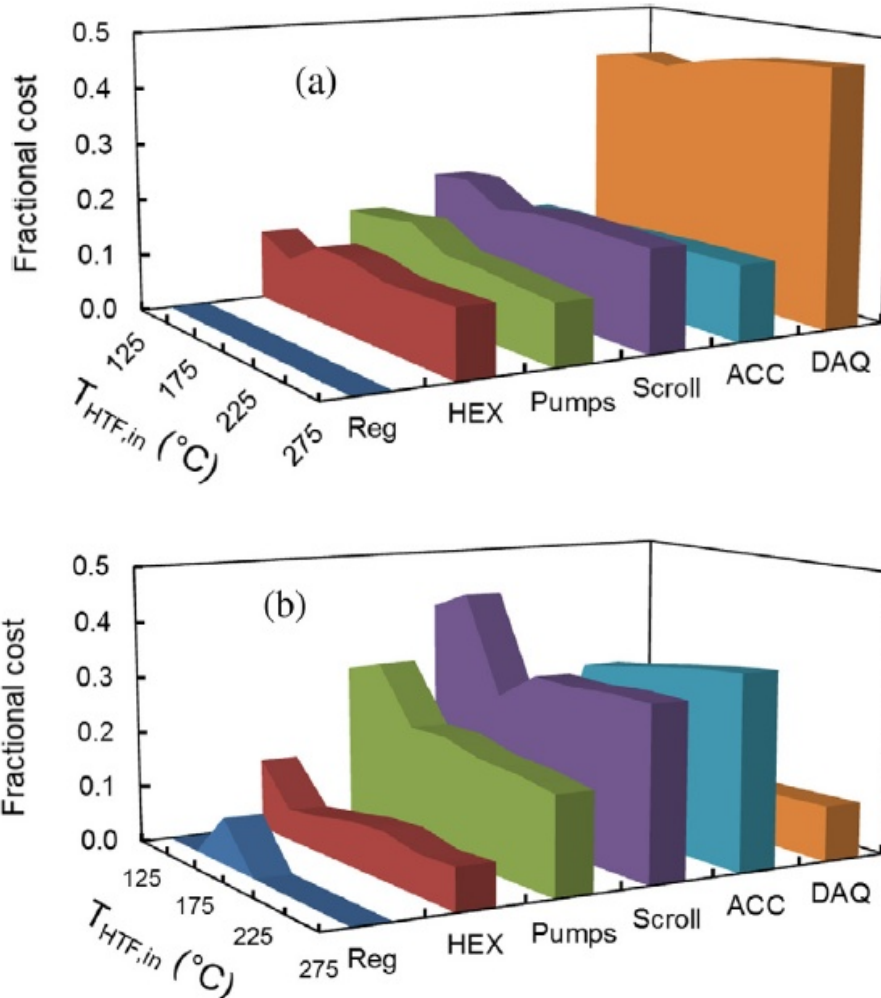
Fig. II.28. *Cost break up for ORC with the lowest specific cost: (a) 5 kW unit, (b) 50 kW unit; in function of regenerator (Reg), heat exchangers of the HRVG (HEX), pumps, scroll devices, air-cooled condenser (ACC), and data acquisition system (DAQ). (Source: Ref. [138])*

Further studies can be found in the literature to optimize each parameter of generic systems applied to different cases of study. For instance, Imran *et al.* [139] used the thermo-economic optimization to compare different architectures with the working fluid HFC-245fa. The parameters assessed were evaporation pressure, superheating, and pinch points. A figure of their

results is depicted in Fig. II.29, which shows that the optimum system also depends on the cycle architecture.
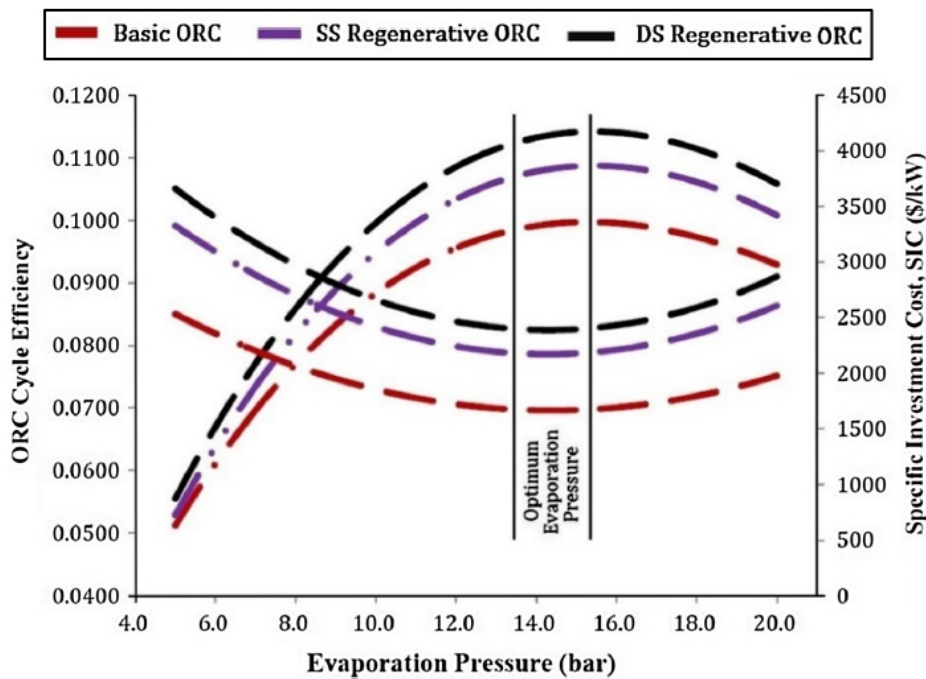
Fig. II.29. *Basic, single regenerative and double regenerative cycles comparison about efficiency and SIC. (Source: Ref. [139])*

5. CONCLUSIONS

The revision conducted has shown that ORC systems have been proven as a suitable technology for small-scale applications. Not only due to the exponential growth of investigations on the topic, but also the availability of commercial small-scale units in the market.

With regard to the investigations, it has been observed that mainly have a technical character. Numerous studies are devoted to finding better organic working fluids, as well as low GWP candidates for a drop-in replacement to the HFC-245fa, which is the most popular fluid among commercial systems. It has also been observed many studies that experimentally characterize the performance of different expansion technologies, which has been pointed as a critical component to reach cost-effective solutions. Other investigations focus on technical issues such as the architecture of the cycle, design of components like feed pump or heat exchangers, or the control strategy operated by the system.

In spite of this advances, there is a lack of knowledge about experimental applications of small-scale ORC systems for waste heat recovery in industrial processes. The main reason has been revealed due to the

difficulty to reach profitable projects, which have a high dependency on the economic regime assigned. In fact, even with medium and large-scale projects the profitability is not guaranteed.

Being aware of the economic feasibility relevance for the ORC adoption in practical applications, more cost-effective solutions are being explored in the literature through thermo-economic optimizations. The investigations reviewed show that there is an optimum value for any of the parameters assessed, including organic working fluid, expander geometry, cycle architecture, superheating value (control strategy), heat exchange surface, or sizing of other components, which in turn depends on the type and scale of the specific application.

For this reason, a thermo-economic optimization based on actual projects could lead to more realistic cost-effective systems and, hence, more reliable projects.

Experimental application & tests
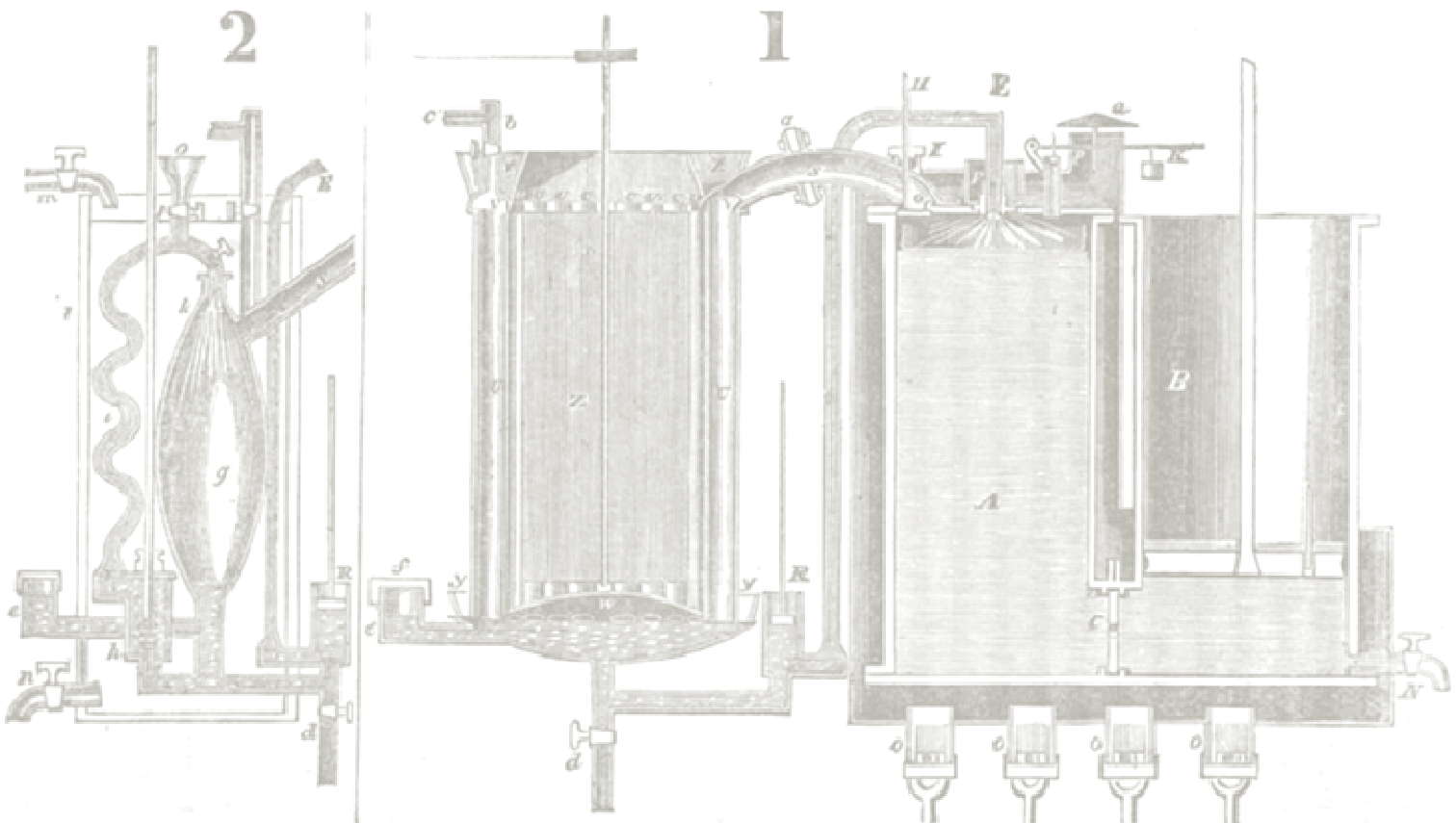
Howard's ether engine (1826)

1. INTRODUCTION

This Chapter focuses on the experimental part of the thesis. In this way, an experimental application is used as a reference case for the subsequent model development and validation from actual data of operation. Specifically, a small-scale ORC system installed in a ceramic furnace for low-grade WHR is addressed.

With this in mind, the description of the facility, monitoring with metering devices, testing procedure conducted, and acquisition and treatment of the data are discussed below.

2. FACILITY DESCRIPTION

This section presents the different parts of the facility distinguishing between industrial process and waste heat recovery system.

2.1. Industrial process

The specific industrial process consists of a ceramic furnace that belongs to a tile industry located in the province of Castellon (Spain) [140].

Ceramic furnaces allow recovering an important fraction of the input energy [141], as well as it occurs in many other industrial processes [47]. In the addressed case, the main heat source recoverable is concentrated on exhaust gases, which are available in the chimneys depicted in Fig. III.1. The first chimney expels flue gases from the firing zone. There is a great potential in this heat source, although the minimum temperature of the gas is usually limited to protect the facility against the acid dew point. The second chimney exhausts the air of the intermediate cooling zone. The thermal power in this chimney is lower compared to such of the first one, but a higher gas temperature is reached due to its proximity to the burners of the firing zone [142]. The last chimney corresponds to the final cooling zone, wherein the thermal power and gas temperature are much lower.
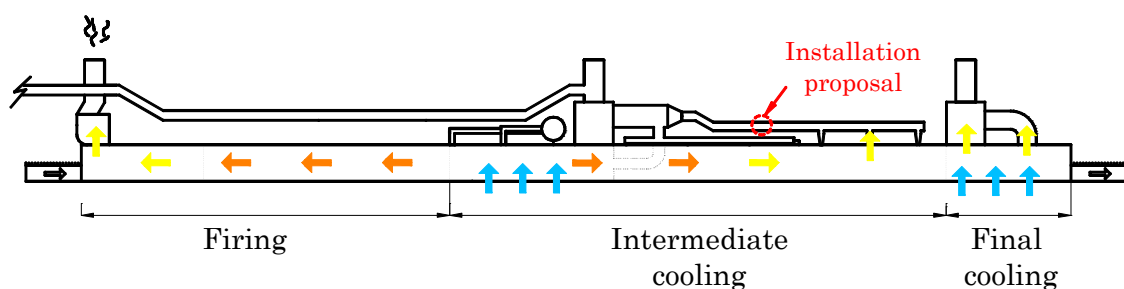
Fig. III.1. *Ceramic furnace scheme. (Source: Ref.* [142]*)*

Attending to temperature criterion, the project was finally focused on the intermediate cooling zone. In particular, it was executed in a duct that accomplished space requirements, which is pointed in the previous figure.

The thermal characteristics available in this duct were determined during the first stage of the project. Some direct measurements were conducted under typical operating conditions. For that, a flue gas analyzer connected to a Pitot-tube-thermocouple was utilized. Thus, through a perforation in the duct, temperature and mean velocity of exhaust air were determined. Moreover, it was found stable operating conditions, appreciable in a quite constant air velocity and a smooth variation of temperatures over time. A summary of these measurements is listed in Table III.1 [143]. In addition, the original facility and a thermography of the duct can be seen in Fig. III.2.

Table III.1. Measurements of the heat source.

Exhaust air temperature (ºC)	[285 – 300]
Duct diameter (m)	0.40
Profile mean velocity (m/s)	[18.8 – 19.0]

(a)   (b)

Fig. III.2. Intermediate cooling zone: (a) image of the original duct, (b) out of scale thermography of the duct.

2.2.   Waste heat recovery system

There are different parts that compose the waste heat recovery system, as Fig. III.3 shows.

Firstly, the section of the ceramic furnace that corresponds to the intermediate cooling zone is depicted in the figure. In this section, there is a duct directed towards the chimney, which originally contained part of the exhaust air. Parallel to this duct there is a bypass, in which a heat exchanger is installed. This heat exchanger allows the heat transfer from

the exhaust air of the industrial process to a secondary fluid. Specifically, a heat transfer loop with thermal oil is used to transport the thermal energy to the ORC unit (set of module and condenser). Taking advantage of the furnace proximity to the wall of the factory, the module of the ORC was placed outdoors (green box). Just above this module, a long heat exchanger can be seen, which is used to release the heat from the ORC unit to the ambient.

Once presented the general scheme of the facility, their main parts can be addressed in detail.
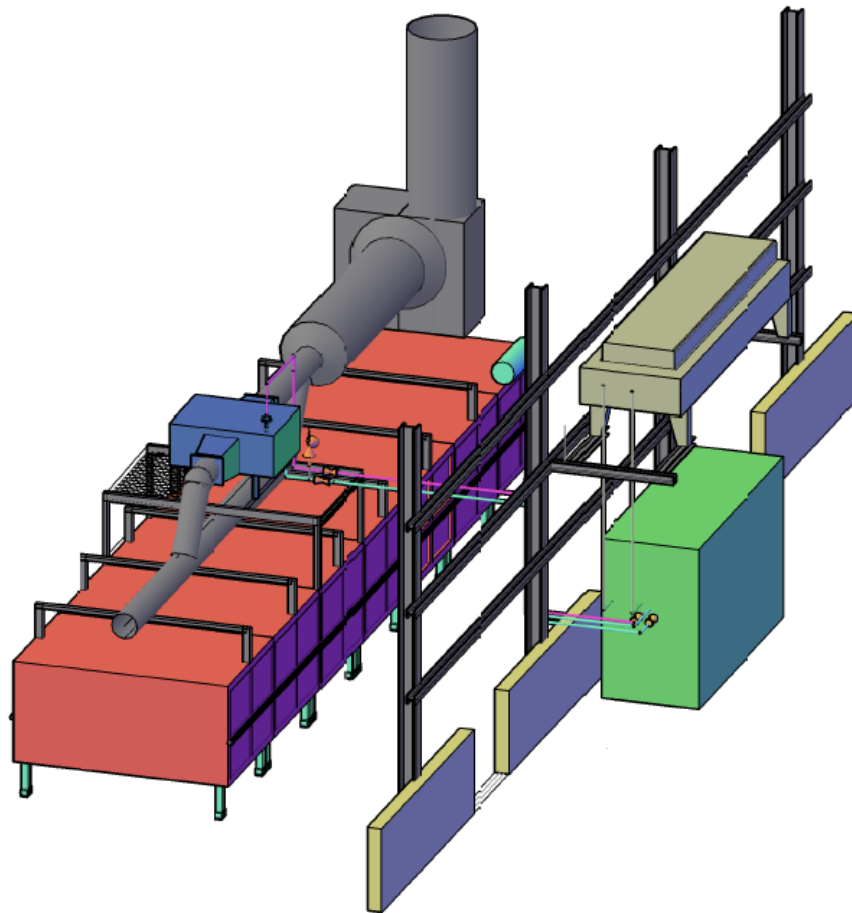
Fig. III.3. *Drawing of the facility.*

2.2.1. Recuperator

The recuperator is the heat exchanger that is installed in the industrial process. Its function consists of allowing the heat transfer between the fluid of the heat source and a secondary fluid. In this case, the fluid of the heat source is exhausted air and the secondary fluid is thermal oil.

Fig. III.4 shows that the recuperator is integrated into a bypass. The main reason is to allow the air flow interruption during maintenance tasks.
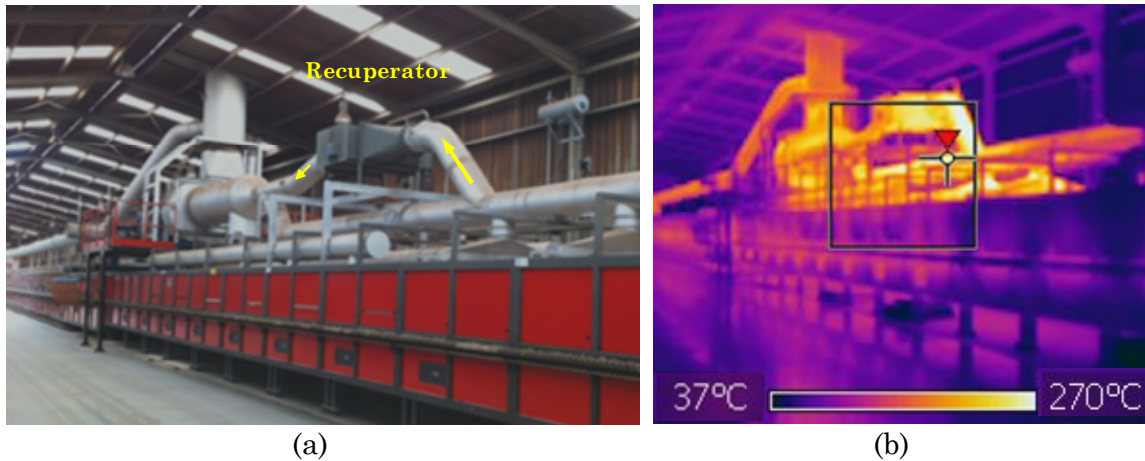
Fig. III.4. *Recuperator integrated into the industrial process: (a) image of heat exchanger, (b) out of scale thermography of the process.*

The thermal power considered for the recuperator design was also determined during the first stage of the project, which also depends on the temperature at which the exhaust gas can be cooled. For instance, as mentioned, the minimum flue gas temperature is commonly restricted to prevent the acid dew point. Typical values that guarantee the chimney protection are 120 ºC for low sulfur content gases and 180 ºC for gases with a higher content of sulfur [144]. In this case, lower values could be reached, since exhaust air is used. However, there is already a bottom heat recovery in the process that restricts the minimum temperature. In particular, a portion of the exhaust air is derived to feed burners and to be used in a dryer. For this reason, the industrial user suggested a minimum temperature around 170 ºC for the recuperator design. Accordingly, it was estimated that a thermal power about 180 kW could be recovered [145].

2.2.2. Heat transfer loop

The use of a heat transfer loop is less efficient, more expensive and conceptually more complex in comparison to a direct recovery system with the organic fluid [146]. However, it is recommended to achieve more reliable practical applications [147]. This is because excessive temperatures may appear during a start-up or a transient, deteriorating the organic fluid. On the other hand, thermal oils are able to support temperatures up to 400 ºC without pressurizing the circuit [148]. In addition, the heat transfer loop damps the heat source variation and allows a smoother cycle operation [80].

The circuit of thermal oil is shown in Fig. III.5, which crosses from the recuperator to the wall of the factory. The thermal oil introduced into the facility is Pirobloc 300A [149]. Moreover, various accessories are required for a safe operation, which are schematized in Fig. III.6 in accordance to thermal fluids regulation [150].

(a)   (b)
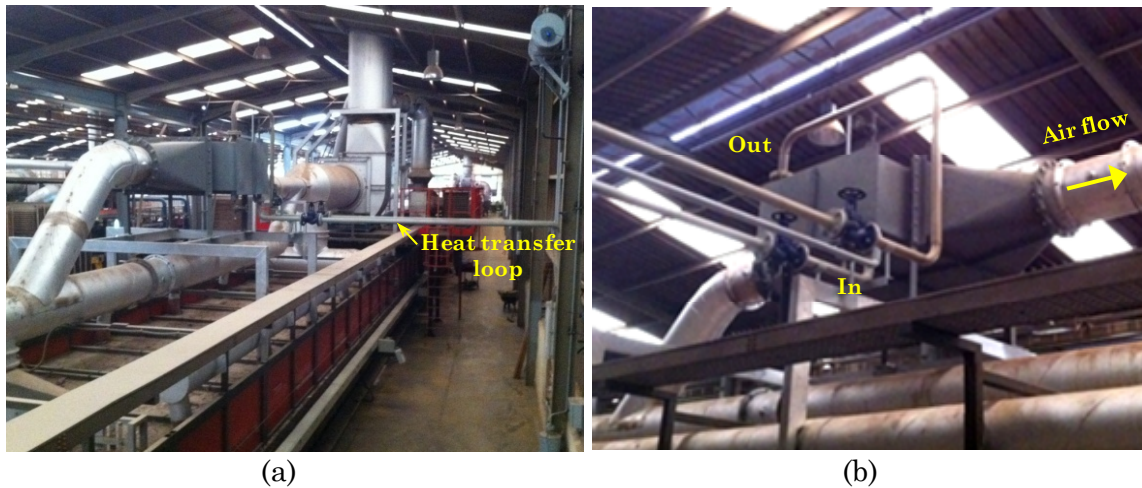
Fig. III.5. *Heat transfer loop: (a) general view (b) connections to recuperator.*
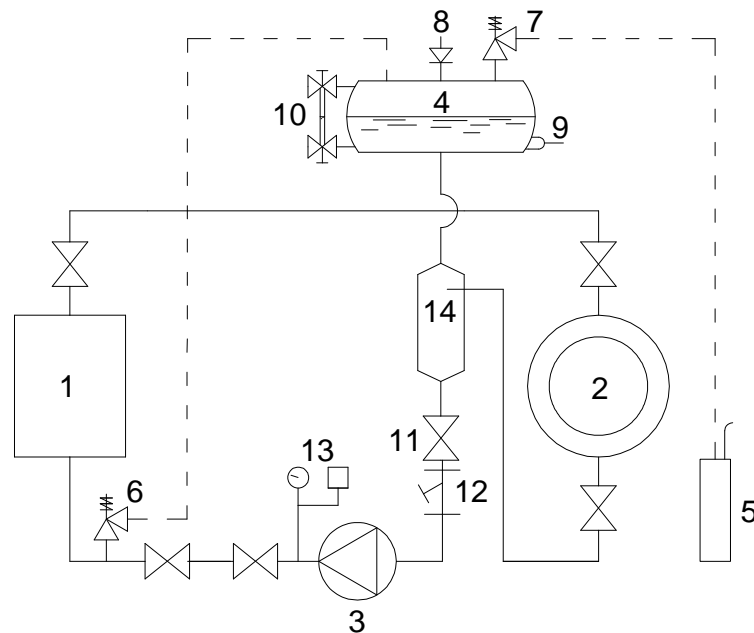
Fig. III.6. *Parts of the heat transfer loop: 1-recuperator, 2-ORC unit, 3-centrifugal pump, 4-expansion tank, 5-open receiver, 6-main safety valve, 7-secondary safety valve, 8-vacuum breaker valve, 9-level switch, 10-level viewer and purge valve, 11-valves, 12-filter, 13-manometer and pressure switch and 14-deaerator.*

2.2.3. Module

The ORC is a 20 kW prototype appreciable in Fig. III.7.a [54]. In particular, the module is the box that contains most of the components, which are indicated in Fig. III.7.b. This module was installed outside of the factory due to both proximity and space requirements.

It was designed with a regenerative architecture, which means that an additional heat exchanger, with respect to the conventional typology presented in Chapter I, is used to allow the internal reuse of the heat that leaves from the expander [53].

With regard to the thermodynamic cycle, it operates in subcritical conditions and with a constant superheating degree at the inlet port of the expander.

The organic fluid used is HFC-245fa. It is a working fluid commonly used among the reviewed ORC manufacturers, since it is a non-flammable fluid with low toxicity (permissible exposure level about 300 ppm) and moderate environmental properties [151].

Surely, the most investigated component among the literature is the expansion technology. In this prototype, a rotary volumetric or positive displacement machine is used. Specifically a twin screw expander, which is considered the best candidate for small to middle power capacity ORC systems [89].

These and other characteristics are collected in Table III.2, and more detailed information about the components will be shown in Chapter IV.

(a)   (b)

Fig. III.7. *Photos of* ORC: *(a) external view of the unit (set of module and condenser), (b) internal view of the module.*

Table III.2. ORC module main characteristics.

Alternator rated power (kW)	20
Architecture	Regenerative
Thermodynamic cycle	Subcritical with superheating
Organic working fluid	HFC-245fa
Expander machine	Twin-screw
Heat exchangers	Compact brazed plate
Feed pump	Diaphragm pump

2.2.4. Air-cooled condenser

The condenser is the heat exchanger that allows the heat transfer between ORC unit and heat sink. Commonly, when further heat integration in a process is not possible, the heat can be rejected to the ambient by direct systems [152]. Thus, since a power only system is assessed in this study, a direct air-cooled condenser can be used. This type of dissipation system allows reducing exergetic losses compared to a dry cooler with cooling water; besides simplifying the scheme, since there is not required another pump, nor its associated safety and control devices.

The condenser can be appreciated in the previous Fig. III.7.a, which is located above the module to save space occupation. Specifically, it consists of a horizontal unit composed of five fans in an induced-draft arrangement, which provides a uniform cooling air flow over the tube bundle and helps to stabilize the operation when changes in ambient conditions occur [153].

3. MONITORING

This section presents the points of the facility that are measured and the metering devices used for that purpose.

3.1. Measured points

The points of the facility measured, as well as numbering of the cycle, are represented in the scheme of Fig. III.8. Among them, there are some parameters that were monitored and registered during tests and other parameters that were directly measured on-site.

Regarding parameters registered, there are numerous temperatures throughout the facility. Thus, air temperatures in the recuperator, thermal oil temperatures in the heat transfer loop, various temperatures of the organic fluid, and the ambient temperature are monitored. Moreover, focusing on the ORC unit, pressure variation along the cycle, organic fluid

mass flow rate, and electrical power produced by the alternator and consumed in feed pump and fans of the condenser are also monitored.

On the other hand, there are some parameters that just were measured on-site during typical operation. In particular, it was measured the velocity of the exhaust air, which was found quite constant, the electrical consumption of the thermal oil pump, which operates at a constant speed, and other energy consumptions reflected in the power output of the ORC unit, related to control devices or energy losses.
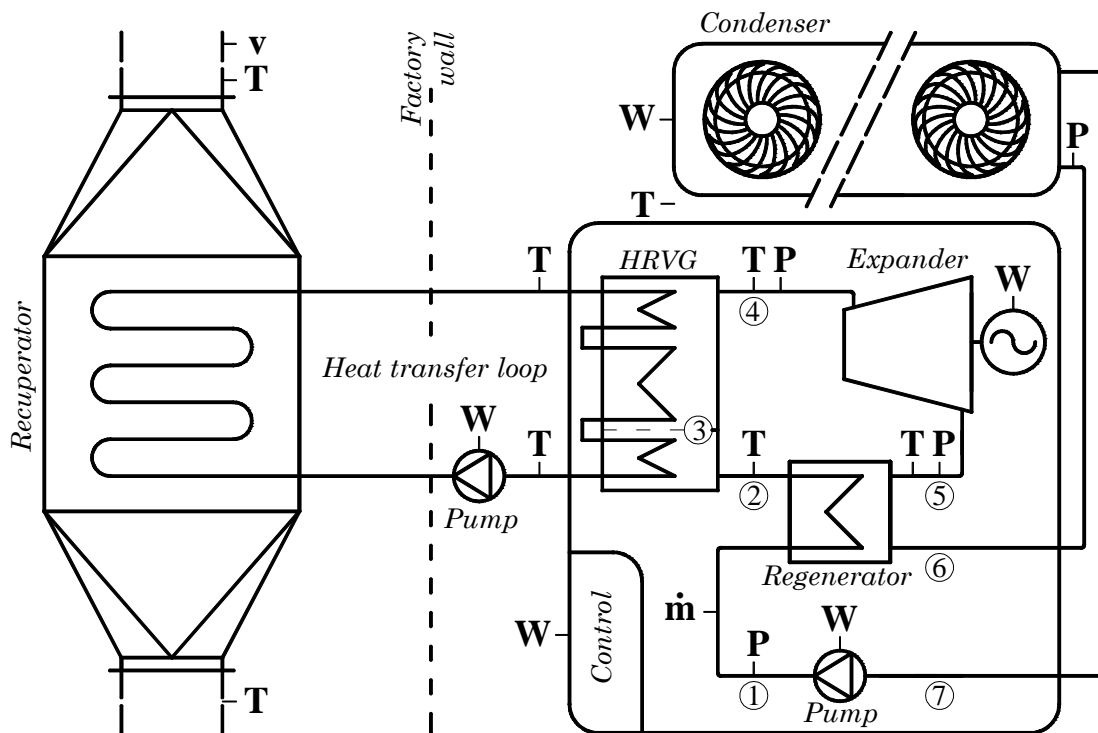
Fig. III.8. *Points measured in the facility.*

3.2.   Metering devices

The characteristics of the metering devices, extracted from manufacturers' data sheets, are collected in Table III.3.

Table III.3. Information of metering devices.

Parameter		Use	Instrument	Accuracy (%)	Range
Temperature	T	ORC	Thermocouple	± 0.4	0 – 750 °C
		Recup.	PT-100	± 0.75	-100 +450 °C
Pressure	P	ORC	Transmitter	± 0.5	0 – 40 bar
Mass flow rate	ṁ	ORC	Coriolis flow meter	± 0.3	< 6500 kg/h
Velocity	v	Recup.	Gas analyzer	± 1.5	-
Electricity	W	ORC	Wattmeter	± 1.2	-
		Other	Grid analyzer	± 0.2	< 80 kW

4. TESTING PROCEDURE

With the aim to obtain performance data of the facility during typical operating conditions, the system was kept running for testing during a complete week. Thus, the monitored parameters of the reference case could be registered. The resolution of the registration was set per second, achieving more than 604,800 points of operation.

5. DATA TREATMENT

After testing, a data treatment is required to extract useful information. In this way, the selection of the data for the model validation is addressed. Furthermore, some performance ratios that also will be used in the validation, and the statistical analysis method followed are described below.

5.1. Data selection

As mentioned, the process is characterized for a stable operation with smooth variations over time. For this reason, suitable results can be obtained through a steady-state model, instead of using a more complex dynamic model. So in order to validate the model, some steady-state points are required.

With this in mind, 21 points (three points per day) representative of the operating range were selected. In particular, the selection was made averaging 15 minutes operation (900 direct measurements), and checking that mean absolute errors remain below 5%, which is a value within the acceptable limits of the standard method for steady-state tests [154]. In representation of these errors, Table III.4 collects the values that correspond to the input temperatures of the system, referred to exhaust air in the recuperator and ambient air in the condenser. The maximum errors

are lower than 1% for the heat source temperature and 4% for the heat sink temperature.

Table III.4. *Errors of steady-state points due to exhaust air and ambient air.*

Day		T heat source	T heat sink		T heat source	T heat sink		T heat source	T heat sink
Monday	1	0.17%	3.56%	9	0.23%	1.26%	17	0.21%	1.50%
Tuesday	2	0.20%	1.28%	10	0.37%	2.05%	18	0.33%	2.39%
Wednesday	3	0.30%	1.48%	11	0.32%	1.48%	19	0.19%	1.47%
Thursday	4	0.14%	2.82%	12	0.59%	1.52%	20	0.19%	1.65%
Friday	5	0.33%	1.47%	13	0.36%	2.13%	21	0.49%	3.15%
Saturday	6	0.25%	3.15%	14	0.18%	3.70%	22	0.18%	3.70%
Sunday	7	0.22%	0.66%	15	0.17%	0.85%	23	0.49%	1.84%

The values of these inputs represent the operating map achieved during tests, which is displayed in Fig. III.9. As can be noted, due to the bounded range of operation obtained, a model able to conduct off-validation simulations is required. For that, a semi-empirical model based on the geometric description of the main components and the establishment of thermodynamic equations can be used [95].
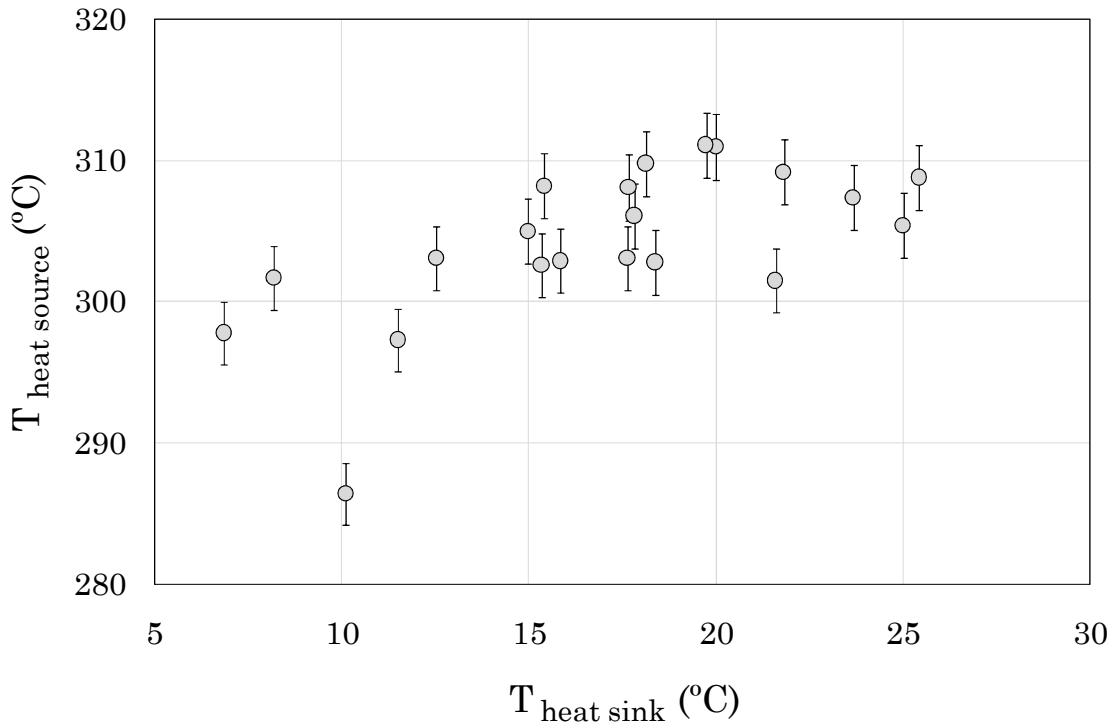
Fig. III.9. *Map of steady-state points.*

The operating range of each parameter obtained from the steady-state points is collected in Table III.5. This table also shows the average values of the parameters that were measured on-site.

Table III.5. *Range of measurements obtained.*

Recuperator	In (exhaust air)	T (ºC) $\bar{v}(m/s)$	286.4 – 311.1 18.85
	Out (exhaust air)	T (ºC)	176.0 – 183.9
Heat transfer loop	In (thermal oil)	T (ºC) $\bar{W}(kW)$	159.3 – 169.6 0.7
	Out (thermal oil)	T (ºC)	127.7 – 135.2
HRVG	In (organic fluid)	T (ºC)	87.0 – 98.7
Expander	In (organic fluid)	T (ºC) P (bar)	147.4 – 155.7 17.3 – 19.7
	Out (organic fluid)	T (ºC) P (bar) W (kW)	109.6 – 121.3 2.7 – 4.1 15.1 – 17.1
Pump	In (organic fluid)	W (kW)	1.8 – 2.5
	Out (organic fluid)	P (bar) $\dot{m}$ (kg/s)	18.1 – 20.7 0.74 – 0.85
Condenser	In (air)	T (ºC) W (kW)	6.8 – 25.4 0.13 – 0.15
	In (organic fluid)	P (bar)	1.9 – 3.5
Other	In	$\bar{W}(kW)$	0.2

5.2. Steady-state points assessment

Despite the stability of the process and the acceptable error of the steady-state points, the use of experimental data for modeling also requires assessing the extent of explainability between inputs and output of a system, as well as the level of noise that points introduce.

For this purpose, there are already tools that conduct an analysis of multivariate steady-state points obtained from experimental data. For instance, GPExp [155] is an open-source package analysis framework written in MATLAB. The methodology of the tool relies on Gaussian Process regression, also known as Kriging regression, which is a nonparametric probabilistic tool.

In this way, an analysis of the steady-state points is conducted. As mentioned above, the inputs of the system are referred to the exhaust air and ambient air, while the gross electrical power of the alternator can be considered as the directly measured parameter that represents the system output.

Thereby, the results of the analysis show that there is a significant correlation between the inputs and the output. Thus, Fig. III.10.a shows the Gaussian probabilistic distribution, in which it can be appreciated that there is not any outliner. The higher deviation is produced in the data point number 2, with an error 1.72 times higher than the standard deviation. Moreover, this tool provides the maximum accuracy that could be reached in a model that use these inputs and output as variables, which is pointed as a coefficient of determination in cross-validation of 96.82%. It also is interesting to appreciate the relationship between these inputs and the output, shown in Fig. III.10.b. As expected, the higher the heat source temperature and the lower the heat sink temperature, the higher the electrical power output.
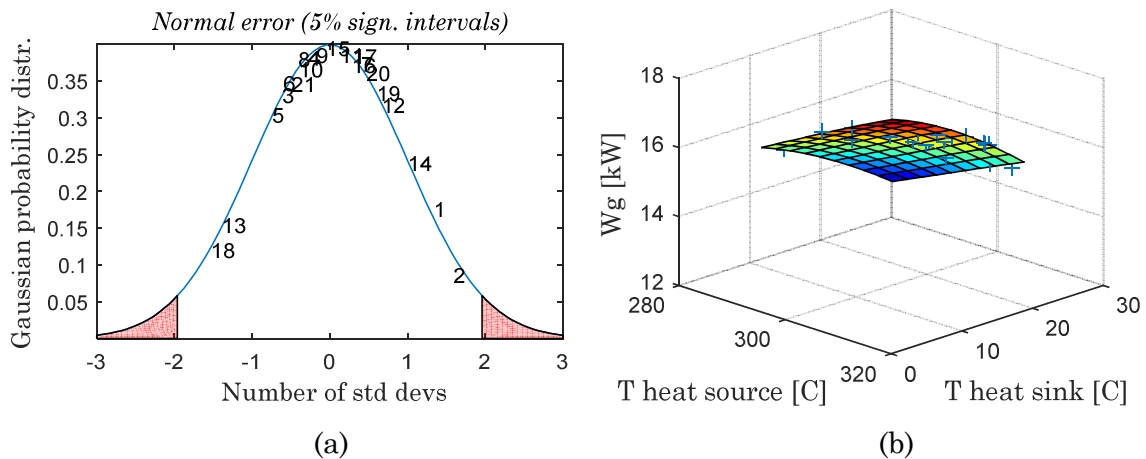
Fig. III.10. *Steady-state points assessment: (a) Gaussian probabilistic distribution, (b) relationship between inputs, referred to exhaust air in the recuperator and ambient air in the condenser, and output, referred to gross electrical power.*

5.3.   Analysis equations

Besides monitored parameters, some analysis ratios are also used for the model validation.

Firstly, the thermal power that is recovered from the heat source can be obtained from Eq. (1), since there is not any phase change. In this expression, the mass flow rate of exhaust air can be calculated using the average velocity and the duct diameter. The thermal power that reaches the organic fluid can be obtained by Eq. (2), since there is a phase change in the HRVG.

One of the main performance ratios sought is the cycle efficiency, which can be expressed in function of gross electrical power as Eq. (3).

With respect to the whole process, the net electricity injected into the grid of the industrial user can be expressed deducting energy consumptions and

losses. Thus, Eq. (4) considers the consumption of the feed pump, fans of the condenser, other consumptions and losses related to the ORC unit, the consumption of the thermal oil pump and such due to the increase of electricity caused in the blower of the industrial process.

Taking this into account, the efficiency of the whole process can be written as Eq. (5). This efficiency can be compared to the maximum ideally reachable according to Carnot efficiency, which is expressed as Eq. (6) with temperatures in Kelvin units.

$$Q_{source} = \left(\rho \cdot \bar{v} \cdot \frac{\pi \cdot D^2}{4} \right) \cdot c_p \cdot \Delta T \tag{1}$$

$$Q_{wf} = \dot{m}_{wf} \cdot \Delta h \tag{2}$$

$$\eta_{cycle} = \frac{W_g}{Q_{wf}} \tag{3}$$

$$W_{net} = W_g - W_p - W_{cond} - W_{other} - W_{oil\,p} - W_{blower} \tag{4}$$

$$\eta_{process} = \frac{W_{net}}{Q_{source}} \tag{5}$$

$$\eta_{Carnot} = 1 - \frac{T_{heat\,sink}}{T_{heat\,source}} \tag{6}$$

Similar to the accuracy that metering devices have, the analysis ratios also present an uncertainty that can be quantified. To do this, Eq. (7) can be used as a function of each measured variable [156]. Thereby, uncertainties calculated are collected in Table III.6.

$$U_y = \sqrt{\sum_{i=1}^{N} \left(\frac{\partial y}{\partial x_i} \right)^2 \cdot U_{x_i}^2} \tag{7}$$

Furthermore, the validation of monitored parameters and analysis ratios with respect to the results predicted by the model can be assessed by a statistical analysis. In this way, the mean absolute error can be obtained by Eq. (8). The error of each measurement can be calculated through Eq. (9), whose maximum absolute value represents the bandwidth of the error. The standard deviation can be quantified using Eq. (10). Moreover, the coefficient of determination, shown in Eq. (11), can be used to assess the prediction accuracy.

Table III.6. Uncertainties of analysis equations.

Thermal power recovered	Q_{source}	1.70%
Thermal power input	Q_{wf}	0.61%
Cycle efficiency	η_{cycle}	1.35%
Net electrical power	W_{net}	1.55%
Process efficiency	$\eta_{process}$	2.30%
Carnot efficiency	η_{Carnot}	0.21%

$$\left|\overline{\chi}\right| = \frac{1}{N} \cdot \sum_{i=1}^{N} \left|\chi_i\right| \tag{8}$$

$$\chi_i = \left(\frac{x_{model,i} - x_{experimental,i}}{x_{experimental,i}} \right) \tag{9}$$

$$\sigma = \sqrt{\frac{1}{N} \cdot \sum_{i=1}^{N} \left(\chi_i - \overline{\chi}\right)^2} \tag{10}$$

$$R^2 = 1 - \frac{\sum_{i=1}^{N} \left(y_i - \hat{y}_i\right)^2}{\sum_{i=1}^{N} \left(y_i - \overline{y}\right)^2} \tag{11}$$

5.4.   Preliminary validation

A preliminary validation is used to check the suitability of the measurements obtained and the analysis ratios described. In this way, Fig. III.11 shows a comparison between the thermal power recovered in the heat source and the thermal power that reaches the organic fluid. In the first place, a linear tendency can be seen, which confirms the adequacy of measurements and calculations. Moreover, a thermal power deviation is also observed, which means that heat losses occur and, hence, require to be considered in the model development.
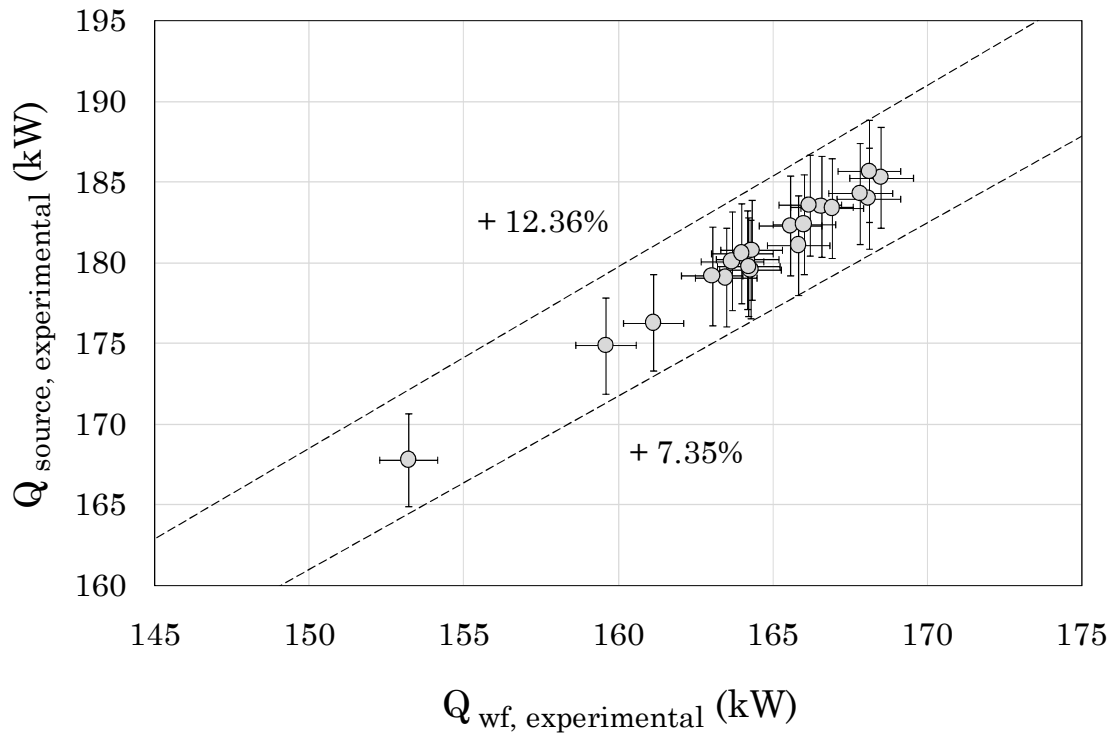
Fig. III.11. *Preliminary validation of thermal power in heat source and in ORC.*

6. CONCLUSIONS

An experimental application has been addressed as a reference case for the subsequent model development and validation from actual data of operation.

The operating data have been obtained from the facility monitoring during a week of tests under typical conditions. As a result, 21 steady-state points have been selected and their explainability assessed.

Besides measurements, performance ratios for the model validation have also been described and their uncertainty calculated, as well as a statistical method for the analysis of the model predictability. Thus, a preliminary validation has confirmed the adequacy of measurements and calculations.

Furthermore, this Chapter has revealed that thanks to the stability of the process and due to the necessity to conduct off-validation simulations, a steady-state and semi-empirical model could be a suitable tool to carry out the thermo-economic assessment.

Chapter IV

Modeling
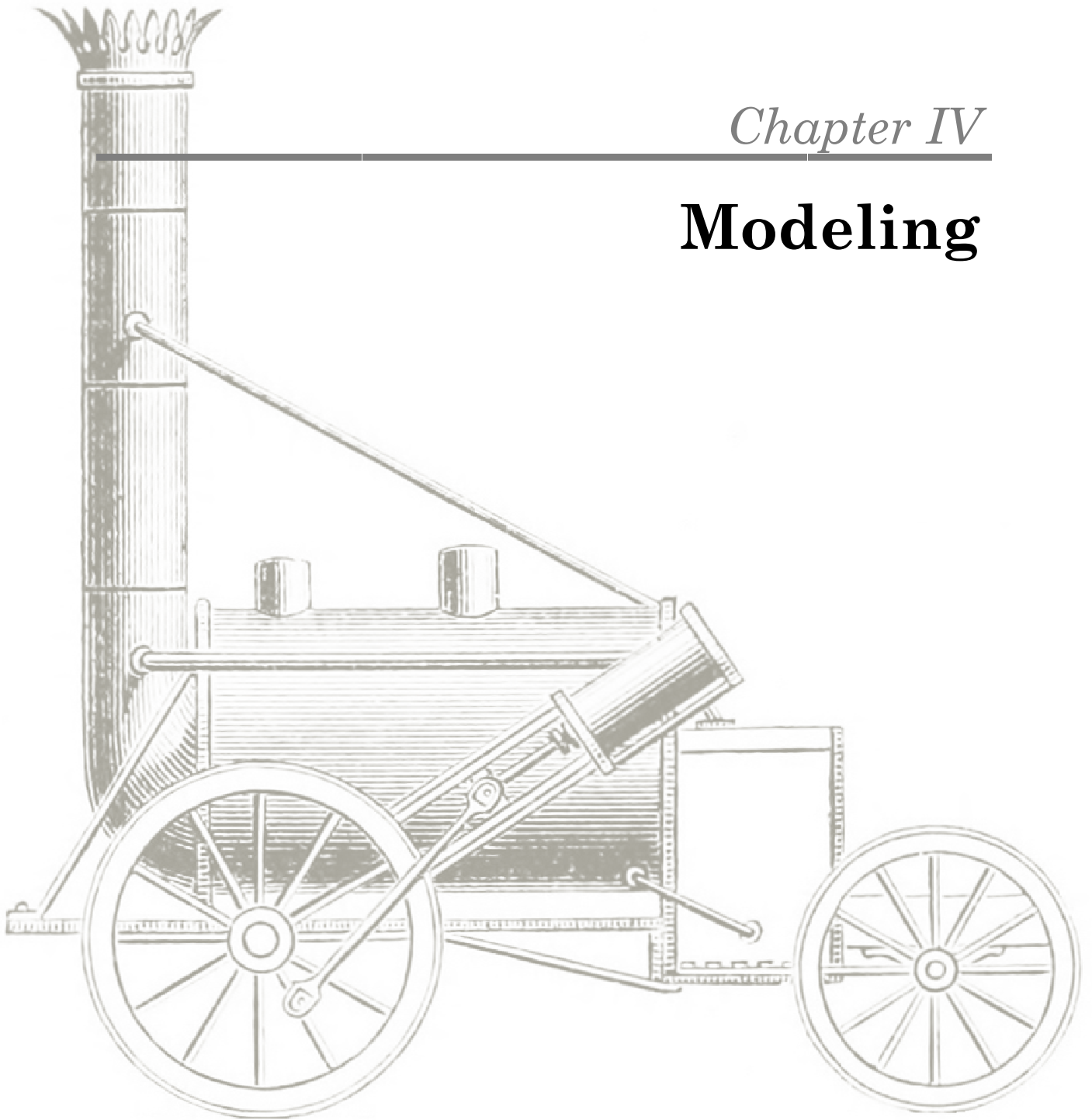
Stephenson's locomotive engine, "The Rocket" (1829)

1. INTRODUCTION

This Chapter describes a comprehensive model of the WHR system presented in Chapter III. In particular, the development of a semi-empirical steady-state model is proposed as a tool to carry out the thermo-economic assessment.

With this in mind, firstly, the approach of the model is exposed. Secondly, the geometric characteristics and the equations that define the thermodynamic performance of the main components are described. And finally, cost correlations and economic feasibility indicators are established.

2. MODEL APPROACH

From a general point of view, the model of the WHR system should predict the net electricity injected into the grid of the industrial user. This prediction should be made from boundary conditions, *i.e.* heat source and heat sink, as Fig. IV.1 shows.
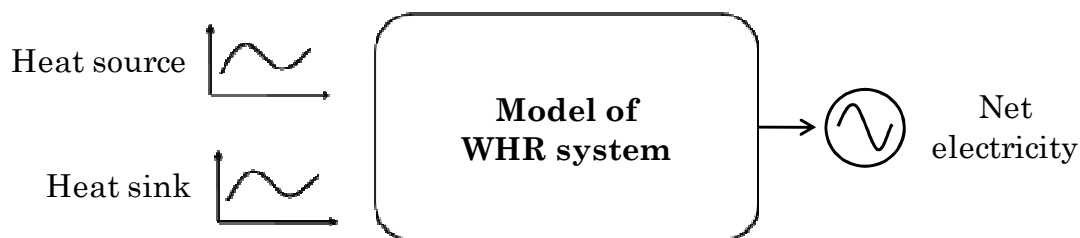
Fig. IV.1. *General approach of the model.*

To achieve this, a tool able to simulate the thermodynamic state of the fluids in each point of the system, the type of control operated by the ORC, and the electrical energy production and consumption is required. Accordingly, a model following the scheme depicted in Fig. IV.2 is developed. This scheme shows that the general model is composed by sub-models of the components, whose main interconnection parameters are also illustrated.

Taking this into account, the steady-state and semi-empirical sub-models of the main components are addressed below distinguishing between heat exchangers, fluid machines, and auxiliary components.
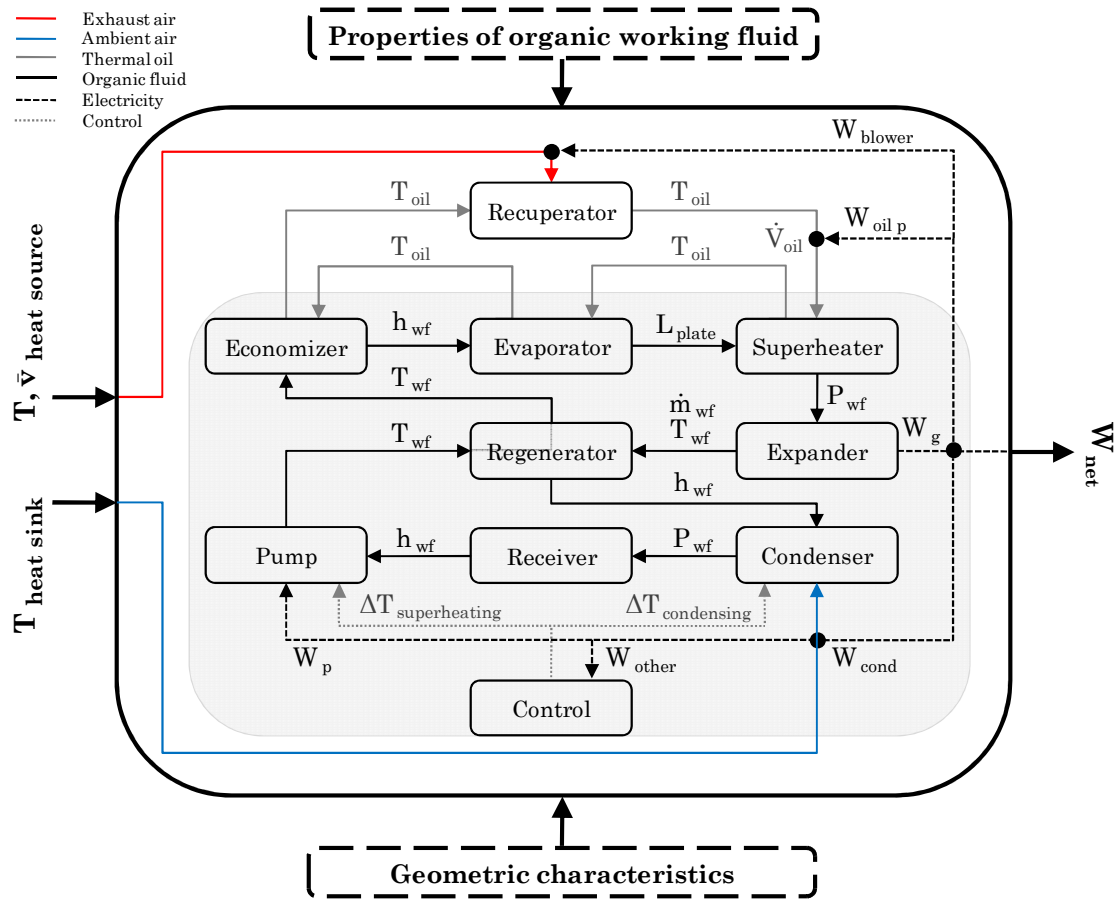
Fig. IV.2. *Scheme followed for the model development.*

3. HEAT EXCHANGERS

This section focuses on sub-models of heat exchangers from the geometric characteristics description and the establishment of heat transfer fundamentals.

3.1. Geometry

Heat exchangers are typically classified according to the flow arrangement and type of construction. In this facility, two types of heat exchangers can be distinguished. Firstly, the type of device used in the heat source and the heat sink is classified as bank of finned tubes. Secondly, the heat exchangers that are installed inside the module of the ORC are classified as plate heat exchangers.

3.1.1. Bank of finned tubes

A bank (or bundle) of tubes is used to transfer heat between a fluid that moves over the tubes and a fluid at a different temperature that passes through the tubes.

This type of construction was chosen for the heat exchangers used in the heat source and in the heat sink. The air in both cases, exhausted from the industrial process or blown from the ambient, corresponds to the external fluid that is forced to flow over the tubes. These tubes can be aligned to the direction of the air velocity, as in the case of the recuperator, or be staggered, as occurs in the case of the condenser. A schematic of this type of construction is shown in Fig. IV.3, along with some nomenclature used in equations.
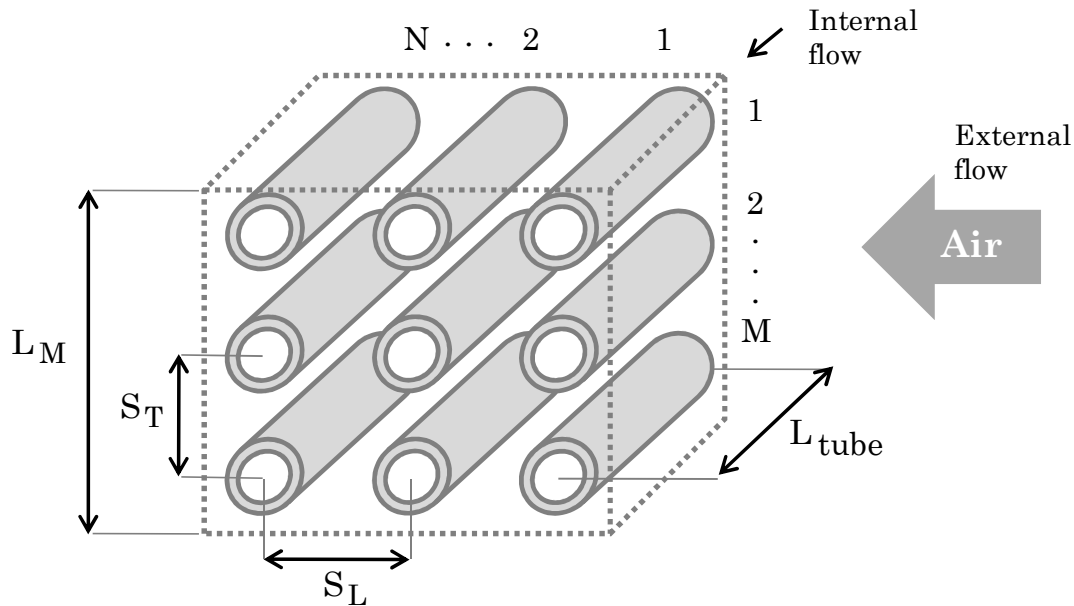
Fig. IV.3. *Bank of tubes with aligned arrangement.*

3.1.1.1. Recuperator

The recuperator is the heat exchanger integrated into the industrial process to recover the available waste heat. The thermal energy is transferred from the exhaust air to a secondary fluid. Specifically, a heat transfer loop with thermal oil is used between the heat source and the ORC unit.

A schematic of the recuperator is depicted in Fig. IV.4. The exhausted air from the process flows across the bank of finned tubes transferring the thermal power. Accordingly, the thermal oil recovers this heat and leaves at a higher temperature.
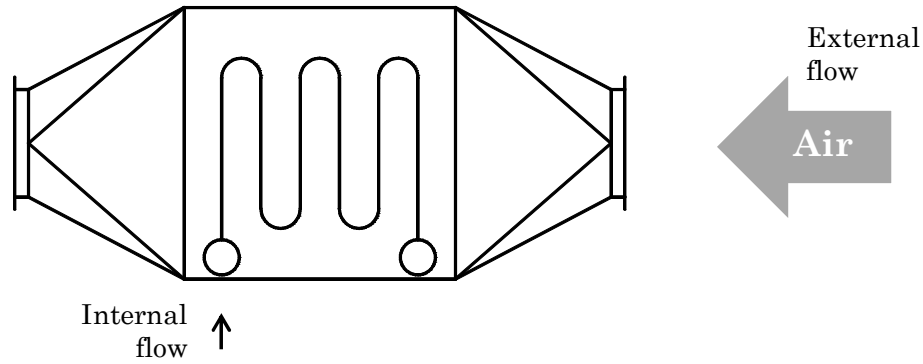
Fig. IV.4. *Recuperator, transversal view of tubes.*

The geometric parameters used to model the recuperator are collected in Table IV.1. This information has been obtained from the calculations and drawings of the recuperator manufacturer.

Table IV.1. *Characteristics of the recuperator.*

L_{tube}	Tube length (m)	1.0
L_M	Air inlet height (m)	0.54
N_{tube}	Number of tubes in direction of flow (-)	14
M_{tube}	Number of tubes in transverse flow direction (-)	8
D_{tube}	Tube size (")	1¼
D_{fin}	Fins diameter (mm)	57.7
t_{fin}	Fin thickness (mm)	1.3
FpM	Fins per meter (-)	200
S_L	Longitudinal pitch (mm)	67.0
S_T	Transverse pitch (mm)	67.0

3.1.1.2. Air-cooled condenser

The direct air-cooled condenser is the heat exchanger used to release the heat from the ORC unit to the ambient. It consists of a bank of finned tubes, in which the organic fluid condenses inside the tubes and the ambient air is blown across the tubes through axial-flow fans.

In particular, the device used consists of a horizontal unit with five fans in an induced-draft arrangement, which is schematized in Fig. IV.5.

The geometric parameters used for modeling are collected in Table IV.2. This information has been extracted from the calculations and drawings of the condenser manufacturer.
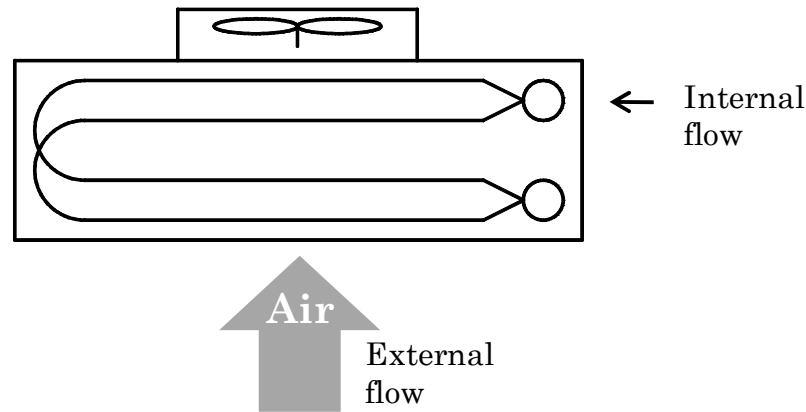
Fig. IV.5. *Induced-draft air-cooled condenser with two passes.*

Table IV.2. *Characteristics of the direct air-cooled condenser.*

L_{tube}	Tube length (m)	9.5
L_M	Air inlet height (m)	1.4
N_{tube}	Number of tubes in direction of flow (-)	4
M_{tube}	Number of tubes in transverse flow direction (-)	30
D_{tube}	Tube size (")	3/4
t_{fin}	Fin thickness (mm)	0.11
$Fin_{spacing}$	Fin spacing (mm)	2.20
S_L	Longitudinal pitch (mm)	25.0
S_T	Transverse pitch (mm)	50.0
N_{fans}	Number of fans	5
D_{fans}	Fans diameter (mm)	900
$W_{m_{fan}}$	Mechanical capacity per fan (kW)	0.22
$W_{e_{fan}}$	Electrical capacity per fan (kW)	0.45

3.1.2. Plate heat exchanger

A plate heat exchanger consists of several plates stacked forming multiple parallel channels. The most common type uses identical corrugated plates, which are pressed with a sinusoid like pattern [157].

This type of heat exchanger has improved its mechanical integrity and sealing aspects over the years, allowing its application in new areas [158]. Thus, the use of Brazed Plate Heat Exchangers (BPHEs) in ORC systems offers compactness, reducing refrigerant charge and leakages, but also allowing operating pressures above 30 bar [157].
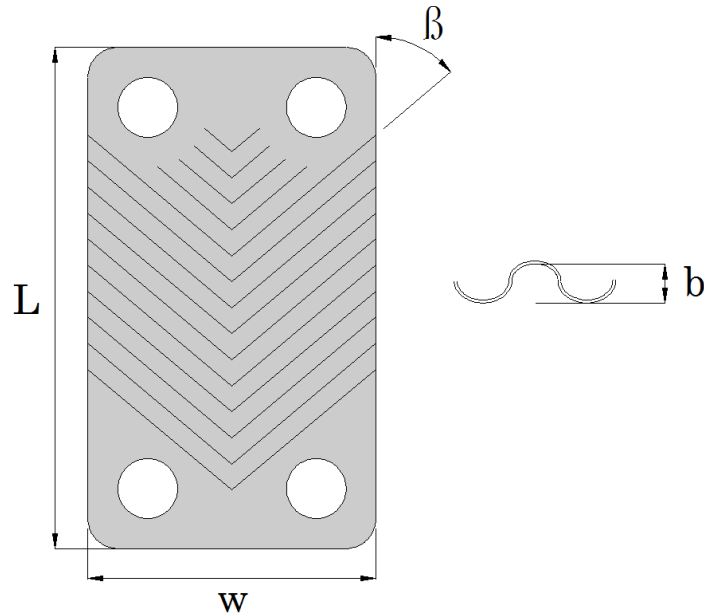
Fig. IV.6. *Plate geometric parameters of a BPHE.*

The geometry of the plates is directly related to the heat transfer performance. Thus, the main geometric parameters are described below.

- *Channels*

  The number of channels varies between inner and outer circuit. Specifically, the outer circuit has one more channel than the inner circuit. Therefore, the number of channels is defined as Eq. (1) and Eq. (2). It should be mentioned that, in the reference case, the inner circuit matches with the side of the cold fluid.

$$N_{\text{channels}_\text{o}} = \frac{N_{\text{plates}}}{2} \tag{1}$$

$$N_{\text{channels}_\text{i}} = \frac{N_{\text{plates}}}{2} - 1 \tag{2}$$

- *Heat transfer area*

  The heat transfer area is calculated as the dimension of a plate by the number of plates, discounting cover surfaces [159], such as Eq. (3) shows.

$$A = \left(N_{\text{plates}} - 2\right) \cdot L_{\text{plate}} \cdot w_{\text{plate}} \tag{3}$$

- *Chevron angle* (β)

  This angle is the half of the included angle of the corrugation pattern with the main flow direction, its value for all BPHEs used is about 40°. It establishes the thermal hydraulics softness (low thermal efficiency and low pressure drop) and hardness (high thermal

efficiency and high pressure drop) [158].

- *Pressing depth* (b)
  This parameter is defined as the actual gap available for the flow, whose value is 2.0 mm. It is represented along with other relevant nomenclature in Fig. IV.6.

- Plate thickness (t)
  The value of the thickness of the plates has been assumed as 0.2 mm.

- *Channel flow area*
  The cross flow sectional area is expressed as Eq. (4) [160].

$$A_c = b \cdot w_{plate} \tag{4}$$

- *Hydraulic diameter*
  The most common definition of hydraulic diameter, when the width of the channel is much larger than the pressing depth, is two times the pressing depth [161], as Eq. (5) shows.

$$D_h = 2 \cdot b \tag{5}$$

- *Mass flux*
  The mass flux per channel of a fluid is defined as Eq. (6).

$$G = \frac{\dot{m}}{N_{channels} \cdot A_c} \tag{6}$$

Different BPHEs are installed inside the module of the ORC. In the first place, the HRVG is composed by two BPHEs, denoted as economizer and evaporator. These heat exchangers are designed to operate with the organic fluid under different thermodynamic states, such as Fig. IV.7 shows. Thus, the economizer mostly works in the single phase (SP) region, transforming subcooled liquid into practically saturated liquid. This BPHE has a heat exchange surface of 1.62 m². The evaporator continuously works in the two-phase (TP) region to achieve saturated vapor, but also in the single phase region to feed the expander with superheated vapor. This BPHE has a heat exchange surface of 5.28 m². In addition, the regenerator mostly works in single phase region to exchange the sensible heat from the vapor side to the liquid side. This BPHE has a heat exchange surface of 12.9 m².
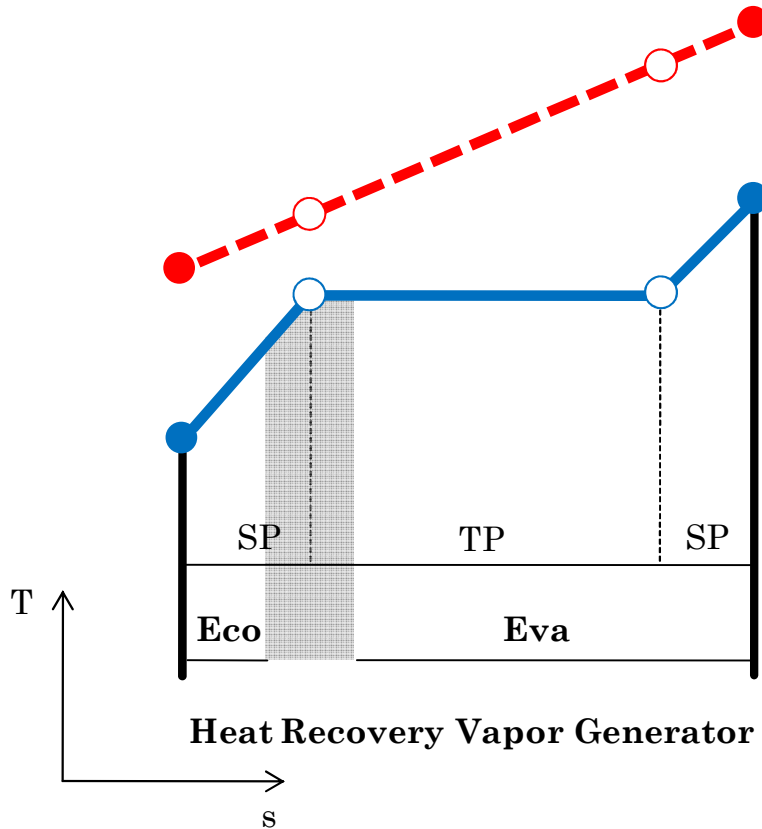
Fig. IV.7. *Heat transfer process between thermal oil and organic fluid represented in a temperature-entropy diagram.*

3.2.   Heat transfer fundamentals

The establishment of heat transfer fundamentals to a specific geometry of heat exchanger allows predicting its thermal performance. Therefore, the thermodynamic equations used are addressed below.

3.2.1. Analysis method

There are two methods for the analysis of heat exchangers: ε-NTU (effectiveness-Number of Transfer Units), and LMTD (Logarithmic Mean Temperature Difference), the last with the F factor when required. On the one hand, the ε-NTU is the recommended method to minimize the number of iterations in problems whose inputs and constructive characteristics are known [162]. On the other hand, the LMTD is the suggested method when different phases can cohabit in the same heat exchanger [163]. This effect is appreciable in the previous figure about the thermodynamic state between economizer and evaporator.

Taking this into account, the LMTD method is considered for the analysis of the heat exchangers that use the organic working fluid. Accordingly, the recuperator is modeled through the ε-NTU method.

3.2.1.1. LMTD

This method defines the thermal power as Eq. (7). In this expression, the LMTD represents the appropriate mean temperature difference between the fluids of the heat exchanger. In the case of the BPHEs analyzed, whose flow direction is countercurrent, the LMTD is expressed as Eq. (8). However, the condenser is a cross-flow heat exchanger. Therefore, this expression is corrected with the F factor of Eq. (9), which is calculated from Eq. (10) to Eq. (12) [164].

$$Q = U \cdot A \cdot LMTD \tag{7}$$

$$LMTD = \frac{\left(T_{h_i} - T_{c_o}\right) - \left(T_{h_o} - T_{c_i}\right)}{\ln\left(\dfrac{T_{h_i} - T_{c_o}}{T_{h_o} - T_{c_i}}\right)} \tag{8}$$

$$F = \frac{\ln\left(\dfrac{1 - R \cdot P_{un}}{1 - P_{un}}\right)}{NTU_{mx} \cdot \left(\dfrac{1}{R} - 1\right)} \tag{9}$$

$$NTU_{mx} = -R \cdot \ln\left(1 + \frac{\ln(1 - P_{un} \cdot R)}{R}\right) \tag{10}$$

$$P_{un} = \frac{T_{h_o} - T_{h_i}}{T_{c_i} - T_{h_i}} \tag{11}$$

$$R = \frac{T_{c_i} - T_{c_o}}{T_{h_o} - T_{h_i}} \tag{12}$$

3.2.1.2. ε-NTU

This method defines the thermal power in function of the maximum ideally reachable and the effectiveness of the heat transfer process, such as Eq. (13) expresses.

$$Q = \varepsilon \cdot Q_{max} \tag{13}$$

The maximum thermal power could ideally be transferred through a countercurrent heat exchanger with an infinite surface. In such heat exchange, one of the fluids experiences the maximum temperature difference, specifically the fluid with the lower thermal capacitance. Therefore, the maximum thermal power is defined as Eq. (14).

$$Q_{max} = C_{min} \cdot \left(T_{h_i} - T_{c_i} \right) \tag{14}$$

The effectiveness depends on the type of heat exchanger. But also depends on if the air, which is the mixed fluid, has the minimum, Eq. (15), or maximum, Eq. (16), thermal capacitance [162]. These expressions also use the capacitance ratio of Eq. (17), and the dimensionless parameter NTU of Eq. (18).

$$\varepsilon = 1 - \exp\left(-C_r^{-1} \cdot \left(1 - \exp\left(-C_r \cdot (NTU) \right) \right) \right) \tag{15}$$

$$\varepsilon = \frac{1}{C_r} \cdot \left(1 - \exp\left(-C_r \cdot \left(1 - \exp(-NTU) \right) \right) \right) \tag{16}$$

$$C_r = \frac{C_{min}}{C_{max}} \tag{17}$$

$$NTU = \frac{U \cdot A}{C_{min}} \tag{18}$$

3.2.2. Overall heat transfer coefficient

The overall heat transfer coefficient is related to the thermal resistance of the heat exchanger between the hot and the cold fluid. This coefficient is defined as Eq. (19).

$$U = \frac{1}{A \cdot R_{total}} \tag{19}$$

The total thermal resistance of the heat transfer process is the sum of the individual resistances, such as Eq. (20) shows [162].

$$R_{total} = R_{conv_c} + R_{w_c} + R_{cond} + R_{w_h} + R_{conv_h} \tag{20}$$

In a general form, the thermal resistance due to convection is defined as Eq. (21). For the case of external flow of a finned tube bank, the convective area also takes into account surface and efficiency of the fins, such as Eq. (22) shows.

Fins efficiency of annular type is calculated from Eq. (23), using Bessel functions, to Eq. (25) [165]. This is the type of fins used by the recuperator. For its part, the condenser uses a plate type of fins with multiple rows in a staggered tube arrangement, which can also be treated as equivalent annular type through the correlations from Eq. (26) to Eq. (28) [166].

$$R_{conv} = \frac{1}{h_{conv} \cdot A_{conv}} \tag{21}$$

$$A_{conv_{eq}} = A_{free\,of\,fins} + A_{fins} \cdot \eta_{fins} \tag{22}$$

$$\eta_{fin} = C_{fin} \cdot \frac{K_1(m_{fin} \cdot r_o) \cdot I_1(m_{fin} \cdot r_{fin}) - I_1(m_{fin} \cdot r_o) \cdot K_1(m_{fin} \cdot r_{fin})}{I_0(m_{fin} \cdot r_o) \cdot K_1(m_{fin} \cdot r_{fin}) + K_0(m_{fin} \cdot r_o) \cdot I_1(m_{fin} \cdot r_{fin})} \tag{23}$$

$$C_{fin} = \frac{D_o / m_{fin}}{r_{fin}^2 - r_o^2} \tag{24}$$

$$m_{fin} = \sqrt{2 \cdot \frac{h_{conv}}{k_{fin} \cdot t_{fin}}} \tag{25}$$

$$r_{fin} = r_o \cdot \left(1.27 \cdot \psi \cdot \sqrt{\beta - 0.3}\right) \tag{26}$$

$$\psi = \frac{S_L}{r_o} \tag{27}$$

$$\beta = \frac{\sqrt{\left(\frac{S_T}{2}\right)^2 + S_L^2}}{2 \cdot S_L} \tag{28}$$

The thermal resistance due to conduction depends on the geometry and the thermal conductivity of the materials. For cylindrical tube walls the expression of Eq. (29) is used. For the plane walls of BPHEs, the resistance is defined as Eq. (30). Regarding the thermal conductivity of materials, Table IV.3 collects values obtained from the literature [167].

$$R_{cond} = \frac{\ln(D_o / D_i)}{2 \cdot \pi \cdot L \cdot k} \tag{29}$$

$$R_{cond} = \frac{t}{k \cdot A} \tag{30}$$

The fouling factor is the thermal resistance due to a build-up of a layer of dirt, or other fouling substance, on tubes and fins surfaces. Typical values for thermal oil and organic fluids are obtained from the literature [168], whilst values for air are directly extracted from the software database [62].

Table IV.3. *Thermal conductivity of materials.*

Component	Material	Conductivity (W/m ·K)
Tube and fins of recuperator	Carbon steel	60
Tubes of condenser	Copper	400
Fins of condenser	Aluminum	240
Plates of BPHE	Stainless steel	16.2

3.2.3. Convection coefficients

The convection coefficient is defined in terms of Nusselt number, thermal conductivity of a fluid, and characteristic length by Eq. (31).

$$h_{conv} = \frac{Nu \cdot k}{D_h} \tag{31}$$

The Nusselt number is a dimensionless parameter that represents the ratio of convective to conductive heat transfer. The expressions of the Nusselt number have been obtained from empirical correlations widely used in the literature. Thus, the different correlations implemented in the model are exposed below.

3.2.3.1. External flow correlation in tube bank

With regard to the air side of the recuperator, Eq. (32) was proposed by Zukauskas [169] to know the average heat transfer coefficient of the entire tube bank. The coefficients shown in the equation are given for the aligned tube rows arrangement in accordance with the operating conditions of the recuperator [162]. This correlation is valid for the range of $0.7 < Pr < 500$ and $1x10^3 < Re < 2x10^6$.

The heat transfer on the air side of the condenser can be characterized through the correlation of Briggs and Young, shown in Eq. (33). This correlation has been extensively used for the flow of cooling air across triangular pitch banks of finned tubes [170]. It is valid for the range of $1x10^3 < Re < 18x10^3$.

$$Nu = 0.27 \cdot Re_{max}^{0.63} \cdot Pr^{0.36} \cdot \left(\frac{Pr}{Pr_s} \right)^{0.25} \cdot 0.96 \tag{32}$$

$$Nu = 0.134 \cdot Re_{max}^{0.681} \cdot Pr^{1/3} \cdot \left(\frac{r_{fin} - r_o}{Fin_{spacing}} \right)^{-0.2} \cdot \left(\frac{t_{fin}}{Fin_{spacing}} \right)^{-0.1134} \tag{33}$$

The Reynolds number is a dimensionless parameter that expresses the ratio between inertial and viscous resistances of a flowing fluid. A general definition, in function of the hydraulic diameter as equivalent length, is shown in Eq. (34).

$$Re = \frac{v \cdot \rho \cdot D_h}{\mu} \tag{34}$$

The velocity of the air entering into the tube bank is calculated by Eq. (35). However, for the case of external flow in tube bank, the velocity that is used in the Reynolds number calculation refers to the maximum reachable. The maximum velocity for the aligned arrangement, as the case of the recuperator, is defined by Eq. (36), while the velocity for staggered arrangement, as the case of the condenser, is obtained as the maximum between Eq. (36) and Eq. (37). The diagonal pitch is calculated as Eq. (38) [162].

$$v_{face} = \frac{\dot{V}}{L_{tube} \cdot L_M} \tag{35}$$

$$v = \frac{S_T}{S_T - D_o} \cdot v_{face} \tag{36}$$

$$v = \frac{S_T}{2 \cdot (S_D - D_o)} \cdot v_{face} \tag{37}$$

$$S_D = \sqrt{S_L{}^2 + \left(\frac{S_T}{2}\right)^2} \tag{38}$$

3.2.3.2. Internal flow correlation in tubes

Two types of correlations of internal flow in tubes are required. Firstly, a single phase correlation for the thermal oil that flows through the tubes of the recuperator. And secondly, a two-phase correlation for the organic fluid that condenses inside the tubes of the direct air-cooled condenser.

The correlation of Gnielinski [162], Eq. (39) has demonstrated a suited accuracy in a wide range of conditions. Therofer, it is implemented to characterize the thermal oil performance in the recuperator. The friction factor for smooth tubes is obtained through Eq. (40). The correlation is valid for the range of $0.5 < Pr < 2000$ and $3000 < Re < 5 \times 10^6$.

$$Nu = \frac{\frac{f}{8} \cdot (Re - 1000) \cdot Pr}{1 + 12.7 \cdot \left(\frac{f}{8}\right)^{0.5} \cdot \left(Pr^{2/3} - 1\right)} \tag{39}$$

$$f = \frac{1}{\left(0.79 \cdot \ln(Re) - 1.64\right)^2} \tag{40}$$

The characteristics of the heat transfer mechanisms for condensation can be directly explained by the Akers *et al.* correlation [171], presented in Eq. (41). The equation of the velocity to calculate the Reynolds number is given by Eq. (42). The correlation is valid for Re < 5x10^4 [172].

$$h = 5.03 \cdot Pr^{\frac{1}{3}} \cdot Re_l^{\frac{1}{3}} \cdot \frac{k}{D_i} \cdot \left(\frac{\chi}{1 - \chi} \cdot \left(\frac{\rho_l}{\rho_v}\right)^{0.5} + 1 \right) \tag{41}$$

$$v = \frac{4 \cdot \dot{m}}{\left(\frac{N}{2} \cdot M\right) \cdot \left(\pi \cdot \rho_o \cdot D_i^2\right)} \tag{42}$$

3.2.3.3. Correlation in plates

Two types of Nusselt correlations are required to characterize the performance of BPHEs in single phase and two-phase regions.

The single phase correlation is used to model the economizer, regenerator, and the superheating part of the evaporator. The Eq. (43) was proposed by Sekhar V. [173] to model commercial BPHEs. The coefficients of the correlation are described in Eq. (44) [174] and Table IV.4. It should be noted that this correlation uses the Chevron angle in radians, and it is validated for the application range of 10 < Re < 1x10^4. In this case, the velocity used to calculate the Reynolds number is obtained from Eq. (45).

$$\frac{Nu}{Pr^y} = \left(C_0 + C_1 \cdot \beta + C_2 \cdot \beta^2\right) \cdot Re_c^{K_0 + K_1 \cdot \beta} + \left(C_3 + C_4 \cdot \beta + C_5 \cdot \beta^2\right) \cdot Re_c^{K_2 \cdot \beta} + C_6 \tag{43}$$

$$y = \frac{1}{3} \cdot \exp\left(\frac{6.4}{Pr + 30}\right) \tag{44}$$

$$v = \frac{\dot{m}}{N_{channels} \cdot \rho \cdot A_c} \tag{45}$$

Table IV.4. *Coefficients of single phase correlation for BPHEs. (Source: Ref.* [174]*)*

C_0	0.236853827	C_5	0.236667683
C_1	-0.429914999	C_6	0.599681567
C_2	0.194375018	K_0	-0.284829132
C_3	0.146176215	K_1	0.696216086
C_4	-0.147253283	K_2	1.120898786

The two-phase correlation is used for the evaporation process of the organic fluid. Dong *et al.* [175] proposed Eq. (46) for working fluids of ORC systems. The equivalent Reynolds number, two-phase mass flux, and Boiling number are defined from Eq. (47) to Eq. (49), respectively [174]. This correlation is valid for the range of $250 < Re < 2.5 \times 10^3$.

$$\mathrm{Nu} = 2.64 \cdot \mathrm{Re_{eq}}^{0.815} \cdot \mathrm{Pr_l}^{0.333} \cdot \mathrm{Bo_{eq}}^{0.343} \tag{46}$$

$$\mathrm{Re_{eq}} = \mathrm{G_{eq}} \cdot \frac{\mathrm{D_h}}{\mu_l} \tag{47}$$

$$\mathrm{G_{eq}} = \mathrm{G} \cdot \left(1 - \chi + \chi \cdot \left(\frac{\rho_l}{\rho_v} \right)^{0.5} \right) \tag{48}$$

$$\mathrm{Bo_{eq}} = \frac{\mathrm{Q}}{\mathrm{N_{channels}} \cdot \mathrm{A} \cdot \mathrm{G_{eq}} \cdot (\mathrm{h_v} - \mathrm{h_l})} \tag{49}$$

3.2.4. Pressure drops

The correlations implemented in sub-models of heat exchangers for the pressure drop characterization are defined as follows.

3.2.4.1. External flow correlation in tube bank

A widely used correlation for the pressure drop across a bank of tubes was given by Zhukauskas in the form of Eq. (50) [176]. Kay and London proposed Eq. (51) as friction factor correlation of a finned tubes bank with aligned rows [177]. These expressions are used to characterize the pressure drop caused in the exhaust air side of the recuperator.

$$\Delta \mathrm{P} = 4 \cdot \mathrm{f} \cdot \mathrm{N_{tube}} \cdot \left(\frac{\rho \cdot \mathrm{v}^2}{2} \right) \cdot 1 \times 10^{-5} \tag{50}$$

$$f = \left(0.44 + \frac{0.08 \cdot \dfrac{S_L}{D_o}}{\dfrac{S_T - D_o}{D_o^{\left(0.43 + 1.13 \cdot \frac{D_o}{S_T}\right)}}} \right) \cdot Re^{-0.15} \tag{51}$$

The pressure drop of the ambient air side of the condenser can be characterized through Eq. (52), which is the correlation for staggered tube arrangement proposed by Robinson and Briggs [178].

$$\Delta P = \left(18.93 \cdot Re^{-0.316} \cdot \left(\frac{S_T}{D_o}\right)^{-0.927} \cdot \left(\frac{S_T}{S_D}\right)^{0.515} \cdot N_{tube} \right) \cdot \frac{\rho \cdot v_{max}^2}{1 \times 10^5} \tag{52}$$

3.2.4.2. Internal flow correlation in tubes

The pressure drop of the thermal oil side in the recuperator is characterized as a fully developed turbulent flow in tubes. Therefore, it can be expressed by Eq. (53) of Darcy-Weisbach in terms of equivalent length. It should be mentioned that the value of the equivalent length is obtained by considering the total tube length and the number of bends [179].

$$\Delta P = \frac{f \cdot L_{eq} \cdot v^2}{2 \cdot g \cdot D_i \cdot 10.2} \tag{53}$$

A generalized correlation for pressure drop during condensation was proposed by Kedzierski, such as Eq. (54) shows [180]. The two-phase friction factor used is defined in Eq. (55).

$$\Delta P = \left(f \cdot L_{eq} \cdot \frac{1/\rho_1 + 1/\rho_v}{D_i} + \left(1/\rho_v - 1/\rho_1\right) \right) \cdot G^2 \cdot 1 \times 10^{-5} \tag{54}$$

$$f = 0.00506 \cdot Re_1^{-0.0951} \cdot \left(\chi \cdot \frac{h_{lv}}{L_{eq} \cdot g} \right)^{0.1554} \tag{55}$$

3.2.4.3. Correlation in plates

The total pressure drop of a BPHE is calculated taking into account ports, static or gravity effect, and frictional pressure drops. Due to the greater significance of the frictional effect [157], the remainder pressure drops have been neglected in the calculations. Consequently, the expression of Eq. (56) is used.

The friction factor depends on the type of fluid. Therefore, for working fluids typically used in ORC systems the Eq. (57) can be used [181]. For more common fluids, like thermal oils, expressions with a widely demonstrated experience can be used. Thus, the Eq. (58) proposed by Thonon [182] is implemented, which is valid for Reynolds values upper 200.

$$\Delta P_f = \left(\frac{2 \cdot L_{plate} \cdot G^2 \cdot f}{D_h \cdot \rho} \right) \cdot 1 \times 10^{-5} \tag{56}$$

$$f = 1\,285 \cdot Re^{-1.25} + 1.73 \tag{57}$$

$$f = 0.6857 \cdot Re^{\,0.172} \tag{58}$$

In the case of two-phase heat exchangers, the correlation also includes the momentum pressure drop, as can be seen in Eq. (59) and Eq. (60). This energy loss takes into consideration the acceleration of the flow due to the increasing vapor quality from the inlet to the outlet of the channel. In this case, the frictional pressure drop is calculated using the two-phase density of Eq. (61) and the Fanning friction factor of Eq. (62) [183].

$$\Delta P = \left(\Delta P_{mom} + \Delta P_f \right) \cdot 1 \times 10^{-5} \tag{59}$$

$$\Delta P_{mom} = G^2 \cdot \left(\frac{1}{\rho_v} - \frac{1}{\rho_l} \right) \tag{60}$$

$$\rho_{tp} = \left(\frac{\chi}{\rho_v} + \frac{1-\chi}{\rho_l} \right)^{-1} \tag{61}$$

$$f = 15.08 \cdot Re_{eq}^{-0.467} \tag{62}$$

3.3. Preliminary validation

Taking into account that heat exchangers are modeled from known geometric characteristics, there is not required a subsequent calibration of any parameter. So a preliminary comparison between simulations and calculations of the respective heat exchangers manufacturers can be used to check the results deviation with respect to initial estimations. For that, simulations from the inputs used during the design stage are conducted. The results referred to thermal capacity, and pressure drops in hot and cold fluids are collected in Table IV.5. In the first place, it should be mentioned that all heat exchangers operate within the valid range of the correlations

proposed. Moreover, a minimum deviation in thermal power transferred and pressure drops caused is observed, which confirms the suitability of the proposed sub-models of heat exchangers.

Table IV.5. *Heat transfer and pressure drop comparisons in the recuperator.*

	Manufacturer information			Sub-model proposed		
	Q (kW)	ΔP_h (bar)	ΔP_c (bar)	Q (kW)	ΔP_h (bar)	ΔP_c (bar)
Recuperator	177.4	19.6E-4	0.80	178.9	17.7E-4	0.82
Condenser	157.9	0.22	-	156.7	0.21	1.6E-4
Economizer	86.36	0.473	0.029	86.02	0.513	0.026
Evaporator	66.91	0.31	0.1	65.84	0.44	0.06
Regenerator	56.93	0.346	0.0045	57.38	0.495	0.0056

4. FLUID MACHINES

This section addresses sub-models of fluid machines from the geometric characteristics description and the establishment of thermodynamic fundamentals.

4.1. Expander

The main geometric characteristics of the expander and the equations used to characterize its performance are defined as follows.

4.1.1. Geometry

The expansion technology used in this application is classified as a volumetric or positive displacement rotary machine. Specifically, it is a twin screw expander, which is characterized by a swept volume of 22.2 m^3/h and a built-in volume ratio of 5.5.

4.1.2. Thermodynamics

An ideal thermodynamic process of expansion is an isentropic transformation. Thus, actual expansion processes can be treated by considering the irreversibilities that appear during this ideal transformation.

Taking this into account, an equivalent expander considering the main energy losses occurred during an ideal expansion process is proposed. This system is depicted in the Fig. IV.8, which distinguishes between internal and external energy losses with respect to the limits of the expander.

Some assumptions have been considered in the equations definition.

- Similar to heat exchangers, the kinematic and potential energies are small relative to enthalpy energies and can be neglected [184].
- Heat losses between expander and ambient are neglected, since the expander is completely insulated.
- As commonly is assumed in models of ORC systems, the influence of the lubricating system over the performance ratios is considered negligible [185].
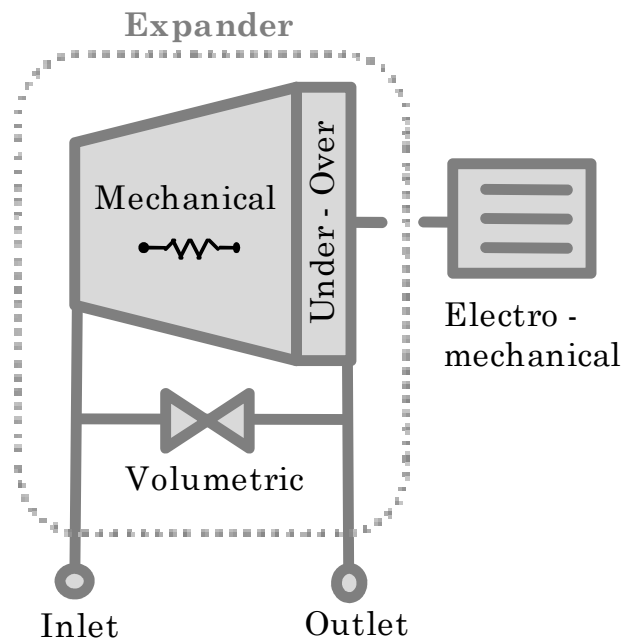
Fig. IV.8. *Equivalent expander and energy losses.*

4.1.2.1. Internal energy losses

All internal energy losses can be lumped in a single performance ratio denoted as isentropic efficiency, which is defined by Eq. (63).

$$\eta_{ise} = \frac{h_i - h_o}{h_i - h_{o\,ise}} \tag{63}$$

However, this efficiency is a consequence of other internal performance ratios that depend on geometric parameters and, hence, can be independently modeled to improve the accuracy of the results [186].

- *Volumetric efficiency*
  One of the most relevant performance ratios is the volumetric efficiency, which is referred to internal leakages due to rotors and wall tolerances. This efficiency can be treated as a unique fictitious leakage path connecting the expander supply and exhaust [187]. It

can be calculated as the relationship between the swept volume and the measured volumetric flow rate at the inlet port of the expander, as Eq. (64) expresses. It can also be calculated inversely, which is denoted as filling factor [188].

$$\eta_v = \frac{\dot{V}_{swept}}{\dot{V}_i} \tag{64}$$

- *Under and over-expansion efficiency*

  The built-in volume ratio is a geometric parameter defined as the relationship between discharge and swept volumes, such as Eq. (65) shows, whose value establishes the optimum expansion ratio. Thereby, an off-design operation is considered an internal energy loss that can be quantified [189].

  The effect of this energy loss is illustrated in Fig. IV.9. When the optimum expansion ratio is lower than the imposed by the system, the expander operates in under-expansion. On the other hand, if the optimum expansion ratio is higher than the imposed by the system, the expander operates in over-expansion.
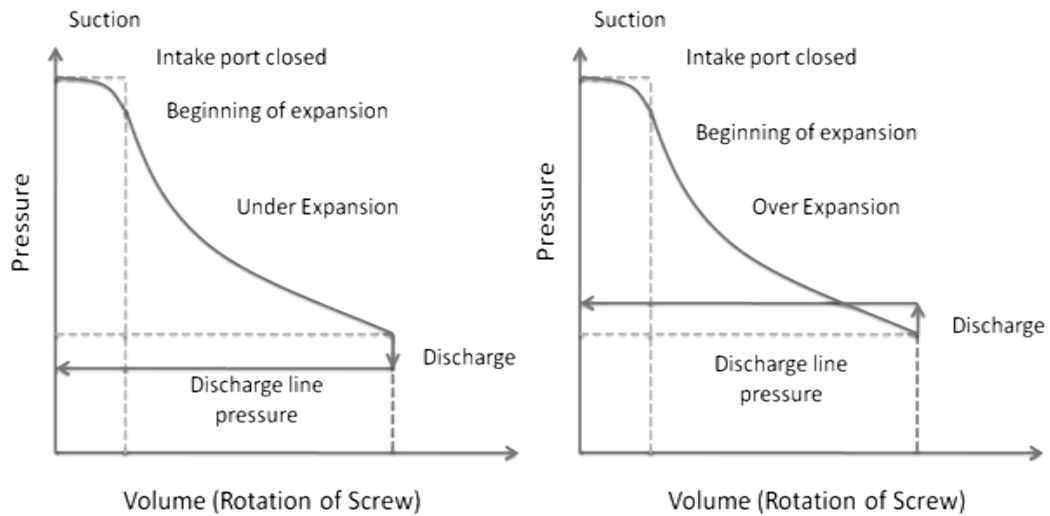
Fig. IV.9. *Under and over expansion losses in a twin screw expander. (Source: Ref. [190])*

This efficiency is usually modeled as an isentropic expansion at the optimum ratio, along with an adiabatic expansion at constant volume, which is defined as Eq. (66) [187].

$$V_r = \frac{\dot{V}_{discharge}}{\dot{V}_{swept}} \tag{65}$$

$$\eta_{UnderOver} = \frac{\left(h_i - h_{V_r}\right) + 100/\rho_{V_r} \cdot \left(P_{V_r} - P_o\right)}{h_i - h_{o_{ise}}} \tag{66}$$

- *Mechanical efficiency*

  Mechanical losses are due to friction between moving elements, like screws or bearings, and internal pressure drops. The value of the mechanical efficiency depends on the specific expander and its operating conditions. So in order to achieve a suitable accuracy, this efficiency should be calibrated from steady-state points.

  Nonetheless, it is demonstrated that geometric characteristics limit the maximum efficiency reachable by an expander. Thus, the higher the discharge volume and the lower the built-in volume ratio, the higher is the expander efficiency. This fact was pointed by Astolfi [191], who presented a map of the maximum efficiency achieved by commercial screw machines, shown in Fig. IV.10, and proposed the regression of Eq. (67).

  Taking this into account, and in order to conduct a system optimization, the correction factor of Eq. (68) is considered. Thereby, the model is turned into a flexible tool able to extrapolate the results to different expander geometries.

$$\eta_{max} = 0.9403305 + 0.0293295 \cdot \ln\left(V_{discharge}\right) - 0.0266298 \cdot V_r \tag{67}$$

$$Fc = \frac{\eta_{max}}{\eta_{reference}} \tag{68}$$

With regard to the enthalpies calculation, the internal enthalpy at the outlet port of the equivalent expander is obtained as Eq. (69), and the enthalpy at the actual outlet can be calculated by Eq. (70).

$$h_{o_{eq}} = h_i - \left(Fc \cdot \eta_m \cdot \eta_{UnderOver} \cdot \left(h_i - h_{o_{ise}}\right)\right) \tag{69}$$

$$h_o = \left(1 - \eta_v\right) \cdot h_i + \eta_v \cdot h_{o_{eq}} \tag{70}$$
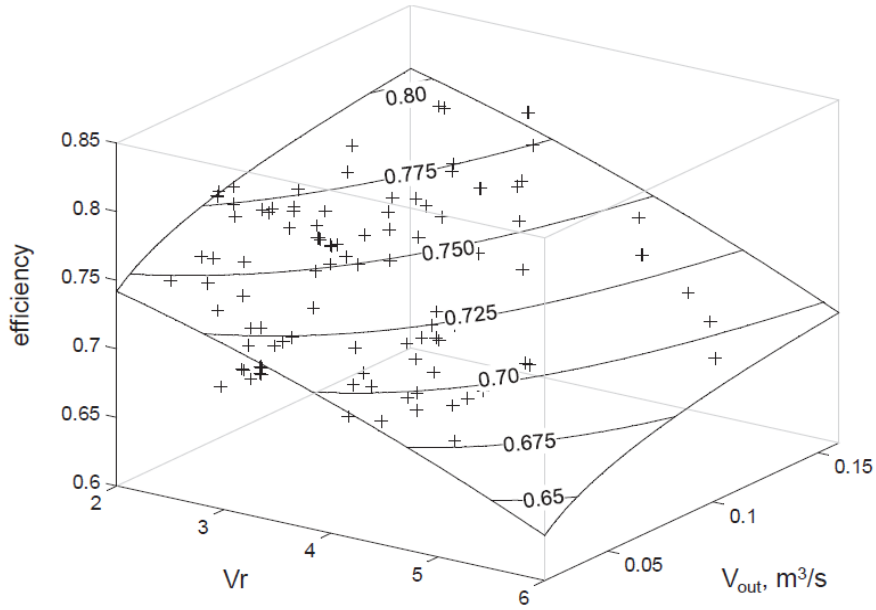
Fig. IV.10. *Maximum efficiency of commercial screw machines. (Source: Ref.* [191]*)*

4.1.2.2. External energy losses

There are more energy losses that reduce the electrical power output. In this way, it can be highlighted mechanical losses due to the coupling between the shafts of expander and alternator, besides electrical losses in the conversion from mechanical to electrical power. Both, mechanical and electrical, losses can be considered in a single performance ratio, which is denoted as electro-mechanical efficiency. This efficiency is defined as Eq. (71), which should be calibrated from the steady-state points to improve the model accuracy.

$$\eta_{em} = \frac{W_g}{\dot{m} \cdot \left(h_i - h_o \right)} \tag{71}$$

4.2. Pumps

Two pumps are used in the system. Firstly, the feed pump of the ORC is used to pressurize the organic liquid up to the maximum pressure of the cycle. And secondly, a thermal oil pump is used in the heat transfer loop to impel the liquid within the closed circuit.

Focusing on the sub-model of the feed pump, just one parameter remains to be calculated. It should be noted that the mass flow rate of the organic fluid mainly depends on the sub-model of the expander. The discharge pressure of the pump is imposed by the balance in the HRVG, besides pressure drops. The suction conditions at the admission of the pump are also imposed by the sub-model of the condenser and the static pressure supplied by the receiver. So only the electrical consumption is required. For this calculation, a

simplified method is commonly used [192]. It consists of using Eq. (72) in function of an overall performance ratio, that can also be extracted from the experimental data.

$$W_p = \frac{\dot{m} \cdot \left(h_{o\,ise} - h_i \right)}{\eta_p} \tag{72}$$

Similarly, the electrical power consumed by the thermal oil pump is also required. If the thermal oil is considered as an incompressible fluid, the electrical consumption of the pump can be defined as Eq. (73). This expression considers the pressure drop related to the recuperator, BPHEs of the HRVG and piping length of the thermal oil circuit, as well as an overall performance ratio experimentally obtained.

$$W_{oil\,p} = \frac{\dot{V} \cdot \left(\Delta P \cdot 100 \right)}{\eta_{oil\,p}} \tag{73}$$

4.3.   Fans

The condenser is equipped with five axial flow fans that impel ambient air to the ORC unit. These fans, in turn, use a variable speed drive to allow the air flow variation and, hence, condensing temperature regulation.

The electrical energy consumption of the condenser can be expressed as Eq. (74). For that, the same mechanical efficiency at full and partial loads is assumed, that can be obtained from Eq. (75). However, it should be highlighted that fans operate at widely varying loads, which means that the electrical efficiency is highly dependent on the capacity ratio. In this topic focused Chirakalwasan, who proposed a method for the electrical efficiency at partial loads calculation [193]. Thus, that performance ratio can be expressed by Eq. (76), in function of electrical efficiency at full load, mechanical capacity ratio and a correction factor related to current losses. In this way, the electrical efficiency at full load is obtained from the information given by the manufacturer by Eq. (77). Moreover, the mechanical capacity ratio is obtained from the operating and rated conditions by Eq. (78).

$$W_{cond} = \frac{\dot{V} \cdot \left(\Delta P \cdot 100 \right)}{\eta_{m\,pl} \cdot \eta_{e\,pl}} \tag{74}$$

$$\eta_{m\,pl} = \frac{\dot{V}_{rated} \cdot \left(\Delta P_{rated} \cdot 100 \right)}{W_{m\,fan} \cdot N_{fans}} \tag{75}$$

$$\eta_{e\,pl} = \frac{\chi_m}{\chi_m + \left(\dfrac{1}{\eta_{e\,fl}} - 1\right) \cdot \left((1 - Fc) + Fc \cdot \left(\chi_m \cdot \dfrac{\eta_{e\,fl}}{\eta_{e\,pl}}\right)^2\right)} \tag{76}$$

$$\eta_{e\,fl} = \frac{W_{m\,fan}}{W_{e\,fan}} \tag{77}$$

$$\chi_m = \frac{\dot{V} \cdot (\Delta P \cdot 100)}{\dot{V}_{rated} \cdot (\Delta P_{rated} \cdot 100)} \tag{78}$$

The partial load calculations are rarely presented in ORC publications. Thus, in order to check the curve that draws the above expressions, an example has been plotted in Fig. IV.11. The correction factor due to current losses is set to 70% in this figure, which is a typical magnitude order value [193]. However, this value requires being experimentally obtained.
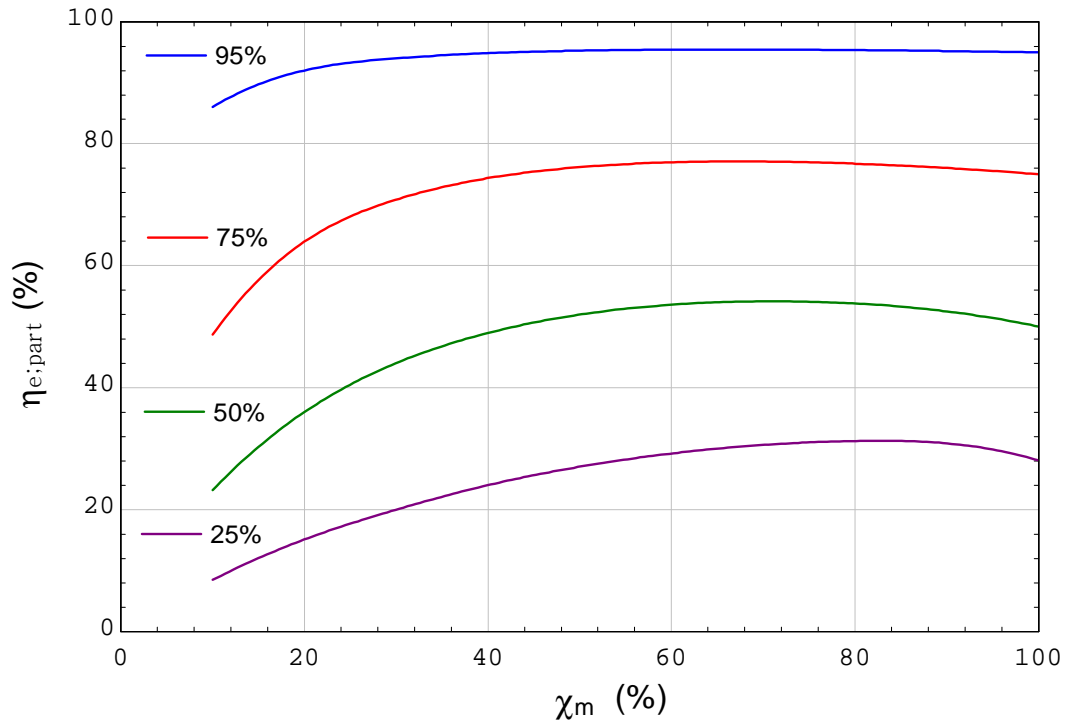
Fig. IV.11. *Electrical efficiency at part loads in function of maximum electrical efficiency and mechanical capacity ratio.*

From these expressions, the electrical power required by the condenser to achieve design conditions used in Table IV.5 is quantified as 2.24 kW. This value is very close to the 2.19 kW provided by the manufacturer. Thus, the validity of these expressions and the previous correlations for the electrical consumption estimation at full load is confirmed.

4.4. Blower

As it was previously mentioned, the recuperator is a heat exchanger installed in the industrial process. Specifically, it is integrated into a new duct that bypasses the original duct of the facility. Both ducts have the same diameter, length, and elbows number. Thus, the additional pressure drop can directly be assigned to the bank of tubes of the recuperator.

Taking this into account, the increase of electrical power required by the industrial blower to overcome the pressure drop introduced by the recuperator can be calculated through the expression of Eq. (79). In this case, the overall efficiency is considered 75%, which is a typical value associated with full load operation [194].

$$W_{blower} = \frac{\dot{V} \cdot (\Delta P \cdot 100)}{\eta_{overall}}$$
(79)

5. AUXILIARY COMPONENTS

This section pays attention to other essential components that help to achieve an operating system.

5.1. Piping and fittings

Piping and fittings connect the above components. The use of these connectors slightly modifies the operating conditions of a process, due to heat losses and pressure drops caused.

5.1.1. Heat losses

The main components of the facility are thermally insulated. However, there are some auxiliary components without insulation whose energy losses should be considered. In this way, Chapter III showed that heat losses occur between the recuperator and the ORC unit. This thermal power difference is explained by the heat losses caused in the about 4 m of the thermal oil circuit located inside of the factory that, contrary to the remaining piping, are not insulated. Similarly, there is a pipe in the circuit of the organic fluid that does not use insulation. Specifically, it is the receiver, whose heat losses to the ambient are considered useful to increase the subcooling degree at the suction line of the feed pump.

Taking this into account, heat losses caused in the components without insulation are characterized as follows.

Similar to the LMTD method, the heat losses calculation also use the overall heat transfer coefficient, such as Eq. (80) shows. Nonetheless, the

temperature variation due to heat losses is much lower compared to that of heat exchangers. Therefore, the temperature difference is expressed through Newton's law of cooling [162]. Notice that the temperature of the cold fluid usually refers to the ambient. However, with regard to heat losses occurred inside of the factory, this temperature corresponds to the furnace surroundings, which usually varies around 40 ºC and, hence, it has been assumed as a constant value.

The methodology for heat transfers characterization is the same than the used with heat exchangers. The expression of Gnielinski for internal flow correlation in tubes is used. On the other hand, referred to the cold fluid, free convection correlations in cylinders are required. Thus, the Nusselt number of Eq. (81) is used for the horizontal pipe of the thermal oil circuit, and Eq. (82) is used for the vertical receiver [162]. The Grashof number is calculated as Eq. (83) in function of the characteristic length in each case.

$$Q_{loss} = U \cdot A \cdot \Delta T \tag{80}$$

$$Nu = 0.125 \cdot \left(Pr \cdot Gr \right)^{1/3} \tag{81}$$

$$Nu = 0.1 \cdot \left(Pr \cdot Gr \right)^{1/3} \tag{82}$$

$$Gr = \frac{g \cdot \beta \cdot \left(T_s - T_{ambient} \right) \cdot L^3}{\left(\mu / \rho \right)^2} \tag{83}$$

5.1.2. Pressure drops

Auxiliary components also introduce an additional pressure drop in each point of the system, which slightly modifies the operating conditions. This pressure drop can be calculated through the previously presented internal flow correlation in tubes of Darcy-Weisbach.

To do this, some assumptions are taken. Thus, since there are not pressure transmitters in each section of the ORC unit, the calibration of individual pressure drops is not possible. Therefore, equivalent pressure drops are considered at the discharge line of the feed pump and at the inlet line of the condenser, which will be calibrated in next Chapter. Moreover, pressure drops of receiver and pipes of the thermal oil circuit are also taken into account through their characteristic length.

5.2. Receiver

The receiver is a tank that collects the liquid that leaves from the condenser. Typically, models of condensers next to receivers consider liquid leaving at saturated conditions [195]. This assumption is also considered in this study.

Nonetheless, it is known that the pump operates with a minimum net positive suction head that avoids the cavitation [80]. Accordingly, the output conditions of the receiver can be modeled considering the liquid height that ensures the static pressure and the heat losses that contributes to the subcooling degree, such as Fig. IV.12 represents.

The output pressure of the receiver is calculated as the pressure that leaves from the condenser, plus the static pressure provided by the liquid height, minus the pressure drop caused, such as Eq. (84) and Eq. (85) show.

The output enthalpy also depends on the liquid height, which was set during the start up, and the thermal energy losses to the ambient. So Eq. (86) is used.

$$P_o = P_i + P_{static} - \Delta P \tag{84}$$

$$P_{static} = \frac{L \cdot g \cdot \rho}{100\,000} \tag{85}$$

$$h_o = h_i + \frac{g \cdot L}{1000} - \frac{Q_{loss}}{\dot{m}_{wf}} \tag{86}$$
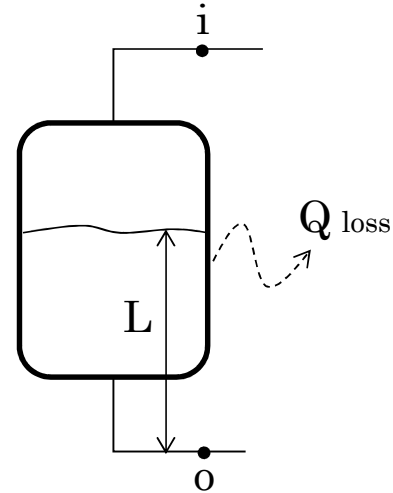
Fig. IV.12. *Schematic of receiver.*

5.3. Control strategy

The control strategy operated by the ORC is also implemented in the model since the goal is to reproduce the performance of the facility. Furthermore, the electrical energy consumption for its operation is also considered in the net electricity calculation.

Firstly, to ensure superheated vapor state at the inlet port of the expander, the superheating degree is controlled. Specifically, a PID (Proportional-Integral-Derivative) controller minimizes the error between measured

superheating degree and the set point value of 35 K implemented in the system.

Secondly, the condensing temperature is also regulated. In particular, a PID controller maintains a fixed difference between condensing and ambient temperatures. The predefined set point value implemented in the controller of the condenser is 25 K.

It should be mentioned that there are not more control devices in the system. For instance, the thermal oil pump and the blower of the industrial process operate at constant speed.

6.   ECONOMIC EQUATIONS

This section addresses economic equations, which are referred to the cost correlations required by the model to conduct the thermo-economic optimization, and economic ratios for the analysis of the project feasibility.

6.1.   Cost correlations

Due to the confidential character of the costs of the components used in commercial ORC systems, thermo-economic assessments are usually based on reported correlations. In this way, cost correlations for small-scale ORC systems have been selected from the literature, but also have been internally checked to ensure that are within the magnitude order of actual costs of the reference case.

6.1.1. ORC unit

The cost correlation of Eq. (87) was reported for commercial screw machines [191]. This correlation is given in U.S. dollars, so an average exchange ratio to Euro of 0.94 is introduced in the equation [196]. Moreover, the cost of the alternator used to produce electricity is correlated from the rated electrical power by Eq. (88) [197].

$$C_{screw} = \left(3143.7 + 217\,423 \cdot \dot{V}_{discharge} \right) \cdot R_{USD} \tag{87}$$

$$C_{alternator} = 2x10^5 \cdot \left(\frac{W_e}{5000} \right)^{0.67} \tag{88}$$

BPHEs can be correlated with the heat transfer area, as Eq. (89) shows [58].

$$C_{BPHE} = 190 + 310 \cdot A \tag{89}$$

The cost of the feed pump is correlated with its electrical power consumption, as Eq. (90) shows [198].

$$C_{pump} = \left(1970 \cdot W_p^{0.35}\right) \cdot R_{USD} \tag{90}$$

An average cost for the total mass of organic fluid is considered using Eq. (91) [137]. The mass of organic fluid depends on the charge, which can be quantified in function of the rated electrical power through Eq. (92) [199].

$$C_{wf} = 20 \cdot M \tag{91}$$

$$M = 5.05 \cdot W_e \tag{92}$$

The costs of the pipes are taken into account through Eq. (93) [135]. About 4 m of piping length is considered for the liquid line, vapor line, and receiver. Moreover, as similar studies assume, the cost of the control system and miscellaneous hardware is set to 800 € [137].

$$C_{piping} = \left(-6.90 + 675 \cdot D_{piping}\right) \cdot L_{piping} \tag{93}$$

The cost of the direct air-cooled condenser can be considered by two equations. Firstly, the tube bank is correlated using the heat transfer area through Eq. (94). Secondly, fans cost is correlated with the diameter and electrical power consumption, such as Eq. (95) shows.

Furthermore, other costs are often valued as a 30% of the main components cost [200], which is a ratio also considered in this study.

$$C_{condenser} = \left(5.6 \cdot A\right) \cdot R_{USD} \tag{94}$$

$$C_{fans} = \left(1887.5 + 159.95 \cdot D_{fans}^2 + 3.53 \cdot D_{fans} + 281.25 \cdot W_{e_{fan}}\right) \cdot N_{fans} \cdot R_{USD} \tag{95}$$

6.1.2. Recuperator

Similar to previous equations, the recuperator can be correlated with the heat transfer area. Accordingly, Eq. (96) is obtained from budget information.

$$C_{recuperator} = 228 \cdot A \tag{96}$$

6.1.3. Heat transfer loop

Costs of the heat transfer loop and commissioning are estimated from budgets around 6,000 €.

6.2. Cost-effective indicators

The economic feasibility is assessed in cost-effective terms when a thermo-economic optimization is conducted. The ratios most extensively used are described as follows.

6.2.1. Specific Investment Cost (SIC)

The SIC is a ratio commonly used as objective function in thermo-economic optimizations with ORC systems [101]. This cost-effective indicator is defined as the ratio between initial investment cost and net electrical power by Eq. (97). It should be noted that literature often focuses on the ORC unit (module and condenser) using Eq. (98).

$$\text{SIC}_{\text{project}} = \frac{C_0}{W_{\text{net}}} \tag{97}$$

$$\text{SIC}_{\text{ORC}} = \frac{C_{\text{ORC}}}{W_g - W_p} \tag{98}$$

6.2.2. Levelized Cost Of Electricity (LCOE)

The LCOE is the constant electricity price needed during the lifetime of the system to reach break even over the lifetime of the project [201]. This ratio is usually used to compare the cost of electricity produced to the cost of electricity consumed from the grid, which is defined as Eq. (99).

$$\text{LCOE} = \frac{\displaystyle\sum_{t=1}^{T} \frac{C_0 + C_m}{(1+r)^t}}{\displaystyle\sum_{t=1}^{T} \frac{E_{\text{final}}}{(1+r)^t}} \tag{99}$$

6.3. Profitability indicators

The economic feasibility of the project can be assessed through different profitability indicators. The most extensively used are described as follows.

6.3.1. Net Present Value (NPV)

The NPV is a ratio that provides the absolute value of the wealth reachable in a project. This ratio can be defined as the difference between present values of cash inflows and outflows, such as Eq. (100) expresses. The project is considered profitable when positive values of NPV are obtained.

$$NPV = \sum_{t=1}^{T} \frac{C_t}{(1+r)^t} - C_0 \qquad (100)$$

6.3.2. Profitability Index (PI)

The PI is an investment appraisal technique that relativizes the NPV. This ratio provides a measure of the profit per unit of capital cost. It can be calculated by dividing the present value of cash inflows to the capital cost, such as Eq. (101) shows. The project is considered profitable when values greater than 1 are obtained.

$$PI = \frac{\sum_{t=1}^{T} \frac{C_t}{(1+r)^t}}{C_0} \qquad (101)$$

6.3.3. Internal Rate of Return (IRR)

The IRR is the discount rate that makes the NPV of all cash flows from a project equal to zero. Generally, the higher the IRR, the more desirable it is to undertake the project.

6.3.4. Discounted Payback Period (DPP)

The DPP, calculated considering the discounted cash flow, is the time required to get the initial investment back. It is a widely used economic index by corporations. The lower the DPP, the better the profitability of the project.

7.   CONCLUSIONS

This Chapter has developed a comprehensive model of the WHR system as a tool to conduct the thermo-economic assessment. In this way, the geometric characteristics and the equations that define the thermodynamic performance of the components have been described. Among the main components, heat exchangers, fluid machines, and auxiliary components highlight.

Each sub-model of heat exchanger has been preliminarily validated by the simulation of design conditions. Thus, a minimum deviation in results is observed between using the correlations proposed and those considered valid by the respective manufacturers.

Similarly, sub-models of fluid machines and auxiliary components have also been developed to allow the performance simulation and the system

optimization. However, some performance ratios require being calibrated from the steady-state points.

Economic equations have also been addressed. Thus, reported cost correlations in thermo-economic assessments have been selected in accordance with actual costs of the ORC unit, while the remaining costs have been provided from the specific experimental application case. Moreover, economic feasibility indicators of the project have been defined.

Calibration & Validation
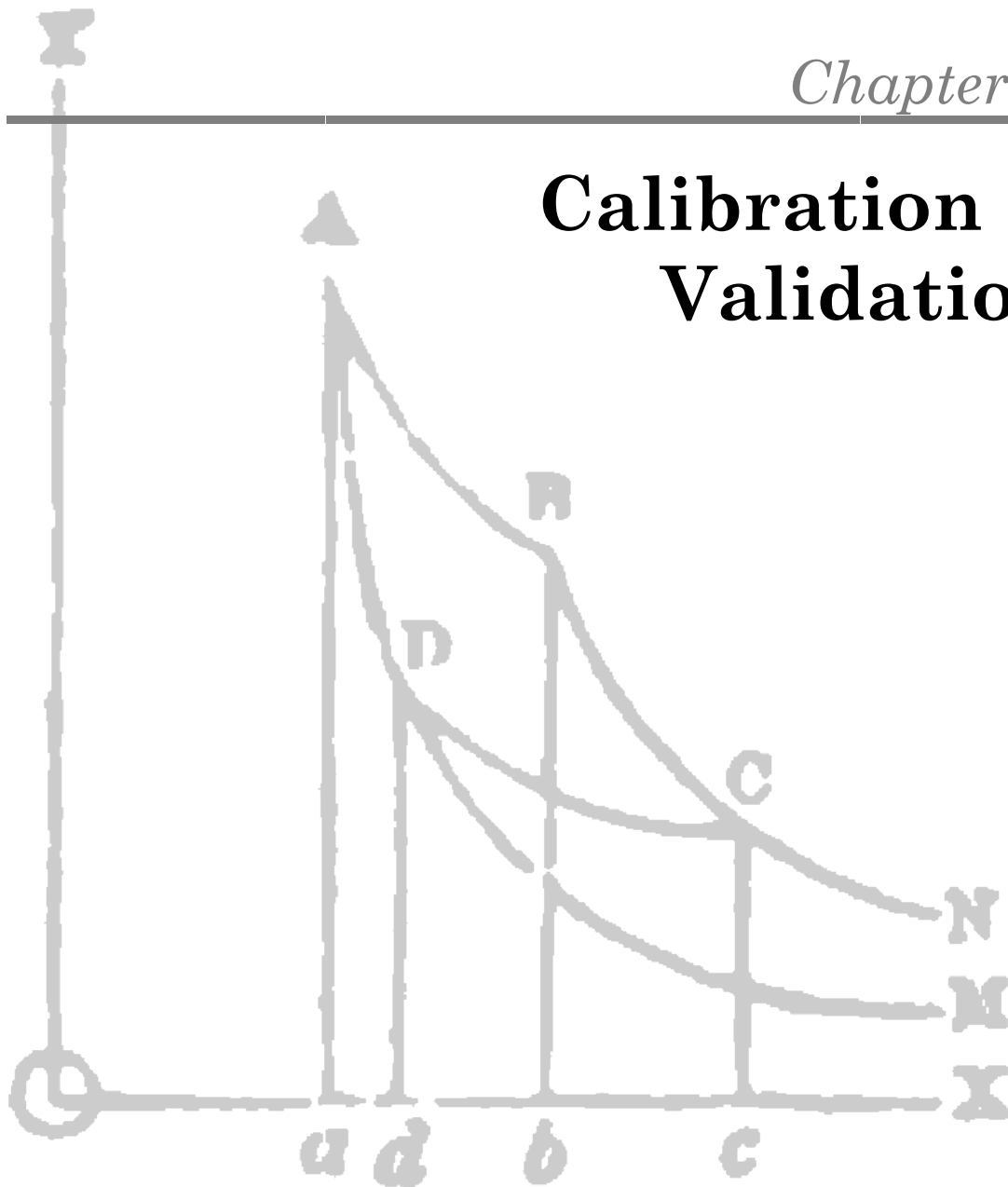
1. INTRODUCTION

The importance of the economic feasibility on the ORC adoption in practical applications has encouraged researchers to focus on thermo-economic assessments. To do this, models of the systems are usually used as a tool to carry out the investigations.

This study addresses the model development from a specific experimental application case, allowing its validation from actual data of operation.

In this way, Chapter IV described sub-models of the components, demonstrating a suitable accuracy concerning to the heat exchangers. However, some parameters related to the experimental performance of fluid machines and auxiliary components require being adjusted from actual data.

With this in mind, this Chapter deals about the calibration and validation of the model.

2. CALIBRATION

This section uses actual data of operation to adjust some performance ratios defined in the sub-models of the components. It should be clarified that constant experimental performance ratios are proposed, instead of regressions of the specific application, since a high flexibility to extrapolate results is imperative in thermo-economic optimizations.

2.1. Expander

The expander was modeled considering the irreversibilities that appear during the expansion process. In this way, some performance ratios were defined to be set from the analysis of the steady-state points.

Thereby, the characterization of internal energy losses requires the calibration of volumetric and mechanical efficiencies. In addition, the characterization of external energy losses requires the calibration of the electro-mechanical efficiency.

2.1.1. Volumetric efficiency

The volumetric efficiency of the expander is the performance ratio used to characterize the internal leakages occurred. This efficiency is validated in Fig. V.1, in which no trend is observed in the data analyzed. Nonetheless, it highlights the small range of variation. So a constant average value of 75.3% is assumed.

2.1.2. Mechanical efficiency

The mechanical efficiency of the expander is the internal performance ratio used to characterize frictional losses and pressure drops. This efficiency is represented in Fig. V.2 in function of the organic working fluid mass flow rate. The value ranges between 70% and 80%, so an average value of 75.07% is considered.
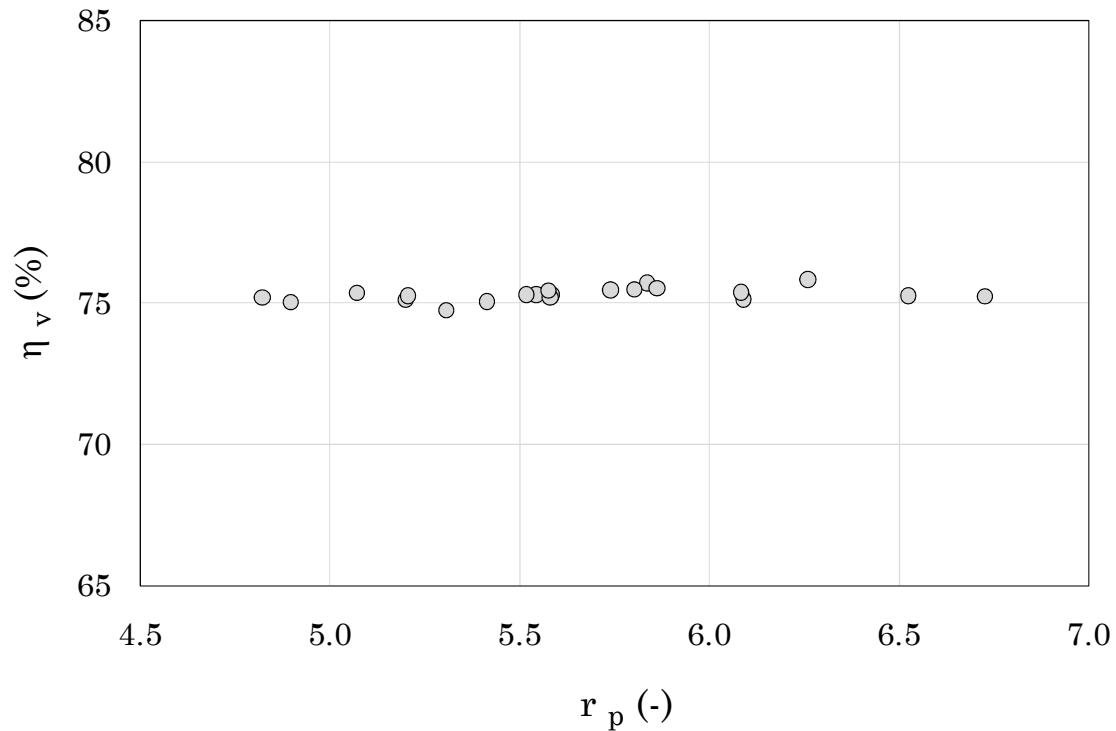
Fig. V.1. *Volumetric efficiency of the expander in function of its pressure ratio.*
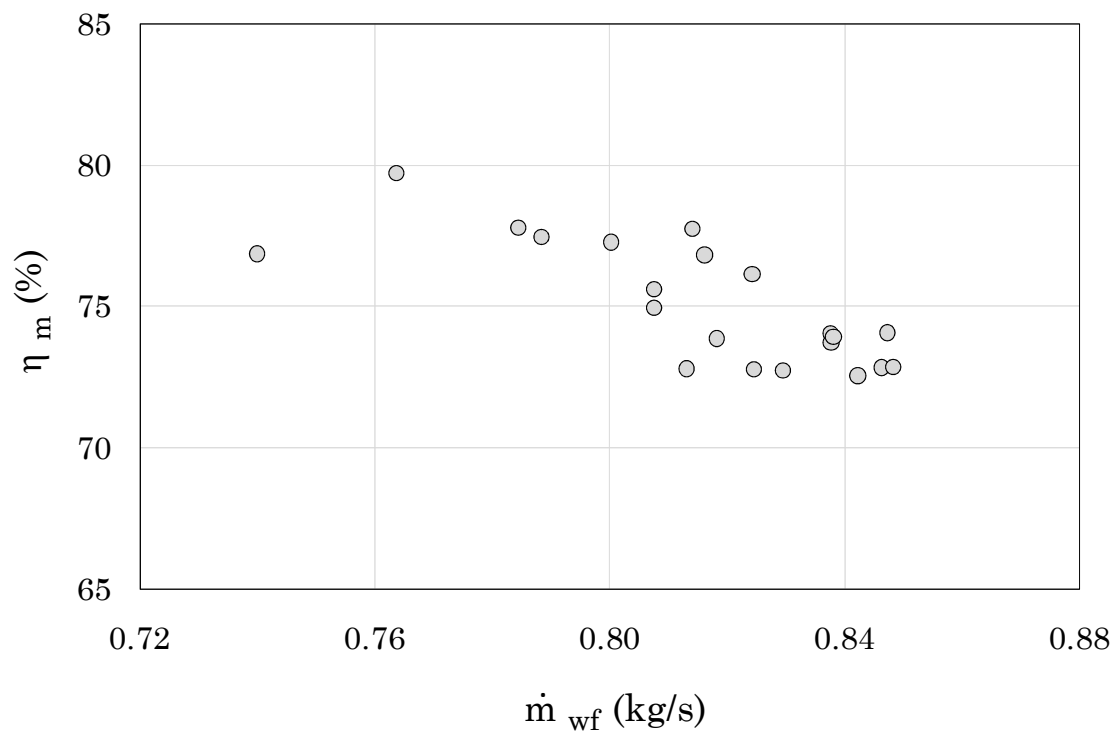
Fig. V.2. *Internal mechanical efficiency in function of working fluid mass flow rate.*

2.1.3. Electro-mechanical efficiency

External energy losses to the limits of the equivalent expander are characterized by a single performance ratio, the electro-mechanical efficiency. This efficiency is shown in Fig. V.3 in function of gross electrical power. Similarly to the volumetric efficiency, there is not any clear tendency. Consequently, a constant average value of 93.80% is considered.

Furthermore, this figure shows that, despite the rated gross electrical power of the ORC unit is 20 kW, a maximum electricity of 17.08 kW is observed in the steady-state points. This fact means that the ORC unit is operating in partial loads ranging between 75.6 – 85.4%.
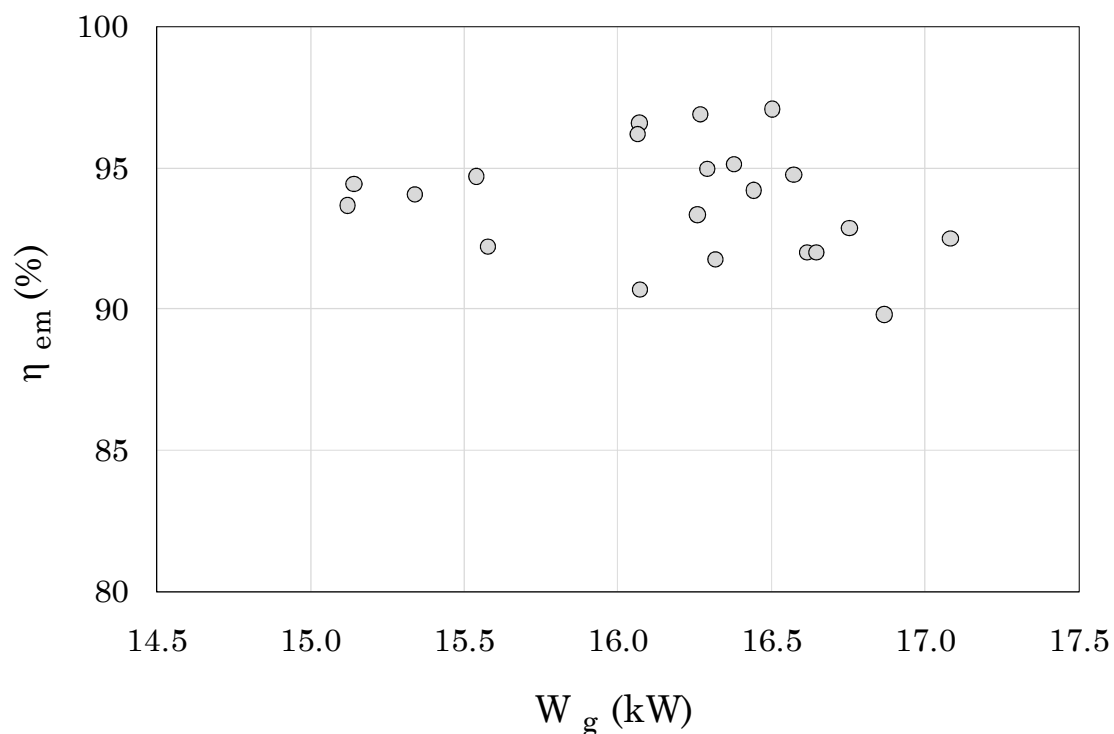
Fig. V.3. *External electro-mechanical efficiency in function of gross electrical power.*

2.2.   Pumps

Regarding the feed pump of the ORC unit, its overall efficiency can be plotted in function of different parameters. For instance, Fig. V.4 represents its variation with respect to the pressure ratio. As can be seen, the efficiency remains quite constant. Thus, in accordance with the simplified method used, a constant average value of 48.02% is considered.

With respect to the pump of the thermal oil circuit, various parameters require being calibrated. In this way, Fig. V.5 shows its overall efficiency in function of the volumetric flow rate calculated at the suction line. In the

first place, since the pump operates at constant speed, a reduced range of variation is obtained. Therefore, constant average values of 40.45% and 9.07 m³/h are assumed, respectively.
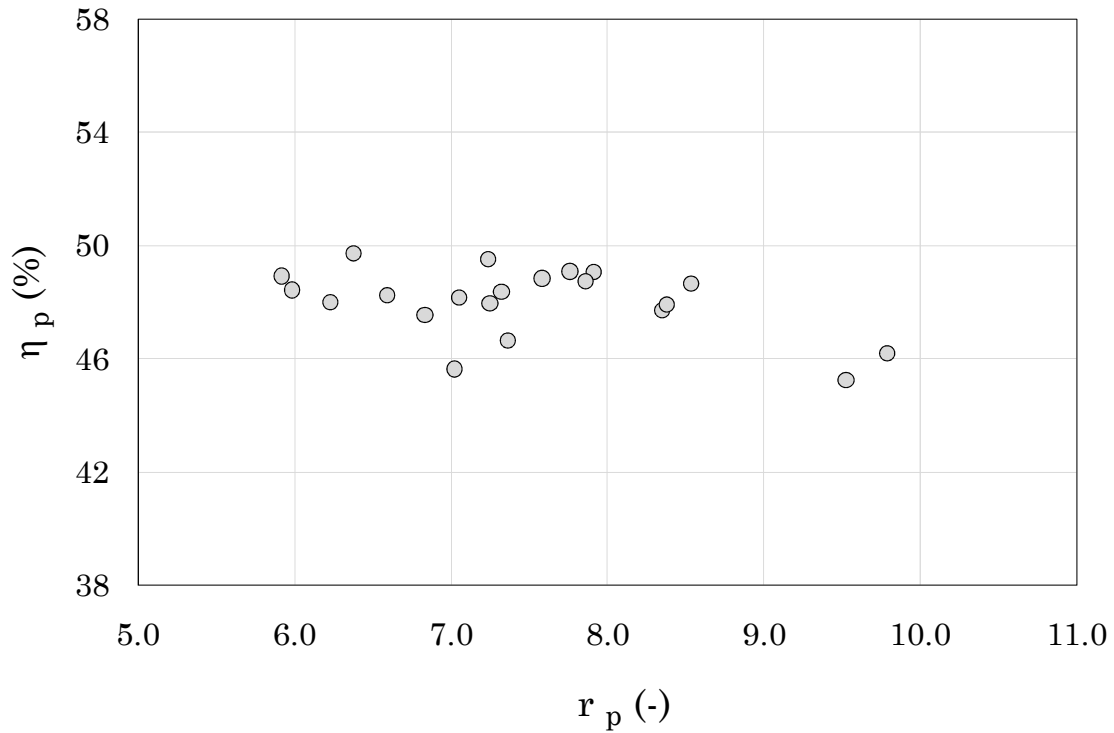
Fig. V.4. *Overall efficiency of ORC feed pump in function of its pressure ratio.*
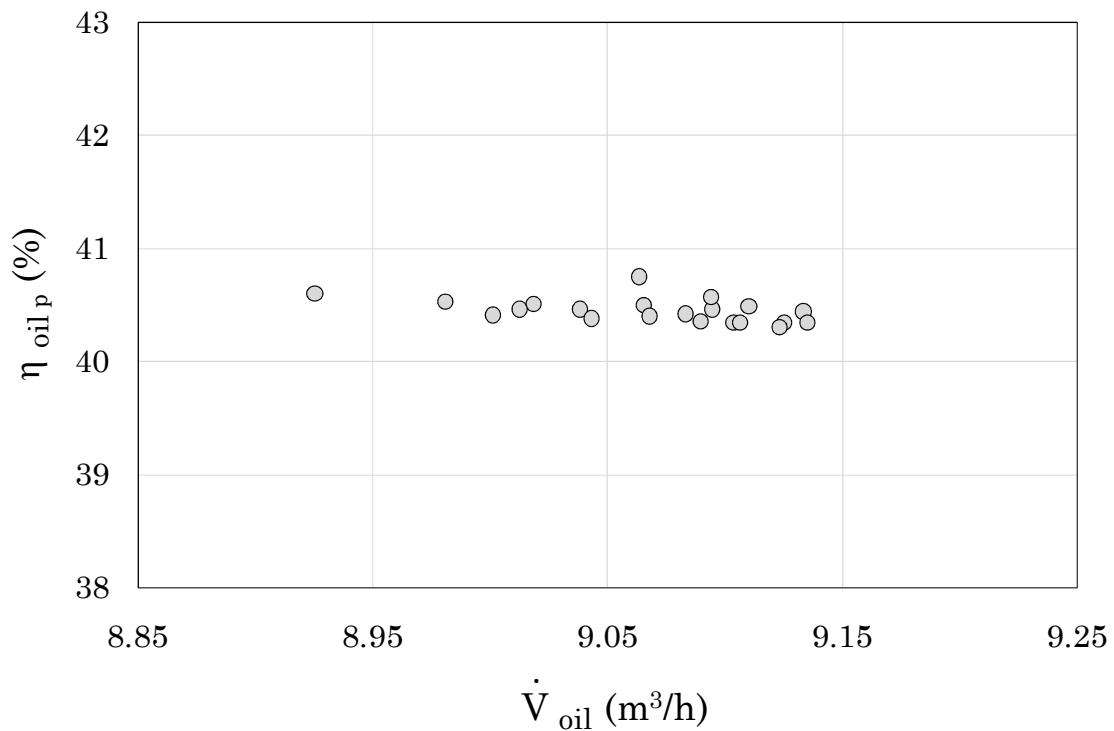
Fig. V.5. *Overall efficiency of thermal oil pump in function of volumetric flow rate.*

2.3. Air-cooled condenser

The electrical power consumed by the fans of the condenser has been characterized taken into account the partial load operation. Thereby, a correction factor related to the capacity ratio was defined in Chapter IV, which requires being calibrated through the steady-state points.

In this way, the variation of the correction factor in function of the actual electrical consumption of the fans is depicted in Fig. V.6. Based on observations, a constant average value of 92.6% is considered.
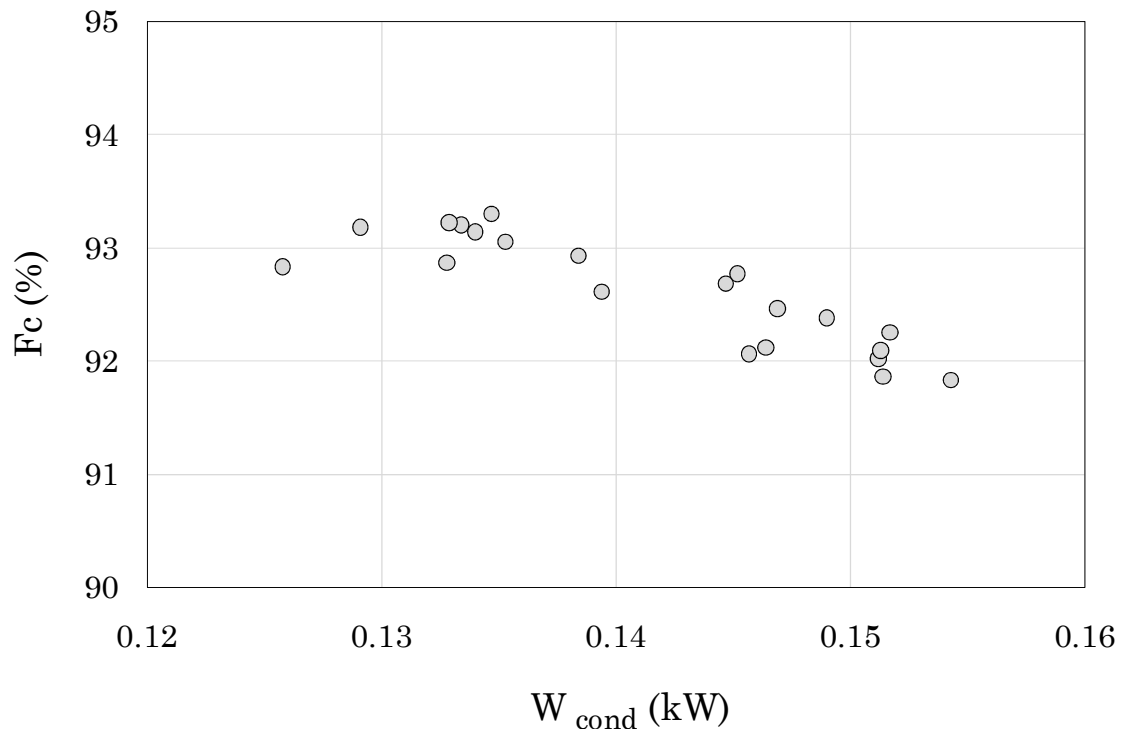
Fig. V.6. *Partial loads correction factor of the fans of the condenser.*

2.4. Piping and fittings

Piping and fittings cause a pressure drop in the circuit of the organic fluid that cannot be directly measured, so a calibration with constant values is considered. For this purpose, the equivalent length of the pipes is calculated in liquid and vapor lines as the difference between the actual pressure drop in each line minus the calculated pressure drop that BPHEs introduce.

As a result, the pressure drop in the liquid line is calibrated using the average equivalent length of 68.70 m illustrated in Fig. V.7. Similarly, the pressure drop in the vapor line is calibrated using the average equivalent length of 9.62 m shown in Fig. V.8.
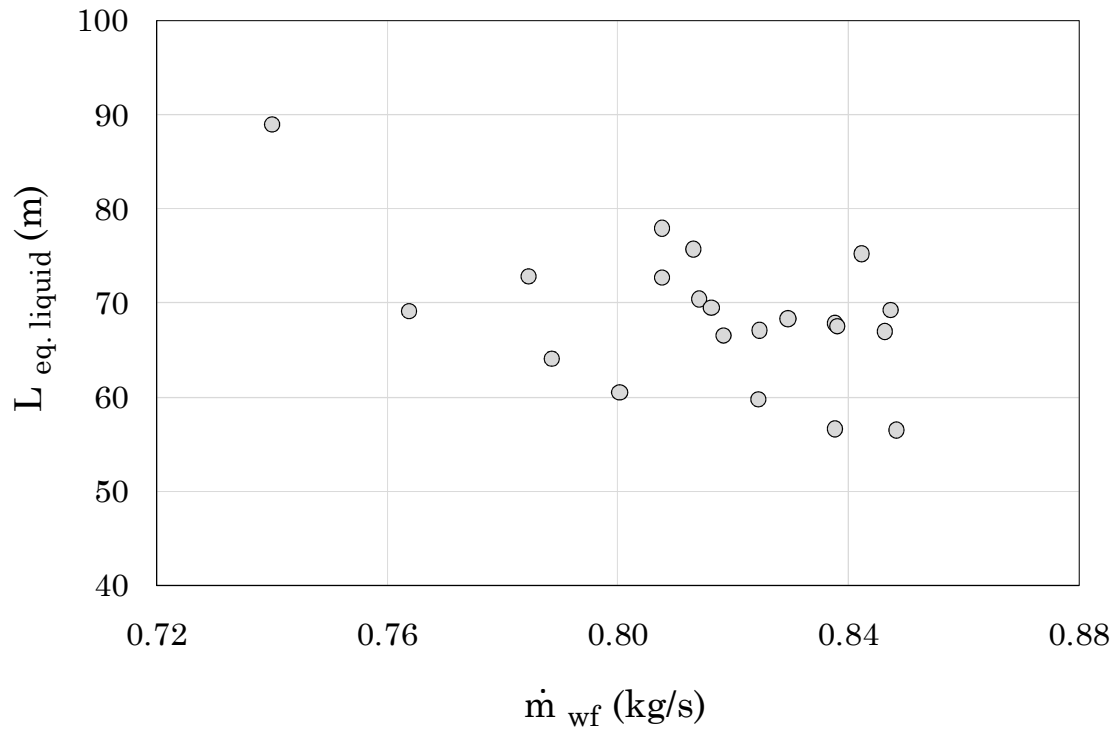
Fig. V.7. *Equivalent length for the liquid line pressure drop calibration.*
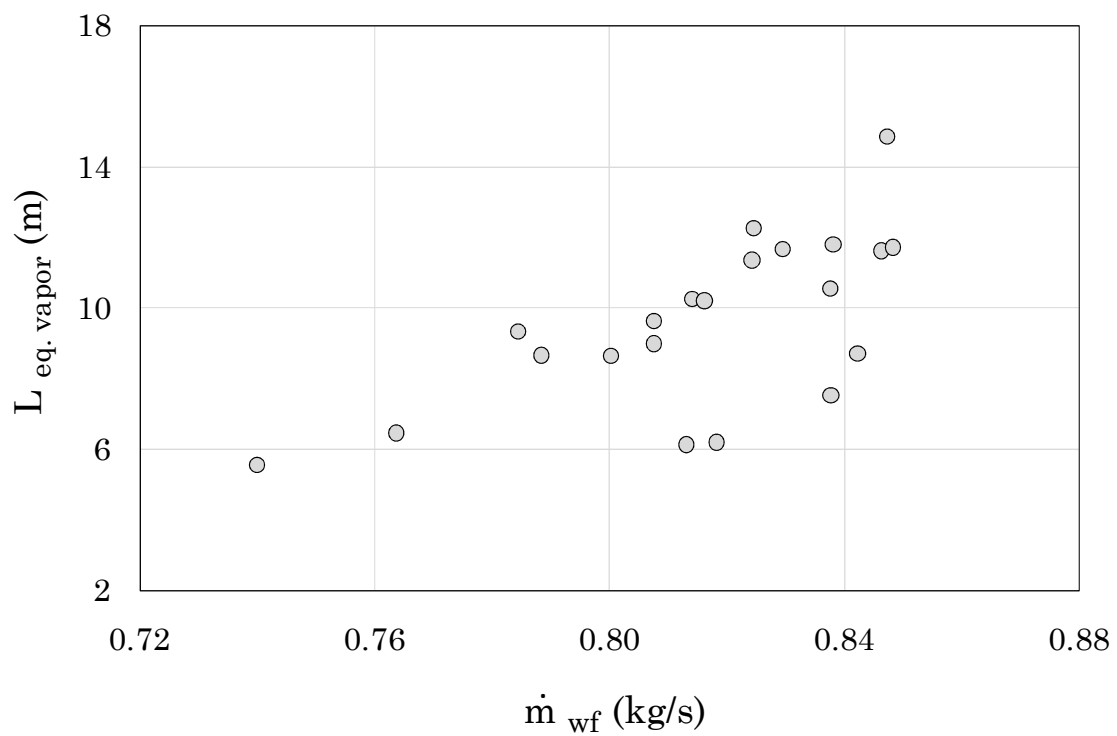
Fig. V.8. *Equivalent length for the vapor line pressure drop calibration.*

3. VALIDATION

Once the calibration is completed, a model able to conduct simulations is achieved. Hence, the conditions obtained during steady-state points can be simulated to allow the values comparison.

3.1.   Monitored parameters

The accuracy and validity of the model to simulate temperatures, pressures, mass flow rates and electrical powers are discussed below.

3.1.1. Temperature

The temperature is a property that was measured in each fluid of the system, like the exhaust air of the heat source, ambient air of the heat sink, thermal oil of the heat transfer loop and organic working fluid of the ORC unit. Regarding temperatures that are not used as inputs by the model, their validation is addressed as follows.

The exhaust air temperature that leaves from the recuperator is validated in Fig. V.9. Focusing on the statistical analysis, all values are included in a bandwidth of 0.92%, excluding error bars. The mean absolute error is 0.36% and a standard deviation of 0.23% is obtained.

These error values are indicative of the model suitability to predict the thermal power recovered from the heat source. Moreover, it highlights that all values are upper 170 ºC. This fact, along with the observed gross electrical powers below 20 kW, points that a higher exploitation of the heat source could be made.

The thermal oil temperatures that enter and leave from the ORC unit are validated in Fig. V.10 and Fig. V.11. The statistical analysis shows that the values are within a bandwidth of 1.22% and 1.54% respectively, excluding error bars. Mean absolute errors of 0.56% and 0.84%, and standard deviations of 0.31% and 0.40% are quantified, respectively.

These error values confirm the model capacity to predict the energy balance between the heat source and the HRVG, as well as the heat losses occurred in the heat transfer loop.

The temperature of the organic working fluid that enters into the HRVG, or that leaves from the liquid side of the regenerator, is validated in Fig. V.12. With respect to the statistical analysis, all values are included in a bandwidth of 5.48%, excluding error bars. The mean absolute error is 3.66% and a standard deviation of 0.99% is calculated.

The temperatures of the organic working fluid entering and leaving from the expander are validated in Fig. V.13 and Fig. V.14. Regarding the statistical analysis, all values are included in a bandwidth of 1.81% and 1.79% respectively, excluding error bars. The mean absolute errors are 0.45% and 0.94%, and standard deviations of 0.54% and 1.01% are obtained, respectively.

The low errors shown about the temperatures in the expander underline the accuracy that the model may achieve to predict the gross electrical power.
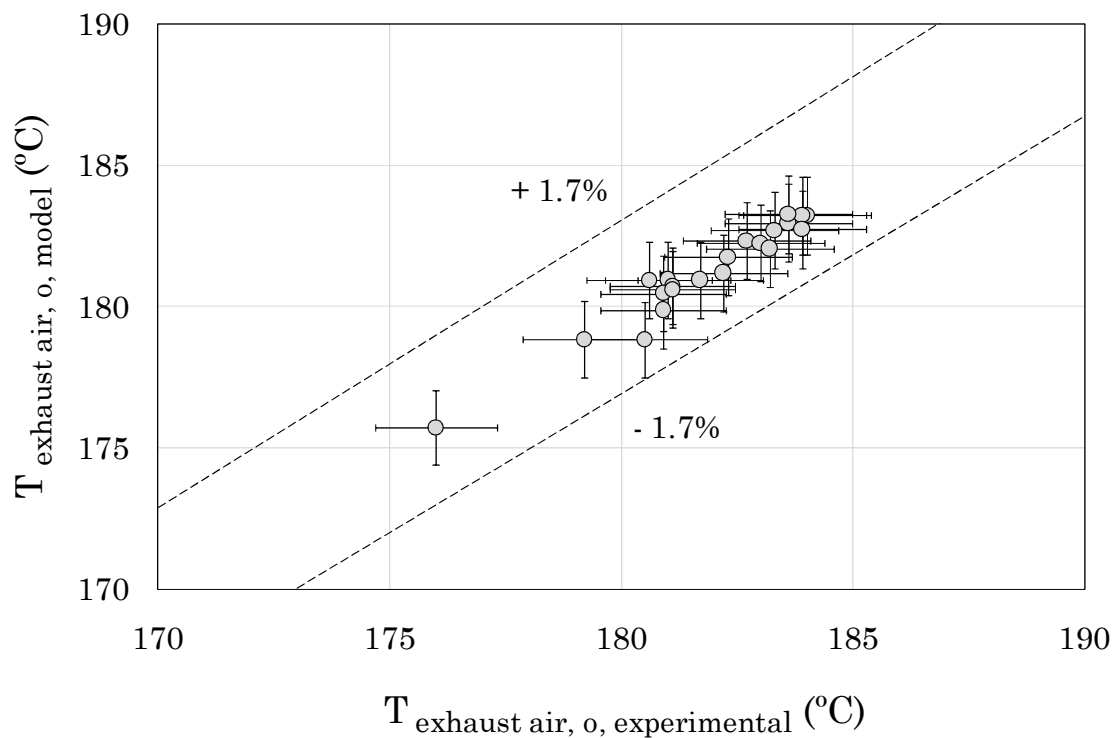
***Fig. V.9.** Exhaust air temperature validation.*
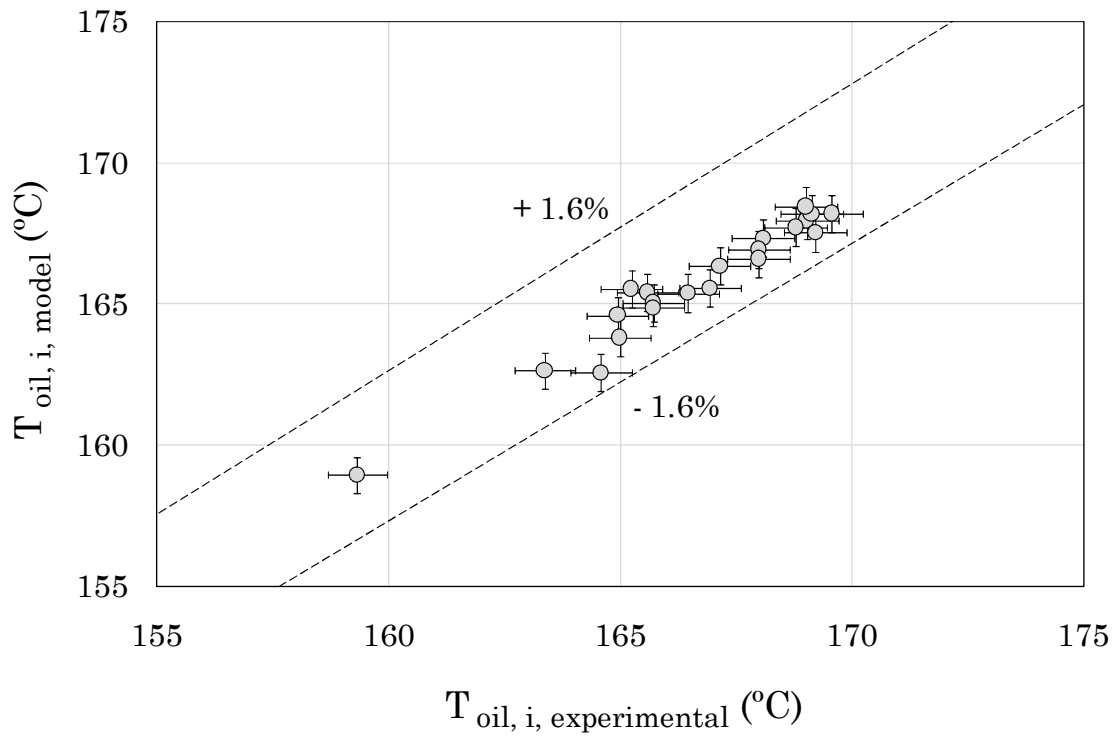
Fig. V.10. Validation of the inlet temperature of thermal oil into the ORC unit.
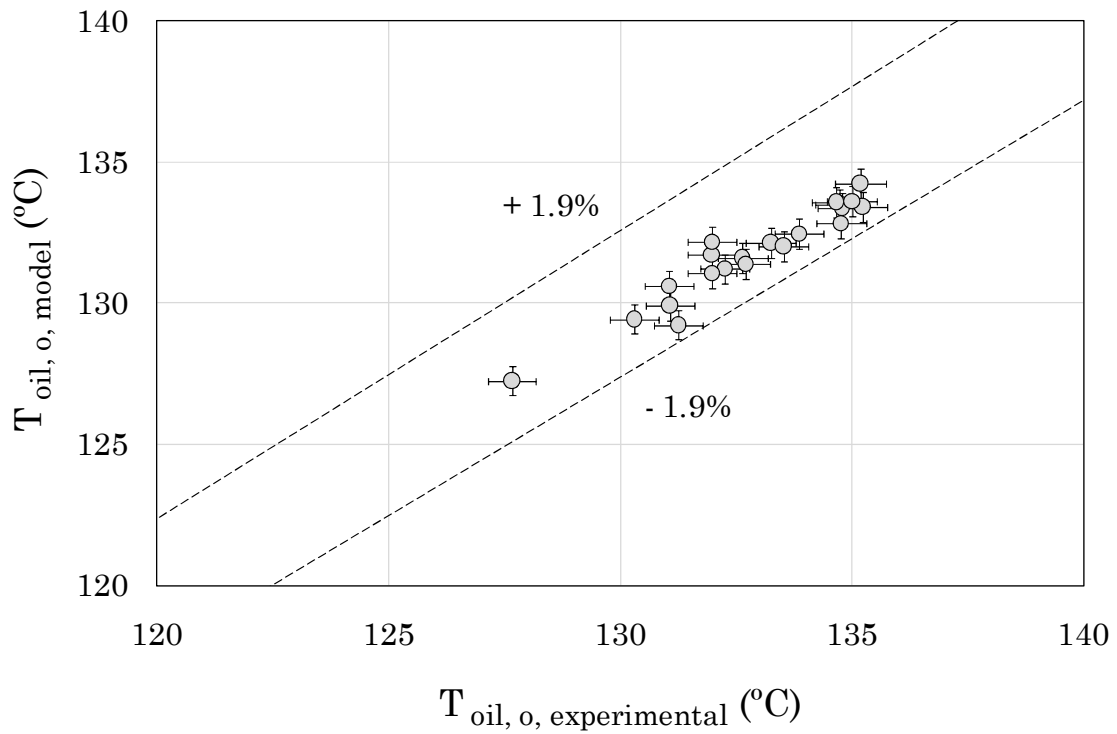
Fig. V.11. Validation of the outlet temperature of thermal oil from the ORC unit.
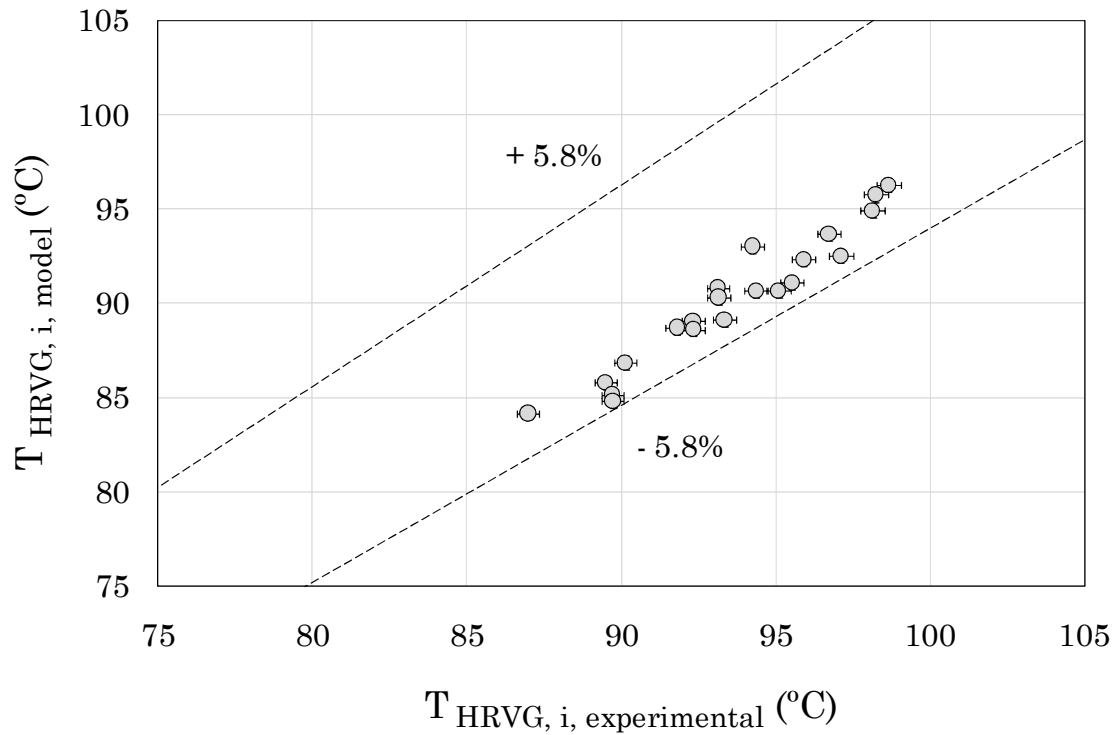
Fig. V.12. *Validation of the inlet temperature of organic fluid into the HRVG.*
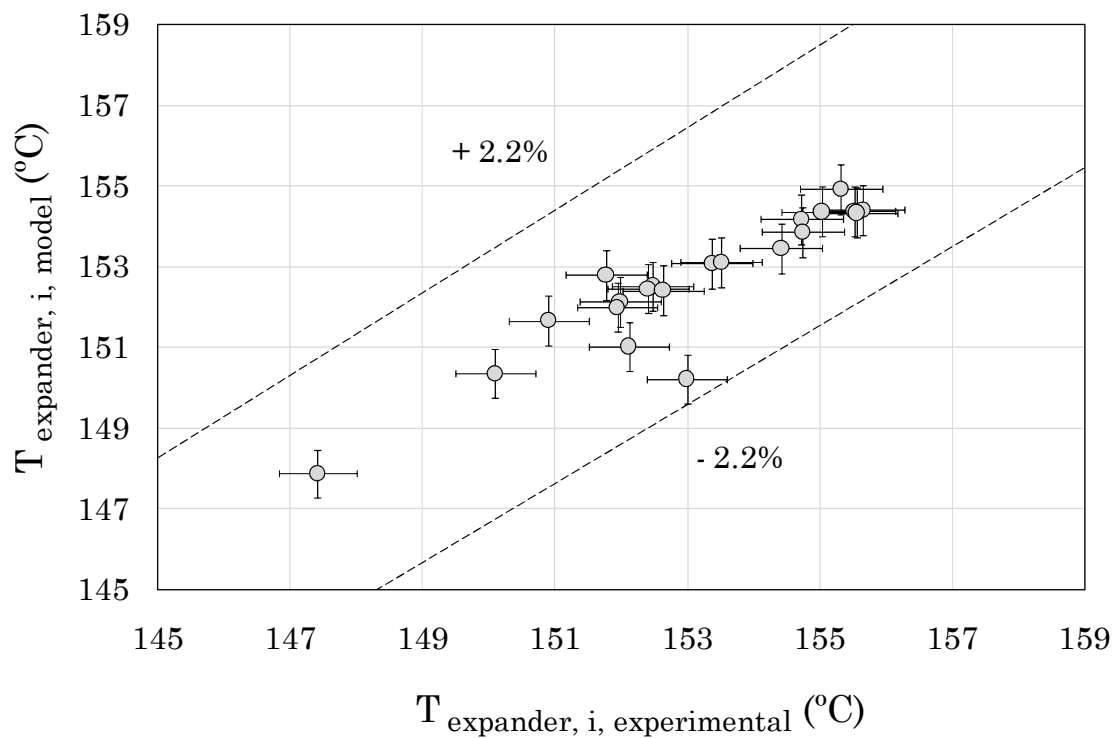
Fig. V.13. *Validation of the inlet temperature of organic fluid into the expander.*
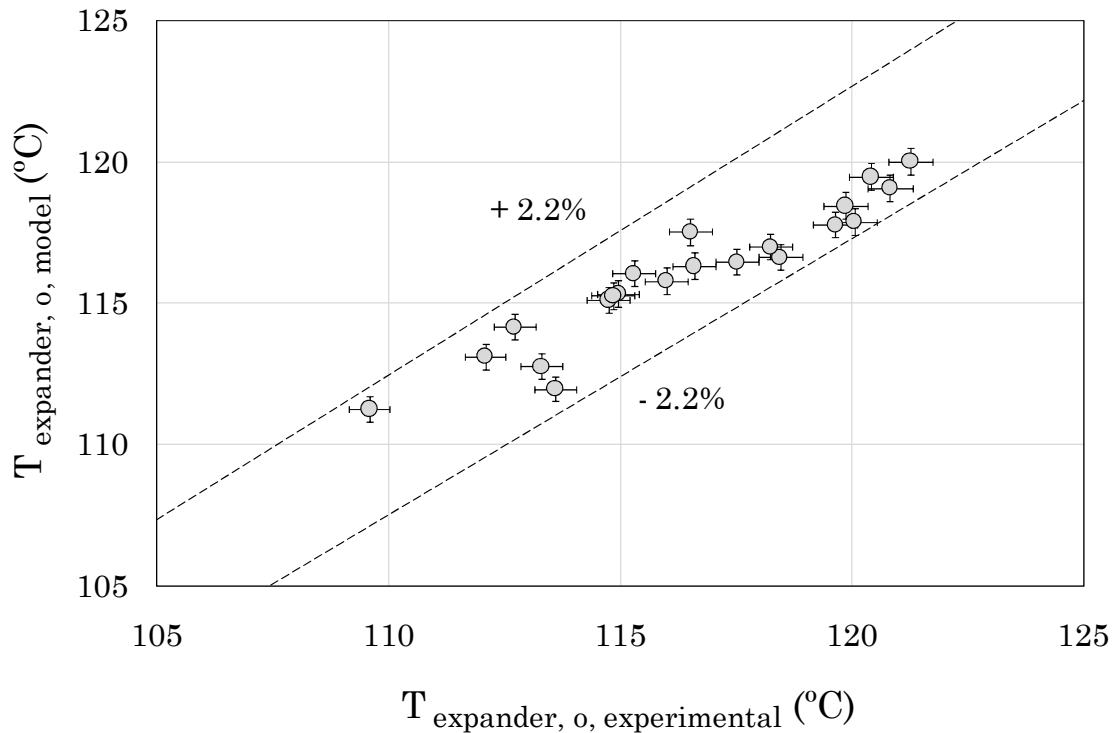
Fig. V.14. Validation of the outlet temperature of organic fluid from the expander.

3.1.2. Pressure

The pressure is a property only measured in the circuit of the organic fluid. Four pressure transmitters are installed in the ORC unit, which are used to monitor high and low operating pressures, as well as to quantify the pressure drops.

The pressure at the inlet port of the expander, which also corresponds to the outlet pressure of the HRVG, is validated in Fig. V.15. Focusing on the statistical analysis, all values are included in a bandwidth of 2.08%, excluding error bars. The mean absolute error is 1.51% and a standard deviation of 0.39% is quantified.

The prediction of this pressure is achieved with a suitable accuracy thanks to the stability of the control operated by the ORC, which maintains a quite constant value of superheating, such as the calibration has shown.
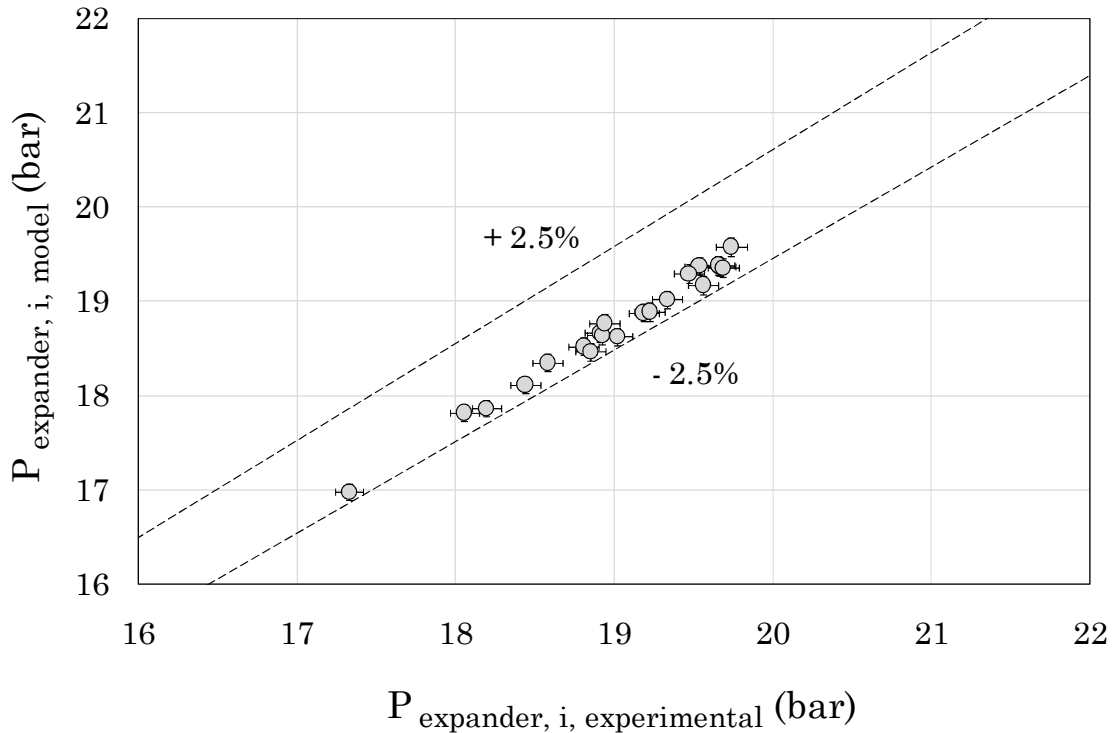
Fig. V.15. *Validation of the inlet pressure of organic fluid into the expander.*

Similarly, the stability of the control of the condensing temperature allows a suitable prediction of the lower pressure measured in the cycle, which is validated in Fig. V.16. The statistical analysis shows that all values are within a bandwidth of 2.03%, excluding error bars. The mean absolute error is 0.62% and a standard deviation of 0.85% is calculated.

The remaining pressures are also predictable thanks to the calibration previously conducted about the pressure drops caused in piping and fittings.

In this way, the validation of the maximum pressure of the cycle, which corresponds to the outlet of the pump, is represented in Fig. V.17. With respect to the statistical analysis, all values are included in a bandwidth of 1.40%, excluding error bars. The mean absolute error is 0.51% and a standard deviation of 0.48% is obtained.

In addition, the validation of the pressure that leaves from the expander, which also is the pressure of the vapor that enters into the regenerator, is shown in Fig. V.18. Regarding the statistical analysis, all values are included in a bandwidth of 5.24%, excluding error bars. The mean absolute error is 3.05% and a standard deviation of 1.27% is quantified.
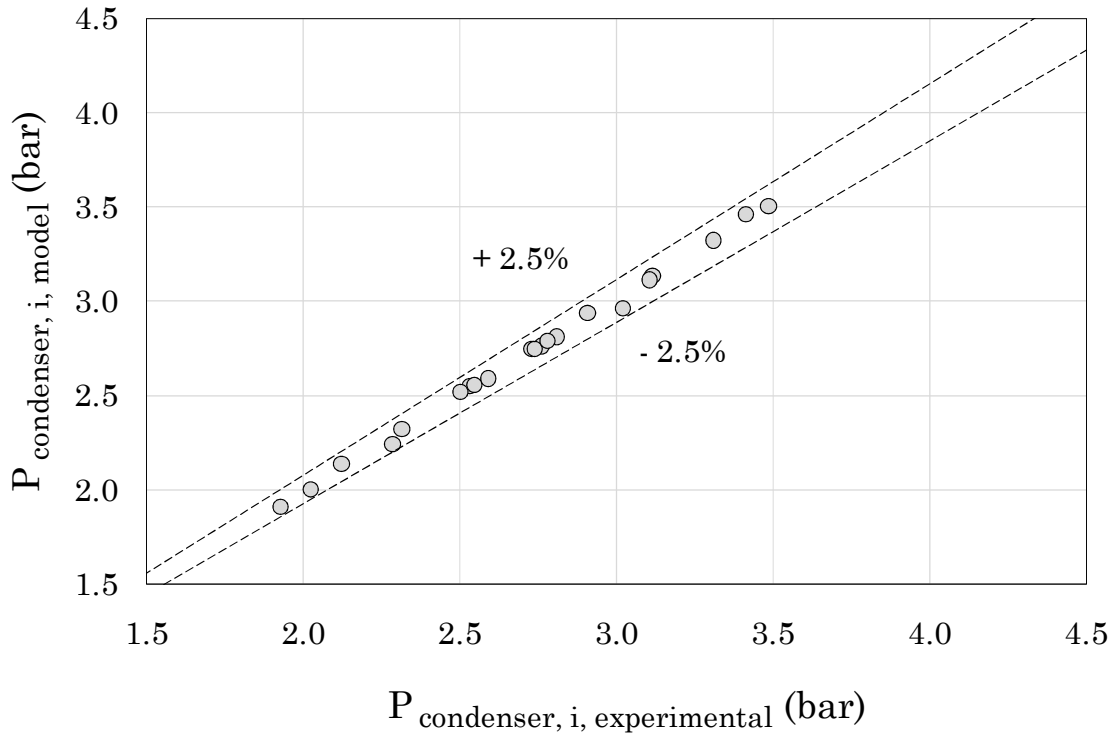
Fig. V.16. *Validation of the inlet pressure of organic fluid into the condenser.*
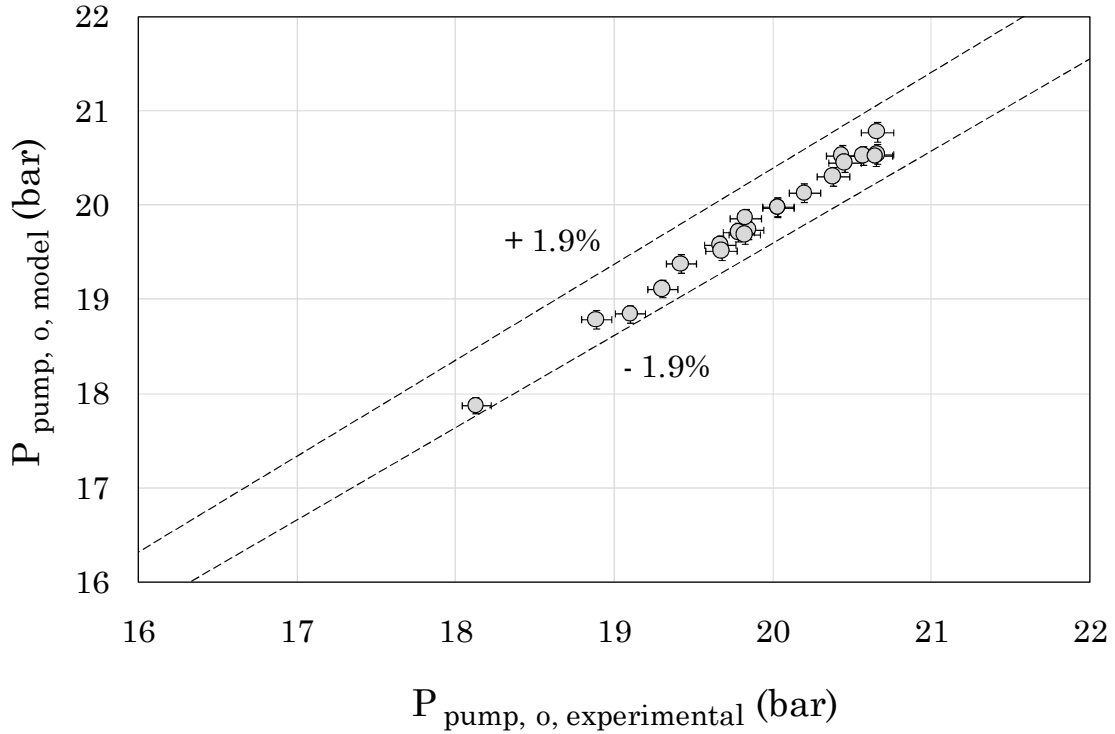
Fig. V.17. *Validation of the outlet pressure of organic fluid from the feed pump.*
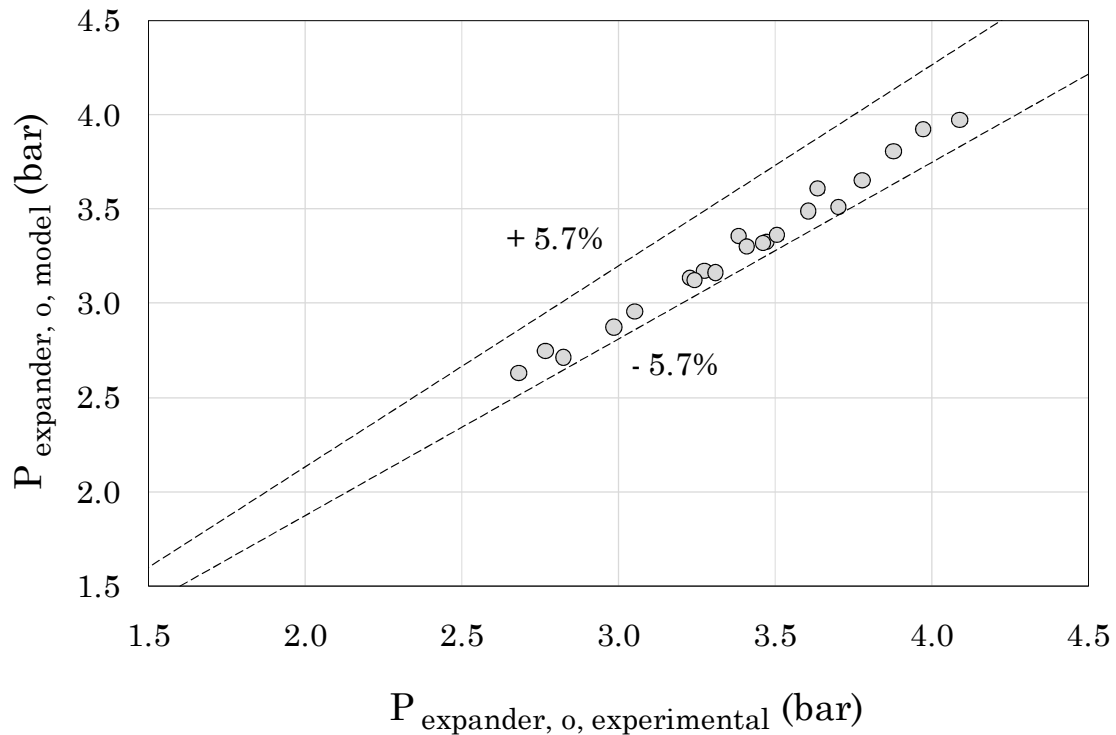
Fig. V.18. *Validation of the outlet pressure of organic fluid from the expander.*

3.1.3. Mass flow rate

The mass flow rate is a parameter only measured at the liquid line of the circuit of the organic fluid. The validation of this parameter is shown in Fig. V.19. Focusing on the statistical analysis, all values are included in a bandwidth of 2.79%, excluding error bars. The mean absolute error is 1.81% and a standard deviation of 0.52% is calculated.

The prediction of the organic working fluid mass flow rate is indicative of the small error assumed considering constant the volumetric efficiency of the expander.
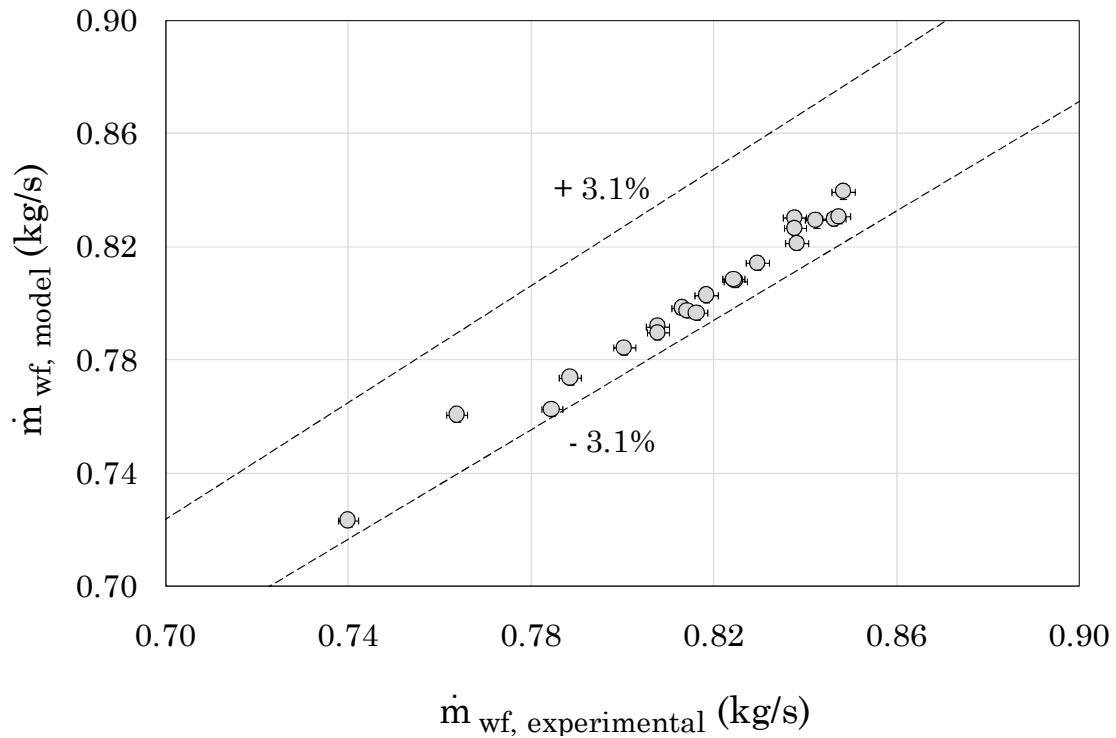
Fig. V.19. *Validation of organic working fluid mass flow rate.*

3.1.4. Electrical power

The electrical power is a parameter used to monitor the electrical production of the alternator, and the electrical consumptions of ORC feed pump and fans of the condenser.

In this way, the gross electrical power produced is validated in Fig. V.20. The statistical analysis shows that all values are within a bandwidth of 3.52%, excluding error bars. The mean absolute error is 1.42% and a standard deviation of 1.49% is obtained.

The validation of the electrical consumption of the ORC feed pump is depicted in Fig. V.21. In this case, the bandwidth that includes all values is 8.12%, excluding error bars. The mean absolute error is 2.65% and a standard deviation of 2.23% is quantified. As can be seen, in spite of the simplified method use, a reasonable error is obtained.

The electrical power consumed by the fans of the direct air-cooled condenser is validated in Fig. V.22. With respect to the statistical analysis, all values are included in a bandwidth of 6.37%, excluding error bars. The mean absolute error is 3.77% and a standard deviation of 4.20% is calculated.

The error that this parameter shows might also be due to other meteorological phenomena beyond the temperature. In fact, it was

experimentally observed that fans velocity increases with the effect of wind and decreases with the rain.
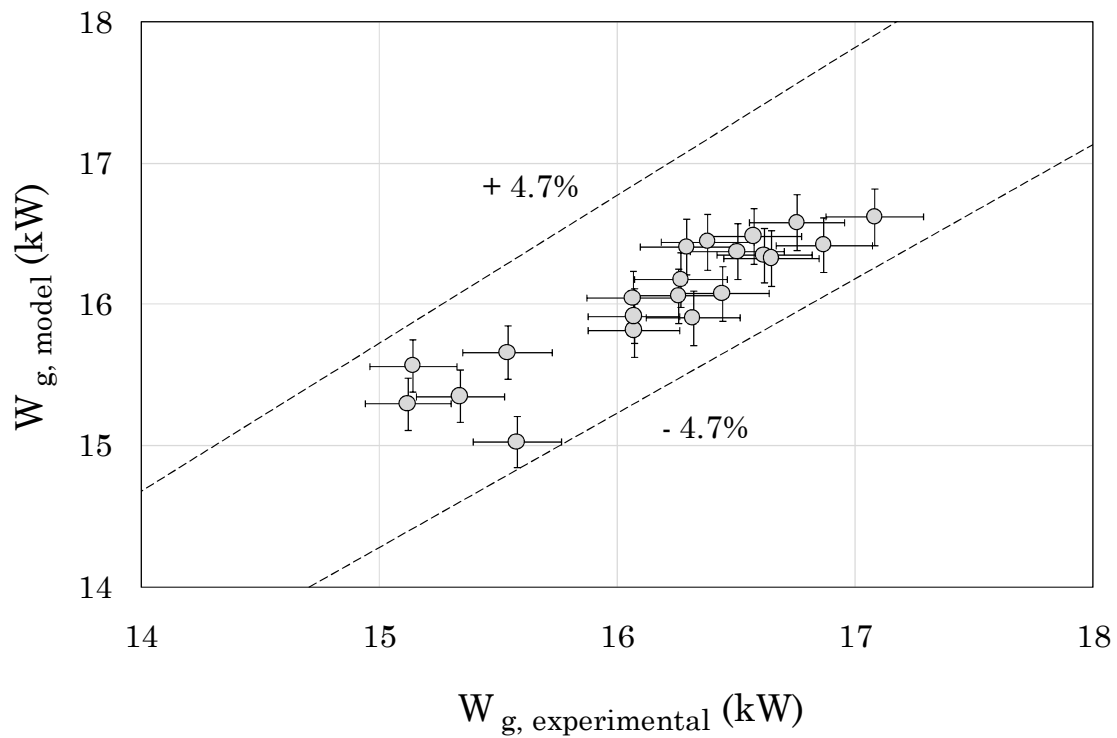
Fig. V.20. *Validation of the gross electrical power produced in the alternator.*
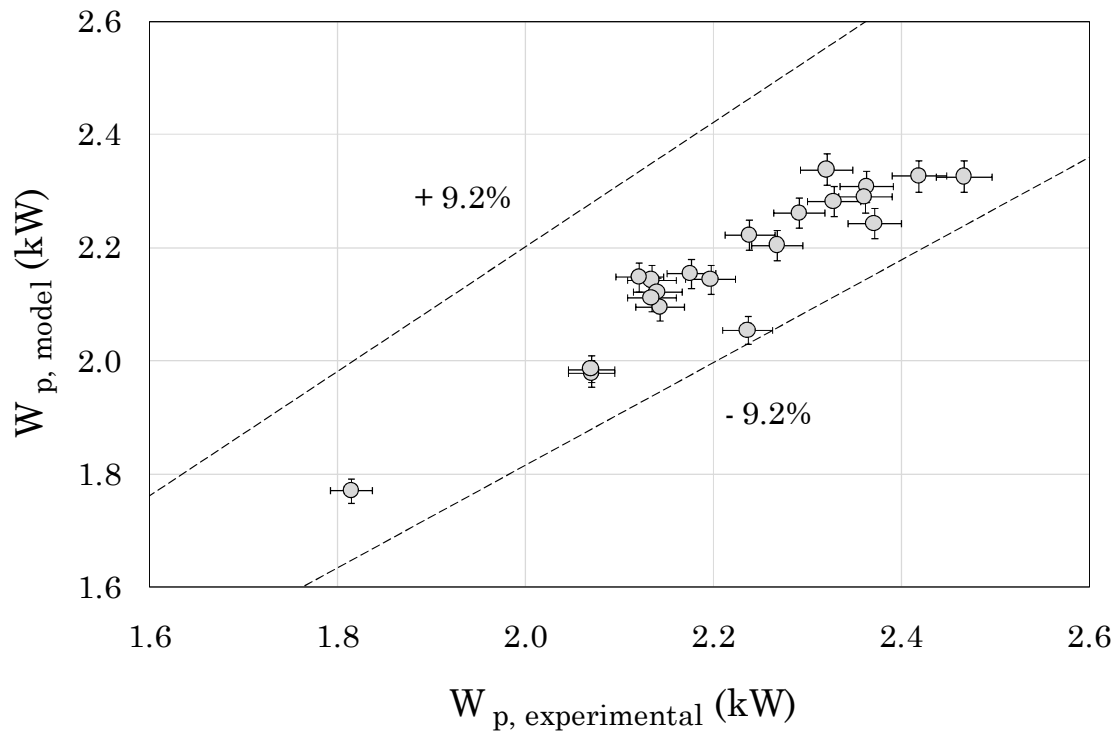
Fig. V.21. *Validation of the electrical power consumed by the ORC feed pump.*
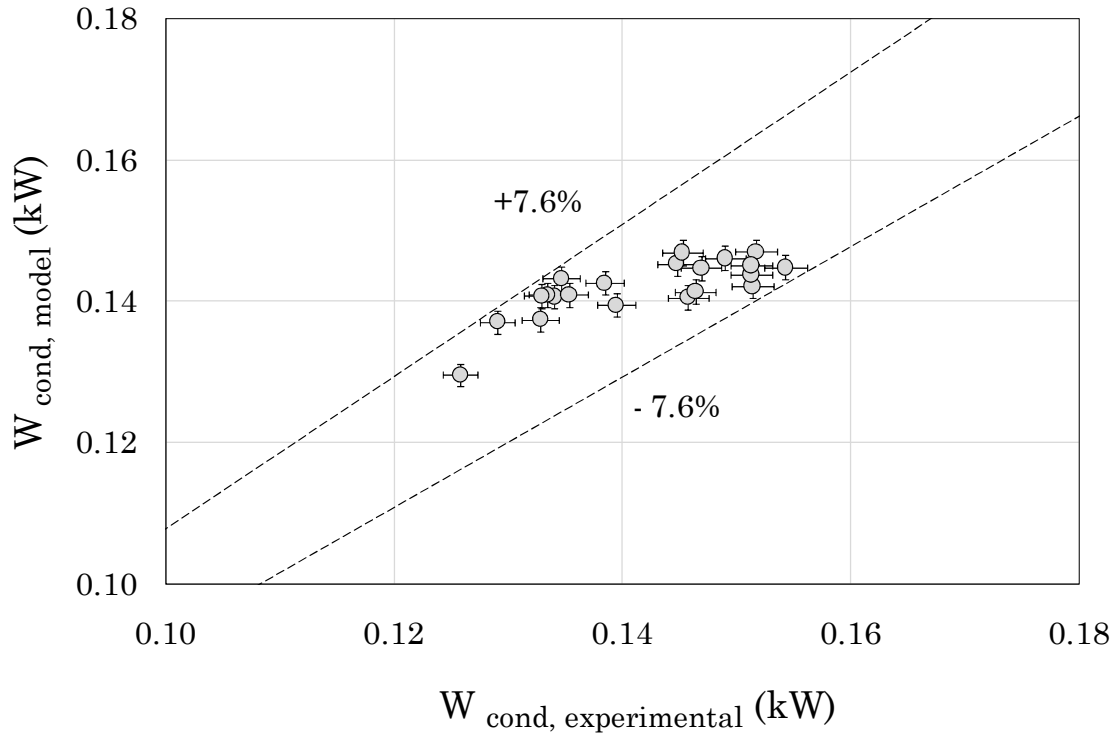
Fig. V.22. Validation of the electrical power consumed by the fans of the condenser.

3.2.   Performance ratios

Besides the use of monitored parameters to validate the model, some performance ratios are also interesting.

In this way, the validation of the gross electrical efficiency of the cycle is represented in Fig. V.23. Regarding the statistical analysis, all values are included in a bandwidth of 4.14%, excluding error bars. The mean absolute error is 1.81% and a standard deviation of 1.55% is obtained.

With respect to the whole process, a second law comparison would show the relationship between the gain obtained and the maximum ideally reachable. So this relationship is illustrated in Fig. V.24 as a comparison of the final efficiency of the process versus the Carnot efficiency.

In addition, the relevance of addressing the whole WHR system in the investigation can be emphasized. Thus, despite a gross electrical efficiency of 10.57% is experimentally reached, the different energy losses caused in the process reduce this value to a net electrical efficiency of 7.27%.
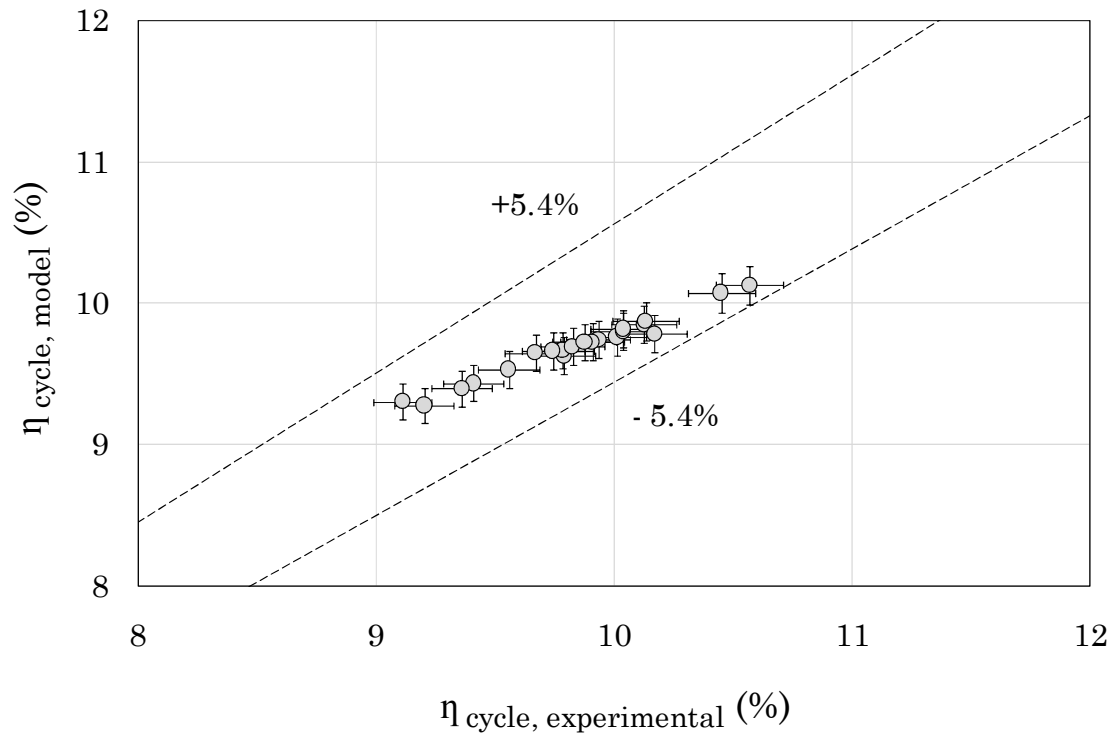
Fig. V.23. *Validation of the gross electrical efficiency of the cycle.*
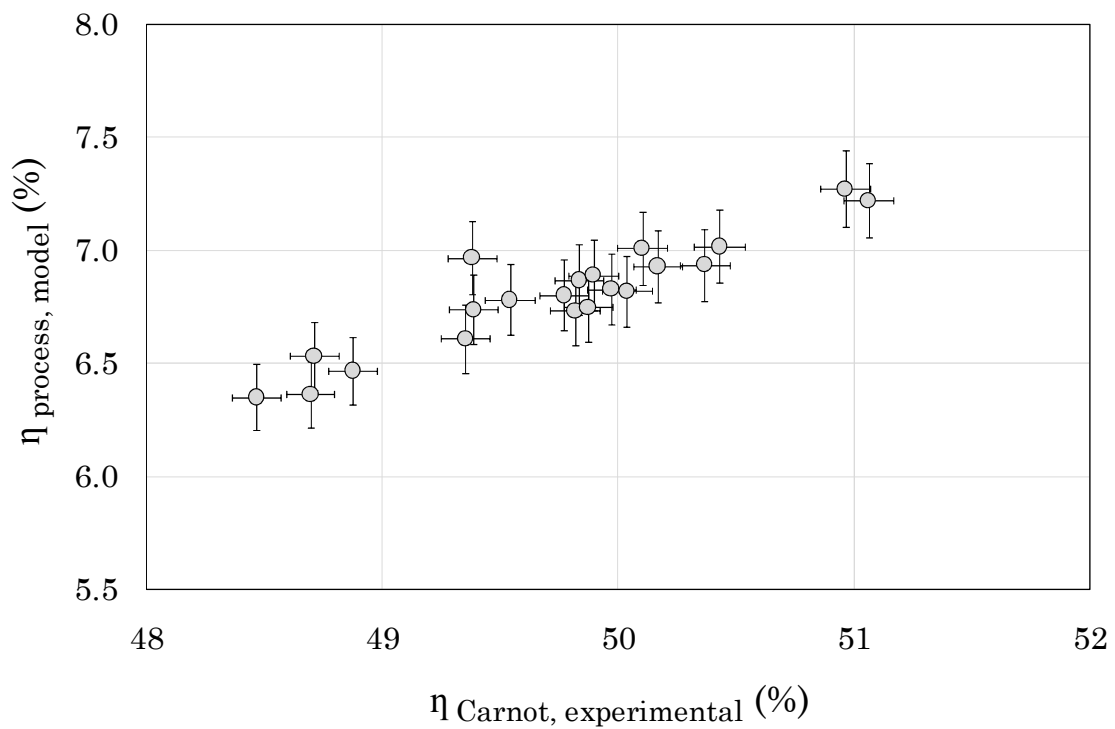
Fig. V.24. *Comparative between process and Carnot efficiency.*

3.3. Cost correlations

The costs of the system can also be validated. To do this, the economic results of the simulations conducted are collected in Table V.1. Values presented for the alternator and the feed pump depend on the operating conditions that will be established in next Chapter.

Thereby, the quantified cost is 55,418 € for the ORC unit (set of module and condenser) and 83,227 € for the whole WHR system. These values are very close to the capital investment cost reported in previous studies based on indications of the ORC supplier. In particular, it was estimated around 60,000 € for the preliminary ORC prototype [145], and about 87,000 € for the whole project [53]. Notice that commercial prices are subject to change.

Table V.1. Calculated cost per component.

$C_{expander}$	Cost of expander (€)	9,881
$C_{alternator}$	Cost of electric generator (€)	4,260
C_{BPHE}	Cost of brazed plate economizer (€)	692
C_{BPHE}	Cost of brazed plate evaporator (€)	1,827
C_{BPHE}	Cost of brazed plate regenerator (€)	4,189
C_{pump}	Cost of feed pump of the ORC (€)	2,413
C_{wf}	Cost of organic working fluid (€)	2,020
$C_{condenser}$	Cost of heat exchange surface of the condenser (€)	5,858
C_{fans}	Cost of the five fans of the condenser (€)	10,092
C_{piping}	Cost of pipes of organic fluid circuit (€)	596
$C_{control}$	Cost of control and miscellaneous hardware (€)	800
C_{other}	Cost of other components (€)	12,789
$C_{recuperator}$	Cost of recuperator (€)	21,809
C_{oil}	Cost of heat transfer loop (€)	6,000

4. CONCLUSIONS

This Chapter has completed the tool required to conduct the thermo-economic assessment.

For that, the steady-state points have been analyzed to calibrate some performance ratios required by the sub-models of fluid machines, as well as heat losses and pressure drops referred to auxiliary components.

Subsequently, a simulation of the conditions obtained in the steady-state

points has been carried out to compare measured parameters and analysis ratios with respect to values predicted by the model.

In this manner, a suitable accuracy of the model has been revealed. The main reason is due to the stability of the control operated by the system, as well as the success achieved through the calibration. In representation of the results obtained, the gross electrical power has been validated with an error bandwidth of 3.52%. The results also show that, after deducting energy consumptions and losses, an electrical efficiency up to 7.27% is reached by the process. Moreover, it has been observed that a higher exploitation of the heat source could be made, which may bring greater benefits.

Regarding the economic prediction of the model, the costs resulting from simulations have been compared to the initial estimations of the project, also confirming their validity.

Chapter VI

Results
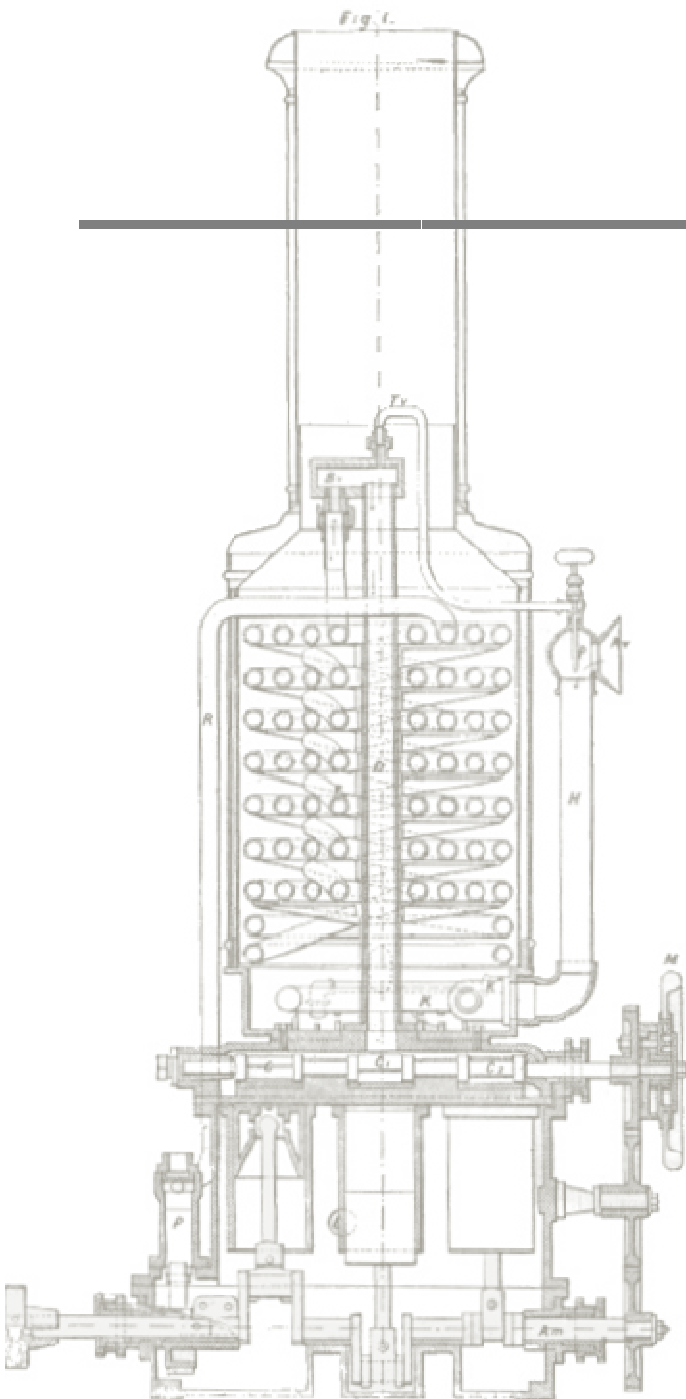
Petroleum vapor launch engine by Ofeldt (1880)

1. Introduction

Previous Chapters have contributed to achieve a validated model of a small-scale ORC integrated into an industrial process as a tool to carry out the thermo-economic assessment.

Accordingly, this Chapter begins with the economic feasibility establishment of the reference case. Subsequently, the thermo-economic optimization is conducted to achieve the most cost-effective solution. Thereby, the economic feasibility reachable through an optimized system in this type of applications is revealed. Finally, profitability indicators of both, reference and optimized, systems are compared and discussed.

2. Economic feasibility of reference case

The specific experimental application has been used throughout the document as a reference case for the model development and its subsequent validation. But also, the establishment of its economic feasibility could be useful to assess the extent of improvement that an optimized system offers.

With this in mind, this section addresses the economic feasibility of the reference case. For that, a year operation is simulated, since there are not annual data at this time. In this manner, from the estimated electricity production, profitability indicators can be quantified. For that, different economic regimes available in the industry are assessed. Moreover, other scenarios are considered by means of a sensitivity analysis.

2.1. Performance simulation

Recalling the general approach of the model, which was illustrated in Fig. IV.1, it can be noted that for the net electricity prediction, performance curves of boundary conditions are required. Consequently, performance curves of heat source and heat sink are determined below. Then, a simulation is conducted to predict the net electrical energy generated during a typical year operation.

2.1.1. Heat source

The model input with respect to the heat source refers to the characteristics of the exhaust air of the industrial process. In particular, air velocity and temperature at the inlet of the recuperator.

As it was discussed in Chapter III, the air velocity remains quite constant, so a mean value is assumed. However, the temperature variation should be considered.

There are not historical records in the industry about the exhausted air temperature. Nonetheless, due to the smooth variation of this parameter over time, quasi-steady-state points can be extracted from the week of tests. In this manner, a typical operating curve of the furnace is obtained.

To do this, values registered of air temperature at the inlet of the recuperator are averaged per hours, achieving 168 quasi-steady-state points. As a result, the temperature profile shown in Fig. VI.1 is obtained. It should be mentioned that, due to the lack of more operating data, this profile has been duplicated in the remaining weeks until completing the annuity.
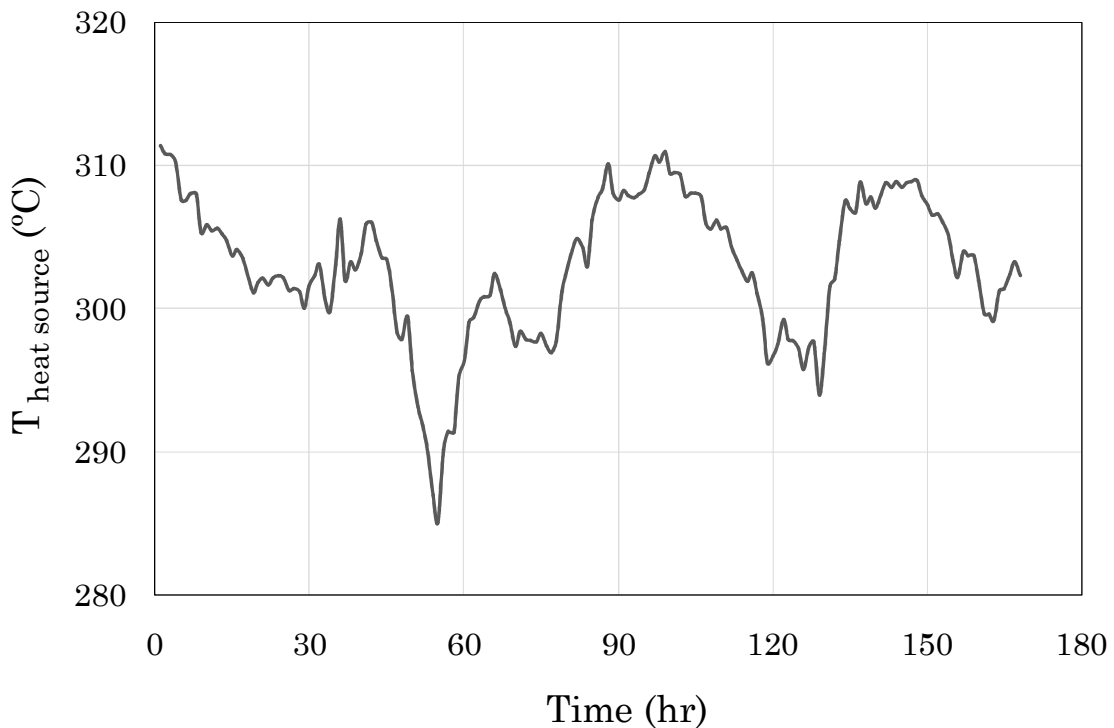
Fig. VI.1. *Temperature profile of heat source during a typical week.*

2.1.2. Heat sink

Regarding the model input referred to the heat sink, the only parameter required is the ambient temperature. It should be noted that, in this case, the air flow is not an input, since it can be known from the control operated by the system.

Taking this into account, a complete year obtained from historical records can be used, instead of just using a week of registrations. Thus, Fig. VI.2 displays values extracted from a meteorological station located around the facility [202].
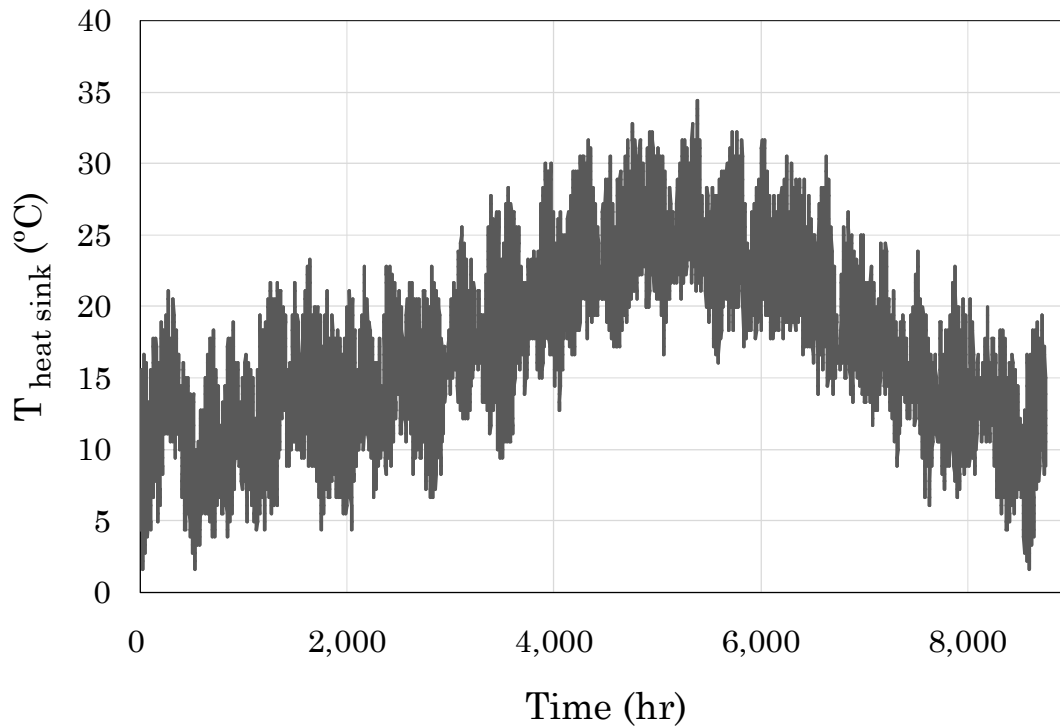
Fig. VI.2. *Temperature profile of heat sink during a typical year.*

2.1.3. Net electricity

The actual electrical energy saving that the industrial user would perceive at the end of a year is unknown. In light of this, the output of the model predicts the net electricity injected into the grid of the factory.

In the annual performance simulation, a month-long outage for maintenance tasks of furnace and WHR system is considered. Specifically, these tasks are usually scheduled for August.

It should be mentioned that due to the amount of equations and variables implemented in the model, above 600, the calculations take almost 3 seconds per point. So the hourly simulation of a year spends about 7 hours of calculations.

As a result, Fig. VI.3 shows the simulation of the net electricity that the system produces during a typical year operation. From the analysis, it highlights that the net electrical power ranges between 9.53 – 14.27 kW. Consequently, an electrical energy generation of 99 MWh is reached, which represents a saving about 1.4% of the electricity consumption of the factory.

The benefits obtained can also be assessed in energy and environmental terms. Thus, the use of this ORC for electricity production saves 203 MWh of primary energy, similarly as occurs in cogeneration power plants [203]. Moreover, in accordance to the energy mix of the country [204], about 27 t/yr of equivalent CO_2 emissions to the atmosphere are avoided.
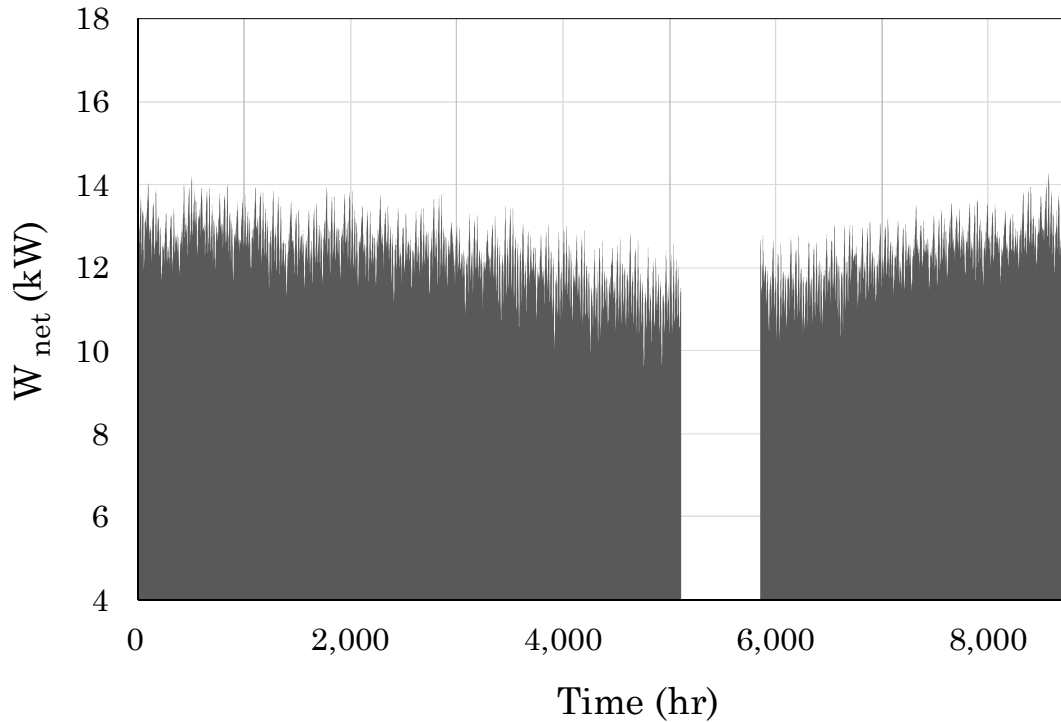
Fig. VI.3. *Simulation of net electricity of the reference case.*

2.2. Profitability study

From the revision of the state of the art, it was observed that the profitability of a project should be analyzed in function of the electricity price and the specific regulation affected. Therefore, the two economic scenarios currently available in the industry are analyzed, which consist of the self-consumption of energy or electricity sale to the energy market.

Some ratios used in the profitability study should be clarified. Firstly, the investment cost presented in Chapter V, and obtained from the operating conditions addressed below, is used. A lifetime of 25 years is assumed in accordance with regulatory values for power systems that recover waste heat from industrial processes [205]. A discount rate of 2% is initially assumed, which is later varied in the sensitivity analysis. And the annual maintenance cost is considered from the ORC supplier indications as 10 €/MWh.

2.2.1. Self-consumption of energy

Under this scenario, the economic benefit that the industrial user perceives is a consequence of the energy consumption reduction. The electricity that the WHR system supplies to the grid of the factory is instantly self-consumed in any process, so a reduction in the energy demand of the factory is achieved.

Regarding the electricity price, Chapter II demonstrated that it depends on the annual consumption of a factory, as well as country and year assessed. Accordingly, the electricity price for an industry with an annual electricity consumption about 7,000 MWh, located in Spain, and using 2015 as reference year (in which tests were conducted), is selected. In particular, an electricity price for the energy saved of 96.15 €/MWh is adopted [122].

With respect to the regulation, in Spain, there is currently an economic charge for the self-consumption of energy [125], even if it is instantly used in the factory. The main reason is to contribute to some energy costs derived from the electrical network, which supports the energy requirements of the factory when a failure in the decentralized system occurs. Specifically, there is a tax that directly affects the price of the electricity, which is shown in Table VI.1 in function of the six-period fee [206]. It should be mentioned that, since an hourly simulation is conducted in this study, the price differentiation according to the six-periods fee is considered [207].

Table VI.1. *Six-period tax for self-consumption of energy.*

Period 1 (€/MWh)	11.775
Period 2 (€/MWh)	11.336
Period 3 (€/MWh)	7.602
Period 4 (€/MWh)	9.164
Period 5 (€/MWh)	9.986
Period 6 (€/MWh)	6.720

Paying attention to the incentives that energy efficiency measures in industry receive in Spain [126], a contribution up to 30% of the total investment of the project is currently available [128]. So this investment incentive is also considered through a bandwidth in the results.

In particular, the results with regard to the economic feasibility of the reference case under the self-consumption regime are displayed in Fig. VI.4 and listed in Table VI.2. In the first place, it can be seen that the project is considered feasible. Thus, the NPV is positive, the PI is greater than the unit, an IRR higher than the discount rated is achieved, a DPP lower that the lifetime of the system is reached, and the price associated to the electricity generated is higher than their production cost (LCOE). However, more profitable ratios are expected to undertake this type of projects. For instance, the literature reviewed expose that payback periods around 3 − 4 years are necessary for the technology diffusion [81].
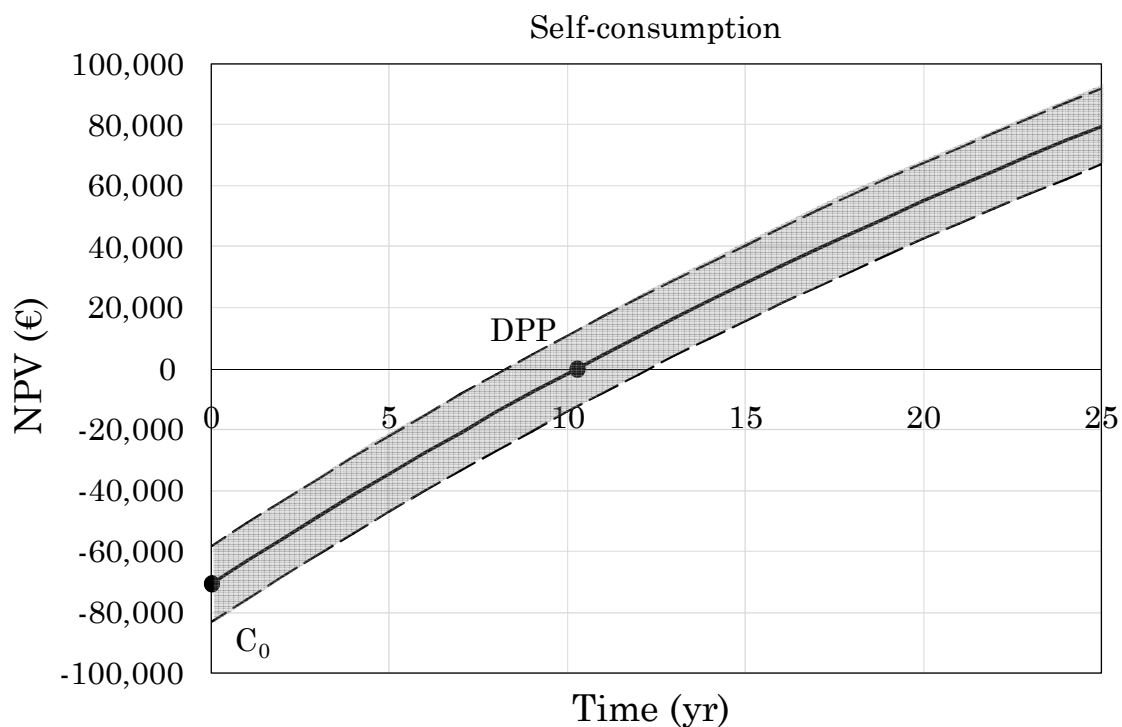
Fig. VI.4. *Profitability of reference case under self-consumption regime.*

Table VI.2. *Mean profitability indicators of reference case in self-consumption regime.*

Electricity generated (kWh)	E_{final}	98,879
Investment cost with 15% incentive (€)	C_0	70,743
Annual cash flow (€)	C_t	7,693
Net Present Value (€)	NPV	79,445
Profitability Index (-)	PI	2.12
Internal Rate of Return (%)	IRR	9.83
Discounted payback period (yr)	DPP	10.27
Average price of electricity (€/MWh)	–	87.80
Levelized Cost Of Electricity (€/MWh)	LCOE	45.93

2.2.2. Sale of electricity to the energy market

There is a different economic regime available in the industry to the self-consumption. In particular, the net electricity can be sold to the energy market [208], besides receiving an economic retribution assigned to the sustainable electricity generation [124].

The price at which the owner of a power plant can sell the electricity to the energy market is determined by the pool price. Therefore averaged values per month of the reference year are used [208].

The economic retribution received depends on the type of application. For the case of waste heat recovery from industrial processes, the tabulated value in the applicable regulation represents an annual income of 1,208 € [205].

In addition, the bandwidth due to the economic incentive that promotes energy efficiency measures in industry is also considered in this scenario.

The results with regard to the economic feasibility of the reference case under the economic regime that consists of the electricity sale to the energy market are displayed in Fig. VI.5 and listed in Table VI.3. As can be seen, worse values are obtained in comparison to the previous scenario. For instance, the IRR has a value close to 5%, which is a measure of the low reliability of a project under this scenario.
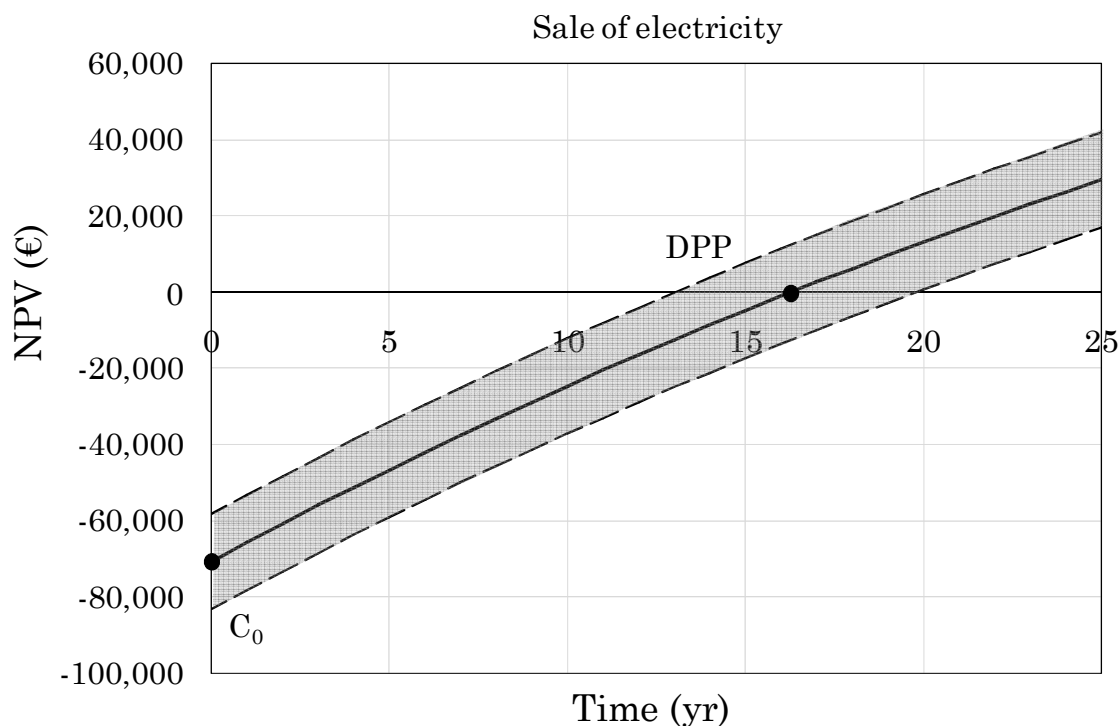
Fig. VI.5. *Profitability of reference case in the sale of electricity regime.*

Table VI.3. Mean profitability indicators of reference case in the sale of electricity regime.

Electricity generated (kWh)	E_{final}	98,879
Investment cost with 15% incentive (€)	C_0	70,743
Annual cash flow (€)	C_t	5,132
Net Present Value (€)	NPV	29,443
Profitability Index (-)	PI	1.42
Internal Rate of Return (%)	IRR	5.22
Discounted payback period (yr)	DPP	16.29
Average price of electricity (€/MWh)	–	61.59
Levelized Cost Of Electricity (€/MWh)	LCOE	45.93

2.3.   Sensitivity analysis

Taking into account the influence of the economic regime on the results, an extrapolation of the reference case to other scenarios is conducted. For that, the discounted payback period is used as a representative indicator of the project profitability, since it has been pointed as the most used feasibility ratio by corporations.

In this way, Fig. VI.6 shows the electricity price influence over the DPP and includes the results bandwidth for investment incentives up to 30%. Notice that the range of electricity prices assessed is in accordance with the values reviewed in Chapter II for different sizes of industries in Spain, as well as countries of the EU-28. Thus, a DPP lower than 10 years can be reached if electricity prices are above 90 €/MWh and investment incentives are received. However, to get close to profitability expectations, the highest value of electricity price and the greatest economic incentive is required. This optimistic scenario can be associated to industries that use the self-consumption regime in Spain, if the annual electricity consumption is under 500 MWh (Fig. II.20), or in Italy, where the industries have the highest electricity price and that receive incentives in the form of white certificates.

The DPP variation (in absence of incentives) in function of electricity price and discount rate is shown in Fig. VI.7. From a general point of view, it is noted the exponential detriment of the DPP with respect to the electricity price reduction, which is more severe the higher the discount rate. Thus, it highlights that electricity prices upper 100 €/MWh are required to ensure payback periods lower than 10 years in absence of incentives.
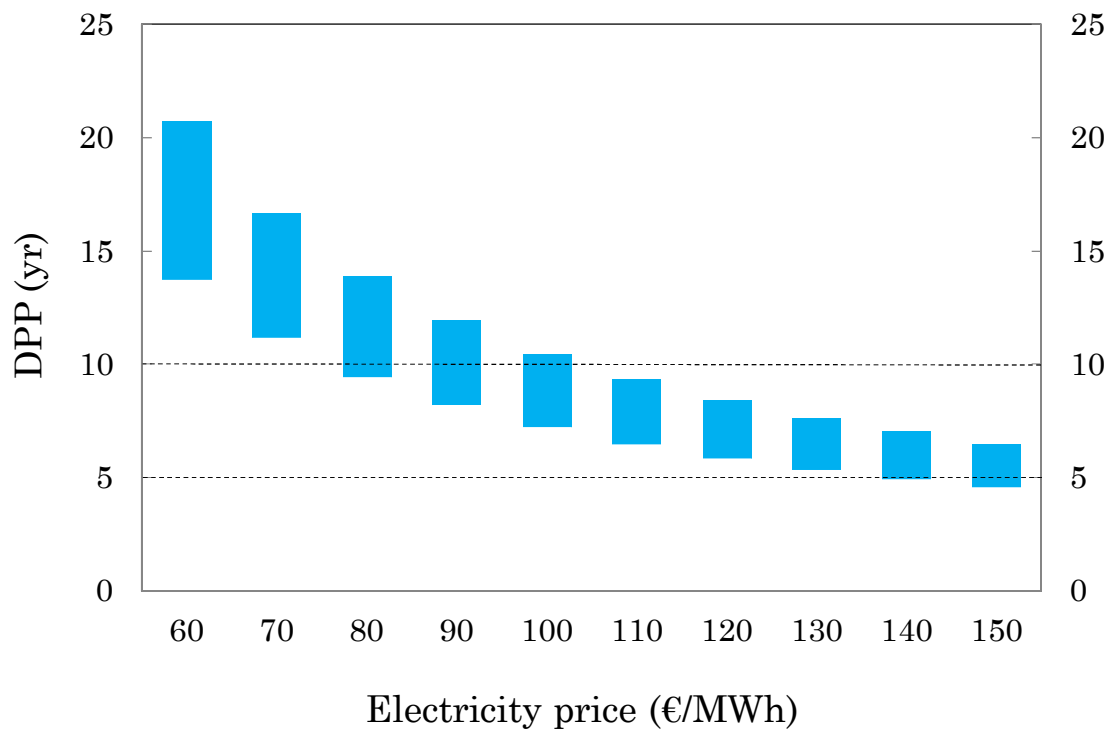
Fig. VI.6. *Sensitivity analysis of reference case.*
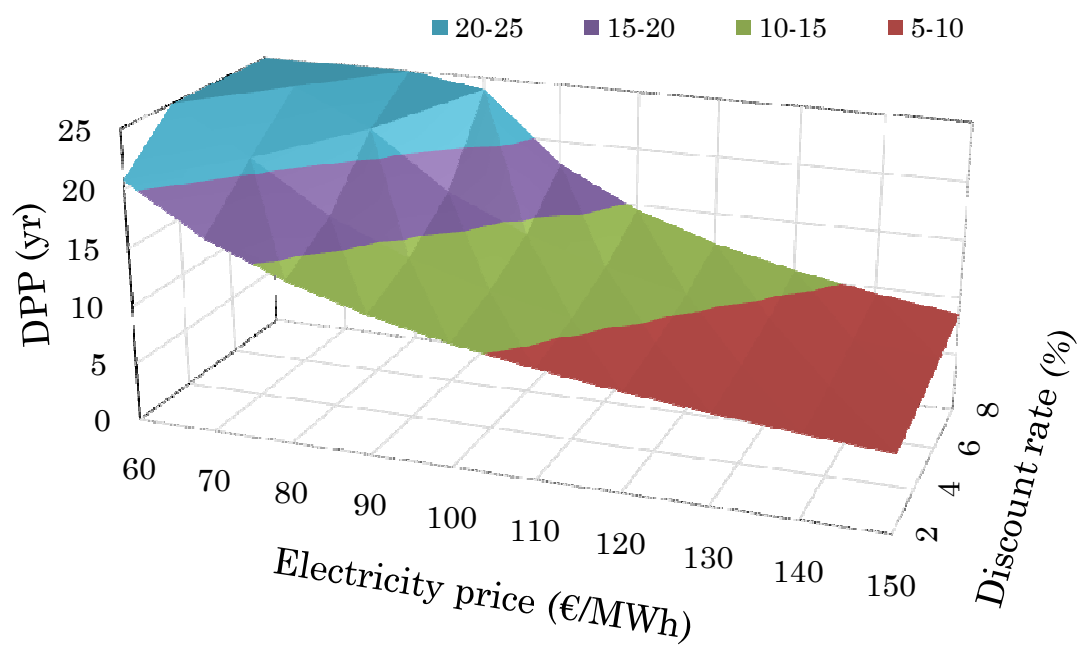
Fig. VI.7. *Sensitivity analysis of discounted payback period of reference case in function of electricity price and discount rate.*

3. THERMO-ECONOMIC OPTIMIZATION

This section addresses the thermo-economic optimization of the system. In this manner, a subsequent economic feasibility study can be conducted to assess the extent of improvement that an optimized system offers.

For that, firstly, the optimization approach is described. Secondly, the relevance of each parameter on the system is analyzed. And thirdly, a multivariable optimization is carried out to find the most cost-effective solution.

3.1.   Optimization approach

Before conducting the optimization, operating conditions, objective function, and main parameters to take into account require being addressed.

3.1.1. Operating conditions

The system optimization can be conducted from representative conditions of the annual system operation. In particular, it is proposed the use of the heat source and heat sink conditions that provide as model output the average annual power of the system.

To do this, and taken into account the bounded range of conditions obtained referred to the heat source, the mean temperature of the exhaust air is assumed. So the equivalent temperature of the heat sink can be inversely calculated. Accordingly, the simulation of the system using the operating conditions of heat source and heat sink listed in Table VI.4 provides as output the average power produced during a typical year. The resulting thermodynamic cycle of mean operating conditions of the reference case is displayed in Fig. VI.8. Notice that the numbering corresponds to Fig. III.8.

Table VI.4. *Operating conditions considered for the thermo-economic optimization.*

Average annual net power (kW)	$\overline{W}_{net}$	12.34
Mean heat source temperature (ºC)	$\overline{T}_{heat\ source}$	302.95
Equivalent heat sink temperature (ºC)	$T_{heat\ sink_{eq}}$	16.67
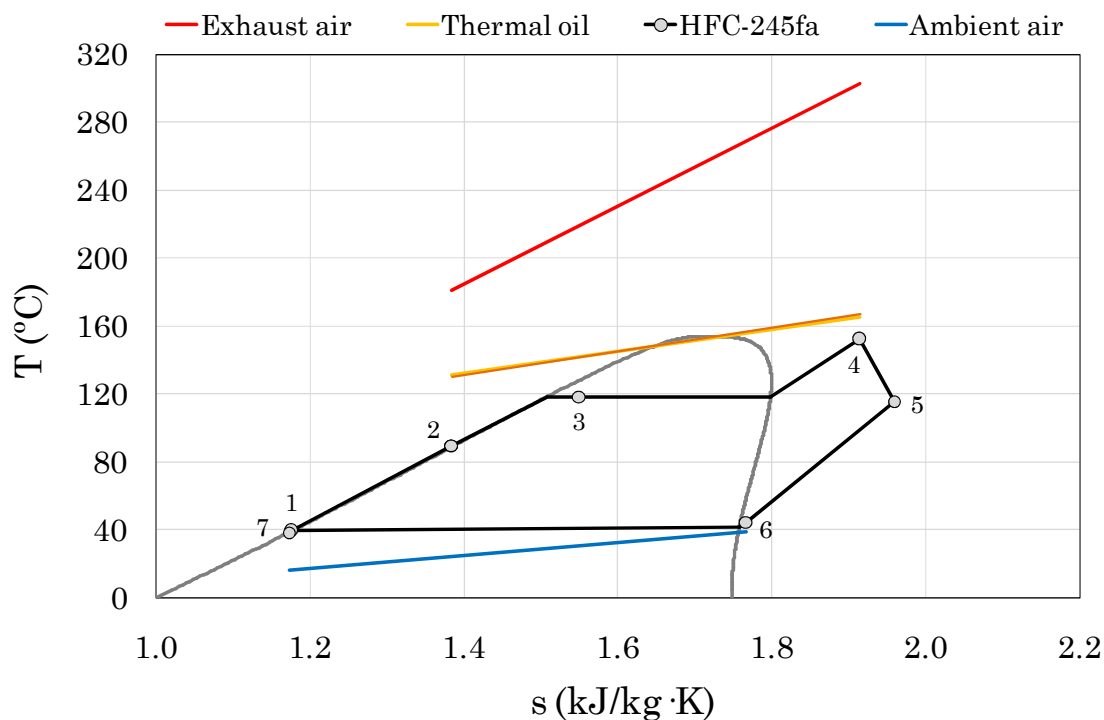
Fig. VI.8. *Reference cycle in a temperature-entropy diagram (numbering corresponds to Fig. III.8).*

3.1.2. Objective function

Chapter II argued that SIC is the most usual cost-effective ratio used in thermo-economic optimizations of ORC systems. This indicator enhances the power output, which is the main goal to help the environmental issue described in Chapter I, but also to provide an economically advantageous solution for industrial users.

The $SIC_{project}$ and other relevant parameters useful for comparisons of reference and optimized systems are listed in Table VI.5.

Table VI.5. *Main objective parameters of reference case.*

$SIC_{project} \left(€ / kW \right)$	6,747
$Q_{source} \left(kW \right)$	180.61
$W_{net} \left(kW \right)$	12.34
$\eta_{process} \left(\% \right)$	6.83

3.1.3. Parameters assessed

The parameters that are going to be individually and together analyzed are listed in Table VI.6. Improvements referred to the control strategy implemented in the system, sizing of heat exchangers and expansion

machine, and working fluid selected are assessed.

Table VI.6. *Main parameters thermo-economically optimized.*

		Reference case
Control Strategy	$\Delta T_{\text{superheating}}\left(K\right)$	35
	$\Delta T_{\text{condensing}}\left(K\right)$	25
	$\dot{V}_{\text{oil}}\left(m^3/h\right)$	9.07
Geometric characteristics of heat exchangers	$N_{\text{Recuperator}}\left(-\right)$	14
	$A_{\text{HRVG}}\left(m^2\right)$	6.9
	$A_{\text{Reg}}\left(m^2\right)$	12.9
	$L_{\text{tube condenser}}\left(m\right)$	9.5
Geometric characteristics of expander	$V_r\left(-\right)$	5.5
	$\dot{V}_{\text{swept}}\left(m^3/h\right)$	22.2
Cycle characteristics	Organic working fluid	HFC-245fa

3.2. Assessment of individual parameters

Before conducting a multivariable optimization, the assessment of individual parameters could lead to the most important topics to pay attention in thermo-economic assessments.

With this in mind, the improvements suggested to optimize ORC systems are individually analyzed below.

3.2.1. Control strategy

The control strategy was experimentally established during the startup of the WHR system. It was implemented to ensure adequate operating conditions for both, ORC and heat source. However, the analysis of experimental data, shown in Chapter V, has revealed that a higher exploitation of the heat source could be made.

Therefore, the different control strategies are assessed. For that, only the restriction of minimum exhaust air temperature of 170 ºC, defined in Chapter III, is considered.

3.2.1.1. Superheating degree

The superheating degree is the temperature difference between the input of the expander and saturated conditions. This difference is maintained quite constant around a set point value that was predefined during the startup.

This variable is typically minimized in the literature, usually considering a set point value of 5 K to ensure vapor quality at the inlet of the expander [101]. The main reason is due to the lower the superheating degree, the higher the recovery capacity of the system.

This effect can be appreciated in Fig. VI.9. Effectively, the lower the value of superheating, the higher the thermal power recovered. Nonetheless, the electrical production reaches a maximum net electrical power of 12.53 kW with a superheating degree of 45 K. This fact is due to the positive superheating influence when certain working fluids in a regenerative architecture are used, such as also was reported in the literature to reach higher temperatures [39]. To clarify, Fig. VI.10 shows that greater pressures and temperatures at the inlet of the expander (point 4) are reached with higher superheating values.
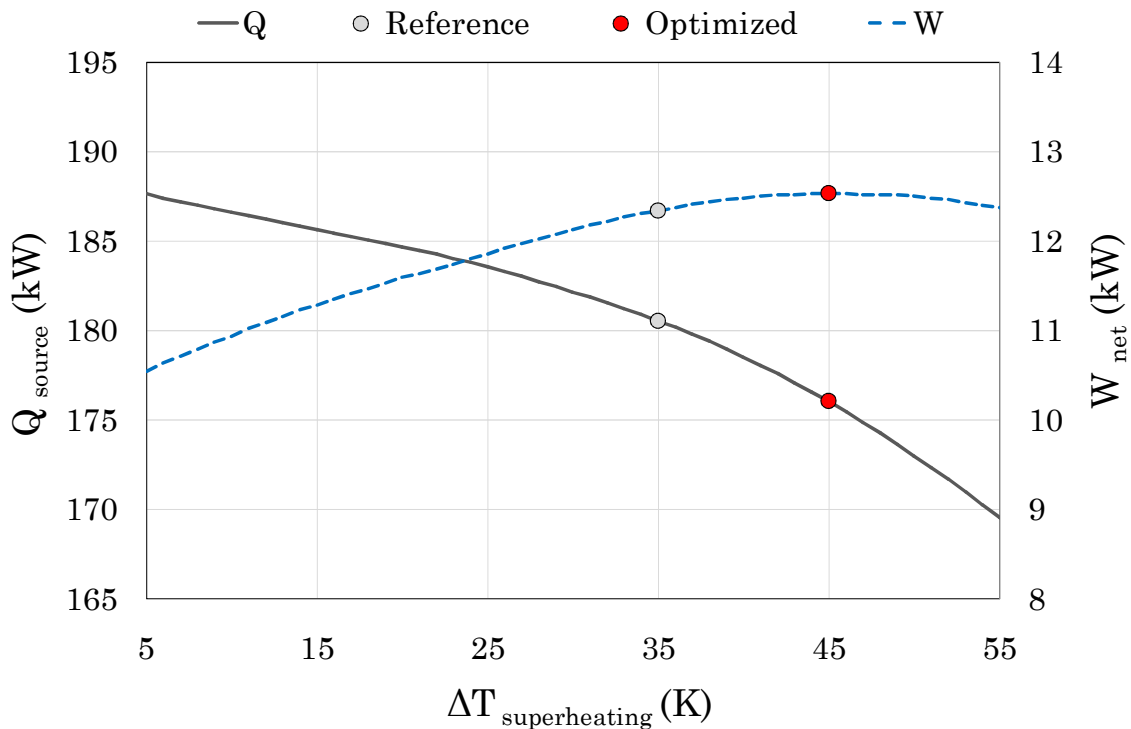
Fig. VI.9. *Superheating degree assessment in function of power input and output.*
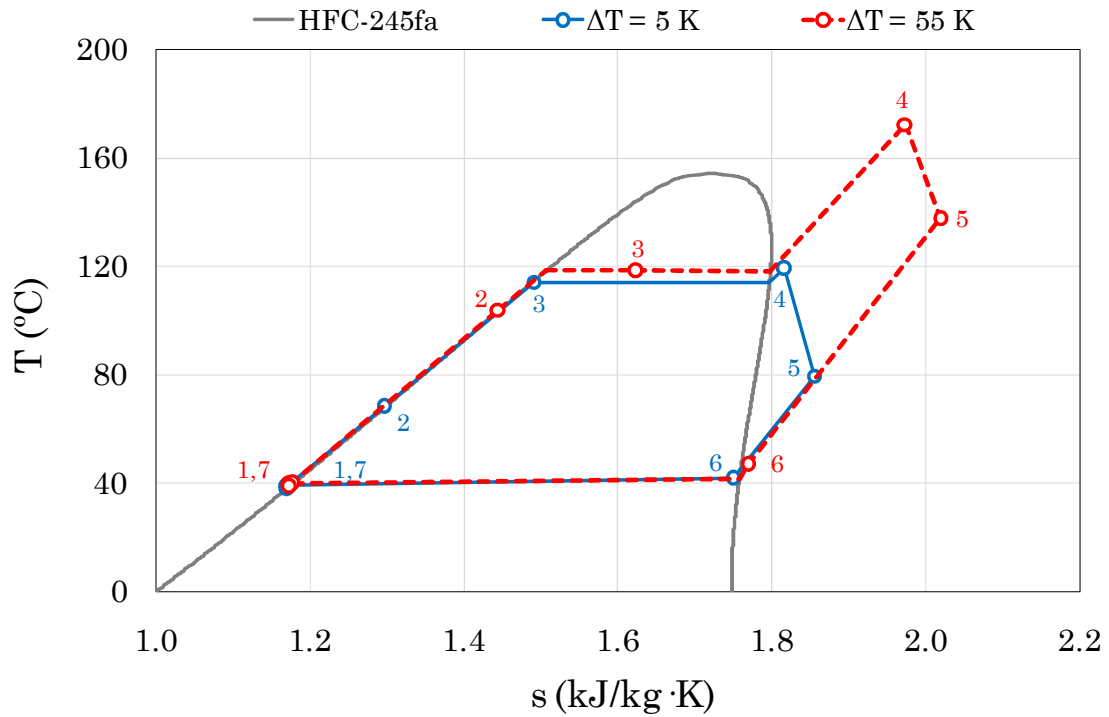
Fig. VI.10. *Superheating degree influence in a temperature-entropy diagram (numbering corresponds to Fig. III.8).*

Regarding the objective function, the SIC $SIC_{project}$ is minimized as the electrical power increases, since the investment cost does not vary with respect to the control strategy. Thus, the ratio of $SIC_{project}$ is reduced to 6,641 €/kW, such as Fig. VI.11 shows.
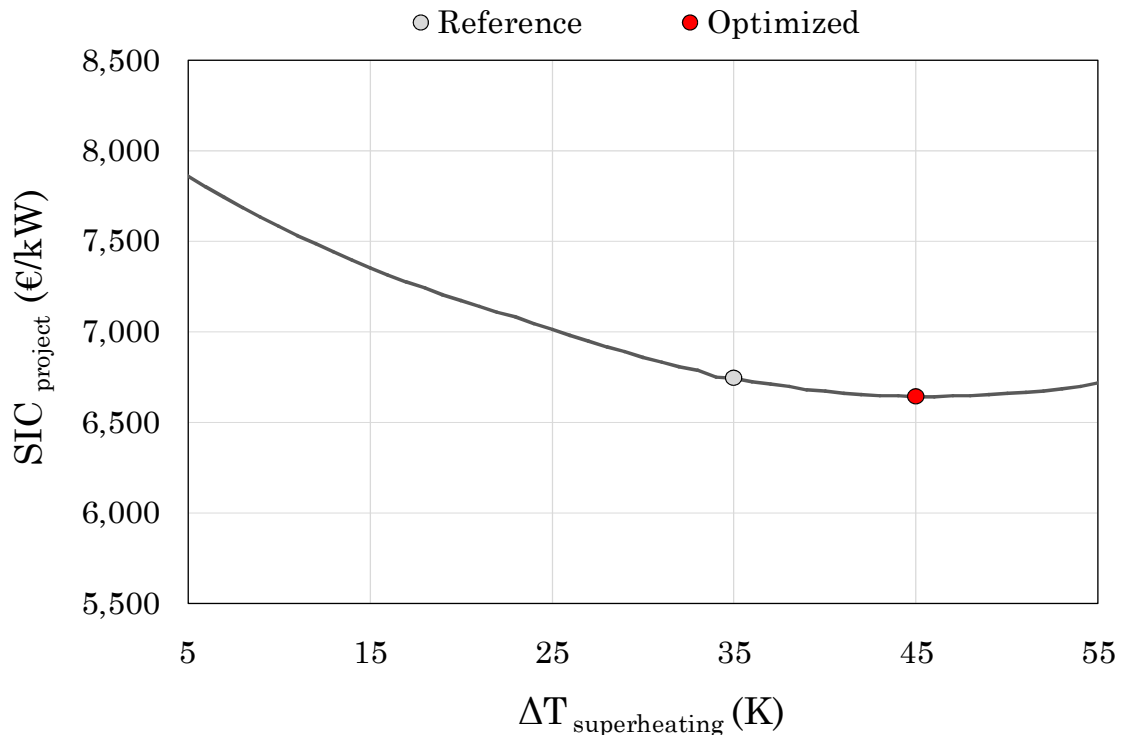
Fig. VI.11. *$SIC_{project}$ assessment in function of superheating degree.*

3.2.1.2. Condensing temperature

Similar to the previous control, the condensing temperature is also regulated from a set point value. This value refers to the temperature difference between condensing conditions of the organic fluid and the ambient temperature.

The results in function of power input and output are depicted in Fig. VI.12. In the first place, it highlights that lower values of set point could provide greater benefits. Thus, the optimum value of 14.5 K allows producing a net electricity of 12.98 kW. It should be clarified that values of air volumetric flow rate remain below the rated capacity of the fans of the condenser.
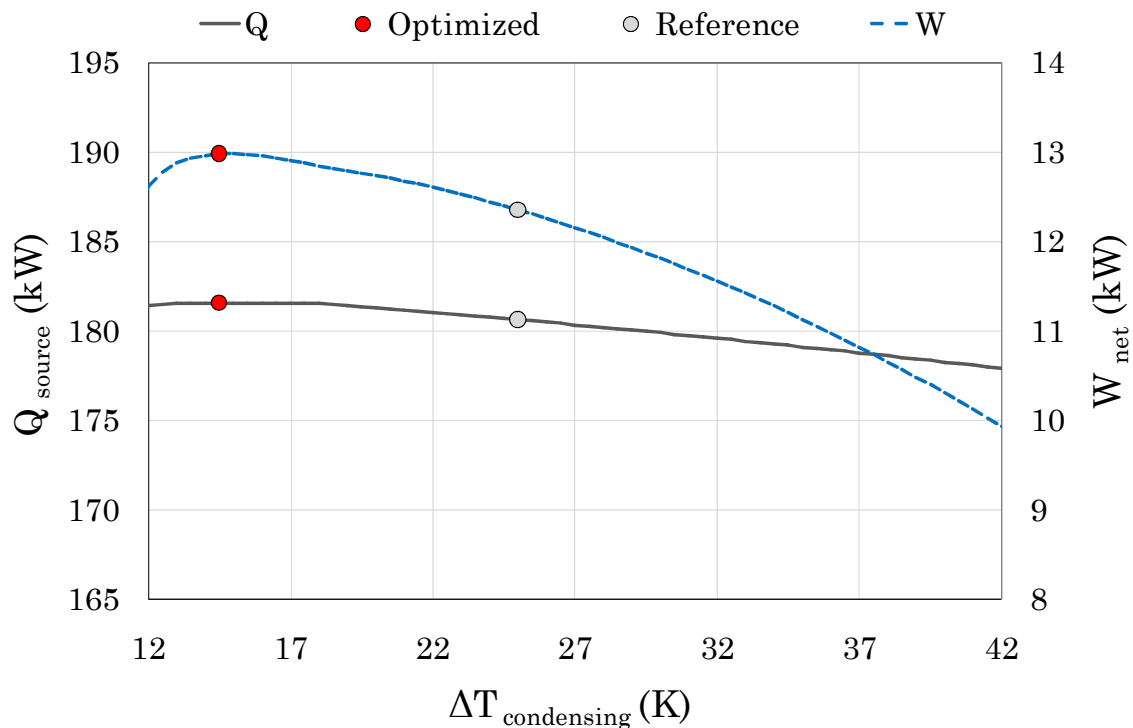
Fig. VI.12. *Condensing temperature control assessment in function of power input and output.*

Since the variation of the set point value in the control system does not modify the investment cost, the improvement of the $SIC_{project}$ is caused by the electrical gain. Thus, a $SIC_{project}$ of 6,416 €/kW is obtained, such as Fig. VI.13 shows.
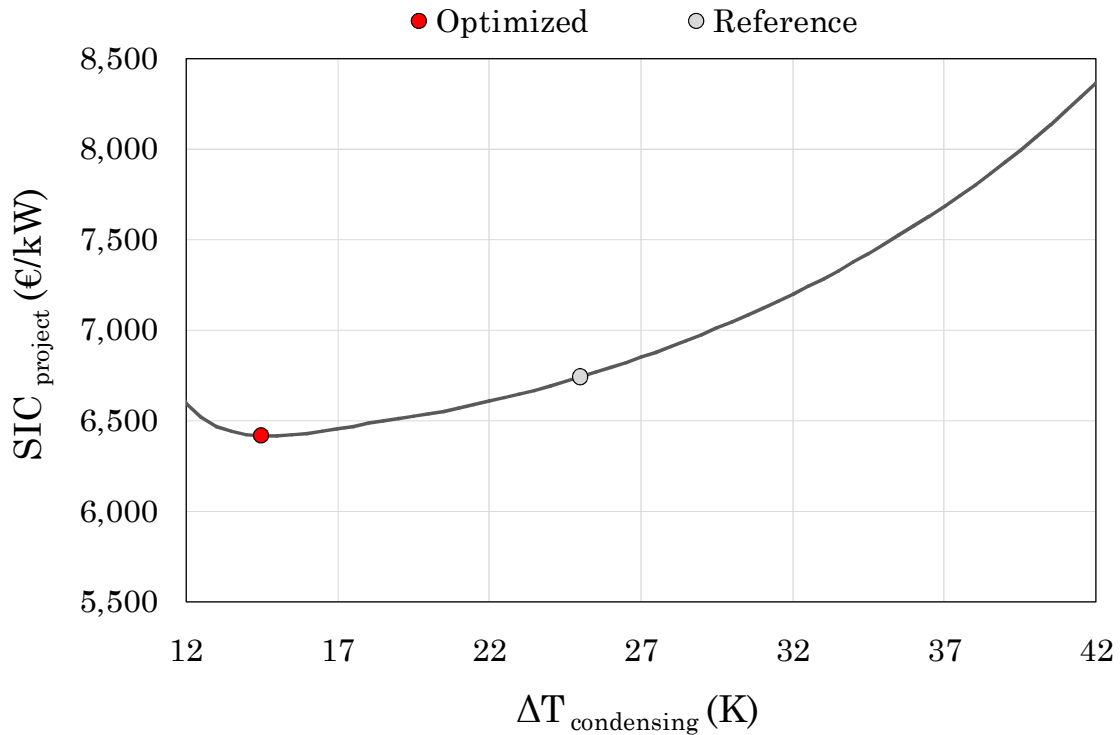
Fig. VI.13. *SIC$_{project}$ assessment in function of condensing temperature control.*

3.2.1.3. Thermal oil circuit

The thermal oil pump operates at a constant rotational speed, set by a speed drive, which may be improved through an optimization. In this way, different values have been simulated and depicted in Fig. VI.14. Firstly, it highlights that the increase of the thermal oil flow rate allows the whole waste heat recovery. However, the increase of electrical power requirements tends to reduce the net electricity. Thus, it highlights that the current flow rate is close to the optimum, which is estimated about 10 m³/h to reach a net electrical power of 12.39 kW.

The SIC$_{project}$ variation in function of thermal oil volumetric flow rate is shown in Fig. VI.15. Thus, an improvement of SIC$_{project}$ to 6,725 €/kW could be reached through the variation of the rotational speed of the pump.
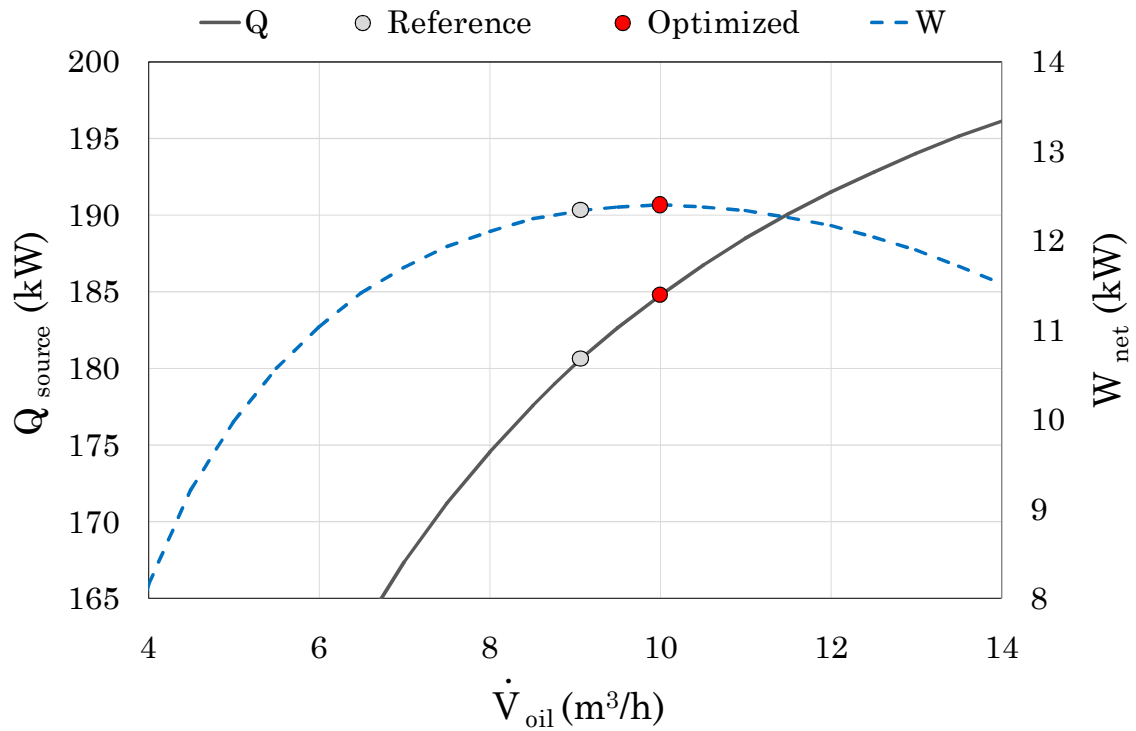
Fig. VI.14. *Thermal oil volumetric flow rate assessment in function of power input and output.*
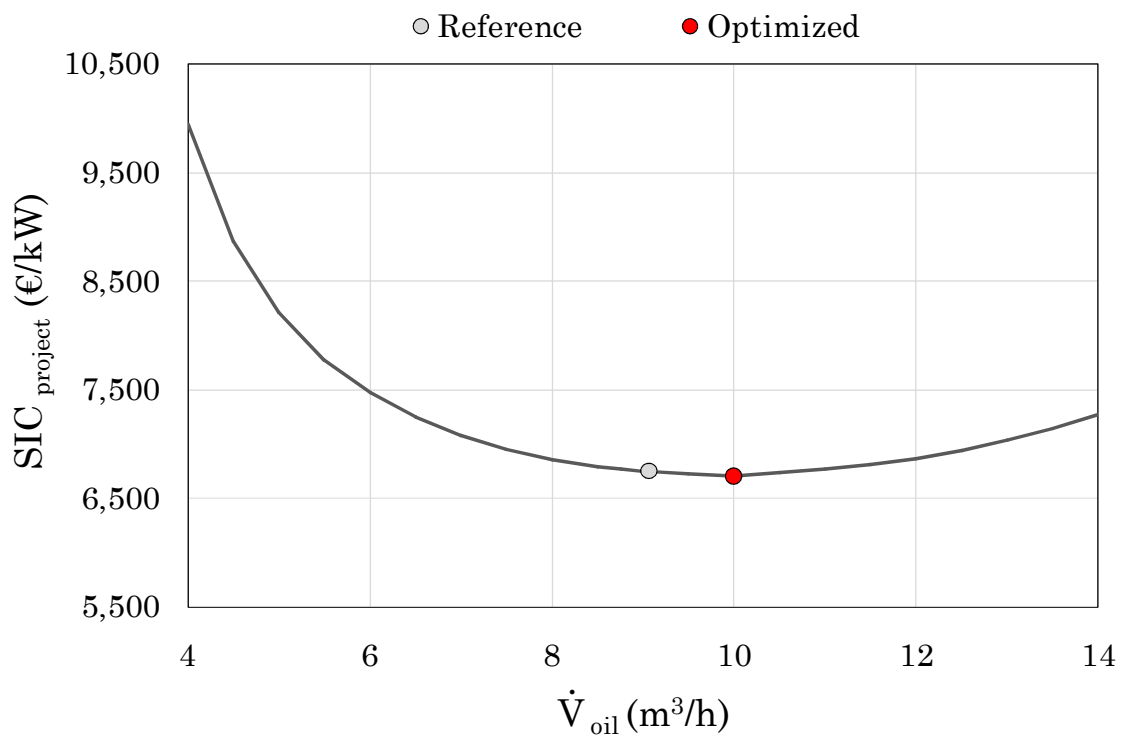
Fig. VI.15. *SIC_{project} assessment in function of thermal oil volumetric flow rate.*

Notice that the combined optimization of the control strategies could lead to a more powerful system that does not require additional investment cost. The results of this proposal are collected in Appendix I.

3.2.2. Geometric characteristics of heat exchangers

The size of the recuperator, HRVG, regenerator, and condenser are thermo-economically assessed as follows.

3.2.2.1. Recuperator

The recuperator is a heat exchanger classified as bank of finned tubes. Their geometric characteristics were designed according to the thermal requirements. Nonetheless, a different exchange surface may improve the economic feasibility of the project. In this way, the analysis is conducted varying the number of passes, or tubes in the direction of the air flow.

The results are displayed in Fig. VI.16. The higher the number of tubes, or exchange surface, the higher the thermal power recovered. In this case, the number of tubes that minimizes the $SIC_{project}$ is 16, which allows producing almost 13 kW of net electrical power.
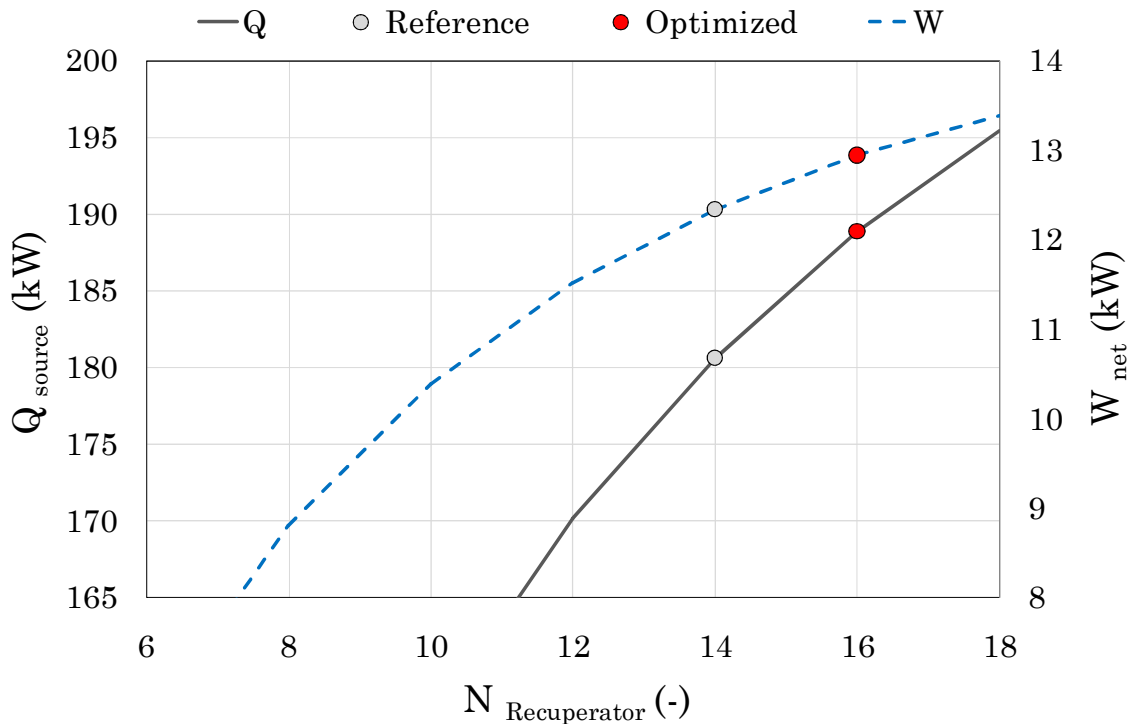
Fig. VI.16. *Recuperator exchange surface (number of passes) assessment in function of power input and output.*

The influence of the exchange surface over the $SIC_{project}$ is shown in Fig. VI.17. In particular, the optimized value obtained is 6,698 €/kW.
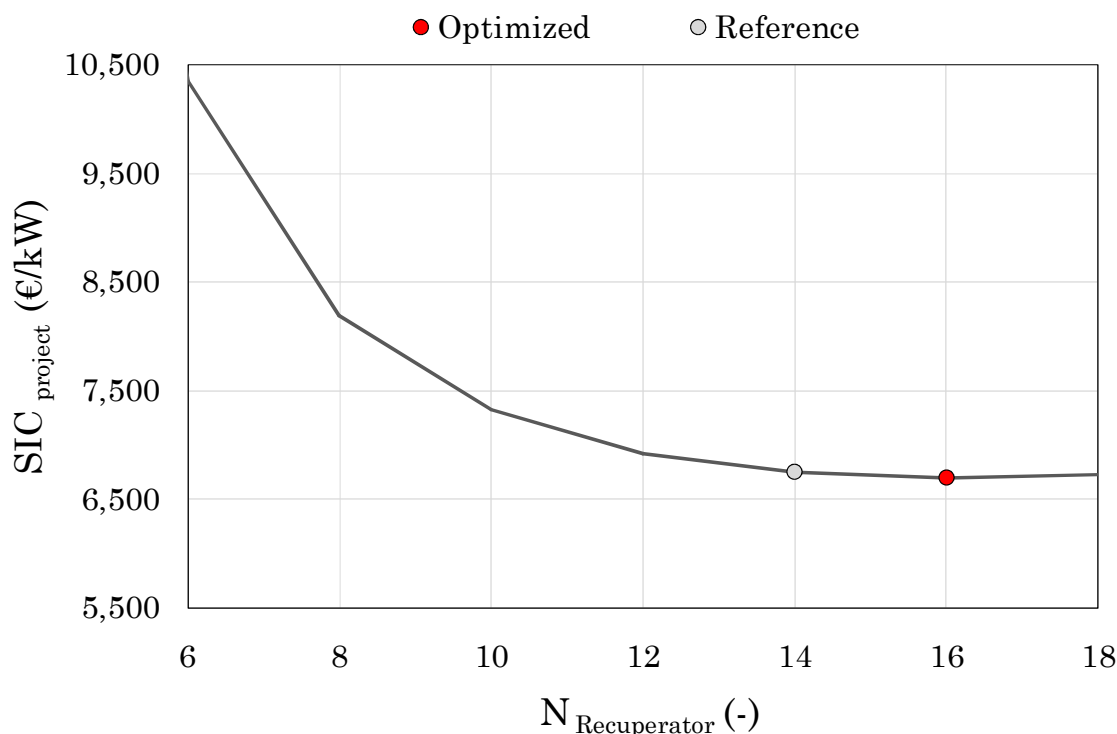
Fig. VI.17. *$SIC_{project}$ assessment in function of recuperator exchange surface (number of passes).*

3.2.2.2. HRVG

The HRVG comprises two BPHEs, the economizer and the evaporator. In order to assess the importance of its sizing on the $SIC_{project}$, the exchange surface has been optimized.

The results are collected in Table VI.7. As can be appreciated, the increase of the exchange surface leads to a better value of $SIC_{project}$. This is due to the electrical power improvement as a consequence of the higher thermal power recovered, as well as the enhancement of the heat exchangers effectiveness and pressure drop reduction.

Table VI.7. *Results of HRVG optimization.*

		Optimized
Exchange surface of HRVG (m²)	A_{HRVG}	8.54
Thermal power input (kW)	Q_{source}	183.48
Electrical power output (kW)	W_{net}	12.88
Specific Investment Cost (€/kW)	$SIC_{project}$	6,607

3.2.2.3. Regenerator

The regenerator is the additional heat exchanger with respect to the conventional architecture of the cycle. This typology is also discussed in the literature, since it allows improving the cycle efficiency, but not always the electrical power output [58]. Taking this into account, the influence of the regenerator is also assessed. For that, the exchange surface has been varied, such as Fig. VI.18 shows.

The results point that the net electrical power increases with the surface of the regenerator. Nonetheless, an increment about 26% of the exchange surface minimizes the $SIC_{project}$ to 6,709 €/kW, such as Fig. VI.19 shows.
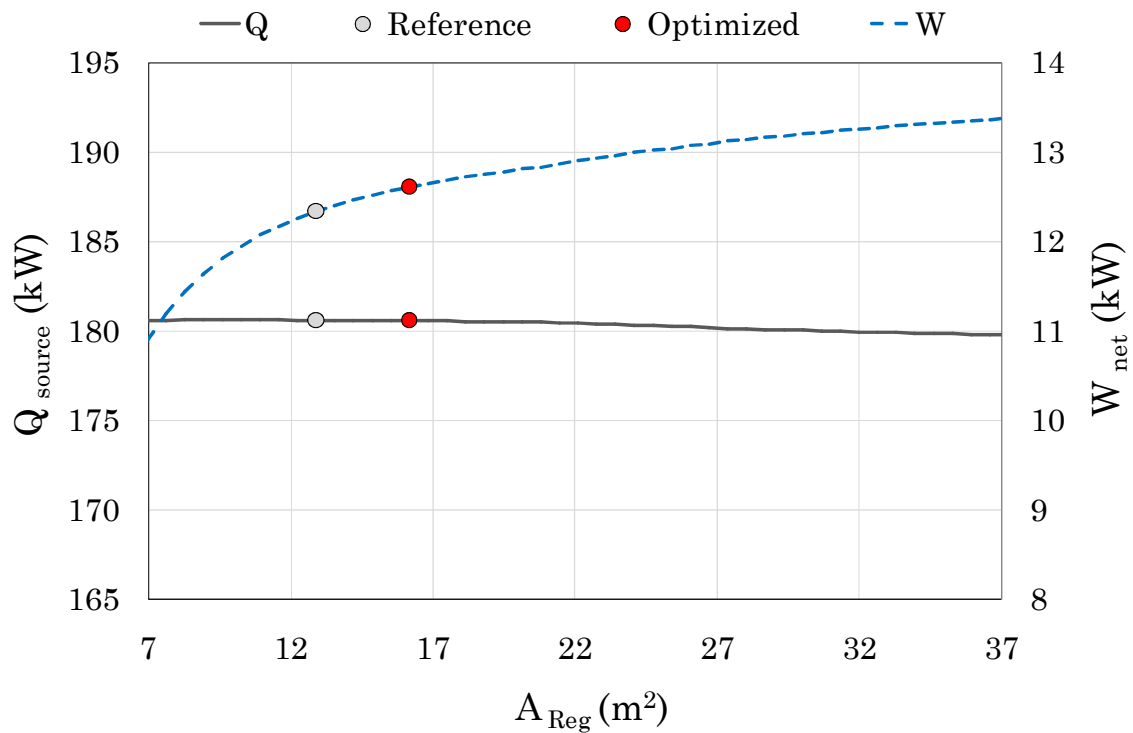
Fig. VI.18. *Regenerator exchange surface (number of plates) assessment in function of power input and output.*
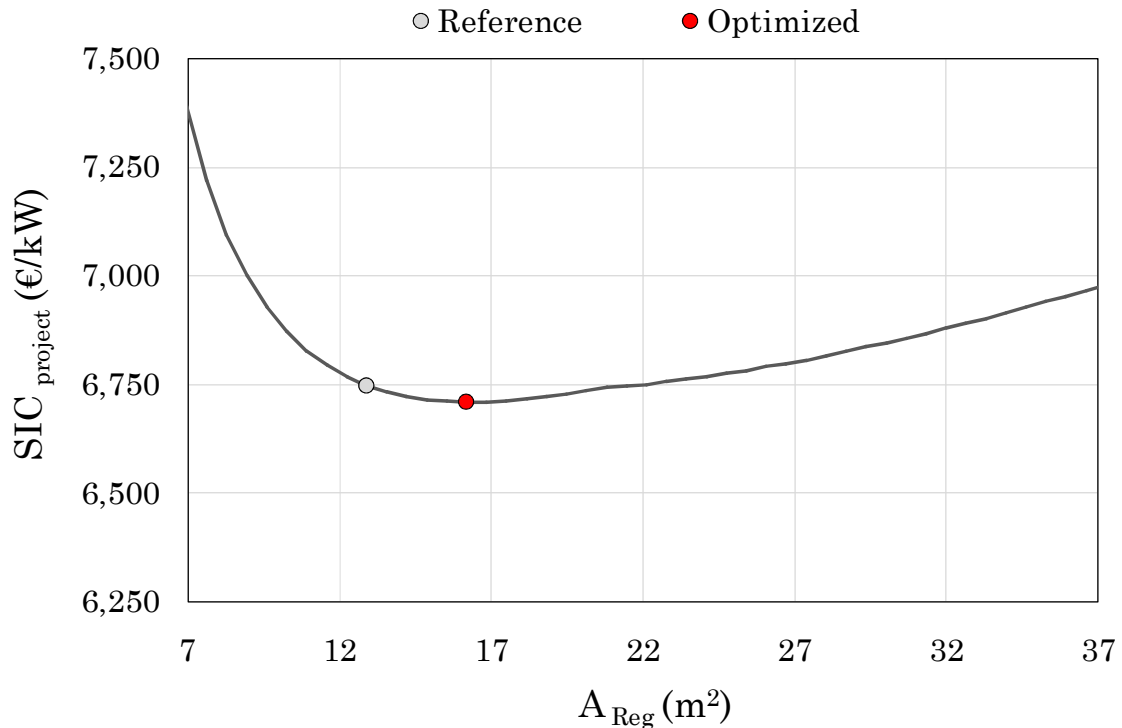
Fig. VI.19. SIC$_{project}$ assessment in function of regenerator exchange surface (number of plates).

3.2.2.4. Condenser

The direct air-cooled condenser is also classified as a bank of finned tubes. In this case, in order to maintain the typology of the heat exchanger, the tube length is the parameter considered to be modified. It should be clarified that the rated fans capacity and the distance between fans have been constrained.

The results confirm that this component is too oversized. The design decision was initially considered to minimize the electrical consumption of fans. However, Fig. VI.20 shows that the electrical power almost does not vary until a half of the tube length. It should be clarified that, despite a higher electrical consumption of fans is required with the tube length reduction, the electrical efficiency of the motors increases as it approaches to rated conditions. So the electrical penalization is minimized. Consequently, a remarkable reduction of 13% in the SIC$_{project}$ is observed in Fig. VI.21, that drops to 5,853 €/kW.
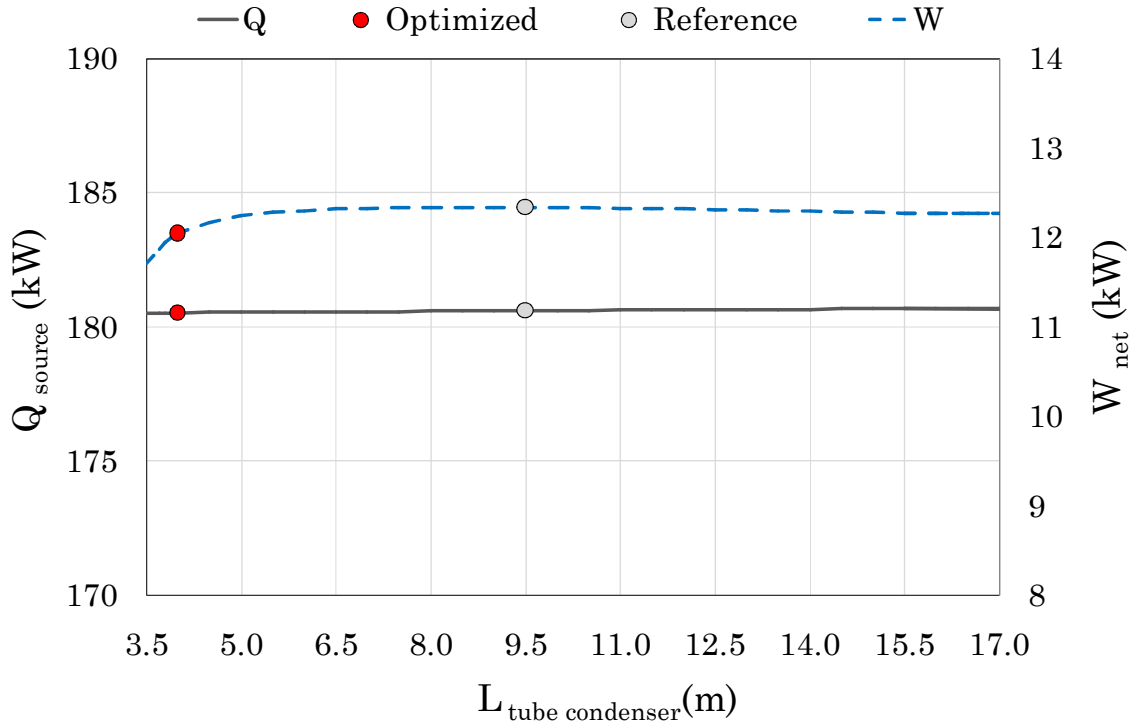
Fig. VI.20. *Condenser exchange surface (tube length) assessment in function of power input and output.*
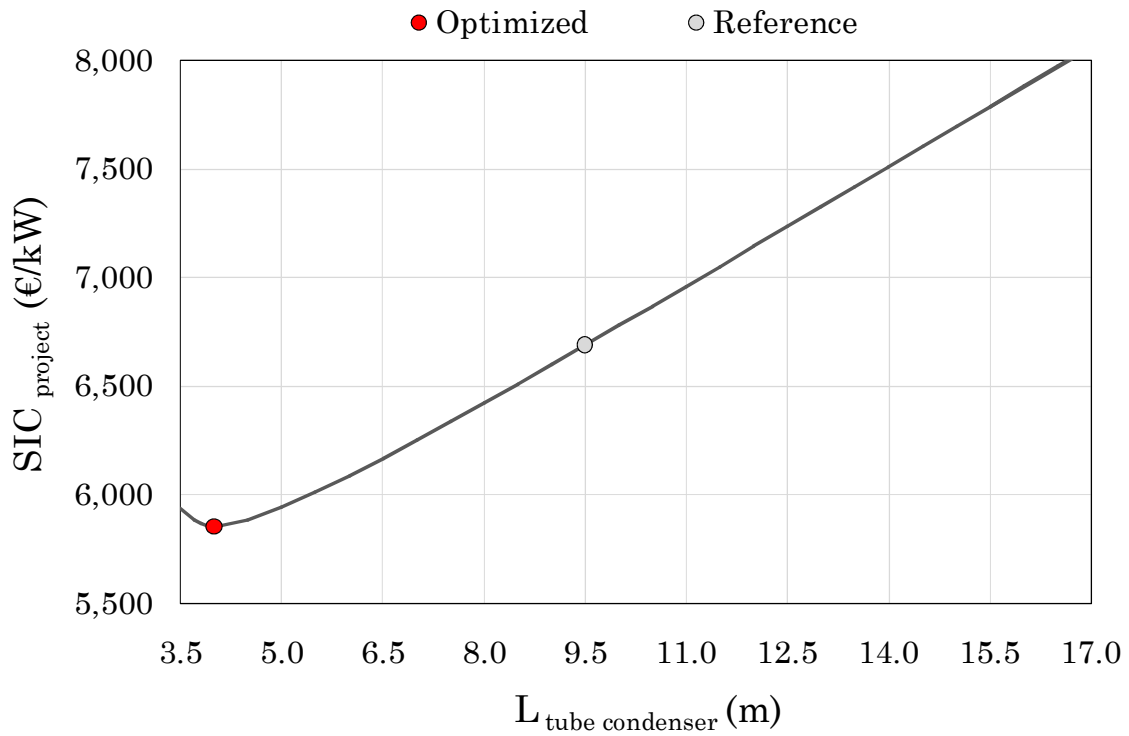
Fig. VI.21. *SIC_{project} assessment in function of condenser exchange surface (tube length).*

3.2.3. Geometric characteristics of the expander

One of the main parameters investigated about the volumetric expansion technology is the influence of the built-in volume ratio over the cycle performance [209]. In this way, Fig. VI.22 shows that there is a value that optimizes the performance of the expander and, hence, maximizes the electrical power output. In this case, the optimum value matches with that used in the reference case, such as Fig. VI.23 shows. In these figures, it is also noted that the higher the built-in volume ratio, the lower the thermal power recovered.

In the same way, Fig. VI.24 shows that the capacity to recover waste heat increases with the swept volume. However, an optimized swept volume of 18 m³/h allows reducing the $SIC_{project}$ to 6,622 €/kW, such as Fig. VI.25 shows
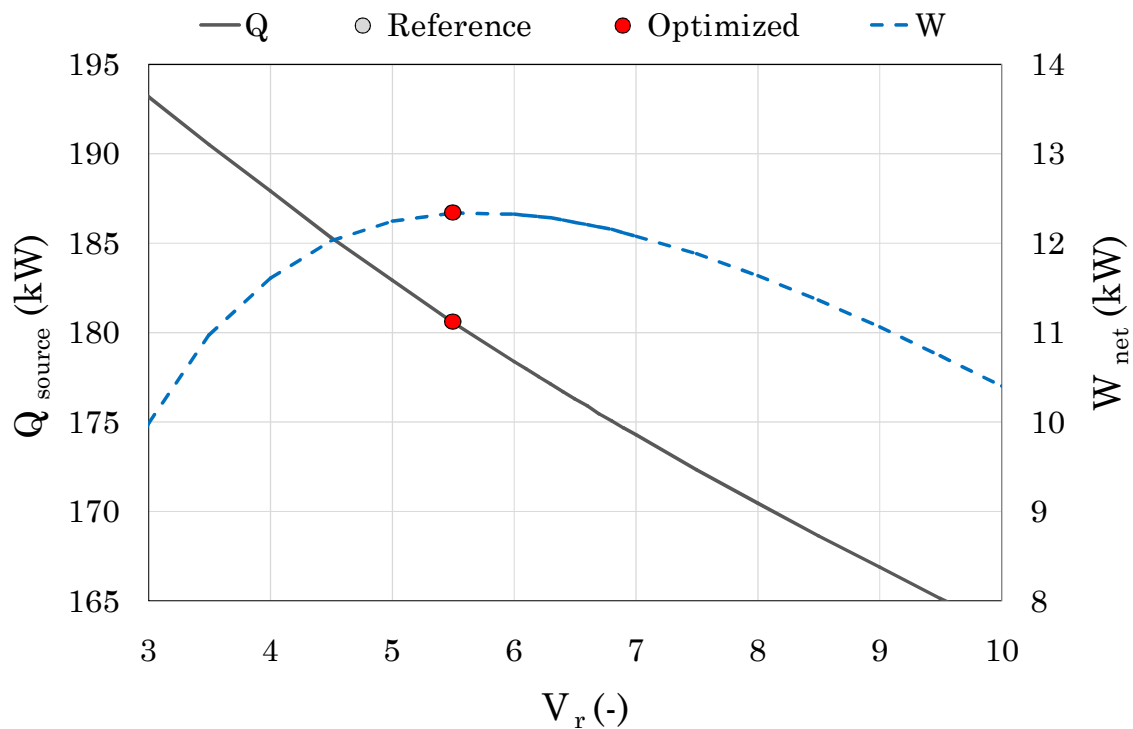
Fig. VI.22. *Built-in volume ratio of expander assessment in function of power input and output.*
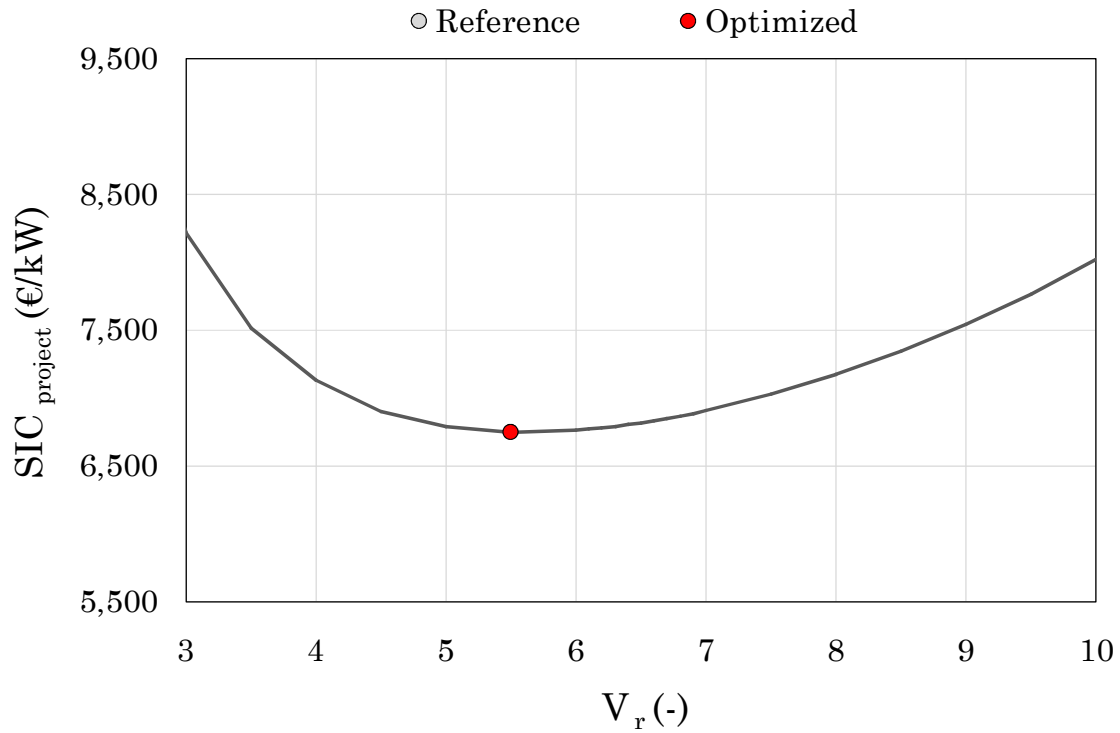
Fig. VI.23. *SIC_project assessment in function of expander built-in volume ratio.*
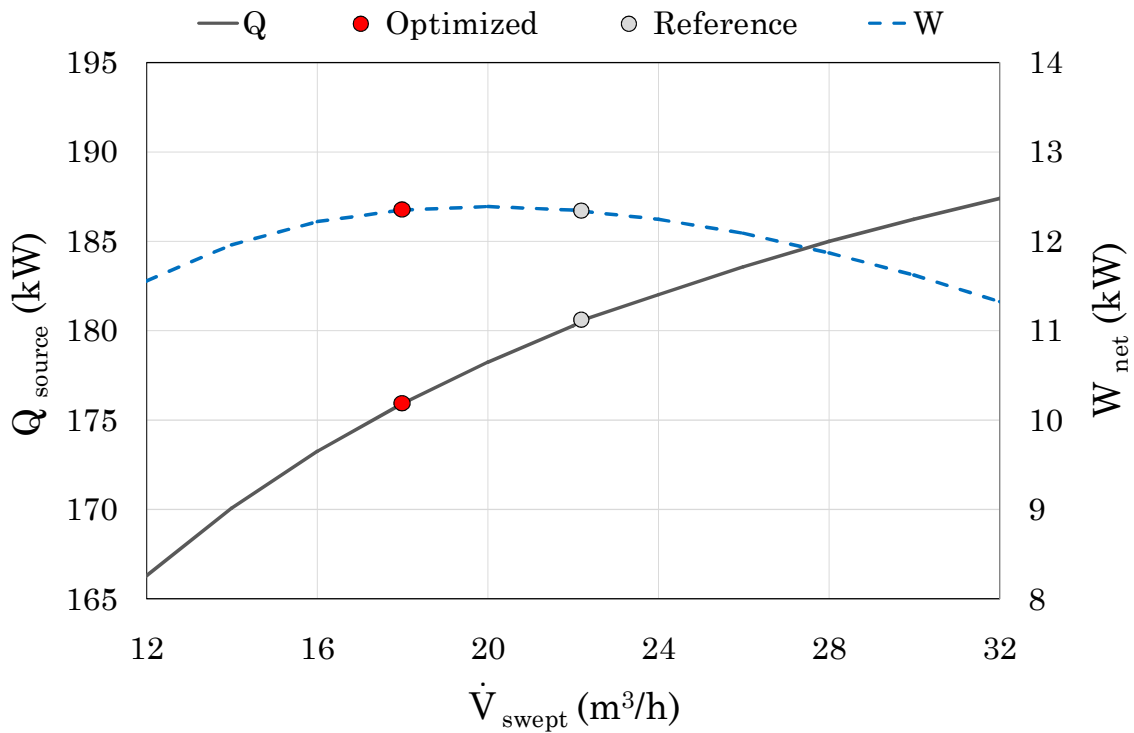
Fig. VI.24. *Swept volume of expander assessment in function of power input and output.*
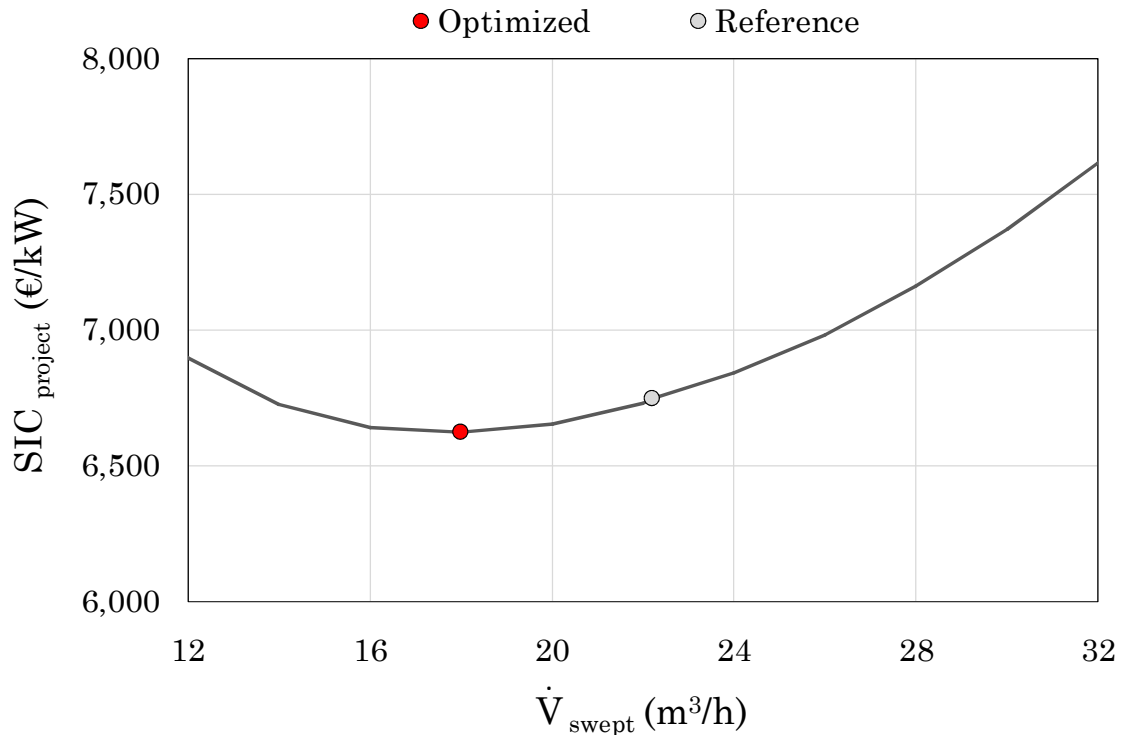
Fig. VI.25. *SIC_{project} assessment in function of expander swept volume.*

3.2.4. Cycle characteristics

As it has been mentioned, the cycle is characterized by subcritical operating conditions, superheating state at the inlet of the expander, and the additional use of a heat exchanger. These characteristics have been previously demonstrated as beneficial for the organic working fluid used. However, there is a growing effort to phase down the production and usage of HFCs and to conduct the replacement by more sustainable alternatives [70]. Therefore, there are numerous low GWP alternatives that are being investigated to replace the hydrofluorocarbon HFC-245fa. For instance, the state of the art addressed in Chapter II revealed that HCFC-1233zd(E) and HFO-1234ze(Z) have been proposed as drop-in alternatives with GWP lower than 1 [74]. In this way, Fig. VI.26 confirms that these alternatives have similar critical temperature and type of slope of the vapor saturated line to the HFC-245fa. Moreover, Table VI.8 shows that both candidates are non-toxic and have lower value of atmospheric lifetime [210].
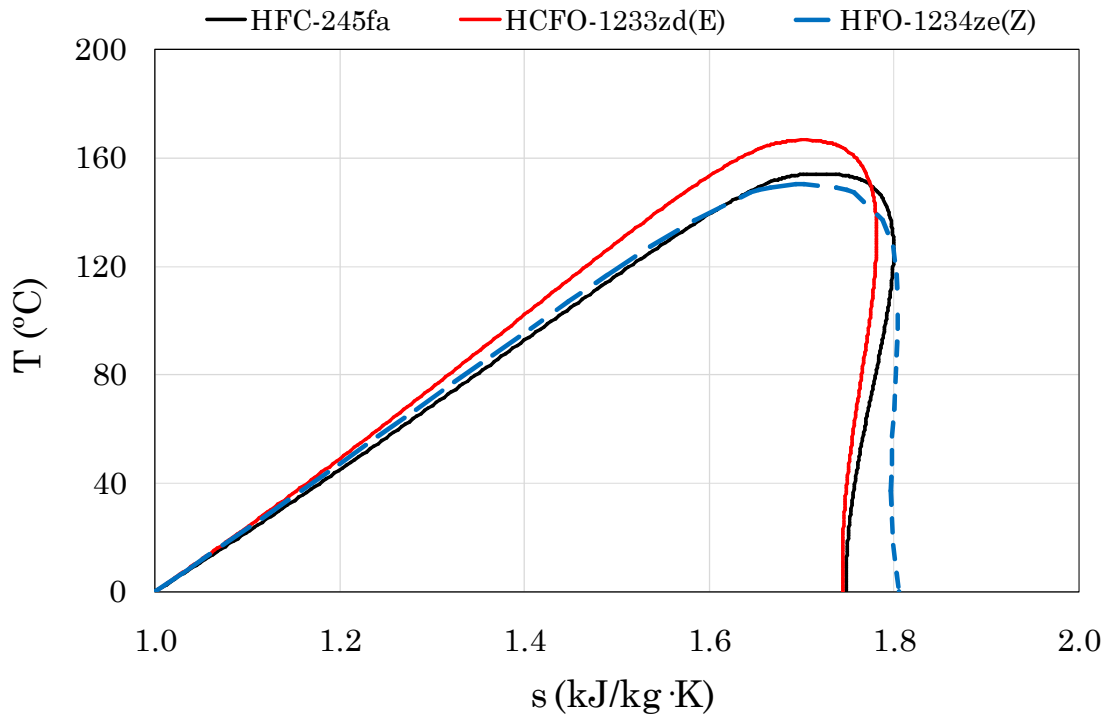
Fig. VI.26. *Temperature-entropy diagrams of organic fluids assessed.*

Table VI.8. *Main characteristics of organic working fluids used.*

	HFC-245fa	HCFO-1233zd(E)	HFO-1234ze(Z)
Critical P (bar)	36.5	35.7	35.3
Critical T (ºC)	154.0	165.6	150.1
Slope	dry	dry	dry
ASHRAE (Std.34)	B1	A1	A2L
ALT (yr)	7.7	0.0712	0.0274
ODP	0	0.00034	0
GWP	858	1	1

The results of the simulation through more friendly working fluids to the HFC-245fa are collected in Table VI.9. It can be appreciated that a drop-in with the fluid HCFO-1233zd(E) could provide an increase of efficiency, but a slight reduction of electricity, which is in accordance with the literature reviewed [73]. A drop-in with the fluid HFO-1234ze(Z) allows a greater thermal power recovery, net electricity production (in accordance with the literature [78]) and, consequently, lower value of $SIC_{project}$. Furthermore, even better results may be expected if a multivariable optimization for each working fluid is conducted.

Table VI.9. Optimization results in function of organic working fluid.

	HFC-245fa	HCFO-1233zd(E)	HFO-1234ze(Z)
$SIC_{project} \left(€ / kW\right)$	6,747	6,778	6,566
$Q_{source} \left(kW\right)$	180.61	174.52	181.42
$W_{net} \left(kW\right)$	12.34	12.27	12.70
$\eta_{process} \left(\%\right)$	6.83	7.03	7.00

3.3.   Multivariable optimization

The individual optimization of each parameter has shown that a more profitable system could be reached. However, the extent of improvement depends on the set of parameters. Consequently, a multivariable optimization is conducted to achieve the most cost-effective solution.

For that, some constraints are assumed in accordance to design criteria. Thus, a minimum velocity in pipes and plates are usually considered to ensure the oil return. For instance, liquid lines are designed for velocities upper 0.5 m/s and vapor lines are designed for minimum velocities around 5 m/s [211]. Similarly, channel velocities in BPHEs upper 0.3 m/s are recommended for fluids in vapor state [161]. Accordingly, these limits are considered in the optimization.

It should be mentioned that, for comparisons between thermo-economic and thermodynamic optimizations, not only the $SIC_{project}$ has been optimized, but also the net electrical power. Thus, both optimization approaches are discussed below.

3.3.1. Maximizing net electrical power

In the first place, the objective function of net electrical power has been maximized. This optimization provides the solution of a thermodynamic optimization, as well as the system that most contributes to the energy and environmental benefits.

As Table VI.10 shows, the current working fluid and the two environmentally friendly alternatives assessed tend to recover the whole thermal power available in the heat source. For that, different values of the parameters are used.

The results also show that the organic working fluid HCFO-1233zd(E) allows reaching the maximum net electrical energy generation, whose thermodynamic cycle is depicted in Fig. VI.27. However, due to the higher

heat exchange surface required, the cost-effective indicator is the least profitable.

Table VI.10. *Results maximizing net electrical power as objective function.*

Working fluid	HFC-245fa	HCFO-1233zd(E)	HFO-1234ze(Z)
$\Delta T_{condensing}\,(K)$	16	18.9	20
$\Delta T_{superheating}\,(K)$	43.2	40.7	42.8
$L_{tube\ condenser}\,(m)$	14	18	12
$N_{Recuperator}\,(-)$	16	20	16
$A_{HRVG}\,(m^2)$	11.2	12.9	11.4
$A_{Reg}\,(m^2)$	26.3	30.8	23.7
$\dot{V}_{oil}\,(m^3/h)$	10.0	8.6	9.93
$\dot{V}_{swept}\,(m^3/h)$	31.01	30.08	30.09
$V_r\,(-)$	4.77	4.40	4.24
$Q_{source}\,(kW)$	196.6	196.6	196.6
$W_{net}\,(kW)$	15.96	16.33	15.70
$E_{final}\,(kW)$	127,951	130,869	125,763
$\eta_{process}\,(\%)$	8.1	8.3	8.0
$SIC_{project}\,(€/kW)$	6,639	7,499	6,275
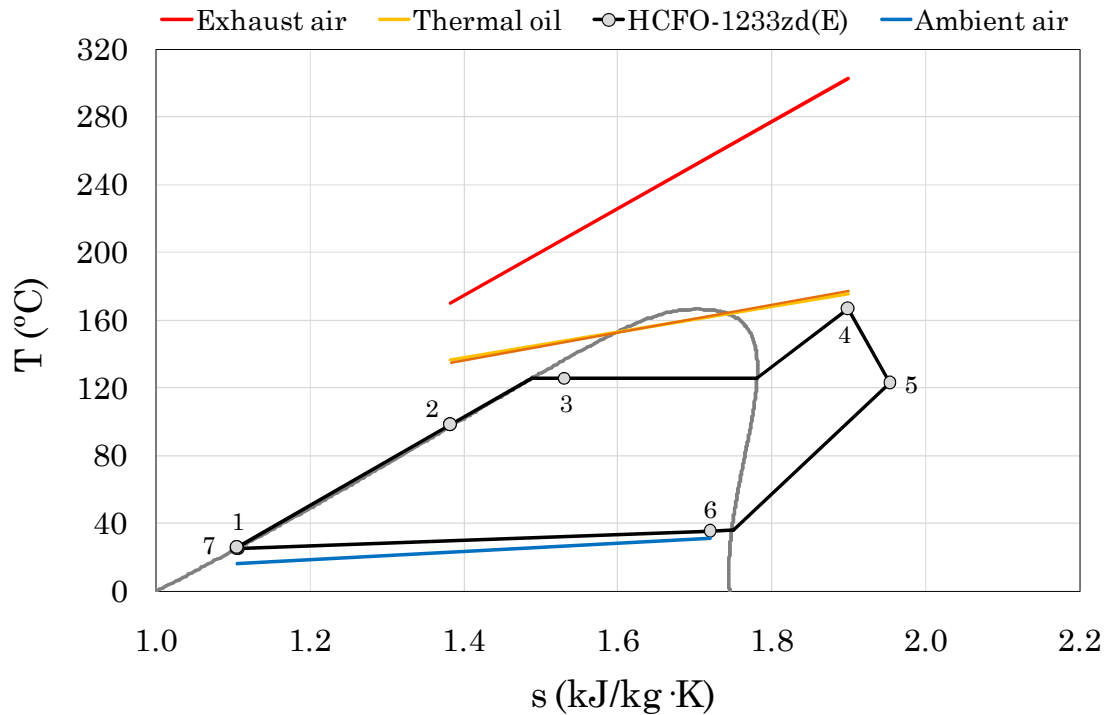
Fig. VI.27. *Maximized net power cycle in a temperature-entropy diagram (numbering corresponds to Fig. III.8).*

3.3.2. Minimizing specific investment cost

On the other hand, to achieve a cost-effective solution, the minimization of the $SIC_{project}$ is considered as objective function. As can be appreciated in Table VI.11, none of the optimizations use the whole thermal power available in the heat source. Nonetheless, substantially better values of $SIC_{project}$ are reached.

The results also show that the organic working fluid HFO-1234ze(Z) can be used to minimize the $SIC_{project}$ and to achieve the most profitable solution. The thermodynamic cycle of the optimized system using $SIC_{project}$ as objective function is shown in Fig. VI.28.

Table VI.11. *Results minimizing specific investment cost as objective function.*

Working fluid	HFC-245fa	HCFO-1233zd(E)	HFO-1234ze(Z)
$\Delta T_{condensing}$ (K)	25.2	20.8	20
$\Delta T_{superheating}$ (K)	33.9	35.4	35.1
$L_{tube\ condenser}$ (m)	4.0	4.5	5.0
$N_{Recuperator}$ (−)	13	13	13
A_{HRVG} (m^2)	10.5	10.3	10.1
A_{Reg} (m^2)	14.2	15.0	13.7
$\dot{V}_{oil}$ (m^3/h)	10.0	9.6	10.0
$\dot{V}_{swept}$ (m^3/h)	20.89	22.45	21.26
V_r (−)	4.6	4.7	4.6
Q_{source} (kW)	178.5	172.1	179.3
W_{net} (kW)	12,41	12.51	13.10
E_{final} (kW)	99,455	100,304	105,015
$\eta_{process}$ (%)	7.0	7.3	7.3
$SIC_{project}$ (€/kW)	5,597	5,734	5,455
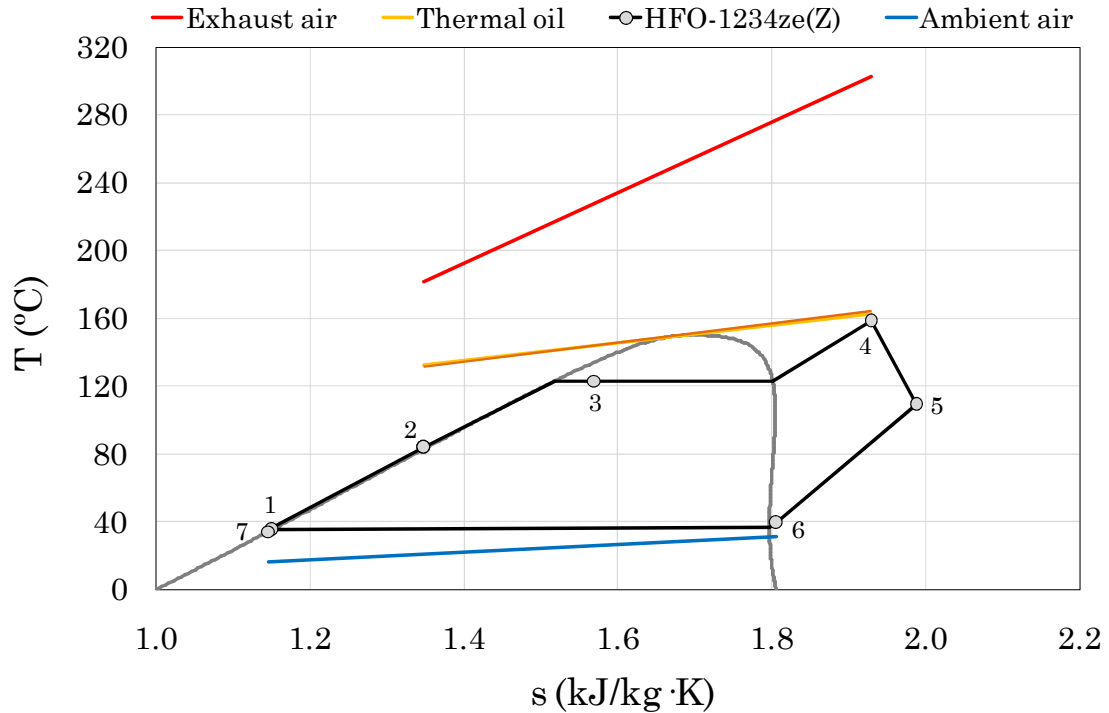
Fig. VI.28. *Minimized SIC_{project} cycle in a temperature-entropy diagram (numbering corresponds to Fig. III.8).*

3.3.3. Optimized system

For comparisons, the results of the reference case, the solution maximizing net electrical power, and the cost-effective solution minimizing SIC_{project} are discussed below. Notice that other relevant performance ratios for readers about the reference and optimized systems are collected in Appendix II.

Fig. VI.29 shows a diagram that represents the gross electrical power produced and the electrical power consumptions that reduce it until reaching the net electrical power. Some conclusions can be extracted from this figure:

- The multivariable optimization of a specific application case results in an electrical power gain.

- From a general point of view, the higher electrical consumption is due to the feed pump of the ORC, followed by the thermal oil pump and blower of the heat source.

- When the SIC_{project} is minimized, the size of the condenser tends to decrease. As a result, the electrical consumption of the fans significantly rises.

- When the net power is maximized, the recuperator sizing tends to increase. As a result, the blower consumption rises to overcome the pressure drop caused.
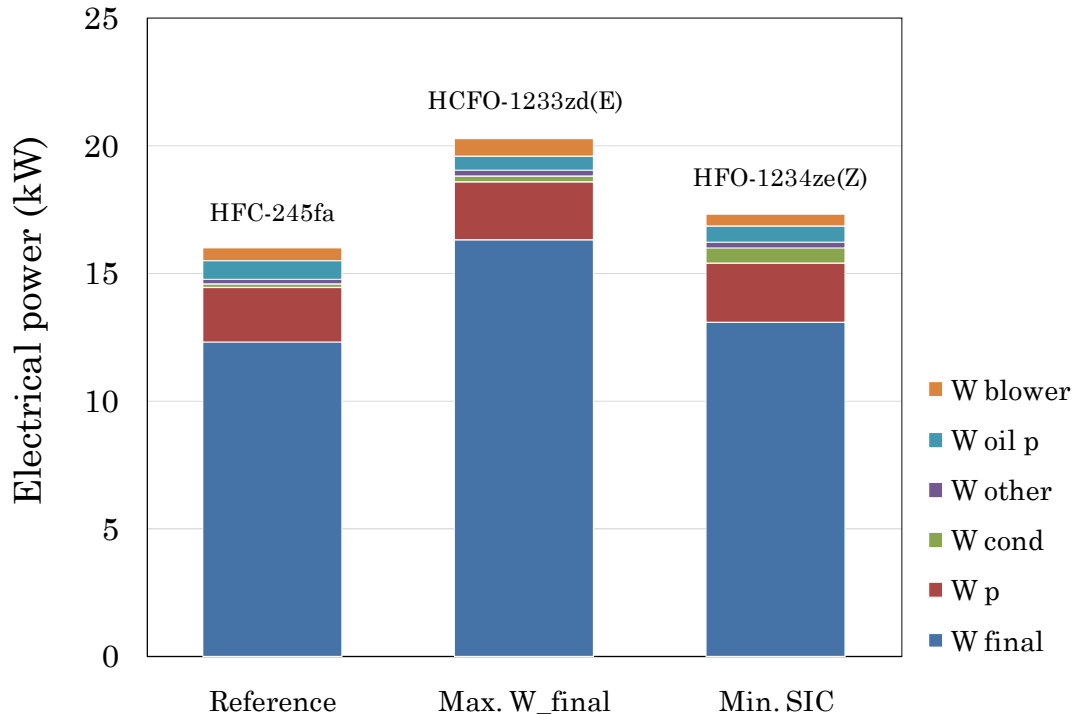
Fig. VI.29. *Comparison of optimization results in function of electrical power.*

On the other hand, Fig. VI.30 shows the significance over the $SIC_{project}$ of each parameter assessed. Some conclusions can be extracted from this figure:

- From a general point of view, the component that most affects to the $SIC_{project}$ is the recuperator.

- The condenser shows an even higher influence when the net power is maximized. However, regarding profitability criterion, a size reduction is more economically feasible.

- Other significant components over the $SIC_{project}$ are the heat transfer loop with thermal oil, regenerator, expander and alternator, besides other costs related to the system.

- Less relevant parameters are due to the economizer, evaporator, feed pump, organic working fluid, piping, and control system.
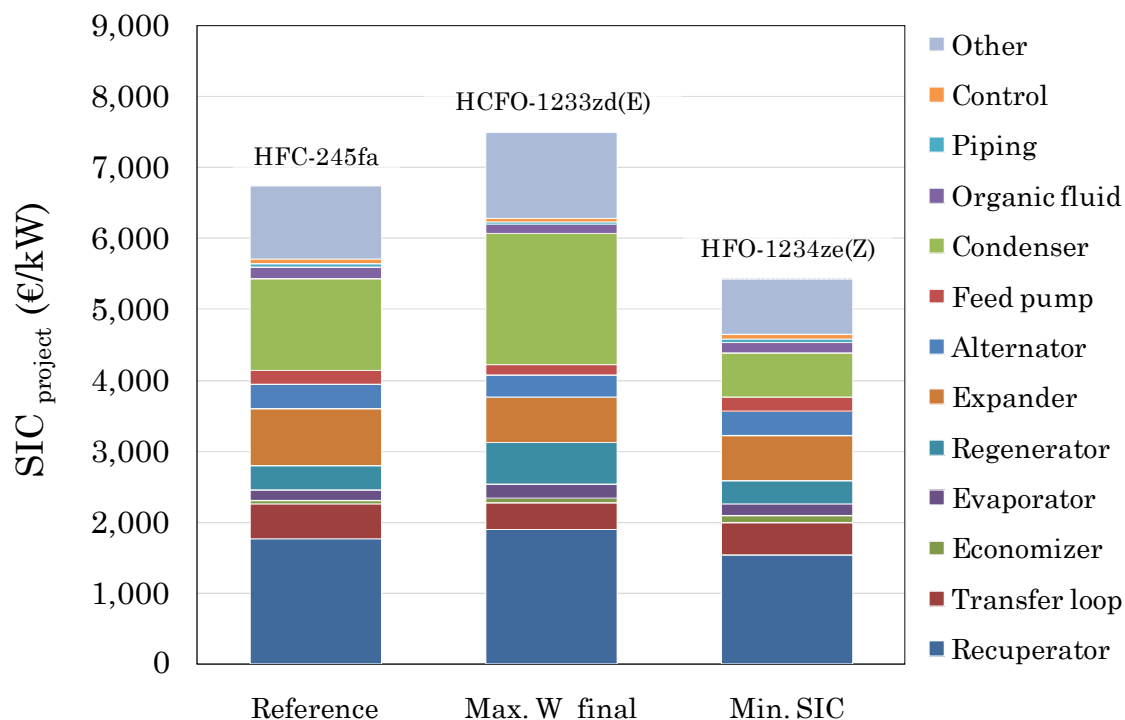
Fig. VI.30. *Comparison of optimization results in function of specific investment cost of the project.*

4. ECONOMIC FEASIBILITY OF OPTIMIZED CASE

Once an optimized system in cost-effective indicators is achieved, the expected improvement in the economic feasibility can be quantified. For that, a typical year operation is simulated, providing the net electricity production required to conduct the profitability study and its subsequent sensitivity analysis.

4.1. Performance simulation

In the same way as the reference case, the annual performance is simulated from temperature profiles of heat source and heat sink, as well as the month-long outage consideration for maintenance tasks.

The results of the simulation are depicted in Fig. VI.31. The net electrical power of the optimized system ranges between 9.91 – 15.29 kW. Consequently, an electricity production above 104 MWh is reached, which represents a saving about 1.5% of the electricity consumption of the factory. This energy generation only differs a 0.8% with respect to the value previously predicted in Table VI.11, confirming the validity of the operating conditions assumed in the previous optimization section.

In this case, the energy and environmental benefits obtained are estimated

as a saving of 214 MWh of primary energy and a reduction of 28 t/yr of equivalent CO_2 emissions to the atmosphere.
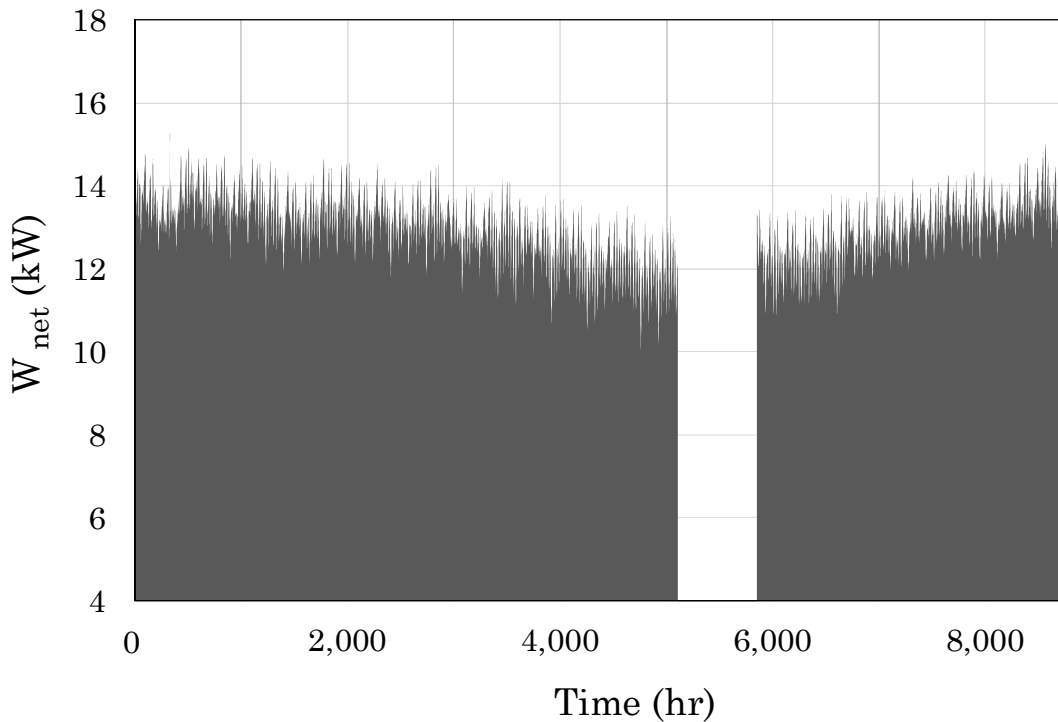
Fig. VI.31. *Simulation of net electricity of the optimized case.*

4.2. Profitability study

From the electrical energy generation and the considerations of economic regimes previously adopted for the reference case, the profitability reachable through the optimized system is assessed.

4.2.1. Self-consumption of energy

This economic scenario considers that the revenue of the project depends on the energy demand reduction. For that, electricity prices for the type of industry addressed and the tax on self-consumption of energy are considered. Moreover, results are framed in a bandwidth that corresponds to investment incentives currently available.

The results of the study are depicted in Fig. VI.32 and listed in Table VI.12. As expected, the use of a cheaper and powerful system enhances the profitability indicators with respect to the reference case. Thus, even in absence of incentives, DPP values lower than 10 years are obtained. Despite this, these values are not enough advantageous to guarantee the technology diffusion.
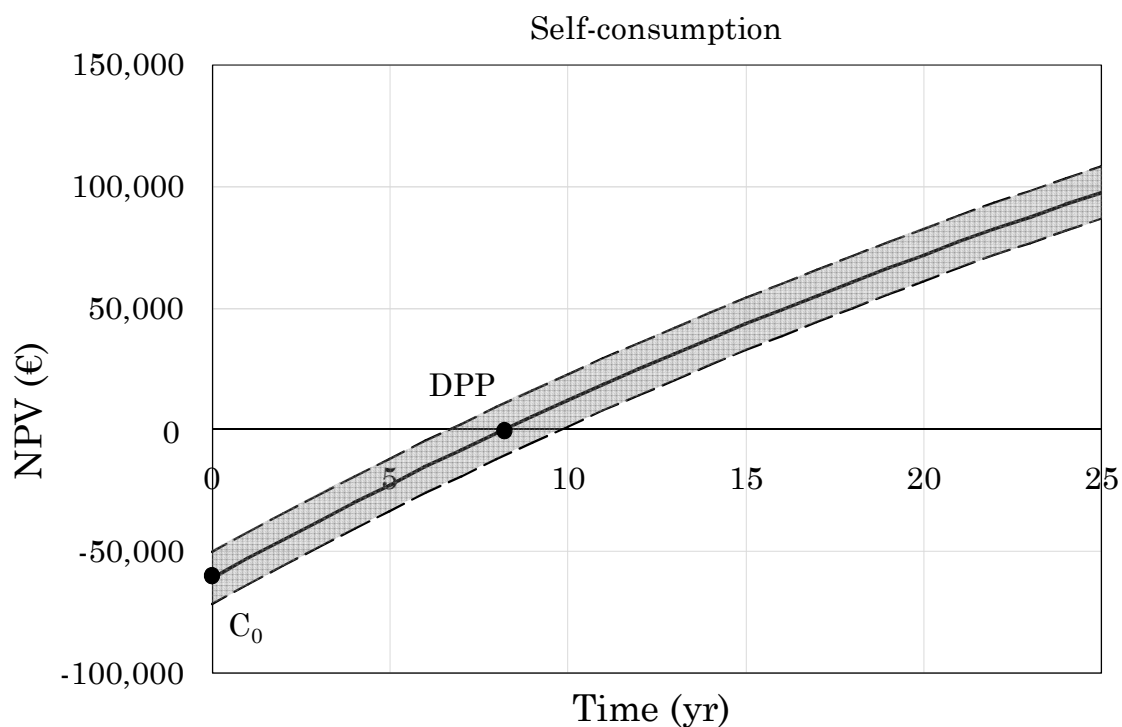
Fig. VI.32. *Profitability of optimized case under self-consumption regime.*

Table VI.12. *Mean profitability indicators of optimized case in self-consumption regime.*

Electricity generated (kWh)	E_{final}	104,183
Investment cost with 15% incentive (€)	C_0	60,741
Annual cash flow (€)	C_t	8,105
Net Present Value (€)	NPV	97,502
Profitability Index (-)	PI	2.61
Internal Rate of Return (%)	IRR	12.67
Discounted payback period (yr)	DPP	8.20
Average price of electricity (€/MWh)	–	87.80
Levelized Cost Of Electricity (€/MWh)	LCOE	39.28

4.2.2. Sale of electricity to the energy market

The electricity sale to the energy market, at pool price in addition to receiving an economic retribution, has been previously proven as a less feasible regime than the self-consumption. Nonetheless, for comparisons between reference and optimized systems, profitability indicators are also quantified under this scenario. Thereby, the results obtained are displayed

in Fig. VI.33 and listed in Table VI.13. It should be highlighted the improvement of the IRR with respect to the reference case in the same scenario, which is an indicator of the reliability that optimized systems offer.
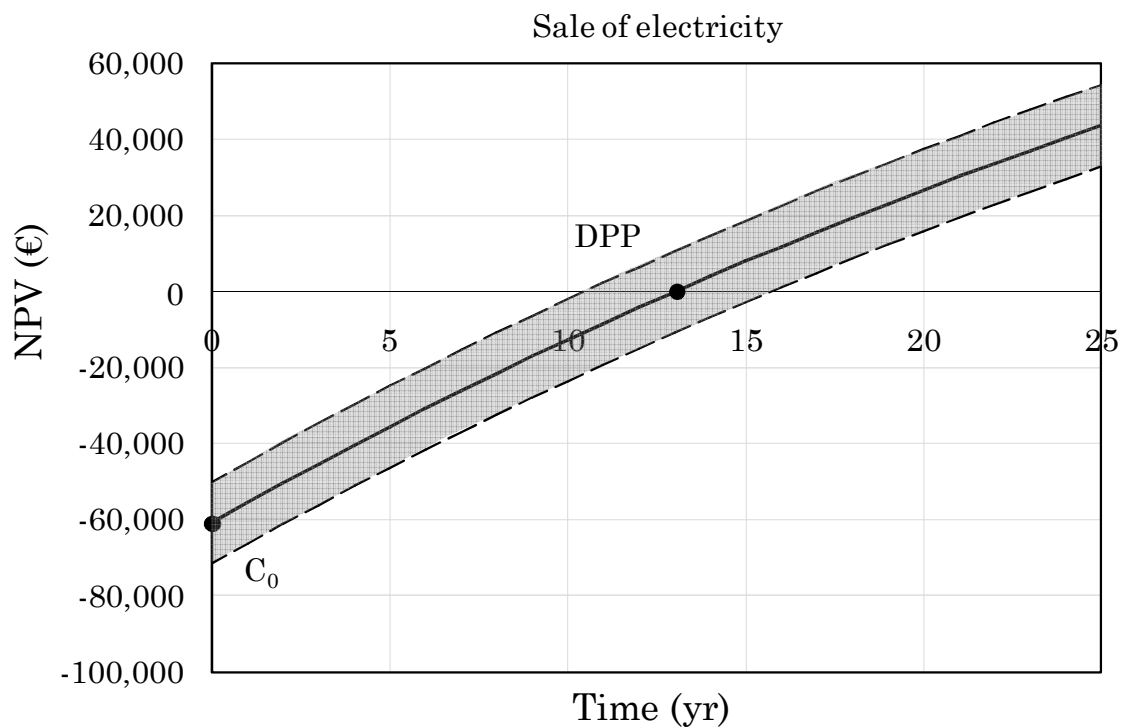
Fig. VI.33. *Profitability of optimized case in the sale of electricity regime.*

Table VI.13. *Mean profitability indicators of optimized case in the sale of electricity regime.*

Electricity generated (kWh)	E_{final}	104,183
Investment cost with 15% incentive (€)	C_0	60,741
Annual cash flow (€)	C_t	5.342
Net Present Value (€)	NPV	43,554
Profitability Index (-)	PI	1.72
Internal Rate of Return (%)	IRR	7.28
Discounted payback period (yr)	DPP	13.03
Average price of electricity (€/MWh)	–	61.59
Levelized Cost Of Electricity (€/MWh)	LCOE	39.28

4.3. Sensitivity analysis

Taking into account the influence of the economic regime on the results, an extrapolation of the optimized system to other scenarios is assessed.

In this way, Fig. VI.34 displays the electricity price influence over the DPP, including the bandwidth of investment incentives up to 30%. It should be recalled that the range of electricity prices assessed is in accordance with different sizes of industries, as well as the countries of the EU-28. Thereby, a DPP lower than 10 years can be reached with electricity prices above 80 €/MWh, besides receiving minor investment incentives. In fact, profitability expectations are met for the case of Spanish industries with annual electrical consumptions below 500 MWh (Fig. II.20), which use the self-consumption regime and receive investment incentives. Similarly, this scenario also relates to industries located in more favorable countries in terms of electricity price, like Italy or Germany, achieving values of DPP about 5 years in absence of incentives.
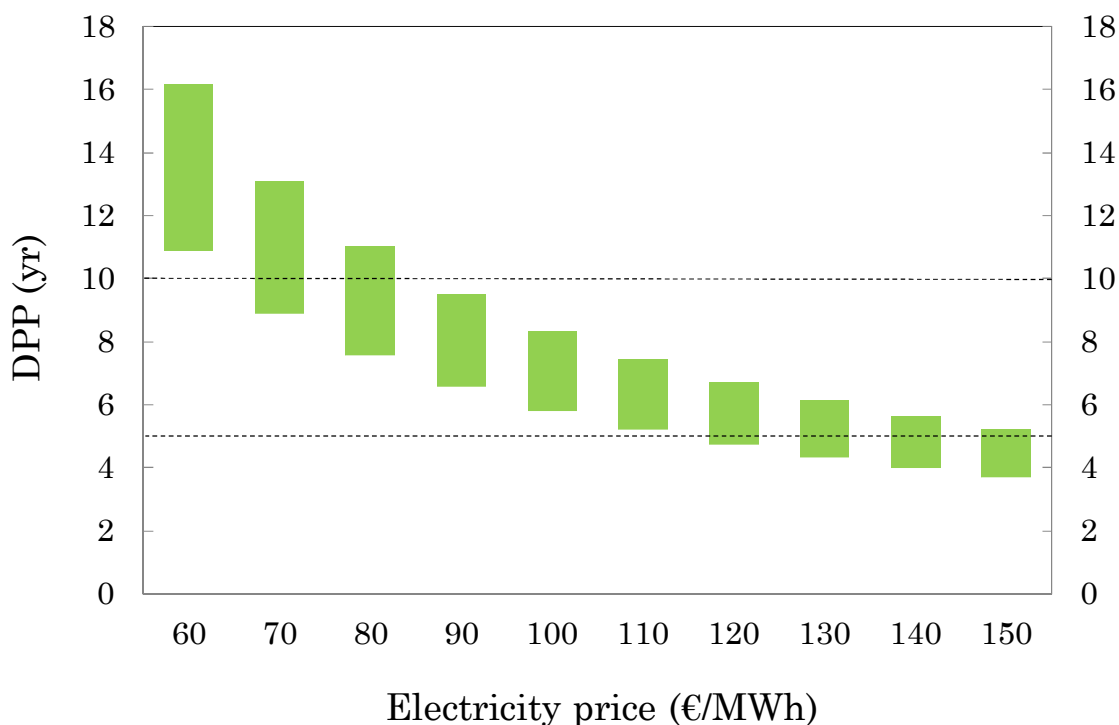
Fig. VI.34. *Sensitivity analysis of optimized case.*

The DPP variation (in absence of incentives) in function of electricity price and discount rate is shown in Fig. VI.35. From a general point of view, electricity prices upper 90 €/MWh are required to ensure payback periods lower than 10 years. Moreover, it should be underlined that the minimum values of DPP are about 5 years, being necessary incentives to reduce this limit.
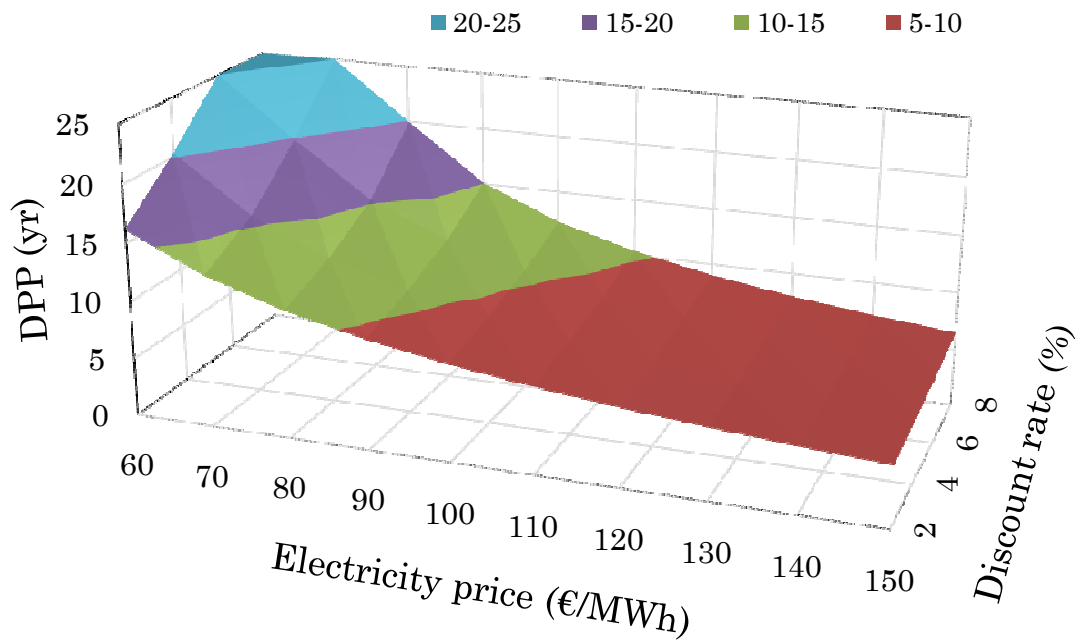
Fig. VI.35. *Sensitivity analysis of discounted payback period of optimized case in function of electricity price and discount rate.*

5. ECONOMIC FEASIBILITY COMPARISON

This section aims to shed light about the improvement that an optimized system offers with respect to the reference case, and to summarize its relevance under the different economic scenarios.

With this in mind, Fig. VI.36 conducts a comparison of the prices and costs associated with the electricity. Firstly, it can be checked that electricity prices are higher than that costs required for its production with the ORC (LCOE), which is an indicator of the suitability of the ORC application in industry. The self-consumption also highlights as a more profitable regime, due to the notable difference with respect to the electricity price under the scenario of energy sale. With respect to the LCOE of the assessed cases, it can be underlined that the improvement achieved thanks to the optimization is comparable to that of receiving an investment incentive higher than 15% in the reference project.

Investment incentive:	0%	15%	30%
Self-consumption	87.80	87.80	87.80
Sale of electricity	61.59	61.59	61.59
LCOE reference	52.27	45.93	39.59
LCOE optimized	44.44	39.28	34.11
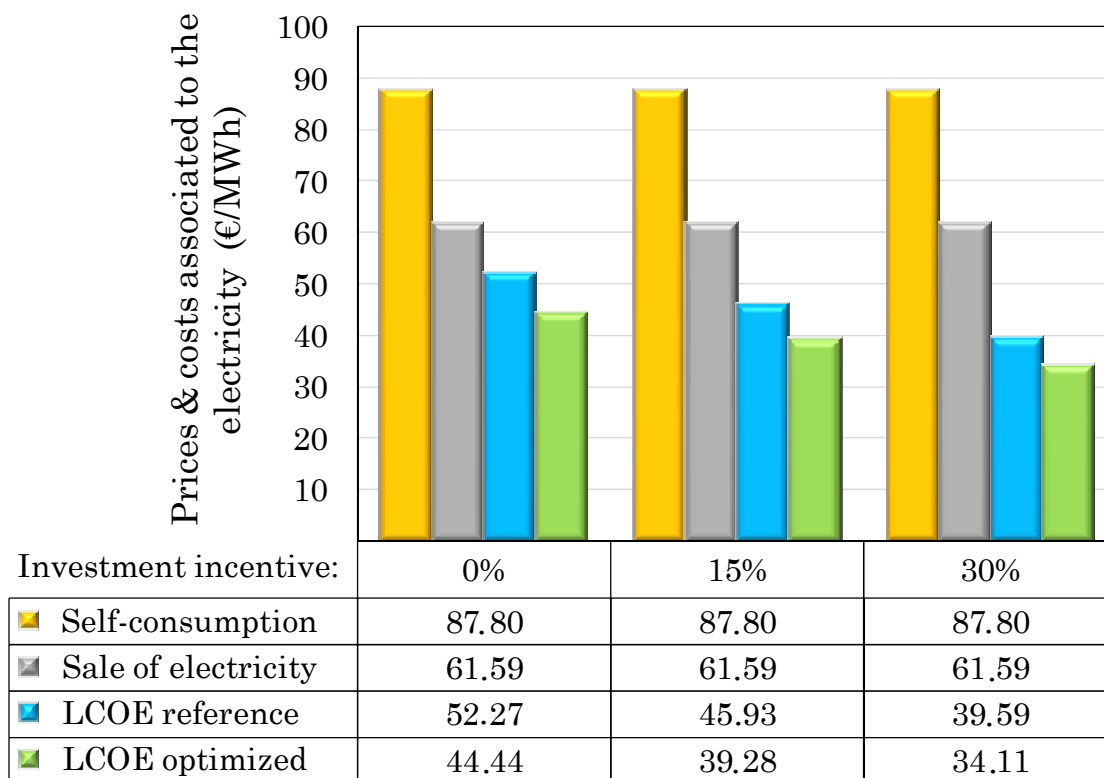
Fig. VI.36. *Prices and production costs associated to the electricity generated.*

A comparison between the DPP of reference and optimized systems under different economic scenarios is depicted in Fig. VI.37. Focusing on the economic regimes, it can be seen that the self-consumption of energy results, even in absence of investment incentives, more profitable than the sale of electricity to the energy market. Furthermore, it is noted that the system optimization allows a DPP reduction around 2 years with respect to the reference case.

The wealth of the project can be appreciated in Fig. VI.38 and Fig. VI.39 in absolute and relative values, respectively. In the first place, it highlights that the better the economic regime and the greater the incentive received, the greater the wealth achievable with the project. Moreover, it can be seen that the lower the incentive receiver, the greater the relevance of conducting optimizations.

Investment incentive:	0%	15%	30%	0%	15%	30%
Reference case	12.32	10.27	8.30	19.80	16.29	13.01
Optimized case	9.80	8.20	6.65	15.72	13.03	10.47
Difference:	2.52	2.06	1.64	4.08	3.26	2.53
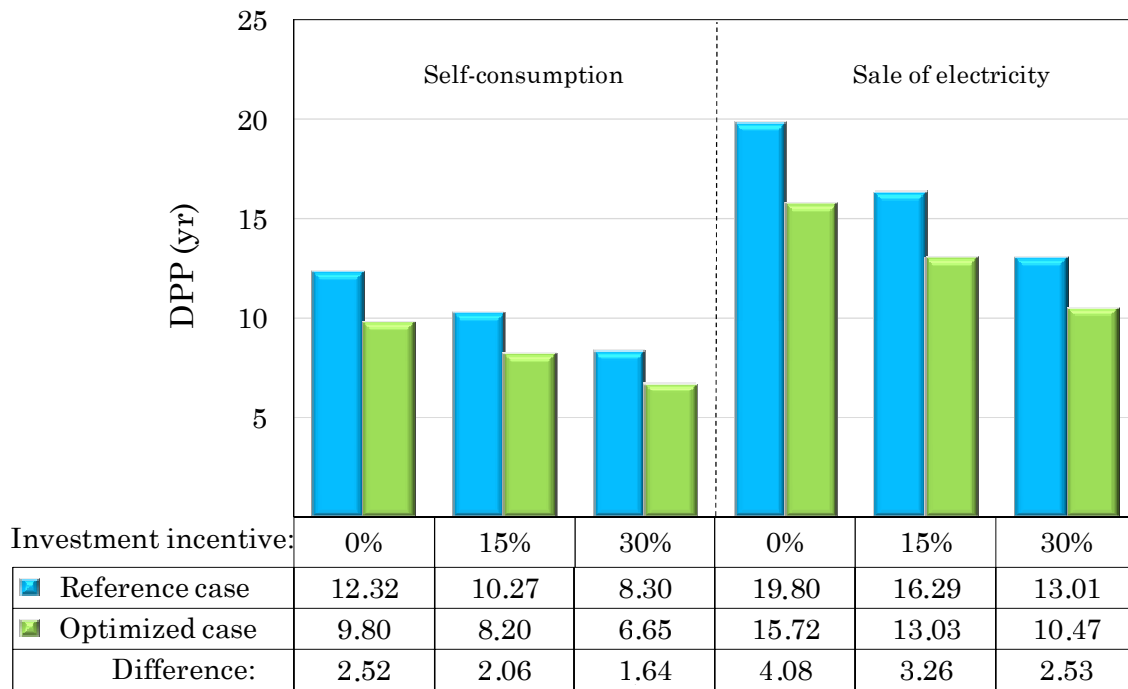
Fig. VI.37. *Comparison of discounted payback period between reference and optimized cases under the different economic scenarios addressed.*

Investment incentive:	0%	15%	30%	0%	15%	30%
Reference case	66,961	79,445	91,929	16,959	29,443	41,927
Optimized case	86,783	97,502	108,221	32,835	43,554	54,273
Difference:	19,822	18,057	16,292	15,876	14,111	12,346
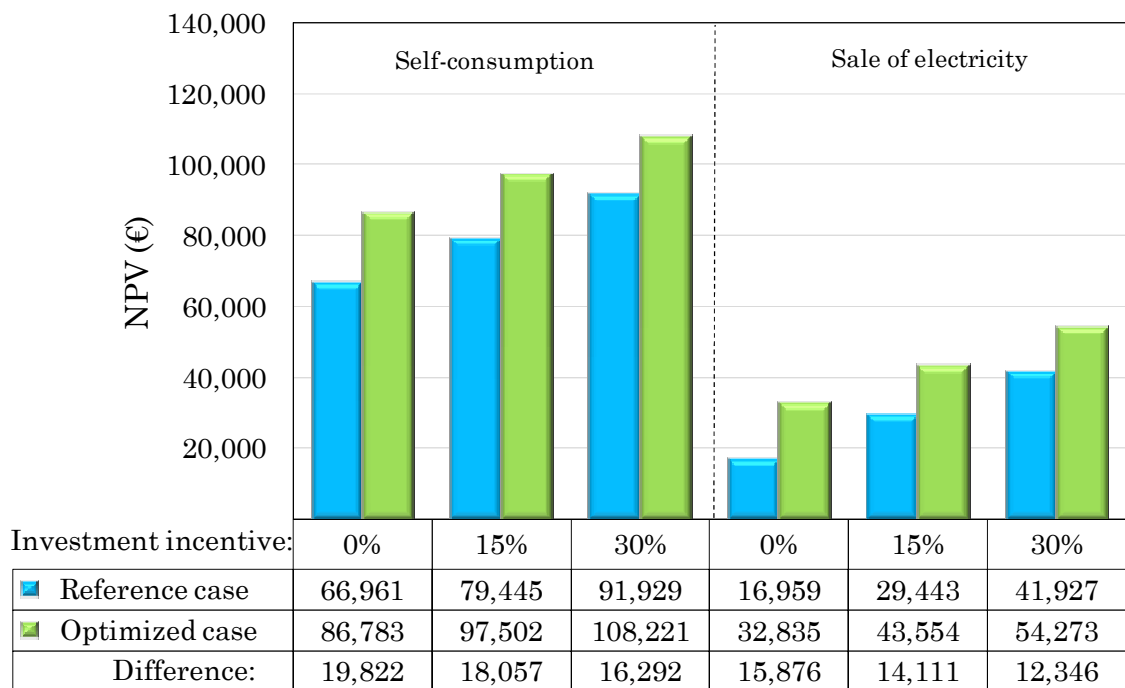
Fig. VI.38. *Comparison of net present value between reference and optimized cases under the different economic scenarios addressed.*

Investment incentive:	0%	15%	30%	0%	15%	30%
Reference case	1.80	2.12	2.58	1.20	1.42	1.72
Optimized case	2.21	2.61	3.16	1.46	1.72	2.08
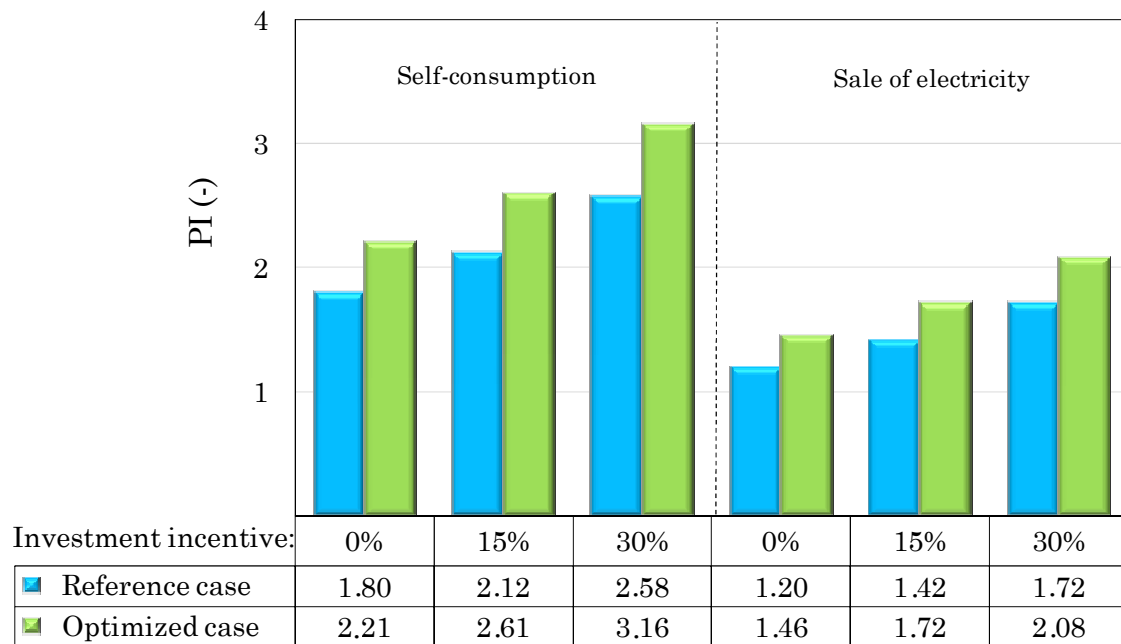
Fig. VI.39. *Comparison of profitability index between reference and optimized cases under the different economic scenarios addressed.*

The reliability of the project is analyzed in Fig. VI.40. Similarly to the previous discussion, the results reveal that the self-consumption of energy is the most reliable economic regime, and the optimization provides an extent of improvement equivalent to an investment incentive of 15% over the reference case.

Investment incentive:	0%	15%	30%	0%	15%	30%
Reference case	7.84	9.83	12.51	3.65	5.22	7.29
Optimized case	10.38	12.67	15.79	5.53	7.28	9.60
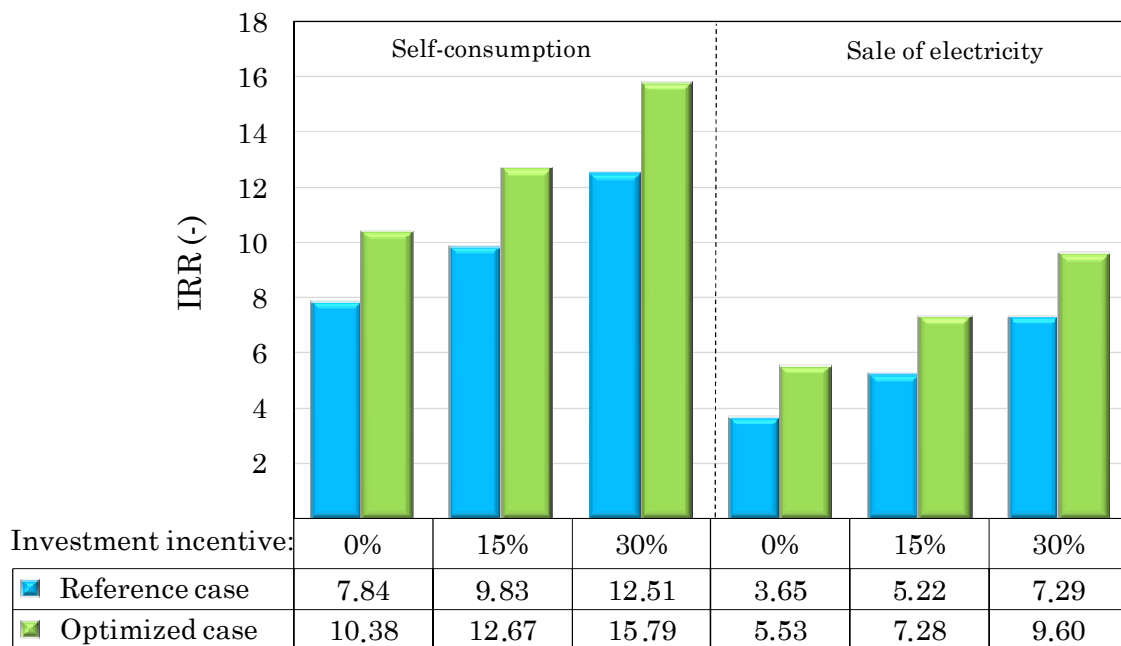
Fig. VI.40. *Comparison of internal rate of return between reference and optimized cases under the different economic scenarios addressed.*

The extrapolation of the comparative to other scenarios is depicted in Fig. VI.41. It is noted that the less advantageous is the scenario, the more significant is the improvement in the DPP due to the optimization. So the optimization guarantees the best cost-effective solution.
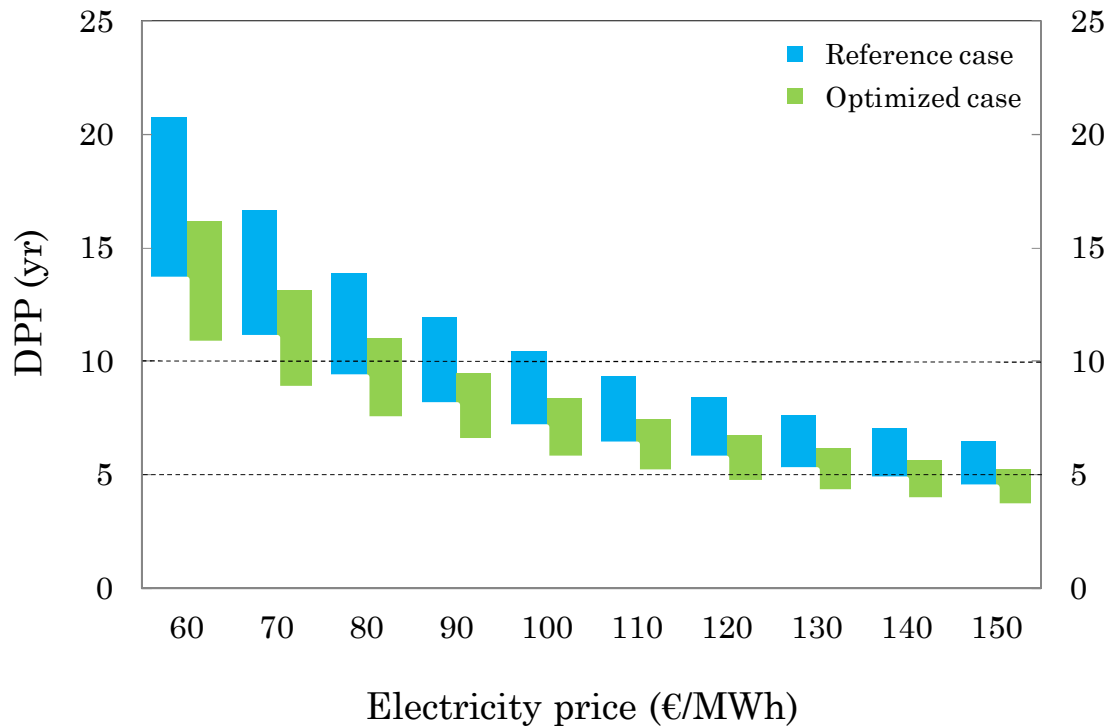
Fig. VI.41. *Sensitivity analysis comparison between reference and optimized cases.*

6.   CONCLUSIONS

This Chapter has begun simulating the performance of the reference case during a typical year operation. Thereby, the economic feasibility of the project has been analyzed under different economic regimes. In particular, the best option currently available for this type of industries is the self-consumption. In that case, an economic charge for the electricity production requires being considered, but also an investment incentive applicable to energy efficiency measures in industry. In this manner, the results show that the discounted payback period ranges between 8.30 and 12.32 years. Nonetheless, the extrapolation of the application to more favorable scenarios has shown that the discounted payback period could be reduced to 5 years if electricity prices about 150 €/MWh and investment incentives around 30% are received.

With the aim to improve the profitability of the project, a thermo-economic optimization has been conducted using the specific investment cost of the whole system as objective function. Thus, the main conclusions obtained can

be summarized as follows:

- The multivariable optimization considering control strategies, geometric characteristics of heat exchangers and expander, and organic working fluid used has provided the most cost-effective solution.

- It has been demonstrated that there is a thermal power, different to the maximum available to be recovered, that optimizes the system. So a thermo-economic assessment to each application case is necessary.

- The greater improvement with respect to the reference case has been obtained by using a more compact direct air-cooled condenser, even in spite of the increase of fans consumption.

- The greatest reduction of the net electrical power is due to the feed pump consumption. Nonetheless, due to the low significance over the $SIC_{project}$, a more efficient component could be used to improve the results.

- Other relevant components over the $SIC_{project}$ of the optimized solution are the recuperator, heat transfer loop, regenerator, expander, and alternator.

As a result, a cheaper and powerful system with respect to the reference case is achieved. Specifically, a net electrical power increase of 6.2% and a $SIC_{project}$ reduction of 19.1% is obtained

If the economic regime of self-consumption is applied to the optimized system, the discounted payback period ranges between 6.65 – 9.80 years. So a mean reduction about 2 years is achieved through the thermo-economic optimization. In other words, the optimization provides an extent of improvement equivalent to an investment incentive of 15% in the reference case. The results extrapolation to other scenarios has shown that the less advantageous is the scenario, the more significant is the improvement in the discounted payback period due to the optimization. In the most favorable scenario, discounted payback periods lower than 5 years can be achieved with minor incentives. In addition, the wealth and reliability of the project using the optimized system result more advantageous, being the optimization a guarantee to reach the best cost-effective solution for a new project.

Chapter VII

Conclusions

CONCLUSIONS

The environmental concern is leading researchers to focus on more sustainable energy systems. In this way, small-scale Organic Rankine Cycles (ORC) have been proven as a suitable technology to produce electricity from low-grade heat sources. This fact is appreciable in the exponential growth of investigations on the topic, but also the current availability of commercial small-scale ORC units in the market.

With regard to the investigations on the topic, the revision of the state of the art has underlined that studies mainly have a technical character, which is at the core of the ORC development. Numerous studies are devoted to finding better organic working fluids, as well as low GWP (Global Warming Potential) candidates for a drop-in replacement to the hydrofluorocarbon HFC-245fa, which is the most popular fluid among the current commercial systems. It has also been observed many studies that experimentally characterize the performance of different expansion technologies, which has been pointed as a critical component to reach cost-effective solutions. Other investigations focus on technical issues such as the architecture of the cycle, design of components like feed pump or heat exchangers, or the control strategy operated by the ORC.

In spite of the advances in research and the availability of commercial small-scale units in the market, there is a lack of knowledge about experimental applications of small-scale ORC systems for waste heat recovery in industrial processes. The interest that raises this application has been underlined in the literature, due to the high amount of waste heat recoverable. However, a scarce number of in-depth experimental investigations are observed as a consequence of the difficulty to reach profitable projects. In fact, even with medium and large-scale projects, the profitability is not guaranteed.

Being aware of the economic feasibility relevance for the ORC adoption in practical applications, more cost-effective solutions are being explored in the literature through thermo-economic optimizations. The investigations reviewed show that there is an optimum value for any of the parameters assessed, including organic working fluid, expander geometry, cycle architecture, superheating value (control strategy), heat exchange surface, or sizing of other components, which in turn depends on the type and scale of the specific application. However, the results achieved cannot be discussed with respect to actual projects implemented in industry, due to its absence.

In light of this, this thesis proposes as a novelty to address the thermo-economic optimization from an experimental application in industry. In particular, a project that was materialized in Spain thanks to a financial support program for business innovation is used as reference case. The application consisted of the installation of a pre-competitive ORC prototype, of a rated electrical power of 20 kW, in a ceramic furnace to take advantage of the low-grade waste heat available in the exhaust air. In this manner, a comprehensive model of the waste heat recovery system is developed based on the reference case and subsequently validated from actual data of operation as a tool to carry out the thermo-economic assessment.

For that, in the first place, the facility was monitored during a week of tests under typical operating conditions. Thus, 21 steady-state points were selected to develop and validate a semi-empirical model. In particular, sub-models of heat exchangers, fluid machines, and auxiliary components are developed based on their geometric characteristics and the equations that define their thermodynamic performance. In addition, the model includes cost-correlations of the components that were selected in accordance with actual costs of the ORC unit, while the remaining costs of the facility are provided from the specific experimental application case. As a result, a comprehensive model of the reference case was obtained, which required the calibration of some parameters related to the experimental performance of the components. Subsequently, the simulation of the conditions obtained in the steady-state points was conducted to compare measured parameters and analysis ratios with respect to values predicted by the model. In this manner, a suitable accuracy of the model has been revealed. The main reason was pointed due to the stability of the control operated by the system, as well as the success achieved through the calibration. In representation of the results obtained, the gross electrical power has been validated with an error bandwidth of 3.52%. The results also show that, despite a gross electrical efficiency of 10.57% is experimentally reached, the different energy losses caused in the process reduce this value to a net electrical efficiency of 7.27%. Furthermore, the costs resulting from simulations have also been compared to the initial estimations of the project, also confirming their validity.

With regard to the results, in the first place, the performance of the reference case during a typical year operation has been simulated. Thereby, the economic feasibility of the project has been analyzed under different economic regimes. In particular, the best option currently available for the type of industry addressed is the self-consumption. In that case, an economic charge for the electricity production requires being considered, but

also an investment incentive applicable to energy efficiency measures in industry. In this manner, the results show that the discounted payback period ranges between 8.30 and 12.32 years. Nonetheless, the extrapolation of the application to more favorable scenarios has shown that the discounted payback period can drop to 5 years if electricity prices about 150 €/MWh and investment incentives around 30% are received.

With the aim to improve the profitability of the project, a thermo-economic optimization has been conducted using the Specific Investment Cost of the whole system, $SIC_{project,}$ as objective function. Thus, the main conclusions obtained can be summarized as follows:

- The multivariable optimization considering control strategies, geometric characteristics of heat exchangers and expander, and organic working fluid used has provided the most cost-effective solution.

- It has been demonstrated that there is a specific thermal power, different to the maximum available to be recovered, that optimizes the system. So a thermo-economic assessment to each application case is necessary.

- The greater improvement achieved with respect to the reference case has been obtained by using a more compact direct air-cooled condenser, even in spite of the increase of fans consumption.

- The greatest reduction of the net electrical power is due to the feed pump consumption. Nonetheless, due to the low significance over the $SIC_{project}$, a more efficient component could be used to improve the results.

- Other relevant components over the $SIC_{project}$ of the optimized solution are the recuperator, heat transfer loop, regenerator, expander, and alternator.

As a result, a cheaper and powerful system with respect to the reference case is achieved. Specifically, a net electrical power increase of 6.2% and a $SIC_{project}$ reduction of 19.1% is obtained

If the economic regime of self-consumption is applied to the optimized system, the discounted payback period ranges between 6.65 – 9.80 years. So a mean reduction about 2 years is achieved through the thermo-economic optimization. In other words, the optimization provides an extent of

improvement equivalent to an investment incentive of 15% in the case addressed. The results extrapolation to other economic scenarios has shown that the less advantageous is the scenario, the more significant is the improvement in the discounted payback period due to the optimization. In the most favorable scenario, discounted payback periods lower than 5 years can be achieved in absence of incentives. In addition, the wealth and reliability of the project using the optimized system result more advantageous, being the optimization a guarantee to reach the best cost-effective solution for a new project.

RECOMMENDATIONS & PERSPECTIVES

From the conclusions of this investigation, some recommendations for future studies can be pointed.

- This study has conducted the model calibration from experimental data assuming constant performance ratios, since a high flexibility to extrapolate results is imperative in thermo-economic optimizations. However, greater accuracies to simulate a specific application case can be obtained using regressions of the performance ratios. For instance, a correlation of the internal mechanical efficiency of the expander reduces the error bandwidth of the gross electrical power to 2.37%.

- Models intended for thermo-economic assessments can also be improved through a deeper effort to minimize assumptions. For instance, recent papers are already proposing correlation of mixtures between working fluids and lubrication oils. Thereby, slightly different performance ratios about the components and a better accuracy of the model could be reached. In the same way, the consideration of heat losses to ambient and kinematic energies of each component of the model could lead to more accurate results.

- The results have revealed that more friendly working fluids to the widely used HFC-245fa can provide greater energy, economic, and environmental benefits. Taking this into account, the use of new generation fluids with low GWP are recommended for future experimental investigations on the topic.

- If an ORC manufacturer conducts a thermo-economic assessment focusing on their own product, an optimized commercial unit to a specific type of application can be accomplished. For that, cost

correlations and range of sizes available in their components should be used to achieve their most competitive solution.

- It has been noted the high influence of the recuperator and the heat transfer loop over the SIC, which represents about the 37% of the total investment cost. This indirect recovery system has been demonstrated as reliable to be experimentally implemented. However, better economic indicators may be reached with a direct recovery system. Notice that direct systems require higher charges of working fluid. However, the significance of the working fluid over the whole SIC has been noted much less significant, specifically less than 3% of total investment cost.

- The investigation performed has focused on a small-scale ORC with a rated power of 20 kW. Nonetheless, due to the SIC reduction with respect to the size of the unit, a future project could focus on a higher size (up to 100 kW in the small-scale range) to achieve better profitability indicators.

- This study has assumed the lifetime of the facility based on the economic regime regulated, as well as some estimations from the ORC supplier, such as annual maintenance. Nonetheless, it is expected to collect information about the experience of the actual lifetime of the whole facility, overhaul or other unexpected expenses, and, in this manner, to contribute with more information of a successful integration of a small-scale ORC into an industrial process.

CONCLUSIONES

La preocupación por el medioambiente está guiando a los investigadores hacia el estudio de sistemas energéticos más sostenibles. En esta línea de estudio, los ciclos Rankine orgánicos (ORC por las siglas en inglés) son considerados una tecnología prometedora para la producción de electricidad a partir de fuentes térmicas de baja temperatura. Este hecho se ve reflejado en el crecimiento exponencial de investigaciones sobre esta temática, así como en la actual disponibilidad de unidades ORC de pequeña escala en el mercado.

En lo referente a investigaciones sobre la temática, la revisión del estado de la técnica ha puesto de manifiesto que la mayoría de los estudios tienen un carácter técnico, lo que se considera un factor clave para el desarrollo del ORC. Así, muchos trabajos se centran en el estudio de fluidos orgánicos que puedan resultar mejores a los actuales, por ejemplo alternativas de bajo Potencial de Calentamiento Atmosférico (PCA) que sirvan para la sustitución directa del hidrofluorocarbono HFC-245fa, siendo éste el más utilizado entre los actuales sistemas comerciales de pequeña escala. Otros estudios focalizan sus esfuerzos en la caracterización experimental de la tecnología de expansión, la cual es considerada como un punto crucial para alcanzar soluciones rentables. Otros aspectos técnicos objeto de estudio en la bibliografía revisada son la arquitectura del ciclo, los principales componentes como la bomba o los intercambiadores de calor, o la estrategia de control que gobierna al ORC.

Sin embargo, cabe destacar que a pesar de los logros conseguidos en las investigaciones y de la disponibilidad de sistemas de pequeña escala en el mercado, todavía persiste la falta de conocimiento en cuanto a aplicaciones experimentales con sistemas ORC de pequeña escala en procesos industriales para la recuperación de calor residual. El motivo principal parece deberse a la dificultad para alcanzar la rentabilidad de los proyectos, la cual ni siquiera está garantizada en aplicaciones de media y gran escala.

Siendo conscientes de la importancia de la viabilidad económica para el uso del ORC en aplicaciones prácticas, las investigaciones más recientes se apoyan en optimizaciones termoeconómicas para lograr soluciones más rentables. En este sentido, los estudios revisados muestran que cualquier parámetro puede ser optimizado, incluyendo el fluido orgánico utilizado, geometría del expansor, arquitectura del ciclo, valor de sobrecalentamiento (estrategia de control), superficie de intercambio térmico o tamaño del resto de componentes; lo que a su vez depende del tipo y tamaño de la aplicación concreta. Sin embargo, la discusión de los resultados obtenidos como fruto

de las investigaciones no puede hacerse con respecto a proyectos reales implementados en las industrias, dada su ausencia.

A la luz de esto, en esta tesis se propone como novedad abordar la optimización termoeconómica a partir de un caso experimental de aplicación en una industria. Concretamente, un proyecto implementado en España gracias a un programa de apoyo financiero a la innovación empresarial es utilizado como caso base. La aplicación consiste en la instalación de un prototipo precompetitivo de ORC, con una potencia eléctrica nominal de 20 kW, en un horno cerámico para el aprovechamiento del calor residual disponible en el aire de escape. De esta forma, puede desarrollarse un modelo íntegro del sistema que sirva como herramienta para llevar a cabo la optimización termoeconómica y que permita, a su vez, la discusión de los resultados con respecto al caso real.

La metodología que se ha mantenido en el trabajo ha consistido, en primer lugar, en la monitorización de la instalación durante una semana de ensayos bajo condiciones típicas de operación. Esto ha permitido extraer 21 puntos en estado estacionario con los que desarrollar y validar el modelo semiempírico. Concretamente, el modelo se ha desarrollado a partir de submodelos de los principales componentes, tales como los intercambiadores de calor, máquinas de fluido, u otros componentes auxiliares. Dichos submodelos han sido constituidos a partir de la definición de las características geométricas de los componentes, las ecuaciones que caracterizan su desempeño termodinámico, y de correlaciones de costes en consonancia con los de la aplicación abordada. Posteriormente, el modelo ha sido calibrado a partir del ajuste de aquellos ratios que dependen del funcionamiento experimental del sistema. De esta forma, se ha procedido a la validación del modelo mediante una comparativa entre los valores medidos y los predichos en la simulación.

Como fruto de la validación se ha revelado una gran precisión en el modelo. En este sentido, si se considera a la potencia eléctrica bruta como un parámetro representativo de la salida del modelo, el error que se obtendría en tal caso quedaría delimitado dentro de un ancho de banda del 3.52%. También cabe destacar la notable diferencia que se observa entre la eficiencia eléctrica bruta de 10.57% y la neta, considerando las pérdidas energéticas de todo el proceso, de 7.27%. Los costes resultantes de la simulación también han podido validarse a partir de las primeras estimaciones del proyecto, confirmando también la adecuación de las correlaciones utilizadas.

En cuanto a los resultados, en primer lugar, se ha procedido a la simulación del funcionamiento que tendría el sistema a lo largo de un año de operación, ya que en la actualidad no hay datos al respecto. De este modo, se ha podido analizar la viabilidad económica del proyecto atendiendo a los diferentes regímenes económicos. Concretamente, la mejor opción actualmente disponible en la industria analizada es el autoconsumo. En tal caso, debe tenerse en cuenta la tasa impuesta sobre la electricidad producida, así como también los incentivos a la inversión aplicables a las medidas de eficiencia energética en industria. De este manera, los resultados muestran que el periodo descontado de retorno varía entre 8.30 y 12.32 años. No obstante, la extrapolación de los resultados de ésta aplicación a escenarios más favorables demuestra que el periodo descontado de retorno se reduciría a 5 años si el precio eléctrico se mantuviera alrededor de 150 €/MWh y se consiguieran incentivos a la inversión de aproximadamente el 30%.

Con la idea de mejorar la rentabilidad obtenida, se procede a la optimización termoeconómica utilizando como función objetivo el coste específico de inversión de todo el proyecto, $SIC_{project}$. Las principales conclusiones obtenidas de la optimización se sintetizan a continuación:

- Por medio de una optimización multivariable que tenga en cuenta la estrategia de control, características geométricas de los intercambiadores de calor y del expansor, y el fluido orgánico de trabajo utilizado se consigue la solución más rentable.

- Ha quedado demostrado que existe una potencia térmica específica, diferente a la máxima disponible para ser recuperada, que optimiza el sistema. Por lo que se requiere una optimización termoeconómica particularizada a cada caso de aplicación.

- La mejora más notable con respecto al caso al caso de referencia se ha conseguido a través del uso de un condensador de tipo directo más compacto, incluso a pesar del aumento del consumo de los ventiladores.

- La reducción más importante de la potencia eléctrica neta se debe al consumo de la bomba principal. No obstante, debido al bajo peso del coste de la bomba sobre el $SIC_{project}$, se podría utilizar un componente de mayores prestaciones.

- Otros componentes importantes sobre el $SIC_{project}$ son el recuperador de calor, el anillo de aceite térmico para la transferencia de calor, el

regenerador o intercambiador de calor interno, el expansor, y el generador eléctrico.

Como resultado de la optimización se he conseguido un sistema más potente y más económico con respecto al caso de referencia. Concretamente, se ha aumentado la potencia eléctrica neta en un 6.2%, al mismo tiempo que se ha reducido el SIC$_{project}$ en un 19.1%.

Si el sistema optimizado es evaluado bajo el régimen económico de autoconsumo, el periodo descontado de retorno obtenido varía entre 6.65 y 9.80 años. Por lo que se ha logrado una reducción media de alrededor de 2 años mediante de la optimización termoeconómica. En otras palabras, la optimización permite un grado de mejora equivalente a un ahorro de inversión del 15% para el caso tratado. La extrapolación de los resultados a otros escenarios económicos muestra que cuanto peor sea el escenario, más importante es la mejora en el periodo descontado de retorno debida a la optimización. En el escenario más favorable, se consiguen periodos descontados de retorno por debajo de 5 años incluso en ausencia de incentivos. A esto cabe añadir que la viabilidad y la riqueza alcanzable con un proyecto que utilice un sistema optimizado es más ventajosa, siendo la optimización termoeconómica una garantía para conseguir la mejor solución en un proyecto nuevo.

RECOMENDACIONES Y PERSPECTIVAS

A partir de las conclusiones de esta investigación se pueden extraer algunas recomendaciones para futuros estudios.

- Este trabajo ha realizado la calibración del modelo a partir de datos experimentales asumiendo ratios de funcionamiento constantes, ya que la flexibilidad para extrapolar resultados es imperativo en una optimización termoeconómica. Sin embargo, para la simulación de un caso específico se sugiere utilizar correlaciones para mejorar la precisión de los resultados. Sirva de ejemplo, el uso de una correlación para la eficiencia mecánica interna en el expansor permitiría reducir el ancho de banda del error de la potencia eléctrica bruta al 2.37%.

- Los modelos destinados a realizar evaluaciones termoeconómicas también podrían mejorarse mediante un mayor esfuerzo para minimizar las suposiciones. Por ejemplo, trabajos recientes ya están proponiendo correlaciones de mezclas de fluidos orgánicos puros y aceites lubricantes. Así, se podría conseguir una ligera mejora en la precisión de los modelos de instalaciones reales. En el mismo sentido,

la consideración de más pérdidas de calor al ambiente y la influencia de la energía cinemática también podría conducir a resultados más precisos.

- Los resultados obtenidos en la tesis han demostrado que fluidos de trabajo más respetuosos con el medioambiente en comparación con el ampliamente utilizado HFC-245fa podrían contribuir con mayores beneficios energéticos, medioambientales y económicos. Por ello, se recomienda el uso de fluidos de nueva generación con bajo PCA para futuras investigaciones experimentales sobre esta temática.

- Si un fabricante de sistemas ORC quisiera llevar a cabo una evaluación termoeconómica basada en su propio producto, podría lograr un sistema comercial optimizado para un tipo concreto de aplicación. Para ello, se recomienda el uso de correlaciones de costes y rango de tamaño de componentes disponible en sus productos para conseguir el equipo más competitivo.

- A partir de los resultados, se ha mostrado la gran influencia del recuperador y el anillo de aceite térmicos sobre el SIC, representando alrededor del 37% del coste total de inversión. Este tipo de sistema indirecto de recuperación de calor resulta fiable para el uso experimental. Sin embargo, podrían alcanzarse mejores indicadores económicos mediante sistemas directos. Nótese que el precio del fluido de trabajo (el cual aumentaría en un sistema directo) sobre el SIC es poco significativo, concretamente menor al 3% del coste total.

- La investigación realizada en este trabajo se ha centrado en un ORC de pequeña escala con una potencia nominal de 20 kW. No obstante, debido a la reducción del SIC con respecto a la escala de los equipos, se recomienda llevar a cabo futuros proyectos de mayor tamaño (de hasta 100 kW dentro del rango de pequeña escala) para conseguir mejores indicadores de rentabilidad.

- En este estudio se han asumido parámetros desconocidos como la vida útil del sistema o el mantenimiento requerido. No obstante, se espera recoger más información de esta experiencia y, así, contribuir con datos reales de la integración exitosa de un ORC de pequeña escala en un proceso industrial.

REFERENCES

[1]   González López A, Amérigo Cuervo-Arango M. Doctoral Thesis. "La preocupación por la calidad del medio ambiente. Un modelo cognitivo sobre la conducta ecológica." Complutense University of Madrid. Faculty of Psychology. ISBN: 84-669-2372-1, 2002.

[2]   UNCHE. United Nations Conference on the Human Environment. Available in: <www.un.org> [accessed 01.03.2017].

[3]   UNEP. United Nations Environment Programme. Available in: <www.pnuma.org> [accessed 01.07.2016].

[4]   BOE-A-1983-7293. "Instrumento de Ratificación de 7 de junio de 1982 del Convenio sobre la contaminación atmosférica transfronteriza a gran distancia, hecho en Ginebra el 13 de noviembre de 1979". vol. 59. 7011-7. 1983.

[5]   UNEP Ozone Secretariat. "Convención de Viena para la Protección de la Capa de Ozono". ISBN: 92-807-2127-5. 2011.

[6]   UN Chronicle. The Magazine of the United Nations. "De Estocolmo a Kyoto: Breve historia del Cambio Climático". vol. XLIV No.2. 2007.

[7]   IPCC. Intergovernmental Panel on Climate Change. Available in: <www.ipcc.ch> [accessed 01.03.2017].

[8]   Houghton JT, Jenkins GJ, Ephraums JJ. Climate Change - The IPCC Scientific Assessment, ISBN: 0-521-40720-6; 1990.

[9]   UNEP Ozone Secretariar. Handbook for the Montreal Protocol on substances that deplete the ozone layer. Available in: <ozone.unep.org> [accessed 01.03.2017].

[10]   UN Department of Economic and Social Affairs. "Declaración de Río sobre el Medio Ambiente y el Desarrollo". Available in: <www.un.org> [accessed 01.03.2017].

[11]   UNFCCC. United Nations Framework Convention on Climate Change. Available in: <unfccc.int> [accessed 01.03.2017].

[12]   IPCC. "Cambio climático 2007: Informe de síntesis". ISBN 92-9169-322-7. 2007.

[13]   "Energía y Sociedad. Manual de la Energia". Available in: <www.energiaysociedad.es> [accessed 01.03.2017].

[14]   Conference of the Parties COP21/CMP11. Available in: <cop21.gouv.fr> [accessed 01.03.2017].

[15]   European Environtment Agency. "El medio ambiente en Europa.

Informe de síntesis, estado y perspectivas 2015". ISBN: 978-92-9213-519-5. 2015.

[16] International Energy Agency. World Energy Outlook 2014. ISBN 978-92-64-20804-9. 2014.

[17] European Commission. Europe 2020 - Europe's growth strategy. Available in: <ec.europa.eu> [accessed 01.03.2017].

[18] Fu B-R, Hsu S-W, Liu C-H, Liu Y-C. Statistical analysis of patent data relating to the organic Rankine cycle. Renew Sustain Energy Rev 2014;39:986–94.

[19] Climate Interactive. Available in: <www.climateinteractive.org> [accessed 01.07.2016].

[20] García-Colín S L. "De la máquina de vapor al cero absoluto (Calor y Entropía)". 1997. ISBN: 978-96-8166-925-6. Fondo de c. 2011.

[21] Rankine WJM. A manual of the Steam Engine and other Prime Movers. 1859. ISBN: 11486250545058. Nabu Press. 2010.

[22] Carnot NLS, Thomson SW. Reflections on the Motive Power of Heat. Accompanied by An Account of Carnot's Theory. Chapman Hall, Ltd 1897.

[23] Stefan PV, Favio CV. "Energía, entropía y religión. Un repaso histórico". ISSN 0370-3908. vol. 34. 2010.

[24] Invernizzi CM. Closed Power Cycles: Thermodynamic Fundamentals and Applications. ISBN: 9781447151395. Springer L. 2013.

[25] KCORC. Knowledge Center Organic Rankine Cycle. Available in: <www.kcorc.org> [accessed 01.03.2017].

[26] Ofeldt. FW. Engine. Patent US611792 A, 1898.

[27] Casati EIM. New Concepts for Organic Rankine Cycle Power Systems. ISBN 978-94-6259-330-5. 2014.

[28] Mazetto BM, Silva JAM Da, Junior SDO. Are ORCs a Good Option for Waste Heat Recovery in a Petroleum Refinery? Int J Thermodyn 2015;18:161.

[29] Agüera Soriano J. "Termodinámica lógica y motores termicos. 6ª edición mejorada". ISBN: 84-86204-98-4. Ciencia 3. 1999.

[30] Yue C, You F, Huang Y. Thermal and economic analysis of an energy system of an ORC coupled with vehicle air conditioning. Int J Refrig 2016;64:152–67.

[31] Peris B, Navarro-Esbrí J, Molés F, González M, Mota-Babiloni A.

Experimental characterization of an ORC (organic Rankine cycle) for power and CHP (combined heat and power) applications from low grade heat sources. Energy 2015;82:269–76.

[32]   Yamada N, Tominaga Y, Yoshida T. Demonstration of 10-Wp micro organic Rankine cycle generator for low-grade heat recovery. Energy 2014;78:806–13.

[33]   Dincer I, Rosen MA. EXERGY: Energy, Environment and Sustainable Development. ISBN: 978-0-08-097089-9. Elsevier L. 2013.

[34]   Chen H, Goswami DY, Stefanakos EK. A review of thermodynamic cycles and working fluids for the conversion of low-grade heat. Renew Sustain Energy Rev 2010;14:3059–67.

[35]   Bombarda P, Invernizzi CM, Pietra C. Heat recovery from Diesel engines: A thermodynamic comparison between Kalina and ORC cycles. Appl Therm Eng 2010;30:212–9.

[36]   Ali Tarique M. PhD Thesis. Experimental Investigation of Scroll Based Organic Rankine Systems. University of Ontario Institute of Technology. The Faculty of Engineering and Applied Science Mechanical Engineering, 2011.

[37]   Tchanche BF, Lambrinos G, Frangoudakis A, Papadakis G. Low-grade heat conversion into power using organic Rankine cycles - A review of various applications. Renew Sustain Energy Rev 2011;15:3963–79.

[38]   Franco A. Power production from a moderate temperature geothermal resource with regenerative Organic Rankine Cycles. Energy Sustain Dev 2011;15:411–9.

[39]   Algieri A, Morrone P. Comparative energetic analysis of high-temperature subcritical and transcritical Organic Rankine Cycle (ORC). A biomass application in the Sibari district. Appl Therm Eng 2012;36:236–44.

[40]   Wang M, Wang J, Zhao Y, Zhao P, Dai Y. Thermodynamic analysis and optimization of a solar-driven regenerative organic Rankine cycle (ORC) based on flat-plate solar collectors. Appl Therm Eng 2013;50:816–25.

[41]   Dolz V, Novella R, García A, Sánchez J. HD Diesel engine equipped with a bottoming Rankine cycle as a waste heat recovery system. Part 1: Study and analysis of the waste heat energy. Appl Therm Eng 2012;36:269–78.

[42]   Wang D, Ling X, Peng H. Performance analysis of double organic Rankine cycle for discontinuous low temperature waste heat recovery. Appl Therm Eng 2012;48:63–71.

References

[43] Wang H, Peterson R, Herron T. Design study of configurations on system COP for a combined ORC (organic Rankine cycle) and VCC (vapor compression cycle). Energy 2011;36:4809–20.

[44] Southon M, Krumdieck S. Preliminary investigation into the current and future growth and affordability of ORC electricity generation systems. Proc. 3rd Int. Semin. ORC Power Syst., 2015, p. 1012–21.

[45] Campana F, Bianchi M, Branchini L, De Pascale A, Peretto A, Baresi M, et al. ORC waste heat recovery in European energy intensive industries: Energy and GHG savings. Energy Convers Manag 2013;76:244–52.

[46] Wang HT, Wang H, Zhang ZM. Optimization of Low-Temperature Exhaust Gas Waste Heat Fueled Organic Rankine Cycle. J Iron Steel Res Int 2012;19:30–6.

[47] Hnat G, Patten JS, Bartone LM, Cutting JC. Industrial Heat Recovery with Organic Rankine Cycles. Proc from Fourth Ind Energy Technol Conf 1982:524–32.

[48] Tchanche BF, Pétrissans M, G. Papadakis. Heat resources and organic Rankine cycle machines. Renew Sustain Energy Rev 2014;39:1185–99.

[49] Ammar Y, Joyce S, Norman R, Wang Y, Roskilly AP. Low grade thermal energy sources and uses from the process industry in the UK. Appl Energy 2012;89:3–20.

[50] Zhou N, Wang X, Chen Z, Wang Z. Experimental study on Organic Rankine Cycle for waste heat recovery from low-temperature flue gas. Energy 2013;55:216–25.

[51] Aneke M, Agnew B, Underwood C, Wu H, Masheiti S. Power generation from waste heat in a food processing application. Appl Therm Eng 2012;36:171–80.

[52] Casci C, Angelino G, Ferrari P, Gaia M, Giglioli G, Macchi E. Heat recovery in a ceramic kiln with an organic rankine cycle engine. J Heat Recover Syst 1981;1:125–31.

[53] Navarro-Esbrí J, Peris B, Collado R, Molés F. Micro-generation and micro combined heat and power generation using "free" low temperature heat sources through Organic Rankine Cycles. Renew Sustain Energy Rev 2013;16 (2012):4175–4189.

[54] Rank®. ORC manufacturer. Castellon (Spain). Available in <rankweb.es> [accessed 01.03.2017].

[55] Scopus. Abstract and citations database. Available in: <www.scopus.com> [accessed 01.03.2017].

[56]   Peris B, Navarro-Esbrí J, Molés F. Bottoming organic Rankine cycle configurations to increase Internal Combustion Engines power output from cooling water waste heat recovery. Appl Therm Eng 2013;61:364–71.

[57]   Kazemi N, Samadi F. Thermodynamic, economic and thermo-economic optimization of a new proposed organic Rankine cycle for energy production from geothermal resources. Energy Convers Manag 2016;121:391–401.

[58]   Quoilin S, Declaye S, Tchanche BF, Lemort V. Thermo-economic optimization of waste heat recovery Organic Rankine Cycles. Appl Therm Eng 2011;31:2885–93.

[59]   Vélez F, Segovia JJ, Martín MC, Antolín G, Chejne F, Quijano A. A technical, economical and market review of organic Rankine cycles for the conversion of low-grade heat for power generation. Renew Sustain Energy Rev 2012;16:4175–89.

[60]   Lemmens S. Cost engineering techniques and their applicability for cost estimation of organic rankine cycle systems. Energies 2016;9, 485.

[61]   "Conselleria de Industria Comercio e Innovación." "Diario Oficial de la Comunidad Valenciana. Resolución de 2 de febrero de 2011, sobre financiación de acciones estratégicas de diversificación industrial". Num. 6459/14.02.2011 (6657).

[62]   EES. Engineering Equation Solver. Academic Commercial V10.092-3D (6/29/16).

[63]   Lemmon E, Huber M MM. NIST REFPROP standard reference database 23. Version 8.0. User's guide. NIST 2007.

[64]   Bao J, Zhao L. A review of working fluid and expander selections for organic Rankine cycle. Renew Sustain Energy Rev 2013;24:325–42.

[65]   Bamorovat Abadi G, Kim KC. Investigation of organic Rankine cycles with zeotropic mixtures as a working fluid: Advantages and issues. Renew Sustain Energy Rev 2017;73:1000–13.

[66]   Modi A, Haglind F. A review of recent research on the use of zeotropic mixtures in power generation systems. Energy Convers Manag 2017;138:603–26.

[67]   Le VL, Kheiri A, Feidt M, Pelloux-Prayer S. Thermodynamic and economic optimizations of a waste heat to power plant driven by a subcritical ORC (Organic Rankine Cycle) using pure or zeotropic working fluid. Energy 2014;78:622–38.

[68]   Gao H, Liu C, He C, Xu X, Wu S, Li Y. Performance analysis and working fluid selection of a supercritical organic rankine cycle for low

grade waste heat recovery. Energies 2012;5:3233–47.

[69] Rahbar K, Mahmoud S, Al-Dadah RK, Moazami N, Mirhadizadeh SA. Review of organic Rankine cycle for small-scale applications. Energy Convers Manag 2017;134:135–55.

[70] UN Environment. Kigali Amendment. <Available in: www.unep.org> [accessed 01.05.2017].

[71] Hodnebrog, Etminan M, Fuglestvedt JS, Marston G, Myhre G, Nielsen CJ, et al. Global warming potentials and radiative efficiencies of halocarbons and related compounds: A comprehensive review. Rev Geophys 2013;51:300–78.

[72] Huck P, Laursen AL, Zia J, Woolley L. Identification and test of Low Global Warming Potential Alternatives to HFC-245fa in Organic Rankine Cycles. ASME ORC, The Netherlands, 2013. 2013.

[73] Eyerer S, Wieland C, Vandersickel A, Spliethoff H. Experimental study of an ORC (Organic Rankine Cycle) and analysis of R1233zd-E as a drop-in replacement for R245fa for low temperature heat utilization. Energy 2016;103:660–71.

[74] Molés Ribera F. Doctoral thesis: "Análisis teórico y experimental de fluidos con bajo potencial de efecto invernadero como alternativas al HFC-245fa en ciclos orgánicos Rankine de baja temperatura". University Jaume I of Castellon (Spain) 2015.

[75] Navarro-Esbrí J, Molés F, Peris B, Mota-Babiloni A, Kontomaris K. Experimental study of an Organic Rankine Cycle with HFO-1336mzz-Z as a low global warming potential working fluid for micro-scale low temperature applications. Energy 2017;133:79–89.

[76] Usman M, Imran M, Yang Y, Lee DH, Park BS. Thermo-economic comparison of air-cooled and cooling tower based Organic Rankine Cycle (ORC) with R245fa and R1233zde as candidate working fluids for different geographical climate conditions. Energy 2017;123:353–66.

[77] Petr P, Raabe G. Evaluation of R-1234ze(Z) as drop-in replacement for R-245fa in Organic Rankine Cycles - From thermophysical properties to cycle performance. Energy 2015;93:266–74.

[78] Ziviani D, Dickes R, Quoilin S, Lemort V. Organic Rankine cycle modelling and the ORCmKit library: analysis of R1234ze (Z) as drop-in replacement of R245fa for low-grade waste heat recovery. 29th Int Conf Effic Cost, Optim Simul Environ Impact Energy Syst 2016:1–13.

[79] Quoilin S. Doctoral Thesis: Sustainable energy conversion through the use of Organic Rankine Cycles for waste heat recovery and solar applications 2011:1–183.

[80] Quoilin S, Broek M Van Den, Declaye S, Dewallef P, Lemort V. Techno-economic survey of organic rankine cycle (ORC) systems. Renew Sustain Energy Rev 2013;22:168–86.

[81] Tocci L, Pal T, Pesmazoglou I, Franchetti B. Small Scale Organic Rankine Cycle (ORC): A Techno-Economic Review. Energies 2017;10:413.

[82] Lemort V, Legros A. Positive displacement expanders for Organic Rankine Cycle systems. Org. Rank. Cycle Power Syst. Technol. Appl., Elsevier Ltd; 2016, p. 361–96.

[83] Song P, Wei M, Shi L, Danish SN, Ma C. A review of scroll expanders for organic Rankine cycle systems. Appl Therm Eng 2014;75:54–64.

[84] Ayachi F, Ksayer EB, Neveu P, Zoughaib A. Experimental investigation and modeling of a hermetic scroll expander. Appl Energy 2016;181:256–67.

[85] Kosmadakis G, Manolakos D, Papadakis G. Experimental investigation of a low-temperature organic Rankine cycle (ORC) engine under variable heat input operating at both subcritical and supercritical conditions. Appl Therm Eng 2016;92:1–7.

[86] Miao Z, Xu J, Zhang K. Experimental and modeling investigation of an organic Rankine cycle system based on the scroll expander. Energy 2017.

[87] Yang SC, Hung TC, Feng YQ, Wu CJ, Wong KW, Huang KC. Experimental investigation on a 3 kW organic Rankine cycle for low-grade waste heat under different operation parameters. Appl Therm Eng 2017;113:756–64.

[88] Kolasinski P, Blasiak P, Rak J. Experimental and numerical analyses on the rotary vane expander operating conditions in a micro organic rankine cycle system. Energies 2016;9.

[89] Tang H, Wu H, Wang X, Xing Z. Performance study of a twin-screw expander used in a geothermal organic Rankine cycle power generator. Energy 2015;90:631–42.

[90] Smith IK, Stošič N, Aldis CA. Development of the Trilateral Flash Cycle System: Part 3: The Design of High-Efficiency Two-Phase Screw Expanders. Proc Inst Mech Eng Part A J Power Energy 1996;210:75–93.

[91] Hsu S-W, Chiang H-W, Yen C-W. Experimental Investigation of the Performance of a Hermetic Screw-Expander Organic Rankine Cycle. Energies 2014;7:6172–85.

[92] EE Publishers. Article of Organic Rankine Cycle for low grade waste

heat recovery. Available in: <www.ee.co.za> [accessed: 01.04.2017].

[93] Desideri A, Gusev S, van den Broek M, Lemort V, Quoilin S. Experimental comparison of organic fluids for low temperature ORC (organic Rankine cycle) systems for waste heat recovery applications. Energy 2016;97:460–9.

[94] Li G, Zhang H, Yang F, Song S, Chang Y, Yu F, et al. Preliminary development of a free piston expander-linear generator for small-scale Organic Rankine Cycle (ORC) waste heat recovery system. Energies 2016;9.

[95] Lemort V., Guillaume L., Legros A., Declaye S. and Quoilin S. A comparison of piston, screw and scroll expanders for small-scale Rankine cycle systems. The 3rd international conference on microgeneration and related technologies, Naples, 2013.

[96] Oudkerk JF, Dickes R, Dumont O, Lemort V. Experimental performance of a piston expander in a small- scale organic Rankine cycle. IOP Conf Ser Mater Sci Eng 2015;90:12066.

[97] Pei G, Li J, Ji J. Analysis of low temperature solar thermal electric generation using regenerative Organic Rankine Cycle. Appl Therm Eng 2010;30:998–1004.

[98] Xu RJ, He YL. A vapor injector-based novel regenerative organic Rankine cycle. Appl Therm Eng 2011;31:1238–43.

[99] Villarini M, Bocci E, Moneti M, Di Carlo A, Micangeli A. State of art of small scale solar powered ORC systems: A review of the different typologies and technology perspectives. Energy Procedia 2014;45:257–67.

[100] Lecompte S, Huisseune H, Van Den Broek M, Vanslambrouck B, De Paepe M. Review of organic Rankine cycle (ORC) architectures for waste heat recovery. Renew Sustain Energy Rev 2015;47:448–61.

[101] Lecompte S, Lemmens S, Huisseune H, Van Den Broek M, De Paepe M. Multi-objective thermo-economic optimization strategy for ORCs applied to subcritical and transcritical cycles for waste heat recovery. Energies 2015;8:2714–41.

[102] Obi JB. State of art on ORC applications for waste heat recovery and micro-cogeneration for installations up to 100kWe. Energy Procedia 2015;82:994–1001.

[103] Bianchi G, Fatigati F, Murgia S, Cipollone R, Contaldi G. Modeling and Experimental Activities on a Small-scale Sliding Vane Pump for ORC-based Waste heat Recovery Applications. Energy Procedia 2016;101:1240–7.

[104] Landelle A, Tauveron N, Haberschill P, Colasson S. Study of Reciprocating Pump for Supercritical ORC at full and part load operation. Proc 3rd Int Semin ORC Power Syst 2015:1–9.

[105] Quolin S. Past and current research trends in ORC power systems. Asme Orc 2015 2015;XXXIII:81–7.

[106] Lazova M, Huisseune H, Kaya A, Lecompte S, Kosmadakis G, De Paepe M. Performance Evaluation of a Helical Coil Heat Exchanger Working under Supercritical Conditions in a Solar Organic Rankine Cycle Installation. Energies 2016;9:432.

[107] Hu K, Zhu J, Li T, Zhang W. R245fa Evaporation Heat Transfer and Pressure Drop in a Brazed Plate Heat Exchanger for Organic Rankine Cycle (ORC). Proc World Geotherm Congr 2015 2015:19–25.

[108] Walraven D, Laenen B, D'Haeseleer W. Comparison of shell-and-tube with plate heat exchangers for the use in low-temperature organic Rankine cycles. Energy Convers Manag 2014;87:227–37.

[109] Zhang C, Liu C, Wang S, Xu X, Li Q. Thermo-economic comparison of subcritical organic Rankine cycle based on different heat exchanger configurations. Energy 2017;123:728–41.

[110] Wei D, Lu X, Lu Z, Gu J. Performance analysis and optimization of organic Rankine cycle (ORC) for waste heat recovery. Energy Convers Manag 2007;48:1113–9.

[111] Hernandez A, Desideri A, Ionescu C, Quoilin S, Lemort V, De Keyser R. Increasing the efficiency of Organic Rankine Cycle Technology by means of Multivariable Predictive Control. vol. 47. IFAC; 2014.

[112] Li L, Ge YT, Tassou SA. Experimental Study on a Small-scale R245fa Organic Rankine Cycle System for Low-grade Thermal Energy Recovery. Energy Procedia 2017;105:1827–32.

[113] ClearPower, ORC manufacturer website. Available in: < www.clearpowersystems.com > [accessed: 01.03.2017].

[114] ElectraTherm, ORC manufacturer website. Available in: < electratherm.com > [accessed: 01.03.2017].

[115] Enertime, ORC manufacturer website. Available in: < www.enertime.com > [accessed: 01.03.2017].

[116] Enogia, ORC manufacturer website. Available in: < www.enogia.com > [accessed: 01.03.2017].

[117] Muhammad Imran, Muhammad Usman, Byung-Sik Park YY. Comparative assessment of Organic Rankine Cycle integration for lowtemperature geothermal heat source applications. Energy

2016;102:473–90.

[118] General Electric, ORC manufacturer website. Available in: < powergen.gepower.com > [accessed: 01.03.2017].

[119] Infinity turbine, ORC manufacturer website. Available in: < www.infinityturbine.com > [accessed: 01.03.2017].

[120] Triogen, ORC manufacturer website. Available in: < www.triogen.nl> [accessed: 01.03.2017].

[121] Zuccato Energia, ORC manufacturer website. Available in: < www.zuccatoenergia.it > [accessed: 01.03.2017].

[122] Commission of the European Communities; European Commission. EUROSTAT-statistical book: Electricity prices for industrial consumers, from 2007 onwards bi-annual data.

[123] Alberta I. AESO, Alberta Energy System Operator. Available: <www.aeso.ca> [accessed: 01.03.2017]:813.

[124] Ministry of Industry, Energy and Tourism. "Real Decreto 413/2014, de 6 de junio, por el que se regula la actividad de producción de energía eléctrica a partir de fuentes de energía renovables, cogeneración y residuos. Boletin Oficial del Estado, N.140.".

[125] Educación MDE, Deporte CY. Ministry of Industry, energy and tourism. "Real Decreto 900/2015, de 9 de octubre, por el que se regulan las condiciones administrativas, técnicas y económicas de las modalidades de suministro de energía eléctrica con autoconsumo y de producción con autoc. Bol Of Del Estado, Miércoles 30 Julio 2014 Sec 2014:60502–11.

[126] Boletin Oficial del Estado N 252. 17 O 2014. Ley 18/2014, de 15 de octubre, de aprobación de medidas urgentes para el crecimiento, la competitividad y la eficiencia 2014:162.

[127] Forni D, Vaccari V, Santo D Di, Baresi M. Heat recovery for electricity generation in industry 2012:523–34.

[128] IVACE IV de CE. RESOLUCIÓN de 17 de mayo de 2017, del presidente del Instituto Valenciano de Competitividad Empresarial (IVACE), por la que se convocan ayudas en materia de eficiencia energética en la industria y en los edificios del sector terciario, con cargo al presup. Docv 2015:27511.

[129] Cavazzini G, Dal Toso P. Techno-economic feasibility study of the integration of a commercial small-scale ORC in a real case study. Energy Convers Manag 2015;99:161–75.

[130] Beith R. Small and micro combined heat and power (CHP) systems.

Advanced design, performance, materials and applications.Woodhead Publishing. ISBN: 978-0-85709-275-5. 2011.

[131] Jung HC, Krumdieck S, Vranjes T. Feasibility assessment of refinery waste heat-to-power conversion using an organic Rankine cycle. Energy Convers Manag 2014;77:396–407.

[132] David G, Michel F, Sanchez L. Waste heat recovery projects using Organic Rankine Cycle technology–Examples of biogas engines and steel mills applications. World Eng Conv 2011.

[133] Forni D, Santo D Di, Campana F. Innovative system for electricity generation from waste heat recovery.:393–403.

[134] Battisti L, Cozzini M, Macii D. Industrial Waste Heat Recovery Strategies in Urban Contexts: a Performance Comparison. Smart Cities Conf (ISC2), 2016 IEEE Int 2016.

[135] Tchanche. BF, Quoilin. S, Declaye. S, Papadakis. DG, Lemort. V. Economic Optimization of small scale organic rankine cycles. 23rd Int Conf Effic Cost, Optim Simul Environ Impact Energy Syst 2010.

[136] Lemmens S, Lecompte S. Case study of an organic Rankine cycle applied for excess heat recovery: Technical, economic and policy matters. Energy Convers Manag 2017;138:670–85.

[137] Lecompte S, Huisseune H, van den Broek M, De Schampheleire S, De Paepe M. Part load based thermo-economic optimization of the Organic Rankine Cycle (ORC) applied to a combined heat and power (CHP) system. Appl Energy 2013;111:871–81.

[138] Garg P, Orosz MS, Kumar P. Thermo-economic evaluation of ORCs for various working fluids. Appl Therm Eng 2016;109:841–53.

[139] Imran M, Park BS, Kim HJ, Lee DH, Usman M, Heo M. Thermo-economic optimization of Regenerative Organic Rankine Cycle for waste heat recovery applications. Energy Convers Manag 2014;87:107–18.

[140] Keros Cerámica. Company specialized in ceramic tiles, Nules, Castellón (Spain). Available in: <www.keros.com> [accessed: 01.03.2017].

[141] Mezquita A, Monfort E, Vaquer E, Ferrer S, Arnal MA, Toledo J, et al. "Optimización energética en la fabricación de baldosas cerámicas mediante el uso de aceite térmico." Bol La Soc Esp Ceram Y Vidr 2012;51:183–90.

[142] Siti Group Datasheet. "Fornos a rolos para pisos. Série F1NH monocanal e bicanal".

[143] Navarro-Esbrí J, Collado-Puig R, González-Piquer M, Martí-Mata J, Peris B. "Aplicación de un equipo de microgeneración Rank(R) para la revalorización energética de humos en un horno cerámico". ISBN: 978-84-86313-14-2. "ESES, II Congr. Serv. Energéticos".Barcelona, 2012.

[144] Roy JP, Mishra MK, Misra A. Parametric optimization and performance analysis of a waste heat recovery system using Organic Rankine Cycle. Energy 2010;35:5049–62.

[145] Peris B, Navarro-Esbrí J, Molés F, Mota-Babiloni A. Experimental study of an ORC (organic Rankine cycle) for low grade waste heat recovery in a ceramic industry. Energy 2015;85:534–42.

[146] Guillen DP. Waste Heat Recovery Research at the Idaho National Laboratory. Technology Forum: Low Temperature Waste Energy Recovery in Chemical Plants and Refineries, Houston, Texas, 2012.

[147] Peris B, Navarro-Esbrí J, Molés F, Collado R, Mota-Babiloni A. Performance evaluation of an Organic Rankine Cycle (ORC) for power applications from low grade heat sources. Appl Therm Eng 2015;75:763–9.

[148] Therminol. Thermal oil manufacturer. Available in: <www.therminol.com> [accessed 01.03.2017].

[149] PIROBLOC. "Fluido térmico 300A". Available in: <www.pirobloc.com> [accessed 01.03.2017].

[150] UNE 9-310-92. "Instalaciones transmisoras de calor mediante líquido diferente de agua", CDU 536.2, 1992.

[151] Sheet SD. Safety datasheet of Honeywell. HFC-245fa , Genetron ®. Regulation (EC) No. 1907/2006. 2016:1–12.

[152] Zhou Y, Dong X, Cheng Y, Hu H. Research on the structure optimization of air-cooled condensers. Energy Science and Applied Technology. ESAT 2016-Fang. ISBN 978-1-138-02973-6.

[153] Serth R. Process Heat Transfer. Chapter 12 Air-cooled heat exchangers. ISBN: 978-0-12-373588-1. 2007.

[154] Standard practice for calculating thermal transmission properties under steady-state sonditions. Annu B ASTM Stand 2012;14:1–13.

[155] Quoilin S, Schrouff J. Assessing steady-state, multivariate thermo-fluid experimental data using Gaussian Processes: the GPExp open-source library. Energies 2016;9, 423:1–16.

[156] Lemort V, Quoilin S, Cuevas C, Lebrun J. Testing and modeling a scroll expander integrated into an Organic Rankine Cycle. Appl Therm Eng 2009;29:3094–102.

[157] Claesson J. Doctoral Thesis. Thermal and Hydraulic Performance of Compact Brazed Plate Heat Exchangers Operating as Evaporators in Domestic Heat Pumps. KTH Energy Technology. ISBN: 91-7283-931-7 2004.

[158] Ayub ZH. Plate Heat Exchanger Literature Survey and New Heat Transfer and Pressure Drop Correlations for Refrigerant Evaporators. Heat Transf Eng 2003;24:3–16.

[159] Quoilin S, Orosz M, Hemond H, Lemort V. Performance and design optimization of a low-cost solar organic Rankine cycle for remote power generation. Sol Energy 2011;85:955–66.

[160] Hsieh YY, Lin TF. Saturated flow boiling heat transfer and pressure drop of refrigerant R-410A in a vertical plate heat exchanger. Int J Heat Mass Transf 2002;45:1033–44.

[161] SWEP plate heat exchangers manufacturer. Available in <www.swep.net> [accessed 01.03.2017].

[162] Incropera F, Dewitt D. Fundamentals of Heat and Mass Transfer. 7th edition. ISBN: 978-0470-50197-9.

[163] Palmer SC, Payne WV, Domanski P a. Evaporation and Condensation Heat Transfer Performance of Flammable Refrigerants in a Brazed Plate Heat Exchanger. Gaithersburg, Maryland: National Institute of Standards and Technology (NIST), 2000.

[164] Jeter S. Effectiveness and LMTD Correction Factor of the Cross Flow Exchanger: a Simplified and Unified Treatment. IceeUsmEdu 2006.

[165] Gardner KA. Efficiency of extended Surfaces. Asme Thermal Engineering Proceedings 1945.

[166] Stewart SW. Doctoral Thesis. Enhanced Finned-Tube Condenser Design and Optimization. Georgia Institute of Technology. 2003:29–100.

[167] Peet MJ, Hasan HS, Bhadeshia HKDH. Prediction of thermal conductivity of steel. Int J Heat Mass Transf 2011;54:2602–8.

[168] Bohnet M. Fouling of heat transfer surfaces. Chem Eng Technol 1987;10:113–25.

[169] Zukauskas, A., "Convective Heat Transfer in Cross Flow," in S. Kakac, R. K. Shah, and W. Aung, Eds., Handbook of Single-Phase Convective Heat Transfer, Wiley, New York, 1987.

[170] Briggs, D. E. and E. H. Young, Convection heat transfer and pressure drop of air flowing across triangular pitch banks of finned tubes, Chem. Eng. Prog. Symp. Ser., 59, No. 41, 1–10, 1963.

[171] Xiaoyong WEI, Xiande F, Rongrong SHI. A Comparative Study of Heat Transfer Coefficients for Film Condensation. Energy Sci Technol 2012;3:1–9.

[172] Thome JR. Condensation in plain horizontal tubes: recent advances in modelling of heat transfer to pure fluids and mixtures. J Brazilian Soc Mech Sci Eng 2005;27:23–30.

[173] Sekhar Gullapalli V. Doctoral Thesis. Estimation of Thermal and Hydraulic Characteristics of Compact Brazed Plate Heat Exchangers. Lund University, Sweden. 2013.

[174] Jaromir Klemes J, Arsenyeva O, Kapustenko P, Tovazhnyanskyy L. Compact Heat Exchangers for Energy Transfer Intensification: Low Grade Heat and Fouling Mitigation. ISBN 9781482232592.

[175] Junqi D, Xianhui Z, Jianzhang W. Experimental investigation on heat transfer characteristics of plat heat exchanger applied in organic Rankine cycle (ORC). Appl Therm Eng 2017;112:1137–52.

[176] R.K. Shah, Subbarao EC, Mashelkar. RA. Heat Transfer Equipment Design. New York: Hemisphere Pub. Corp., c1988. ISBN: 0891167293. 1988.

[177] Zare aliabadi H, Seyed Hussein N, Khoshnoodi M, Atashi H. Experimental & Theoretical Investigation of Pressure Drop across Tube Bundle of a THPHE and Introducing a New Correlation. 5th Int Chem Eng Congr Exhib Kish Island, 2 - 5 January 2008.

[178] Mon MS. Doctoral thesis. Numerical investigation of air-side heat transfer and pressure drop in circular finned-tube heat exchangers. TU Bergakademie Freiberg. 2003:151.

[179] ASHRAE, editor. 2013 ASHRAE Handbook—Fundamentals. ISBN: 978-1-936504-46-6. 2013.

[180] Choi JY, Kedzierski M a, Domanski P a. Generalized Pressure Drop Correlation for Evaporation and Condensation in Smooth and Micro-Fin Tubes 2001.

[181] Amalfi RL, Thome JR. High resolution infrared measurements of single-phase flow of R245fa and R236fa within a compact plate heat exchanger, Part 1: Experimental setup and pressure drop results. Appl Therm Eng 2015;101:545–54.

[182] Táboas Touceda F. Doctoral thesis. "Estudio del proceso de ebullición forzada de la mezcla amoniaco/agua en intercambiadores de placas para equipos de refrigeración por absorción". Universitat Rovira i Virgili. ISBN: 978-84-690-7588-3, 2007.

[183] Amalfi RL, Thome JR, Solotych V, Kim J. High resolution local heat

transfer and pressure drop infrared measurements of two-phase flow of R245fa within a compact plate heat exchanger. Int J Heat Mass Transf 2016;103:791–806.

[184] Cengel Y, Boles M. Thermodynamics An Engineering Approach, 5th Ed. ISBN: 0072884959. 2006.

[185] Minea V. Power generation with ORC machines using low-grade waste heat or renewable energy. Appl Therm Eng 2014;69:143–54.

[186] Imran M, Usman M, Park BS, Lee DH. Volumetric expanders for low grade heat and waste heat recovery applications. Renew Sustain Energy Rev 2016;57:1090–109.

[187] Lemort V, Declaye S, Quoilin S. Experimental characterization of a hermetic scroll expander for use in a micro-scale Rankine cycle. Proc Inst Mech Eng Part A J Power Energy 2012;226:126–36.

[188] Zanelli R, Favrat D. Experimental investigation of a hermetic scroll expander-generator. 12th Int Compress Eng Conf Purdue 1994:459–64.

[189] Lei B, Wang W, Wu Y-T, Ma C-F, Wang J-F, Zhang L, et al. Development and experimental study on a single screw expander integrated into an Organic Rankine Cycle. Energy 2016;116:43–52.

[190] Singh Panesar A. Doctoral thesis. A study of organic Rankine cycle systems with the expansion process performed by twin screw machines. City University London. 2012.

[191] Astolfi M. Techno-economic Optimization of Low Temperature CSP Systems Based on ORC with Screw Expanders. Energy Procedia 2015;69:1100–12.

[192] Dickes R, Dumont O, Legros A, Quoilin S, Lemort V. Analysis and comparison of different modeling approaches for the simulation of a micro-scale organic Rankine cycle power plant. Proc ASME -ORC 2015 2015:1–10.

[193] Chirakalwasan R. Motor load and efficiency. ASHARE J 2006 - 2007.:21–33.

[194] Hariharan C, Govardhan M. Improving performance of an industrial centrifugal blower with parallel wall volutes. Appl Therm Eng 2016;109:53–64.

[195] Le VL, Feidt M, Kheiri A, Lemort V. Sizing and Parametric Optimization of a Waste Heat To Power Plant Based on Transcritical Organic Rankine Cycle. Paper ID: 189. 3rd Int Semin ORC Power Syst Oct 12-14, 2015, Brussels, Belgium.

[196] European Central Bank reference exchange ratio: US dollar. Available in: <www.ecb.europa.eu> [accessed 01.03.2017].

[197] Astolfi M, Romano M, Bombarda P, Macchi E. Binary ORC (Organic Rankine Cycles) power plants for the exploitation of medium-low temperature geothermal sources 2014;66:435–46.

[198] Rettig A, Müller U, Sergi T. Exemplary Thermodynamic Assessment of a small ORC Application using dynamic Simulations. 3rd Engine ORC Consort Work 2016, Belfast, North Ireland.

[199] Collings P, Yu Z, Wang E. A dynamic organic Rankine cycle using a zeotropic mixture as the working fluid with composition tuning to match changing ambient conditions. Appl Energy 2016;171:581–91.

[200] Nusiaputra Y, Wiemer H-J, Kuhn D. Thermal-Economic Modularization of Small, Organic Rankine Cycle Power Plants for Mid-Enthalpy Geothermal Fields. Energies 2014;7:4221–40.

[201] Walraven D, Laenen B, William D. Minimizing the levelized cost of electricity production from low- temperature geothermal heat sources with ORCs : Water or air cooled ? 2015;142:144–53.

[202] "Estación de Climatología - Universitat Jaume I de Castelló". Available in: <www.climatologia.uji.es> [accessed 01.03.2017].

[203] Directive 2012/27/EU of the European Parliament of the Council of 25 October 2012 relative to energy efficiency. Official J Eur Union, 2012.

[204] A practical guide for calculating emissions of greenhouse gases: "Oficina Catalana del Canvi Climatic" (OCCC). Available: <canviclimatic.gencat.cat> [accessed 01.03.2017].

[205] Ministry of Energy, Tourism and Digital diary. "Orden ETU/130/2017, de 17 de febrero, por la que se actualizan los parámetros retributivos de las instalaciones tipo aplicables a determinadas instalaciones de producción de energía eléctrica a partir de fue.

[206] Ministry of energy, tourism and digital diary. "Orden ETU/1976/2016, de 23 de diciembre, por el que se establecen los peajes de acceso de energía eléctrica para 2017. Boletín Oficial del Estado, N. 314". BOLETÍN Of DEL ESTADO Miércoles 30 Julio 2014 Sec 2014;2014:60502–11.

[207] ORDEN ITC/2794/2007, de 27 septiembre, por la que se revisan las tarifas eléctricas a partir del 1 de octubre de 2007. Boletin Oficial del Estado, N. 234".

[208] OMIE. Market and system operators OMI-POLO Español S.A. Available: <www.omie.es> [accessed: 01.03.2017].

[209] Zhu Y, Jiang L, Jin V, Yu L. Impact of built-in and actual expansion ratio difference of expander on ORC system performance. Appl Therm Eng 2014;71:548–58.

[210] Navarro-Esbría J, Peris B, Molés F, Mota-Babilonia A, Barragán-Cerveraa Á. Theoretical Optimization of High Temperature Heat Pumps (HTHP) using Low GWP working fluids. The 4th International Symposium Waste heat valorization in industrial processes. 23-24 May 2016, Kortrijk, Belgium. Evolution (N Y) 2016.

[211] ASME code for Pressure Piping, B31. The American Society of Mechanical Engineers. Process ASME B31.3 (2002).

I.   COMBINED CONTROL STRATEGY OPTIMIZATION FOR THE REFERENCE CASE

If an optimization is conducted combining control strategies, an improvement of power output of the reference case without additional investment cost is reachable. Thus, the SIC of the process has been minimized, which is equivalent to maximize the final electrical power.

The results are collected in Table A.1. As can be seen, the change of the set point values implemented in the control system allows a final electricity increase about 6.6%. Moreover, it highlights that the gain obtained has been reached with a lower waste heat recovery than the current case, which emphasizes the necessity of using a model to find the best solution.

Table A.1 *Results of combined control strategy optimization for the reference case.*

Superheating degree (K)	46.08
Condensing and ambient temperature difference (K)	15.32
Thermal oil volumetric flow rate (m³/h)	9.18
Thermal power input (kW)	176.70
Electrical power output (kW)	13.15
Specific Investment Cost (€/kW)	6,328

II. RELEVANT PARAMETERS OF REFERENCE AND OPTIMIZED SYSTEMS

This investigation focuses on parameters that concern to the economic feasibility of ORC systems. However, depending on the topic of the investigation conducted, there are other ratios that are of interest. In this way, Table A.2 provides some relevant parameters distinguishing between reference and optimized systems.

Table A.2. *Other relevant results obtained from the thermo-economic optimization.*

	Reference	Max. W	Min. SIC
Organic working fluid (-)	HFC-245fa	HCFO-1233zd(E)	HFO-1234ze(Z)
Investment cost (€)	83,227	122,422	71,468
SIC of ORC unit (€/kW)	3,997	4,738	3,018
Cycle efficiency (%)	9.7	11.3	10.7
Thermal power output (kW)	147.70	158.70	144.20
Evaporating temperature (ºC)	118.50	125.90	123.20
Condensing temperature (ºC)	39.53	25.58	35.43
Expander inlet temperature (ºC)	152.28	166.53	158.23
Expander inlet pressure (bar)	18.57	17.59	21.47
Pressure ratio in expander (-)	5.75	7.16	7.57
Pressure ratio in pump (-)	6.90	10.47	6.94
Subcooling degree (K)	5.39	7.42	5.07
Expander isentropic efficiency (%)	56.0	54.8	54.1
Regenerator effectiveness (%)	91.9	99.2	93.8
Recuperator effectiveness (%)	70.6	79.3	70.6
Pinch Point in HRVG (K)	20.49	18.52	17.93
Pinch Point in condenser (K)	3.17	4.22	5.04
Mass flow rate (kg/s)	0.79	0.87	0.71
Pressure drop in exhaust air (bar)	1.7E-03	2.4E-03	1.6E-03
Pressure drop oil circuit (bar)	1.13	0.95	0.96
Pressure drop in ORC liquid side (bar)	1.07	0.17	0.18
Pressure drop in ORC vapor side (bar)	0.57	0.59	0.48

Scientific productivity

Papers indexed in Journal Citation Report

- Bernardo Peris, Joaquín Navarro-Esbrí, Francisco Moles, Adrian Mota-Babiloni. Experimental study of an ORC (organic Rankine cycle) for low grade waste heat recovery in a ceramic industry. Energy 85 (2015) 534–542.

- Bernardo Peris, Joaquín Navarro-Esbrí, Francisco Moles, Jose Pascual Martí, Adrian Mota-Babiloni. Experimental characterization of an Organic Rankine Cycle (ORC) for micro-scale CHP applications. Applied Thermal Engineering 79 (2015) 1–8.

- Bernardo Peris, Joaquín Navarro-Esbrí, Francisco Moles, Manuel González, Adrian Mota-Babiloni. Experimental characterization of an ORC (organic Rankine cycle) for power and CHP (combined heat and power) applications from low grade heat sources. Energy 82 (2015) 269–276.

- Bernardo Peris, Joaquín Navarro-Esbrí, Francisco Moles, Roberto Collado, Adrian Mota-Babiloni. Performance evaluation of an Organic Rankine Cycle (ORC) for power applications from low grade heat sources. Applied Thermal Engineering 75 (2015) 763-769.

- Bernardo Peris, Joaquín Navarro-Esbrí, Francisco Moles. Bottoming organic Rankine cycle configurations to increase Internal Combustion Engines power output from cooling water waste heat recovery. Applied Thermal Engineering 61 (2013) 364–371.

- Joaquín Navarro-Esbrí, Francisco Moles, Bernardo Peris, Adrian Mota-Babiloni, Konstantinos Kontomaris. Experimental study of an Organic Rankine Cycle with HFO-1336mzz-Z as a low global warming potential working fluid for micro-scale low temperature applications. Energy 133 (2017) 79–89.

- Francisco Molés, Joaquín Navarro-Esbrí, Bernardo Peris, Adrián Mota-Babiloni. Experimental evaluation of HCFO-1233zd-E as HFC-245fa replacement in an Organic Rankine Cycle system for low temperature heat sources. Applied Thermal Engineering 98 (2016) 954–961.

- Francisco Moles, Joaquín Navarro-Esbrí, Bernardo Peris, Adrian Mota-Babiloni, Konstantinos Kontomaris. Thermodynamic analysis of a combined organic Rankine cycle and vapor compression cycle system activated with low temperature heat sources using low GWP fluids. Applied Thermal Engineering 87 (2015) 444–453.

- Francisco Molés, Joaquín Navarro-Esbrí, Bernardo Peris, Adrián Mota-Babiloni, Ángel Barragán-Cervera, Konstantinos Kontomaris. Low GWP alternatives to HFC-245fa in Organic Rankine Cycles for low temperature heat recovery: HCFO-1233zd-E and HFO-1336mzz-Z. Applied Thermal Engineering 71 (2014) 204–212.

International Conferences

- Bernardo Peris, Joaquín Navarro-Esbrí, Carlos Mateu-Royo, Francisco Molés, Adrián Mota-Babiloni. Virtual Test Bench of Power Cycles. First International Conference on Engineering Education for the XXI Century– ICEE21C 2017. 6-7 July 2017, Castelló (Spain).

- Francisco Molés, Joaquín Navarro-Esbrí, Bernardo Peris, Adrián Mota-Babiloni. R1234yf and R1234ze as alternatives to R134a in Organic Rankine Cycles for low temperature heat sources. 9th International Conference on Applied Energy, ICAE2017, 21-24 August 2017, Cardiff, UK.

- Bernardo Peris, Joaquín Navarro-Esbrí, Francisco Molés, Adrián Mota-Babiloni, Angel Barragán-Cervera. Sensitive Study of Reversible HTHP/ORC ststems for waste heat valorization. IV International Seminar on ORC Power Systems, ORC2017, 13-15 September 2017, Milano, Italy.

- Francisco Molés, Joaquín Navarro-Esbrí, Bernardo Peris, Adrián Mota-Babiloni, José Pascual Martí, Roberto Collado, Manuel González. Combined cold, heat and power system, based on an organic Rankine cycle, using biomass as renewable energy heat source for energy saving and emission reduction in a supermarket. IV International Seminar on ORC Power Systems, ORC2017, 13-15 September 2017, Milano, Italy.

- Bernardo Peris, Joaquín Navarro-Esbrí, Francisco Molés, Adrián Mota-Babiloni, Angel Barragán-Cervera. Optimization of invertible HTHP/ORC system for cooling water waste heat recovery from internal combustion engines. 3RD Annual Engine ORC Consortium Workshop For Automotive and Stationnary Engine Industries. 14-16 September, 2016, Belfast (U.K).

- Bernardo Peris, Olivier Dumont, Sylvain Quoilin, Joaquín Navarro-Esbrí. Internal Combustion Engines Cooling Water Valorization through Invertible HTHP/ORC systems. The 4th International Symposium Waste Heat Valorization in industrial processes. 23-24 May, 2016, Kortrijk (Beligium).

- Joaquín Navarro-Esbrí, Francisco Molés, Bernardo Peris, Adrián Mota-Babiloni, Antonio Real Fernández. Análisis Termodinámico de un sistema combinado de Ciclo de Compresión de vapor y Ciclo Rankine Orgánico activado con fuente de calor de baja temperatura y utilizando fluidos de bajo GWP. CYTEF 2016 – VIII Congreso Ibérico | VI Congreso Iberoamericano de las Ciencias y Técnicas del Frío, Coimbra-Portugal, 3-6 mayo, 2016.

- Bernardo Peris Pérez, Joaquín Navarro-Esbrí, Francisco Molés, Adrián Mota-Babiloni, Angel Barragán-Cervera. Low grade heat recovery using small scale ORC systems. Interfaces Against Pollution. Environmental Challenges & Opportunities. 4 -7 Septiembre, 2016, Lleida (Spain).

- Bernardo Peris, Joaquín Navarro-Esbrí, Francisco Molés, Adrián Mota-Babiloni. ORC Applications from Low Grade Heat Sources. ASME ORC 2015. 3rd International Seminar on ORC Power Systems. 12-14 October, 2015, Brussels (Belgium).

- Joaquín Navarro-Esbrí, Francisco Molés, Bernardo Peris, Adrián Mota-Babiloni. Small scale ORC design for a Cogeneration Solar Biomass supported application. ASME ORC 2015. 3rd International Seminar on ORC Power Systems. 12-14 October, 2015, Brussels (Belgium).

- Bernardo Peris, Joaquín Navarro-Esbrí, Francisco Molés, Adrián Mota-Babiloni, Ángel Barragán-Cervera, Roberto Collado. Mejora de un sistema de cogeneración mediante el ciclo Rankine orgánico. XIII

Congreso Ibero-Americano de Climatización y Refrigeración (CIAR). 28-30 abril, 2015, Madrid (España).

- Joaquín Navarro-Esbrí, Bernardo Peris, Roberto Collado, Francisco Molés. Título del trabajo: Micro-generation and micro combined heat and power generation using "free" low temperature heat sources through Organic Rankine Cycles. Renewable Energy and Power Quality Journal 2013, (ISSN 2172-038, No.11).

National Conferences

- Bernardo Peris, Joaquín Navarro-Esbrí, Francisco Molés, Adrián Mota-Babiloni, Theoretical analysis of an Invertible HTHP/ORC system to profit from low grade waste heat sources. 10º Congreso Nacional de Ingeniería Termodinámica, 28-30 Junio, 2017, Lleida (España).

- Bernardo Peris, Joaquín Navarro-Esbrí, Francisco Molés, Adrián Mota-Babiloni. Modelado del ciclo Rankine orgánico (ORC) a partir de datos experimentales. 9º Congreso Nacional de Ingeniería Termodinámica (CNIT 9), 3-5 junio, 2015. Cartagena (España). ISBN: 978-84-606-8931-7

- Bernardo Peris, Joaquín Navarro-Esbrí, Francisco Molés, Adrián Mota-Babiloni. Optimización teórica del ciclo Rankine orgánico (ORC) para el aprovechamiento de fuentes térmicas de baja temperatura. 9º Congreso Nacional de Ingeniería Termodinámica (CNIT 9), 3-5 junio, 2015. Cartagena (España). ISBN: 978-84-606-8931-7

- Francisco Molés, Joaquín Navarro-Esbrí, Bernardo Peris, Adrián Mota-Babiloni. Evaluación teórica de fluidos de trabajo con bajo potencial de efecto invernadero como alternativas al HFC-245fa en ciclos orgánicos Rankine. 9º Congreso Nacional de Ingeniería Termodinámica (CNIT 9), 3-5 junio, 2015. Cartagena (España). ISBN: 978-84-606-8931-7

- Bernardo Peris, Joaquín Navarro-Esbrí, Francisco Molés. Evaluación teórica de fluidos para el aprovechamiento de fuentes térmicas de muy baja temperatura mediante ciclos orgánicos Rankine. VIII Congreso Nacional de Ingeniería Termodinámica (CNIT 8). 19-21 junio, 2013. Burgos (España). ISBN: 978-84-92681-62-4.

- Joaquín Navarro Esbrí, Roberto Collado Puig, Manuel González Piquer, José Pascual Martí Mata, Bernardo Peris Pérez. Aplicación de un equipo de microgeneración Rank para la revalorización energética de humos en un horno cerámico. II Congreso de Servicios Energéticos. ESES Gestión eficiente de la energía: un ahorro necesario. 13, 14 marzo, 2012. Barcelona (España). ISBN: 978-84-86313-15-9.

- Bernardo Peris Pérez, Joaquín Navarro-Esbrí, Bárbara Franch Salvador. Diseño y optimización de una instalación de recuperación de calor para sustitución de consumo de energía primaria en los secaderos de una planta de productos químicos básicos. 16-17 junio, 2011. Bilbao (España). ISBN: 84-95416-79-4.